Generation of a stem cell driven *in vitro* culture of polarized cells to study gastric tissue homeostasis and response to infections

D I S S E R T A T I O N

zur Erlangung des akademischen Grades

Doctor rerum naturalium
(Dr. rer. nat.)
im Fach Biologie

eingereicht an der
Lebenswissenschaftlichen Fakultät der Humboldt-Universität zu Berlin

von
Biochemikerin M.Sc., Sarah Wölffling

Präsidentin der Humboldt-Universität zu Berlin
Prof. Dr.-Ing. Dr. Sabine Kunst

Dekan der Lebenswissenschaftlichen Fakultät
der Humboldt-Universität zu Berlin
Prof. Dr. Bernhard Grimm

Gutachter/innen

1. Prof. Dr. Thomas F. Meyer

2. Prof. Dr. David Horst

3. PD Dr. Alexander Link

Tag der mündlichen Prüfung: 20.05.2020

“What we know is a drop, what we don’t know is an ocean.”

(Isaac Newton)

i. Selbstständigkeitserklärung

Hiermit erkläre ich, Sarah Wölffling, die Dissertation selbstständig und nur unter Verwendung der angegebenen Hilfen und Hilfsmittel angefertigt zu haben. Ich habe mich anderwärts nicht um einen Doktorgrad beworben und besitze keinen entsprechenden Doktorgrad. Ich erkläre, dass die Dissertation oder Teile davon nicht bereits bei einer anderen wissenschaftlichen Einrichtung eingereicht, angenommen oder abgelehnt wurden. Ich erkläre die Kenntnisnahme der dem Verfahren zugrunde liegenden Promotionsordnung der Lebenswissenschaftlichen Fakultät der Humboldt-Universität zu Berlin vom 5. März 2015. Weiterhin erkläre ich, dass keine Zusammenarbeit mit gewerblichen Promotionsberatern stattgefunden hat und dass die Grundsätze der Humboldt-Universität zu Berlin zur Sicherung guter wissenschaftlicher Praxis eingehalten wurden.

I, Sarah Wölffling, hereby declare that I completed the doctoral thesis independently based on the stated resources and aids. I have not applied for a doctoral degree elsewhere and do not have a corresponding doctoral degree. I have not submitted the doctoral thesis, or parts of it, to another academic institution and the thesis has not been accepted or rejected. I declare that I have acknowledged the Doctoral Degree Regulations which underlie the procedure of the Faculty of Life Sciences of Humboldt-Universität zu Berlin, as amended on 5th March 2015. Furthermore, I declare that no collaboration with commercial doctoral degree supervisors took place, and that the principles of Humboldt-Universität zu Berlin for ensuring good academic practice were abided by.

Berlin, …….. ……
Sarah Wölffling

ii. Publications

Parts of this thesis have been or will be published:

Woelffling, S., A. Imai-Matsushima, K. Fritsche, C. Goosmann, M. Schmid, M. del Mar Reines-Benassar, L. Pfannkuch, V. Brinkmann, J. Bornschein, P. Malfertheiner, J. Ordemann, A. Link, T. F. Meyer and F. Boccellato. "EGF and BMPs govern differentiation and patterning in human gastric glands" (**in submission)**

Boccellato, F., S. Woelffling, A. Imai-Matsushima, G. Sanchez, C. Goosmann, M. Schmid, H. Berger, P. Morey, C. Denecke, J. Ordemann, and T. F. Meyer. 2018. "Polarised epithelial monolayers of the gastric mucosa reveal insights into mucosal homeostasis and defence against infection", *Gut*.

iii. Zusammenfassung

In der humanen Magenschleimhaut regulieren eine Vielzahl von Interaktionen zwischen verschiedenen Zellpopulationen die Verdauung und die Überwachung von Infektionen. Epithelzellen in der Schleimhaut differenzieren in spezialisierte Zelltypen, die schützenden Schleim (Mukus), Magensäure, Verdauungsenzyme oder Hormone produzieren. Diese Zellen sind räumlich geordnet, um eine einfache säulenförmige Monoschicht zu bilden, die in ununterbrochenen engen Invaginationen gefaltet ist, die als Magendrüsen bezeichnet werden. Neben ihrer Funktion bei der Verdauung schützen sie den Magen aktiv vor Selbstverdauung und auch vor mikrobieller Besiedlung. Eine Infektion mit *Helicobacter pylori* kann sich dieser Überwachung häufig entziehen und die Gewebehomöostase fehlregulieren, was die Wahrscheinlichkeit erhöht, dass an der Infektionsstelle ein Magengeschwür, ein Adenokarzinom oder letztendlich Magenkrebs auftritt. Stammzellen sind für die Regeneration und Homöostase der Magendrüse verantwortlich, und der größte Teil des aktuellen Wissens über Stammzellen basiert auf Lineage-Tracing-Experimenten an Mäusen, bei denen es gelungen ist, die für die Aufrechterhaltung der Stammzellen erforderlichen Nischenfaktoren zu identifizieren. Dieses Bild der Drüsenhomöostase erklärt jedoch nicht, wie die Zellen differenzieren, um ihre spezifische Funktion zu erlangen, und die Nischenfaktoren, die dieses Phänomen bestimmen, sind noch unbekannt.

In dieser Arbeit wird die Entwicklung eines neuartigen *in vitro* Kulturmodells für humane primäre Magenepithelzellen, die sogenannte Mukosoidkultur, gezeigt. Die Mukosoidkulturen sind repräsentativ für Epithelbarrieren und rekapitulieren die meisten Funktionen der menschlichen Magenschleimhaut *in vivo*, einschließlich der Schleimproduktion, und ermöglichen eine langfristige und stabile Kultivierung von Epithelzellen sowie Infektionsstudien mit *Helicobacter pylori*.

Die Mukosoidkulturen wurden von verschiedenen Stellen des menschlichen Magens erzeugt, d.h. Antrum und Corpus. Das Genexpressionsprofil von Mukosoidkulturen aus Antrum und Corpus zeigt Unterschiede, die darauf hinweisen, dass die Zellen ein Gedächtnis für ihre Positionsidentität behalten. Mukosoidkulturen erzeugt aus Corpus wurden verwendet, um die Nischenfaktoren zu untersuchen, die die Differenzierung von Oberflächenepithelzellen, Hauptzellen und Parietalzellen (Belegzellen) fördern, welche Mukine, Verdauungsenzyme bzw. Salzsäure produzieren. EGF erwies sich zusammen

mit BMP/Noggin als ein wichtiger Regulator bei Differenzierungs- und Zellschicksalsentscheidungen. Während EGF für die Differenzierung von Oberflächenepithelzellen unverzichtbar ist, ist es für Haupt- und Belegzellen nachteilig. Aktives BMP-Signal unterstützt die Differenzierung von Oberflächenepithel- und Parietalzellen, wobei hohe BMP-Konzentrationen sich negativ auf die Hauptzellen auswirken.

Stromazellen sind Teil der *Lamina propria* der Magenschleimhaut und haben bekanntermaßen einen Einfluss auf die Krebsentwicklung und -progression, indem sie das Tumorwachstum und den Übergang von Epithel zu Mesenchym induzieren. Sie interagieren auch mit Immunzellen während einer Entzündung, über die Wechselwirkung mit dem Epithel unter homöostatischen Bedingungen und bei bakteriellen Infektionen mit *Helicobacter pylori* ist jedoch nur sehr wenig bekannt.

Die Co-Kultur von humanen primären Stromazellen des Magens mit Epithelzellen unter Verwendung des Mukosoidkultur-Modells zeigte die aktive Signalübertragung zwischen beiden Zelltypen auf. Unter physiologischen Bedingungen scheiden Stromazellen Wnt-Signalweg-Inhibitoren aus, die den Wnt/β-Catenin-Signalweg in Epithelzellen blockieren und die Differenzierung von Oberflächenepithelzellen induzieren. Darüber hinaus wurden Mukosoidkulturen erfolgreich mit *Helicobacter pylori* infiziert. Genexpressionsprofile von *H. pylori*-infizierten, co-kultivierten Epithelzellen ergaben, dass Stromazellen aktiv mit Cytokin- und Chemokinexpression auf eine epitheliale Infektion reagieren. Gleichzeitig erhöhten Stromazellen die NFκB-gesteuerte Entzündungsreaktion in Epithelzellen.

Die in dieser Arbeit entwickelten Mukosoidkulturen haben neue Einblicke in die Homöostase des Epithels geliefert und versprechen, ein nützliches Instrument zu sein, um die epitheliale Reaktion auf Infektionen und pathologische Veränderungen in der Magenschleimhaut zu verstehen.

iv. Abstract

In the human gastric mucosa, multiple interactions between different cell populations regulate digestion and surveillance of infections. Epithelial cells in the mucosa differentiate into specialized cell types to produce protective mucins, gastric acid, digestive enzymes or hormones. These cells are spatially ordered to form a simple columnar monolayer folded in continuous tight invaginations called gastric glands. Beside their function in digestion they actively protect the stomach from self-digestion and also against microbial colonization. Infection with *Helicobacter pylori* is often able to elude this surveillance and it dysregulates the tissue homeostasis increasing the chance to develop a gastric ulcer, adenocarcinoma or ultimately gastric cancer at the site of infection. Stem cells are responsible for the regeneration and homeostasis of the gland and most of the current knowledge on stem cells is based on lineage tracing experiments in mice where it has been possible to identify the niche factors required for their maintenance. This picture of the gland homeostasis does not explain how cells differentiate to acquire their specific function and the niche factors governing this phenomenon are still unknown.

In this thesis, the development of a novel *in vitro* culture model for human primary gastric epithelial cells, called the mucosoid culture, is shown. The mucosoid cultures are representative of epithelial barriers and recapitulate most of the functions of the human gastric mucosa *in vivo*, including mucus production, and allow long-term and stable cultivation of epithelial cells as well as infection studies with *Helicobacter pylori*.

The mucosoid cultures were generated from different sites of the human stomach i.e. – antrum and corpus. Gene expression profiling of antral and corpus derived mucosoid cultures shows differences indicating that the cells retain a memory of their positional identity. Corpus derived mucosoids were used to investigate the niche factors that promote the differentiation of foveolar cells, chief cells, and parietal cells, producing respectively protecting mucins, digestive enzymes, and hydrochloric acid. EGF was found to be a major regulator in differentiation and cell fate decisions together with BMP/Noggin. While EGF is indispensable for foveolar cell differentiation, it is detrimental for chief and parietal cells. Active BMP signaling supports foveolar and parietal cell differentiation but high BMP concentrations have a negative impact on chief cells.

Stromal cells are part of the *lamina propria* of the gastric mucosa and are known to have an influence on cancer development and progression by inducing tumor growth and epithelial-to-mesenchymal transition. They also interact with immune cells during inflammation but very little is known about the interaction with the epithelium under homeostatic conditions and during bacterial infections with *Helicobacter pylori*.

The co-culture of human primary gastric stromal cells with epithelial cells using the mucosoid culture model demonstrated the active signaling between both cell types. Under physiologic conditions, stromal cells secrete Wnt pathway inhibitors which block the Wnt/β-Catenin pathway in epithelial cells and induce foveolar differentiation. Furthermore, mucosoid cultures were successfully infected with *H. pylori.* Gene expression profiling of co-cultured epithelial cells infected with *H. pylori* revealed that stromal cells actively respond to epithelial infection with cytokine and chemokine expression. Concurrently stromal cells increased the NFκB-driven inflammatory response in epithelial cells.

The mucosoid cultures developed in this thesis have provided novel insight into epithelial homeostasis and they promise to be a valuable tool to understand the epithelial response to infections of human cells and also pathological changes in the gastric mucosa.

v. Acknowledgement

First and foremost, I would like to thank Prof. Dr. Thomas F. Meyer for the great and unique opportunity to work on such a complex and diversified research topic, his scientific guidance and supervision. I really appreciated our meetings, your availability for fruitful discussions and your support during my PhD. Also, I would like to thank Prof. David Horst and Dr. Alexander Link who kindly agreed to review my thesis.

Further I would like to thank Dr. Francesco Boccellato for his great co-supervision and his support since the beginning of my PhD. Thanks for your experience and knowledge, your overwhelming optimism and all the fruitful discussions which brought these projects forward and to the next level.

Next, I would like to thank our clinical collaborators Dr. Christian Denecke and Prof. Dr. Jürgen Ordemann for their contribution and the continuous supply with primary material which was the basis for this work. I am grateful to the IMPRS IDI/ZIBI Graduate School for the PhD fellowship and their support in all workshops, conferences and courses that I attended.

Furthermore, I would like to thank the MPIIB Core facility Microscopy for their excellent service, especially Dr. Christian Goosmann for the fruitful discussions and his tireless and ambitious commitment, patience and support in all concerns of electron microscopy. I would like to thank also Monika Schmid for her input and expertise in mass spectrometry and the analysis of my samples. Likewise, I would like to thank the MPIIB Core facility Microarray for their help and excellent services.

I would like to thank all my colleagues and former colleagues from the Department of Molecular Biology for all the advices and fruitful discussions in all the seminars and clubs but also during daily lab life and for the pleasant atmosphere. I am grateful to Dr. Kristin Fritsche, Dr. Maria del Mar Reines, Dr. Hilmar Berger, Dr. Lennart Pfannkuch, Dr. Aki Imai, Dr. Stephanie Zimmermann, Friderike Weege and Dr. Amina Ifthekar. I express my gratitude to all technicians of the Department. In particular I would like to thank Dagmar Frahm, Kirstin Hofmann, Marina Drabkina, Stefanie Müllerke and Jörg Angermann.

Special gratitude goes to Janine Sigulla, Christine Harnack, Stefanie Koster, Dr. Paulina Dziubanska-Kusibab and Silke Lehmann. My PhD time would not have been the same without you. Thank you girls for your friendship, the time we spent together, all the fantastic conversations and your support in all ups and downs.

Finally, I would like to thank my parents, my brother and my boyfriend Paul for their love and their unconditional belief in me and my abilities. You motivated me in all the dark phases and celebrated the successful days with me. Without your unconditional support I would not have made it that far. Thank you.

vi. Table of contents

i. Selbstständigkeitserklärung 7

ii. Publications 8

iii. Zusammenfassung 9

iv. Abstract 11

v. Acknowledgement 13

vi. Table of contents 15

vii. Abbreviations 19

viii. List of figures 24

ix. List of tables 27

1. INTRODUCTION 29

1.1. The human gastric mucosa 29

1.1.1. The antral gland 31

1.1.2. The corpus gland 34

1.1.3. Stromal cells of the *lamina propria* 40

1.2. Embryonic development and patterning of the stomach 44

1.3. Signaling pathways 48

1.3.1. BMP signaling 48

1.3.2. WNT signaling 50

1.3.3. EGFR signaling 52

1.4. Culture systems of primary cells 54

1.4.1. 2D cell culture systems 54

1.4.2. 3D cell culture systems 55

1.5. *Helicobacter pylori* 60

1.5.1. History, prevalence, and transmission 60

1.5.2. Biology of *H. pylori* 61

1.6. Aim of the study 63

2. MATERIALS AND METHODS 65

2.1. Material 65

2.1.1. Human material 65

2.1.2. Cell lines 65

2.1.3. Bacterial Strain 66

2.1.4. Chemicals and Reagents 66

2.1.5. Buffer, solutions and media 69

2.1.6. Kits 73

2.1.7. Arrays 73

2.1.8. Primer 73

2.1.9. Antibodies 76

2.1.10. RNAScope probes 77

2.1.11. Consumables 78

2.1.12. Lab instrumentation 79

2.1.13. Software and databases 80

2.2. Methods 81

2.2.1. Cell culture and primary cell culture 81

2.2.2. Bacterial Cell Culture 88

2.2.3. RNA and DNA techniques 90

2.2.4. Immunohistochemistry and Microscopy 98

2.2.5. Protein biochemistry 101

2.2.6. Statistics 105

3. RESULTS 106

3.1. Development of the mucosoid culture model 106

3.1.1. Mucosoid cultures resemble the *in vivo* situation 106
3.1.2. WNT and RSPO influence foveolar differentiation in antral mucosoids 112
3.2. Differentiation dynamics of the oxyntic gland 118
3.2.1. Characterization of human corpus tissue 118
3.2.2. Corpus derived mucosoids are different from antrum derived mucosoids but lack important *in vivo* characteristics 121
3.2.3. Mapping of morphogens in the human corpus gland 123
3.2.4. BMP and EGF play important roles in foveolar differentiation in the corpus gland 127
3.2.5. EGF regulates chief cell differentiation through MAPK pathway 133
3.2.6. Inhibition of proliferation together with BMP4 guide parietal cell differentiation 139
3.3. Communication between epithelium and stroma 147
3.3.1. Isolation of a human gastric stromal cell population from the *lamina propria* 147
3.3.2. Gastric stromal cells induce differentiation in epithelial cells by blocking the Wnt/β-Catenin pathway 149
3.3.3. Infection of epithelial cells with *H. pylori* induced an inflammatory response in stromal cells 153

4. DISCUSSION 162
4.1. Development of the mucosoid culture model 162
4.2. Differentiation niche factors of the oxyntic gland 166
4.3. Communication between stroma and epithelium 176

5. CONCLUSION 183
6. REFERENCES 185

7. APPENDIX 203

7.1. Electronic appendix 203

7.2. MaxQuant MS data analysis 204

vii. Abbreviations

%	percentage
µg	microgram
µL	microliter
µm	micrometer
2D	two dimensional
3D	three dimensional
Å	angstrom
ALI	air-liquid interface
AO	Acridine Orange
APC	adenomatosis polyposis coli
app	approximatley
AREG	amphiregulin
ATCC	American Type Culture Collection
ATP	adenosine triphosphate
ATP4A	H^+/K^+ ATPase α-subunit
ATP4B	H^+/K^+ ATPase β-subunit
Bapx1	bagpipe homeobox homolog 1
BARX	homeobox BarH-like
BHI	brain heart infusion
bHLHA15	class A basic helix-loop-helix protein 15
BMP	bone morphogenetic protein
BMPR	bone morphogenetic protein receptor
bp	base pair
BSA	bovine serum albumin
CagA	cytotoxin-associated gene A
cagPAI	cytotoxin-associated gene pathogenicity island
CCL	CC-chemokine ligand
CD	cluster of differentiation
cDNA	complementary deoxyribonucleic acid
CDX2	caudal type homeobox 2
CHD1	E-Cadherin
CHGA	Chromogranin A
CI	confidence interval
cm	centimeter
CO_2	carbonate dioxide
CRC	conditional reprogramming of cells
CSF	Colony stimulating factor
CTNNB	β-Catenin
CXCL	chemokine (C-X-C motif) ligand
ddH_2O	double distilled water
DKK	dickkopf
DKKL	Dickkopf like acrosomal proteim
DMEM	Dulbecco's Modified Eagle's Medium
dNTP's	dioxynucleotide triphosphates
DPBS	Dulbecco's phosphate buffered saline

DTT	Dithiotreitol
e.g.	exempli gratia (for example)
ECL	enterochromaffin like cell
ECM	Extracellular matrix
EDTA	Ethylenediaminetetraacetic acid
EGF	epidermal growth factor
EGFR	epidermal growth factor receptor
ELK1	ETS like-1
EM	electron mircoscopy
EPC	epithelial cells
EPCAM	Epithelial cell adhesion molecule
ERK	extracellular signal regulated kinase
ESC	embryonic stem cell
EtBr	ethidium bromide
f	female
F	forward
FCS	fetal calf serum
FDR	false discovery rate
FGF(R)	fibroblast growth factor (receptor)
FZD	frizzled
g	gramm
GA	glutaraldehyde
GAPDH	glyceraldehyde-3-phosphate dihydrogenase
GAST	gastrin
GATA4	GATA binding protein 4
GFP	green fluorescent protein
GHRL	ghrelin
GIF	gastric intrinsic factor
GOI	gene of interest
GSC	gastric stromal cells
GSC CM	gastric stromal cell conditioned medium
GSEA	gene set enrichment analysis
GSK3	glycogen synthase kinase 3
h	hour
H&E	hematoxylin and eosin
H. pylori	*Helicobacter pylori*
H^+	hydrogen ion/proton
HCl	hydrochloric acid
hGAT	human Gastric Adipose Tissue
HGF	hepatocyte growth factor
His	histamine
HKG	house keeping gene
hpi	hours post infection
hTERT	human telomerase reverse transcriptase protein
i.e.	id est
ID1	DNA-binding protein inhibitor
IF	immunofluorescence
IgG	immunglobulin G

IL	interleukin
ILC	innate lymphoid cells
IRX	Iroquois Homeobox Protein
K^+	potassium ion
kb	kilobase pair
kDa	kilodalton
KRT	keratin
LC-MS/MS	liquid chromatography-mass spectrometry/mass spectrometry
LEF	lymphoid enhancer-binding factor
LFQ	lable free quantification
LGR5	leucine-rich repeat-containing G-protein coupled receptor 5
LOD	limit of detection
Log	logarithm
logFC	logarithm fold change
LRP5/6	lipoprotein receptor-related protein 5/6
M	molar
m	male
m/z	mass to charge ratio
MAPK	mitogen activated protein kinase
MEK	mitogen-activated protein kinase kinase
MEKi	MEK inhibitor
mg	milligram
MHC	major histocompatibility complex
min	minute
MIST1	muscle, intestine and stomach expression 1
mL	milliliter
mM	millimolar
mm	millimeter
mm^3	cubic millimeter
MMP	matrix metalloproteinase
MOI	multiplicity of infection
MPIIB	Max Planck Institute for Infectionbiology
mRNA	messenger ribonucleic acid
MS	mass spectrometry
MSC	mesenchymal stromal cells or mesenchymal stem cell
MUC5AC	mucin 5AC
MUC6	mucin 6
NFκB	nuclear factor κB
NI	Non-infected
NIC	nicotinamide
nL	nanoliter
nm	nanometer
norm.	normalized
NT	Non-treated
OD	optical density
PBS	phosphate buffered saline
PCF	polycarbonate
PCR	Polymerase chain reaction

Pen/Strep	Penicillin/Streptomycin
pFA	para-formaldehyde
PGC	pepsinogen C
pH	potential of hydrogen
PI3K	phosphoinositol-3-kinase
PSC	pluripotent stem cell
PVDF	polyvinylidene fluoride
R	reverse or R-spondin
RA	retinoic acid
RNA	ribonucleic acid
RNF43	ring finger protein 43
ROCK	Rho-associated, coild-coil containing protein kinase
RSK	ribosomal s6 kinase
RSPO	R-spondin 1
RT	room temperature or reverse transcriptase
RT-PCR	real time polymerase chain reaction
RUNX1	runt-related transcription factor 1
SD	standard deviation
SDS-PAGE	sodium dodecyl sulfate polyacrylamide gel electrophoresis
sFRP	secreted frizzled related protein
Shh	sonic hedgehog
SOX2	sex determining region Y-box 2
SPEM	Spamolytic polypeptide expressing metaplasia
SST	somatostatin
STD	standard
T4SS	type IV secretion system
Taq	*Thermus aquaticus*
TBE	Tris-Borate EDTA
TBS	Tris-buffered saline (with Tween20)
TBS-T	Tris-buffered saline containing Tween20
TCF	T-cell factor
TEM	transmission electron mircoscopy
TFF 1/2/3	trifoil factor 1/2/3
TGF	tumor growth factor
TLR	toll like receptor
TNF(α)	tumor necrosis factor (alpha)
Treg	regulatory T-cell
Tris	tris(hydroxymethyl)aminometha
Troy	tumor necrosis factor receptor superfamily, member 19
U/mL	Units per milliliter
USAG	sclerostin domain containing protein
UV	ultra violet
v/v	volume per volume
VacA	vacuolating toxin A
vs	versus
W	WNT3A
W/R	WNT3A and R-spondin 1
w/v	weight per volume

WB	western blot
WIF	Wnt inhibitory factor
Wnt	Wingless-Type MMTV Integration Site
WT	wilde type
XBP1	X-box binding protein 1
αSMA	alpha smooth muscle actin

viii. List of figures

Figure 1: Anatomy and histology of the human stomach. 30
Figure 2: Stromal cells can be activated into a secretory phenotype with an immunomodulatory effect and communicate with adjacent cell types. 43
Figure 3: The stomach originates from the posterior foregut of the endoderm.. 46
Figure 4: BMP signaling pathway.. 49
Figure 5: The canonical Wnt signaling pathway.. 51
Figure 6: Schematic representation of *H. pylori*-induced Correa's cascade. 61
Figure 7: Scheme of the gastric gland with the determination of the regions' "top" and "base" for the analysis of *in situ* hybridization samples.. 96
Figure 8: Primary stomach material and schematic representation of the mucosoid culture.. 107
Figure 9: Development of the polarized epithelial monolayer over time. 108
Figure 10: Mucosoid cultures show typical characteristics of a polarized monolayer present in the human stomach.. 109
Figure 11: Mucosoid cultures are long-living and can be re-grown into organoids.. ..110
Figure 12: Mucosoid cultures show stable longevity through propagation keeping their characteristic features.. 111
Figure 13: Mucosoid cultures comprise the cell types of the stomach gland *in vivo.*. 112
Figure 14: Inactivation of the Wnt pathway in mucosoid cultures restraint β-Catenin in the cytoplasm and reduced *LGR5* expression.....113
Figure 15: Inactivation of the Wnt pathway induced a higher proliferation rate in mucosoid cultures.. 114
Figure 16: Removal of WNT3A and RSPO1 induced foveolar differentiation in epithelial cells. 115
Figure 17: Removal of either RSPO1 or WNT3A from the cultivation medium induced partial foveolar differentiation in mucosoid cultures.. 116
Figure 18: Foveolar differentiation of mucosoids was permanent and not reversible. 117
Figure 19: Localization of the proliferative zone in the corpus gland.. 118
Figure 20: Localization of MUC5AC secreting foveolar cells and MUC6 secreting mucus neck cells. 119
Figure 21: Localization of chief cells and parietal cells in human corpus tissue.. 120

Figure 22: Corpus derived mucosoids are different from antrum derived mucosoids but do not fit the *in vivo* situation.. 122
Figure 23: BMP4 and BMP2 showed higher expression in the pit region than in the base.. 124
Figure 24: Noggin is expressed by *muscularis mucosae* cells below the base of gastric glands. 125
Figure 25: EGF and TGFα showed significantly higher expression in the pit region than in the base..... 126
Figure 26: Removal of WNT3A and RSPO1 induced foveolar differentiation in corpus mucosoid cultures.. 128
Figure 27: Depletion of Noggin leads to activation of the BMP pathway in corpus mucosoid cultures and foveolar differentiation. 129
Figure 28: Influence of EGF on foveolar differentiation in corpus mucosoids. 130
Figure 29: Foveolar differentiation highly depends on EGF and the BMP concentration.. 131
Figure 30: Inhibition of EGF signaling pathway with MEKi blocked foveolar differentiation.. 132
Figure 31: Depletion of EGF promoted chief cell differentiation. 134
Figure 32: Absence of EGF is crucial for chief cell differentiation.. 135
Figure 33: Inhibition of the EGFR-MAPK pathway induced chief cell differentiation, while a high concentration of BMP4 inhibited the differentiation.. 136
Figure 34: IF labeling against PGC confirmed a significant increase in chief cells when the EGFR pathway was inhibited.. 137
Figure 35: Electron microscopic images of chief cells after 12 days of treatment with MEKi..... 138
Figure 36: MEKi treated corpus mucosoids accumulated less mucus and showed PGC secretion.. 139
Figure 37: EGF is involved in parietal cell differentiation..... 140
Figure 38: Regulation of intrinsic BMP concentration by administration of increasing Noggin concentration.. 141
Figure 39: Intrinsic BMP as well as extrinsic BMP4 induced parietal cell differentiation, which is additionally stimulated by histamine. 143
Figure 40: Extrinsic BMP4 and stimulation with histamine induced differentiation into functional parietal cells.. 144

Figure 41: Electron microscopic image of a parietal cell. 146
Figure 42: Stromal cells were isolated from the *lamina propria* of human gastric tissue and show typical fibroblast phenotype. 147
Figure 43: Western Blot analysis for E-Cadherin and vimentin to test the purity of epithelial cell and stromal cell culture.. 148
Figure 44: Schematic representation of the co-culture system of gastric primary epithelial cells and stromal cells. 149
Figure 45: Secreted GSC factors inactivate the Wnt pathway in EPC.. 150
Figure 46: GSCs inhibit GFP signal expression in WNT3A reporter cell line in concentration dependent manner. 151
Figure 47: GSCs express different Wnt pathway inhibitors.. 152
Figure 48: GSCs induce partial foveolar differentiation in epithelial cells.. 153
Figure 49: *H. pylori* attached to the epithelial surface and translocated CagA into the host cell 154
Figure 50: Schematic representation of the *H. pylori* infection of co-cultured mucosoids.. 155
Figure 51: *H. pylori* infection induced an early NFκB driven immune response in epithelial cells independent of GSC co-culture. 156
Figure 52: GSCs respond to the *H. pylori* infection of overlaying EPCs.. 158
Figure 53: Time course of IL8 mRNA expression in EPC and GSC after *H. pylori* infection of co-cultured mucosoids.. 159
Figure 54: EPC infection induced a strong immune response in GSC.. 161
Figure 55: Proposed model for involved processes in the luminal-basal axis patterning of the oxyntic gland.. 175

ix. List of tables

Table 1: Human material 65
Table 2: Cell lines 65
Table 3: Bacterial strain 66
Table 4: Chemicals and reagents 66
Table 5: Composition of Adv++ and Adv+++ medium 69
Table 6: Primary epithelial cell culture medium 69
Table 7: Primary stromal cell medium 70
Table 8: Differentiation media for corpus mucosoid cultures to induce secretory cell lineage differentiation. 70
Table 9: General buffer and solutions 70
Table 10: Kits 73
Table 11: Arrays 73
Table 12: Primer 73
Table 13: Primary antibodies 76
Table 14: Secondary antibodies and antibody conjugates 77
Table 15: *in situ* hybridization probes 77
Table 16: Consumables 78
Table 17: Lab instrumentation 79
Table 18: Software and databases 80
Table 19: Motility scoring for *H. pylori* 89
Table 20: Reverse Transcription PCR setting 91
Table 21: Composition of one PCR reaction 92
Table 22: Programm setting of the PCR cycler 92
Table 23: Programm setting of the RT-PCR cycler 93
Table 24: Composition of one RT-PCR reaction 94
Table 25: Top 100 hits of the MaxQuant MS data analysis. 204

1.INTRODUCTION

1.1. The human gastric mucosa

The adult human stomach can be divided anatomically into five parts: cardia, fundus, corpus, antrum, and pylorus (Figure 1A). The cardia forms the entrance of the stomach and connects the esophagus with the rest of the stomach forming the gastric-esophageal junction. A thick ring of muscles, the cardiac sphincter, functions as a valve regulating the entrance of food from the esophagus into the stomach and prevents the backward movement of food or gastric acid into the esophagus. The fundus is on the left, adjacent to the cardia. The largest and main part of the stomach is constituted by the corpus. Here, ingested food is mixed and digestion starts through secretion of digestive enzymes e.g. trypsin, pepsin, and lipase. The antrum forms the lower part of the stomach which is adjacent to the most distal part of the stomach, the pylorus. The pylorus connects the stomach with the small intestine and includes the pylorus sphincter, a ring of muscles acting as a valve as in the cardia to regulate the emptying of the stomach into the duodenum. Moreover, the sphincter also prevents that food from the duodenum flows back into the stomach. (Martini, Timmons, and Tallitsch 2012).

Histologically the stomach wall is structured into four layers of tissue as shown schematically in Figure 1B: the serosa, the muscularis, the submucosa and the mucosa. In an empty stomach, the mucosa shows longitudinal folds so-called rugae which disappear when the stomach is filled with food (Martini, Timmons, and Tallitsch 2012). The gastric mucosa can be further divided into *muscularis mucosa, lamina propria*, and epithelium. The epithelium is made up of a monolayer of simple columnar epithelial cells which forms closely packed tubular invaginations, the gastric glands. Each gland opens into the gastric pit forming the outer stomach surface (while several glands unify into one pit). The gastric gland and pit together resemble the gastric unit. In general two types of gastric units can be defined (Figure 1C and D): zymogenic units (fundic units) in the corpus/fundus and mucus units in the antrum. While fundic units have a short pit region and glands are straight, the antral units have longer pits and the glands are branched and coiled.

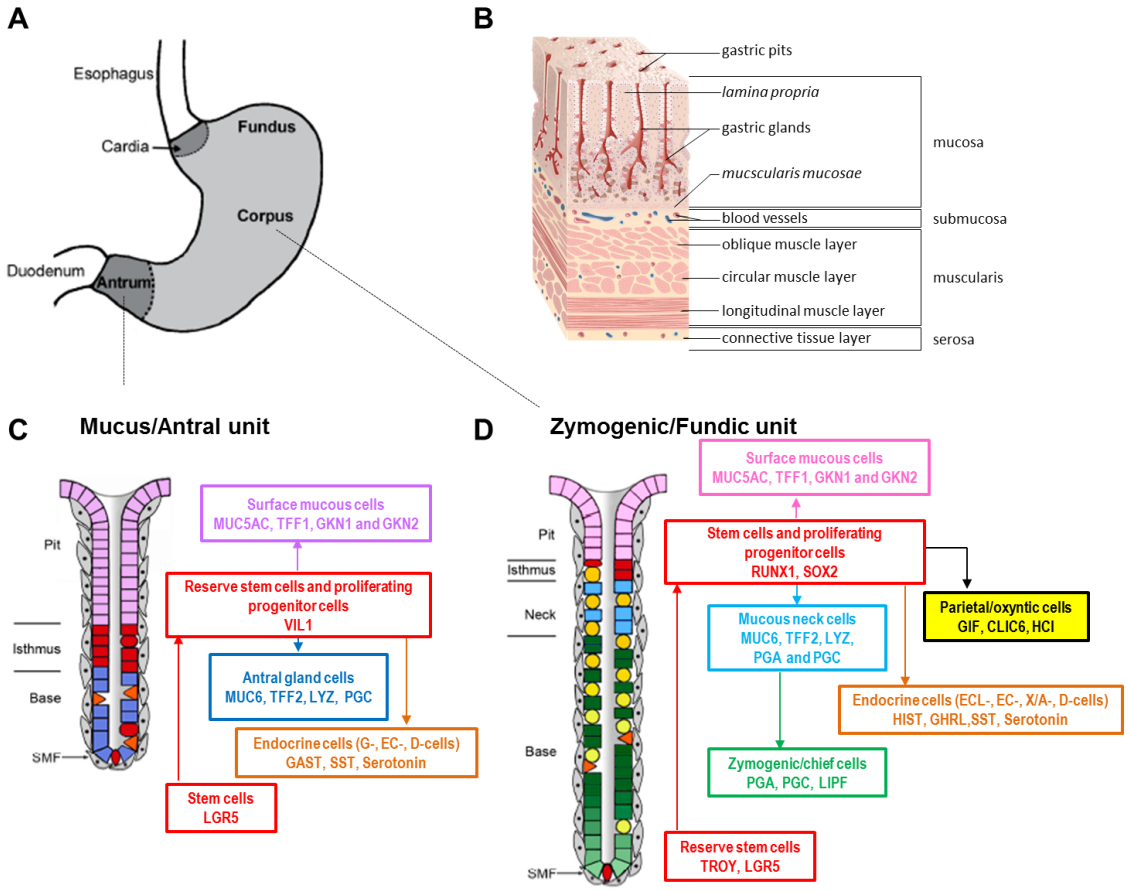

Figure 1: Anatomy and histology of the human stomach. (A) The human stomach can be divided anatomically into five parts: cardia, fundus, corpus, antrum, and pylorus. Cardia and pylorus form the junction with the adjacent esophagus and duodenum, respectively. (B) The stomach wall consists of several layers: the serosa, the muscularis, the submucosa and the mucosa. The latter is delimited by the *muscularis mucosae* and harbors the gastric glands which are surrounded and separated by the *lamina propria*. (C-D) Two different gastric units can be distinguished in the gastric mucosa of the stomach: (C) the antral unit and (D) the fundic unit. Both types are structured into pit, isthmus, neck, and base. The two types are different in their localization in the stomach and the composition of terminally differentiated cell types. The antral units in the antrum mainly consist of mucus-producing cells (pit cells and gland cells) while the fundic units in corpus and fundus harbor gastric acid-producing parietal cells and enzyme secreting chief cells. Figure 1A, C, D were adapted and modified from Hoffmann (2015). Figure 1B was modified from Encyclopædia Britannica https://www.britannica.com/science/stomach/media/1/567085/68634; retrieved on 08.07.2019]

The gastric glands can be subdivided into isthmus, neck, and base and constitute of different functional, highly specialized cell types. The abundance of specific cell types in the gastric units depends on the stomach region and differs between corpus and antrum. The zymogenic units are more complex, harboring more mature cell types but the antral units show a higher turnover (Hoffmann 2008). For some cell types e.g.

parietal cells, no sharp border exists between the stomach regions and the transition is diffuse, thus so-called mixed gland types occur in the antrum (Choi et al. 2014). In general, each gland consists of mucus-secreting cells, enzyme-producing cells, enteroendocrine cells, gastric acid-producing cells, and stem cells while the latter the origin and precursor of every functional cell type are. The epithelium is covered by a protective mucus layer produced by different mucus-producing cells especially in the pit region of the gastric units. The mucus forms a physical barrier protecting the epithelial cells from self-digestion and damage by the gastric acid and also against infection by pathogens like *Helicobacter pylori*.

1.1.1. The antral gland

The antral glands are mainly characterized by mucus-producing cells and hormone-producing endocrine cells which originate from adult stem cells.

1.1.1.1. The stem cell compartment

In the murine antrum stem cells are located in the gland base and are responsible for the self-renewal and repopulation of the entire gland and all resident cell lineages in a monoclonal fashion (Vries, Huch, and Clevers 2010). For a long time, the specific marker of antral stem cells was unknown. In the small intestine which is adjacent to the antrum, *Lgr5* was found to be the specific marker for intestinal stem cells. With the help of $Lgr5^{EGFP\text{-}ires\text{-}CreERT2}$/Rosa26R-LacZ reporter mice, lineage tracing experiments were conducted. In these mice, Cre recombinase was activated after tamoxifen administration leading to lacZ labeling of *Lgr5* expressing cells. Through this approach evidence was given that in mice all intestinal cell types within a crypt originate from the *Lgr5* positive, LacZ labeled stem cell in the crypt base (Barker et al. 2007). Extensive investigations in the antrum using the same approach have revealed that three to four cells in the base of the gland express *Lgr5* and thus were determined as stem cells by lineage tracing, giving rise to all cell lineages (Barker et al. 2010; Leushacke et al. 2013). Another quiescent stem cell population was described by Qiao et al. (2007) which is located in the isthmus of antral glands and is activated by inflammatory

stimuli. The authors showed that upon interferon γ (IFNγ) stimulation these stem cells start to divide and regenerate the entire gland. The lineage tracing experiments by Barker et al. (2010) identifying *Lgr5* to be the stem cell marker instead showed that quiescent stem cells in the isthmus also initially originate from the *Lgr5* stem cells in the base. After the stem cell marker was identified further investigations were made on the characterization of the stem cell niche and its homeostasis. Thus, it was reported that Notch signaling is essential for the homeostasis of *Lgr5*+ antral stem cells as pathway inhibition decreased the proliferation of the stem cells and progenitor cells (Demitrack et al. 2015). Moreover, *Lgr5* is a target gene of the Wnt/β-Catenin pathway, thus the stem cell niche in the intestine and consequently also in the antrum highly depends on the presence of WNT as fuel for *Lgr5* expression to maintain the stemness (Vries, Huch, and Clevers 2010). In addition to *Lgr5,* Sigal et al. (2017) showed that in the murine antrum a further stem cell compartment exists which is A*xin2* positive and is located right above the *Lgr5*+ stem cells. This second stem cell population is as well able to repopulate the antral gland.

1.1.1.2. Mucus producing cells

The pit region is populated by mucus-producing pit cells or foveolar cells which secrete surface mucus dominated by the mucin 5AC (MUC5AC). The transcription factor *FOXQ1* regulates MUC5AC expression in pit cells (Verzi et al. 2008). Foveolar cells are terminally differentiated and short-living with a turnover of three days, developing through constant migration from the stem cell compartment and shed into the lumen when they reach the outer surface (Kim and Shivdasani 2016). Moreover, foveolar cells express Trefoil factor (TFF) 1 which can be used as a cell-specific marker as TFF1 is only expressed in foveolar cells (Karam, Tomasetto, and Rio 2004). The differentiation of the cells into foveolar is regulated by the Wnt/β-Catenin signaling pathway. *In vitro* experiments using organoids have shown that constant supplementation with WNT and RSPO maintains the stemness and longevity of the organoid culture while the removal of both factors induced foveolar differentiation in antral organoids marked by MUC5AC expression (Schlaermann et al. 2014; Bartfeld et al. 2015). Moreover, in mice, it was shown that BMP2, which might originate from mesenchymal cells, has also an impact on foveolar differentiation (Itoh et al. 2006).

Other mucus-producing cells are located deeper in the antral gland. These mucus gland cells secrete acidic mucus enriched in mucin 6 (MUC6) that covers the epithelial cells from the base to the sub-foveolar region (De Bolos, Garrido, and Real 1995; Bartman et al. 1998). Furthermore, mucus gland cells co-express TFF2 also known as spasmolytic polypeptide. TFF2 is a further mucus gland cell specific marker as it is only expressed in MUC6 positive cells (Hanby et al. 1993).

1.1.1.3. Endocrine cells

The antral gland is also populated by hormone-secreting endocrine cells which are distributed among the non-endocrine cells. Two different types of endocrine cells with important function are present in the antrum: (1) G-cells secrete gastrin which is a specific marker for the antrum as these cells are only to be found in the antrum (Choi et al. 2014). G-cells are so-called “open” endocrine cells as the activation is due to luminal content. The gastrin release is triggered by proteins, amino acids and amines in the lumen and gastrin, in turn, activates the gastric acid secretion of parietal cells in the gastric corpus. (2) D-cells are as well “open” endocrine cells producing somatostatin which inhibits locally the gastrin secretion in G-cells. The somatostatin secretion is activated by gastric acid from the corpus and functions as a negative-feedback regulation to control the gastrin release. Somatostatin producing D-cells are also to be found in the corpus but seem to have different functions in the two compartments (Vassallo, Capella, and Solcia 1971; Dockray, Varro, and Dimaline 1996; Latorre et al. 2016). Chromogranin A is a further hormone that is widely expressed in the gastrointestinal tract including the stomach, pancreas, and intestine. The expression is not restricted to a specific cell type and can be found for example in G-cells in the antrum (Dockray, Varro, and Dimaline 1996; Portela-Gomes and Stridsberg 2002).

1.1.2. The corpus gland

In comparison to the antral gland, the corpus gland also called oxyntic gland has a more complex structure. It forms deeper invaginations and harbors more specialized cell types including mucin-producing pit cells and mucus neck cells, different endocrine cell types, zymogenic or chief cells and parietal cells. The two latter ones serve for the main function of the stomach – digestive enzyme secretion and gastric acid production. The mature specialized cells types develop postnatal in mice (Li, Karam, and Gordon 1996).

1.1.2.1. The stem cell compartment

According to the most recent reports (Han et al. 2019) the location of the stem cell compartment is different between antrum and corpus. While it is widely accepted that in the murine antrum the stem cell compartment is localized in the gland base (and it expresses *Lgr5* and/or *Axin2*), in the corpus two stem cell compartments are reported, one in the base of the gland and a second in the isthmus region. It is still under debate which of these two compartments is the driving force for the repopulation of the gland. The early studies of Karam and Leblond (1993a); (1993b, 1993c, 1993d) showed by nucleotide labeling studies in mice that the nucleotides were mainly incorporated in isthmus cells indicating the highest proliferative potential. They further characterized these cells as granule-free, immature cells and determined these cells as the progenitors of all other cell types of the corpus gland. Furthermore, they hypothesized that firstly immature precursors of every mature specialized cell type i.e. pre-pit cells, pre-mucous neck cells, pre-parietal cells or pre-zymogenic cells arise from the immature, granule free stem cell and further differentiate into the mature cell type. Contrary to the stem cells in the antrum, the isthmal stem cells do not express *Lgr5* and a specific stem cell marker has still not been found. Several markers were tested but they all have failed in lineage tracing experiments to label strongly and exclusively the isthmal stem cells. Among these markers, RUNX1, as well as SOX2, were described to be expressed in isthmal stem cells but both are not exclusive markers for these as they are expressed in chief cells in case of RUNX1 or all other cell types for SOX2 as well (Arnold et al. 2011; Matsuo et al. 2017). Although the Wnt target gene *Lgr5* is not expressed by the isthmal stem cells, which are most probably responsible for the daily renewal of the

corpus gland, *in vitro* studies with corpus organoids have revealed that the longevity and propagation of these organoid cultures highly depend on the supplementation of the cultivation medium with WNT and RSPO. Without both factors, the organoid cultures die after one passage as in antral organoid cultures (Schlaermann et al. 2014; Bartfeld et al. 2015). Additionally,to the proliferative stem cell compartment in the gland isthmus, another quiescent stem cell population was described to be present at the gland base exactly where the very characteristic chief cells are located. Lineage tracing experiments in mice using *Lgr5* as a tracer, labeled chief cells to be *Lgr5* positive in the gland base, but no fast renewal and tracing were observed originating from this cell population. Under homeostatic conditions, this stem cell population gives rise to the entire gland in a long-term process, after month. Upon damage with a high dose of tamoxifen, the stem cell capacity of chief cells is activated and they start to slowly regenerate the damaged gland showing the plasticity of this cell type. Thus, chief cells represent a reserve stem cell compartment (Leushacke et al. 2017). Similar findings were published by the Clever's group (Stange et al. 2013) showing a population of chief cells to be positive for the stem cell marker *Troy*. Also in this study lineage tracing experiments revealed that under homeostatic conditions these *Troy*+ chief cells did not have an impact on the "daily" renewal of the corpus gland. Only upon damage and ablation of the proliferative compartment in the isthmus, the stem cell ability of chief cells is activated. *Troy*+ chief cells re-entered the cell cycle and regenerated the injured gland, but with much slower kinetics than isthmal stem cells or *Lgr5*+ stem cells in the pylorus did. A recent study brought some more insight into the dynamics of both stem cell compartments. In the work from Han et al. (2019), the researchers compared three theories about the impact of the two stem cell compartments on the short-term and long-term renewal of the corpus gland and the longevity of the stem cells. They hypothesized that (1) either fast-cycling stem cells in the isthmus repopulate the entire gland through bi-directional migration or (2) the stem cells in the base are responsible in long-term for the repopulation of the gland from base to the pit or (3) both stem cell compartments repopulate the gland with the isthmal stem cells migrating up and regenerating the upper part of the gland and the base stem cells to be responsible for the repopulation of the gland from the base to the isthmus. Long-term tracing experiments in mice over 18 months confirmed that indeed isthmal stem cells are the active cycling and proliferating stem cell population regenerating the isthmus-pit-neck region on a daily basis. The stem

cell compartment in the base is quiescent and rare proliferative (Han et al. 2019). Although lineage tracing offers a potent tool to investigate the origin of the cells, the anatomical differences in the stomach between rodents and men should always be taken into account when inferring for humans the results obtained in mice.

1.1.2.2. Chief cells

Under homeostatic conditions chief cells are long-living (turnover of app. six month in mice estimated by Karam and Leblond (1993c)), fully differentiated cells, releasing digestive enzymes e.g. the zymogen pepsinogen C (PGC) also called progastricsin which is an inactive 42 kDa precursor protein. Pepsinogen C is activated into pepsin (34 kDa) under acidic conditions through hydrochloric acid and stays only active at acidic pH. Pepsin C is an endopeptidase of the aspartic protease family cleaving polypeptides from the C-terminal end between hydrophobic and preferably aromatic amino acids such as tyrosine, tryptophan and phenylalanine (Kageyama 2002; Shen, Jiang, and Yuan 2017). The decrease in PGC expression was described to be correlated with gastric cancer development (Shen, Jiang, and Yuan 2017).

Chief cells develop through trans-differentiation from mucus neck cells which migrate down from the stem cell compartment in the isthmus to the base (Karam and Leblond 1993c). The differentiation dynamics which also include signaling pathways and differentiation niche factors that are involved in the differentiation process of stem cells into chief cells are still poorly understood. In 2009 it was reported (Bredemeyer et al.) that the presence of parietal cells in the gastric gland has an impact on the maturation of chief cells however the authors did not reveal the maturation mechanisms. The authors hypothesized that parietal cells regulate the mucus neck cell to chief cell transition. Mucus neck cells are in close contact with parietal cells and form thereby a pseudostratified epithelium in the neck region while the chief cells in the base are structured in a monolayer. Although the presence of parietal cells seems to be necessary for the neck cell development may be due to secreted factors from the parietal cells, the ablation of parietal cells does not hamper the neck cell to chief cell differentiation. The authors finally hypothesized that parietal cells act more indirectly on the differentiation process of chief cells. Furthermore, the presence of histamine was also demonstrated to

have an influence on chief cell differentiation because in histamine deficient mice a significant increase in the number of chief cells was observed (Nozaki et al. 2009). Ramsey et al. (2007) analyzed the genetic profile of isolated chief cells from mice and found the transcription factor *Mist1* to be required for the maturation of mucus neck cells into chief cells. They defined zones of neck cells and chief cells in the gastric unit and a transition zone in which the mucus neck cells turn into chief cells and show features of both cell types. In the absence of *Mist1* (*Mist1* $^{-/-}$ mice) mucus neck cells still develop, but the further maturation into chief cells was impaired and an increase of transitional cells occurred, which showed intermediate phenotype with neck cell and chief cell morphology. Furthermore, the expression of *Mist1* was exclusively restricted to chief cells and transitional cells but never detected in mucus neck cells. *Mist1* is responsible for the induction and maintenance of the secretory architecture of the chief cells. The forced expression of *Mist1* for instance in parietal cells that normally do not express this gene, induced the formation of secretory granules on their apical side (Lo et al. 2017). The expression of *Mist1* is induced by the transcription factor *XBP1*. Although chief cells also develop in the absence of *XBP1*, this transcription factor was shown to be absolutely essential for the structural differentiation and maturation of chief cells in mice (Huh et al. 2010).

1.1.2.3. Parietal cells

A further frequent and important cell type in the corpus gland is the parietal cell, serving for the production of gastric acid. Parietal cells are large in size and show a very characteristic morphology with a triangular shape. They are terminally differentiated, non-proliferating and long-living cells with a turnover of 54 days in mice (Karam 2010). The localization is scattered throughout the gland, present mainly in the isthmus and neck, less in the base and in the foveolar region (Karam and Leblond 1992). The number of parietal cells comprises 12 % of corpus epithelial cells in humans (Helander, Leth, and Olbe 1986). In mice, on average 26 parietal cells per 194 epithelial cells per gland were estimated (Karam and Leblond 1992). It is suggested that parietal cells lose their functionality during aging, a process that is connected with the migration of the cells to the base or to the pit region of the gland (Karam 2010). Parietal cells release gastric acid, which is chemically hydrochloric acid, in ionic form through an active

ATP-driven process. Chloride ions flow through a chloride channel to the lumen. The proton (H^+) transport is mediated by the H^+/K^+ ATPase, which is located in tubulovesicular and canalicular membrane structures in the cytoplasm. In exchange for one H^+ transport into the lumen, one potassium ion (K^+) is transported into the cytoplasm. This process needs energy, delivered by adjacent mitochondria. The H^+/K^+ ATPase is a heterotetramer of two ATP4A subunits, which have the catalytic and cation transport activity, and two smaller, glycosylated ATP4B subunits. Upon activation of the parietal cells for gastric acid release the morphology of the cell changes. The intracellular tubulovesicles fuse with residual canalicular membranes, leading to intra-canalicular microvilli, forming a membrane network connected to the apical side to expand the surface for acid release. The cytoplasm is packed with mitochondria which concentrate around the canaliculi to provide energy for the active transport (Yao and Smolka 2019). Different agents stimulate the release of gastric acid from parietal cells: (1) by gastrin released by antral G cells (hormonal pathway) either directly through binding to cholecystokinin (CKK_2) receptor or indirectly by stimulating histamine secretion in enterochromaffin-like cells (ECL) in the corpus; (2) by histamine secreted from ECL cells (paracrine pathway) in the corpus which binds to the H_2 receptor on parietal cells and (3) by acetylcholine secreted by oxyntic and antral intramural postganglionic neurons (neural pathway) binding to a M_3 muscarinic receptor (Yao and Smolka 2019). The knowledge of how parietal cells differentiate from stem cells is still limited. The observation that parietal cells express Sonic hedgehog (Shh) supports the hypothesis that Bone morphogenetic proteins (BMP's) play a major role in the differentiation and maintenance of mature parietal cells as Shh induces the expression of BMP in the local environment and BMP in turn negatively regulates Shh expression (Van Den Brink et al. 2001; van den Brink et al. 2002; Katoh and Katoh 2006). In the canine model, the treatment of isolated parietal cells with BMP4 induced expression of ATP4A, demonstrating an impact of BMP4 on differentiation and maintenance of parietal cells (Nitsche et al. 2007). Using a transgenic mouse model which overexpresses the BMP antagonist Noggin under the promoter of the H^+/K^+-ATPase, Shinohara et al. (2010) showed the possible impact of BMP for the presence of parietal cells. They reported increased gland height, less parietal cells to be present and increased number of mucus neck cells and chief cells when BMP is inhibited by Noggin. These findings indirectly suggest a supporting role of BMP inhibition on chief

cell differentiation. In a follow-up study (Todisco et al. 2015) the role of gastrin on the abundance of parietal and chief cells in corpus glands was analyzed. Therefore the Noggin overexpressing mice were bred with gastrin knock-out mice. The combination of BMP pathway inhibition and the absence of gastrin lead to a reduction in the number of parietal cells and chief cells in these mice demonstrating a crucial role of gastrin in the differentiation and maturation of both cell types. Additionally, lower cell proliferation was detected indicating the involvement of gastrin in the cell proliferation of epithelial cells as well. In *in vitro* experiments, it was confirmed that the supplementation with BMP4 is needed for the definite differentiation of human fundic organoids containing parietal cells from pluripotent stem cells (McCracken et al. 2014) but further details about the differentiation are lacking. Besides Shh, parietal cells are a source of other morphogens like Transforming growth factor alpha (TGFα) (Beauchamp et al. 1989) and Parathyroid hormone-like hormone (Pthlh) (Jain and Samuelson 2007; Al Menhali et al. 2017). Parietal cells express further the glycoprotein Gastric intrinsic factor (GIF), which oppositely in mice is expressed in chief cells, demonstrating a clear and undeniable difference between these two species. Hence, GIF is used as a chief cell marker in mice and as a parietal cell marker in humans beside ATP4A and ATP4B. GIF is secreted into the lumen, transported with the pre-digested food in the intestine where it binds cobalamin at neutral pH and is therefore needed for the absorption of vitamin B_{12} in the ileum of the small intestine (Fedosov 2012).

1.1.2.4. Mucus producing cells

The pit region is constituted of surface mucus-producing pit/foveolar cells expressing the mucin MUC5AC and TFF1 similar to the antral gland. MUC6 secreting mucus cells are also present in the corpus gland located below the isthmus, in the neck region of the gland intermingling with parietal cells (Bredemeyer et al. 2009). Here, the mucus neck cells are not only an independent mucus-producing cell lineage but also the progenitors of chief cells as described before. Moreover, mucus neck cells express TFF2 similar to the antrum (Karam, Tomasetto, and Rio 2004). A special focus is given to TFF2 expressing mucus neck cells as the characteristic expansion of this cell type is correlated with the so-called spasmolytic polypeptide expressing metaplasia (SPEM). This phenotype occurs in diseased conditions in the corpus as a consequence of oxyntic

atrophy, the loss of parietal cells caused by mucosal injury associated with chronic *Helicobacter pylori* infection and gastric adenocarcinoma. In the advanced status of SPEM, chief and parietal cells are replaced by TFF2 expressing mucus neck cells leading to an antralization of the corpus gland. It is still under debate whether mature chief cells are the origin or progenitors of SPEM by transdifferentiation back into mucus neck cells (Goldenring et al. 2010).

1.1.2.5. Endocrine cells

Several types of endocrine cells are scattered throughout the whole gland. Although little is known about the endocrine cells in the stomach compared to the intensively characterized endocrine cells in the intestine, the two most important and best-characterized endocrine cells in the corpus are (1) enterochromaffin-like cells (ECL) secreting histamine upon gastrin activation and (2) X/A-like cells secreting the appetite-stimulating hormone ghrelin. ECL cells are classified as “closed” endocrine cells, located at the basal membrane only sensitive to stimuli from the basal side. ECL derived histamine stimulates gastric acid secretion in parietal cells as previously described (Dockray, Varro, and Dimaline 1996). Ghrelin secreting cells are very specific and only present in the corpus, thus being a potent marker for corpus glands (Choi et al. 2014).

1.1.3. Stromal cells of the *lamina propria*

Stromal cells also termed mesenchymal stromal cells (MSCs) are a diverse and heterogeneous cell population of non-epithelial ($EPCAM^-$), non-hematopoietic ($CD45^-$) and non-endothelial cells ($CD31^-$) including all fibroblast and myofibroblast populations and immunological stromal cells of the lymphoid tissue. Ultimately stromal cells derived from mesenchymal stem cells (as well MSC) of the bone marrow (Owens 2015) but can also arise from endothelial or epithelial cells through endothelial-to-mesenchymal or epithelial-to-mesenchymal transition (Zeisberg et al. 2007; Kalluri and Weinberg 2009). A growing body of evidence suggests that multiple stromal cell populations with distinct functions and localizations exist within the same tissue. Stromal cells are responsible for the synthesis of extracellular matrix (ECM)

components e.g. fibronectin, laminin and collagen type I, III, IV and V, but also matrix metalloproteinases (MMPs) for ECM degradation to balance the ECM homeostasis, maintaining the structural framework of the tissue. Furthermore, stromal cells are involved in the regulation of epithelial differentiation and proliferation, regulation of inflammatory processes and wound repair. Fibroblasts can be activated by different stimuli mainly through tissue damage and the release of growth factors like transforming growth factor β (TGFβ), epidermal growth factor (EGF) or fibroblast growth factor 2 (FGF2) by damaged epithelial cells or infiltrating immune cells. Activated fibroblasts are termed myofibroblasts and are characterized by the expression of α smooth muscle actin (α-SMA). Upon activation myofibroblasts express elevated amounts of MMPs and growth factors e.g. EGF, FGF2 and hepatocyte growth factor (HGF), which in turn influences adjacent epithelial cells (Kalluri and Zeisberg 2006) (Figure 2). Besides α-SMA stromal cells express vimentin and are negative for epithelial marker E-Cadherin and EPCAM and hematopoietic marker CD45 and endothelial marker CD31. However, characteristic and exclusive positive markers for stromal cells are still unknown. Unfortunately, many stromal cell markers are also expressed by other cell types. Thus, a panel of markers needs to be used to define stromal cells and to delimit them from other cell types by negative exclusion. The International Society for Cellular Therapy defined minimal criteria to identify and define multipotent MSCs. These criteria include that MSC are plastic-adherent in *in vitro* cultures. Furthermore, they must be positive for the surface markers CD73, CD90 and CD105 and negative for CD34, CD45, HLA-DR, CD14 or CD11b and CD79α or CD19. Finally, MSCs differentiate into adipocytes, osteoblasts or chondroblasts *in vitro* (Dominici et al. 2006). Additionally, Stro-1 was described to be one of the best-known stromal cell markers (Kolf, Cho, and Tuan 2007). Gastric stromal cells (GSC) are part of the *lamina propria* in the gastric mucosa, surrounding and separating the gastric glands. A further population of myofibroblasts is located in the *muscularis mucosae* below the gastric glands separating the mucosa from the submucosa. Almost nothing is known about the role of stromal cells in the gastric mucosa and the communication with adjacent cell types under physiological but also pathophysiological conditions like bacterial infections except the impact of stromal cells in cancer initiation and progression by cancer-associated fibroblasts and gastrointestinal stromal tumors. The research on intestinal stromal cells instead is more advanced. It was shown that the

mesenchymal stromal cells close to the colon crypt base, express BMP pathway antagonists e.g. gremlin or chordin-like to protect the crypt stem cells from BMP as it inhibits the Wnt/β-Catenin pathway in crypt stem cells and induces differentiation (Kosinski et al. 2007). On the other hand stromal cells in the villus region of the crypt express BMPs, maintaining the differentiation in epithelial cells after leaving the stem cell compartment by migration (Powell et al. 2011). Moreover, mesenchymal cells along the crypt-villus axis in the small intestine as well as in the colon are a source of different Wnt signaling components including non-canonical Wnts e.g. Wnt2b, Wnt4, Wnt5a and Wnt5b and antagonists e.g. DKK3, sFRP1 (Gregorieff et al. 2005).

In vitro co-culture studies by Katano et al. (2015) with murine stromal and epithelial cells revealed a supporting role of stromal cells on epithelial stem cell activity and proliferation. Recently, Sigal et al. (2017) showed that murine gastric stromal cells of the antrum in proximity to the stem cell compartment express R-spondin 3 and thereby support the self-renewal of the stem cell niche *in vivo*. In a follow-up study the authors demonstrated that upon *H. pylori* infection, myofibroblastic R-spondin 3 activates *Lgr5*+ stem cells to differentiate into a secretory phenotype expressing antimicrobial factors (Sigal et al. 2019). This study reveals the active communication between stroma and epithelium under pathological conditions revoking once more the dogma that stromal cells are passive structural subjects.

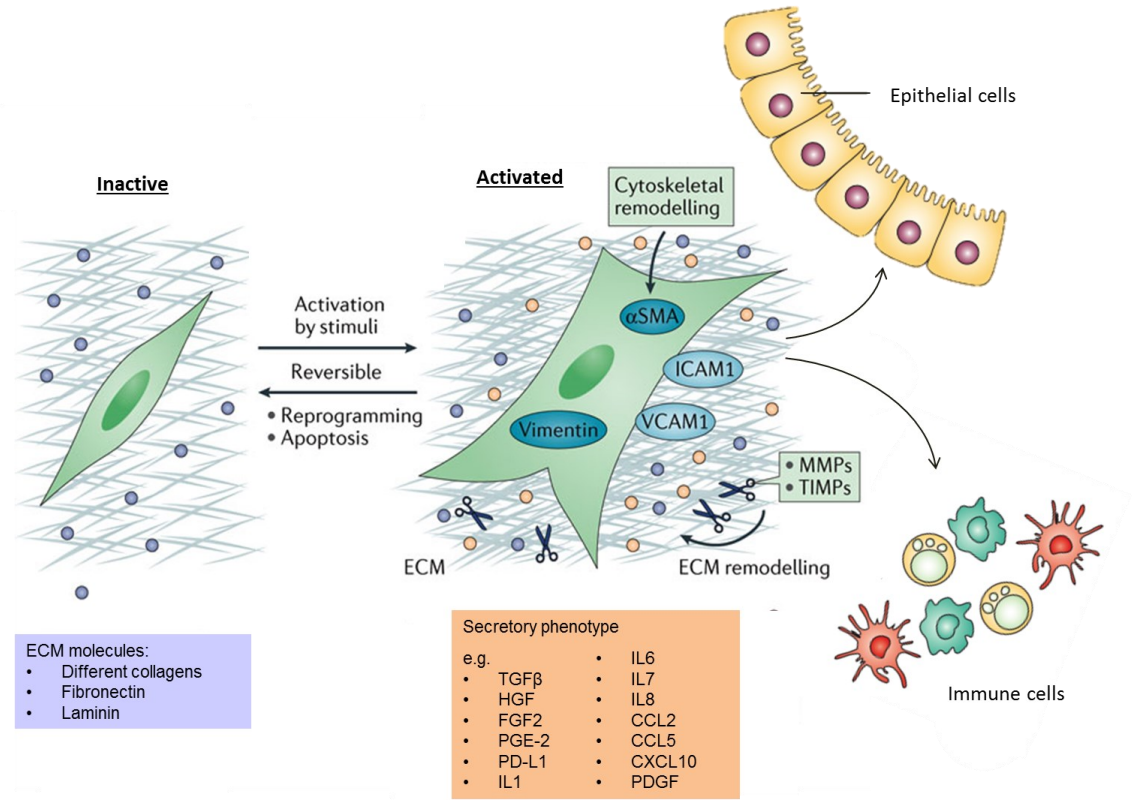

Figure 2: Stromal cells can be activated into a secretory phenotype with an immunomodulatory effect and communicate with adjacent cell types. Schematic representation of a stromal cell in the inactive state and after activation by a stimulus like an injury. Stromal cells produce ECM constituents like fibronectin, laminin and different types of collagen. After activation, stromal cells express αSMA, vimentin, different MMPs and a panel of cytokines, chemokines, growth factors and cell surface molecules with pro- or anti-inflammatory effects depending on the microenvironment. Secreted molecules influence adjacent cell types like immune cells or epithelial cells. TIMP: Tissue inhibitor of matrix metalloproteinase; ICAM: Intercellular adhesion molecule 1; VCAM1: Vascular cell adhesion molecule 1. The figure was adapted and modified from Kalluri and Zeisberg (2006); Kalluri (2016) (by permission of Springer Nature Customer Service Centre GmbH).

It is accepted that stromal cells belong to the group of antigen-presenting cells and are declared as non-professional immune cells as they show immunomodulatory characteristics by secretion of chemokines and cytokines having an impact on tolerance or active immunity (Mueller and Germain 2009). Figure 2 represents the activation of stromal cells into a secretory phenotype influencing adjacent immune cells and epithelial cells. Through secretion of plethora panel of chemokines, cytokines and cell surface molecules MSCs actively interact with different types of immune cells having either pro-inflammatory or anti-inflammatory and immunosuppressive effects which indicate the high plasticity of this cell type (Hoogduijn 2015). During an early

inflammation process, MSCs are able to enhance the pro-inflammatory response through secretion of chemokines which induce the recruitment of lymphocytes to the side of inflammation (Bernardo and Fibbe 2013). Amongst others, these are e.g. TGFβ, HGF, prostaglandin-E2 (PGE-2) or programmed death-ligand 1 (PD-L1) activating immunosuppressive immune cells like regulatory T cells (Treg), macrophages or B cells (Di Nicola et al. 2002; Aggarwal and Pittenger 2005; Augello et al. 2005). Furthermore, in many tissues, stromal cells continuously express IL33 and IDO1 under homeostatic conditions to nourish Tregs and innate lymphoid cells (ILC) and hamper T cell proliferation (Buechler and Turley 2018). On the other hand, MSCs secrete pro-inflammatory chemokines and cytokines like interleukin (IL) 1β, IL6, IL7, IL8 or chemokine ligand 2 (CCL2) to attract and activate immune cells (Hoogduijn 2015; Romieu-Mourez et al. 2009). Although MSCs do not function as classical immune cells, they are able to present antigens through major histocompatibility complex (MHC) class I molecules on their surface and are equipped with pattern recognition receptors like toll like receptors (TLRs) to recognize antigens from e.g. microbial pathogens (Hoogduijn 2015).

Although many general properties and characteristics of stromal cells are described and known as summarized above, a massive lack of knowledge exists regarding the distinct and precise role and function of tissue-specific stromal cells especially gastric stromal cells of the *lamina propria* in the communication with the adjacent epithelium.

1.2. Embryonic development and patterning of the stomach

The stomach derives from the posterior foregut of the endoderm in a multistep and complex process, which is still not fully understood. A highly conserved network of tightly regulated transcription factors and growth factors controls the organogenesis. Of note, the timing plays a crucial role in the whole organogenesis as the responsiveness and susceptibility of one cell population to a set of growth factors changes in the different developmental stages (Zorn and Wells 2009). The organ formation begins with the gastrulation in which the three germ layers mesoderm, endoderm, and ectoderm are formed (Figure 3A). In all vertebrate species, Nodal, a growth factor of the TGFβ

superfamily, is the driving force in the segregation of endoderm and mesoderm (Aoki et al. 2002; Ben-Haim et al. 2006; Hagos and Dougan 2007). The endoderm is further patterned into the foregut, midgut, and hindgut. This primitive gut tube is surrounded by mesoderm, the later mesenchyme, which is a source of growth factors that directly affect the developing epithelium and supports the anterior-posterior-axis patterning of the endoderm. The foregut develops into the esophagus, trachea, stomach, lung, thyroid, liver, biliary system and pancreas while the midgut forms the small intestine and the hindgut develops into the large intestine (Figure 3A). Through cell proliferation and differentiation during the fetal stage, finally, functional organs arise (Zorn and Wells 2009). The whole process of gastrulation and organ formation is tightly controlled and regulated through a complex and interacting network of growth factors including FGF, BMP, Wnt, Retinoic Acid (RA), Hedgehog and Notch (Figure 3B) (Dessimoz et al. 2006; Ameri et al. 2010; Tiso et al. 2002; Narita et al. 2000; Huelsken et al. 2000; Bayha et al. 2009; Litingtung et al. 1998; Kikuchi et al. 2004). In the early stage of organ formation of the endoderm, active Wnt signaling and FGF10 together with BMP, originating from the adjacent mesoderm, drive intestinal patterning of the hindgut characterized by the expression of the transcription factor *Cdx2* (Figure 3B) (Sherwood, Chen, and Melton 2009; Sherwood et al. 2011). The foregut expresses *Sox2,* a high mobility group-box gene transcription factor. BMP negatively regulates *Sox2* and repression of BMP signaling during the early stages of stomach development is therefore essential (Figure 3B) (Rodriguez et al. 2010). Another important transcription factor in the stomach specification is *BARX1,* which is expressed by the mesenchyme adjacent to the nascent stomach, demonstrating the important endodermal-mesoderm interaction. *BARX1* induces the expression of Wnt antagonists like secreted frizzle-related proteins (sFRP) leading to a regional inhibition of the Wnt pathway (Kim et al. 2007; Kim et al. 2005) to generate a sharp stomach-intestine boundary. The boundary of the stomach to other organs is also regulated by differential expression of transcription factors and gradients of growth factors (Kim and Shivdasani 2016).

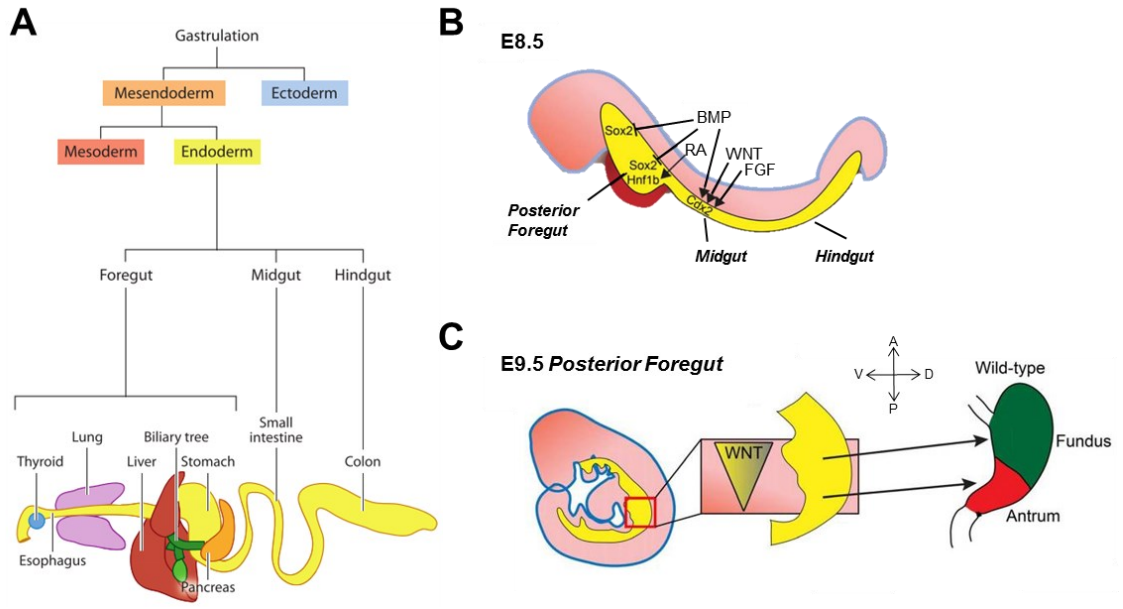

Figure 3: The stomach originates from the posterior foregut of the endoderm. (A) During organogenesis, the stomach develops in a complex and tightly controlled process from the posterior foregut of the endoderm. (B) The endoderm patterning into foregut, midgut, and hindgut occurs during embryonic stage E8.5 in mice. Active Wnt, BMP and FGF signaling promote midgut and hindgut pattering characterized by the transcription factor expression *Cdx2*. *Sox2* is expressed in the posterior foregut and the expression is repressed by BMP. RA is involved in the posterior patterning of the foregut, inducing the expression of the transcription factor Hnf1b. (C) A Wnt/β-Catenin gradient along the anterior-posterior axis of the posterior foregut promotes the further patterning of the stomach. Active Wnt/β-Catenin pathway stimulates the fundus specification in the stomach, while the inactivation of the Wnt pathway leads to antrum specification. Figure 3A modified from Zorn and Wells (2009), Figure 3B/C adapted from McCracken et al. (2017) (with permission from Annual Reviewes Inc. and Elsevier, conveyed through CCC).

After the initial stomach specification is completed, the regionalization, specification, and patterning of the stomach compartments into fundus, corpus, and antrum and the gland formation take place. The regionalization and patterning of the proximal-distal stomach axis are driven by strong epithelial-mesenchymal interactions. A set of differentially expressed transcription factors along this axis patterns the regional epithelium. The mouse stomach is differently structured than in humans. It additionally consists of a forestomach adjacent to the glandular stomach. The latter is similarly structured to the human stomach into fundus/corpus and antrum. In mice, high levels of *Sox2* expression lead to forestomach specification, while a reduction in *Sox2* provokes the expression of genes specific for the glandular stomach (Que et al. 2007). Further transcription factors which were described to be important in mice are *GATA4* for glandular stomach specification and the mesenchymal expressed *Bapx1* for the specific

antral stomach development (Jacobsen et al. 2002; Verzi et al. 2009). Moreover the regionalization is driven by active Wnt signaling and FGF10 as *in vitro* and *in vivo* studies have shown. Mutations in FGF10 or its receptor FGFR2 lead to defects in glandular stomach growth and a decrease in epithelial cell proliferation in the mouse model (Spencer-Dene et al. 2006). While the Wnt pathway is inhibited in the foregut during endoderm patterning (active Wnt would induce intestine development), an active Wnt pathway is necessary for the patterning of the stomach regions into fundus and antrum (Figure 3C). Furthermore, the deletion of the BMP receptor BMPR1A in foregut endoderm in mice had no effect on the stomach organogenesis, epithelial proliferation, and morphogenesis per se, but the loss of BMP signaling has an impact on gastric patterning, leading to anteriorization (Maloum et al. 2011). This again demonstrates the time-dependent effect of these pathways during organogenesis as also demonstrated by others (McCracken et al. 2017; Kim et al. 2005).

The epithelium of the early foregut and the future stomach shows a simple cuboidal shape, which needs to transit into the typical columnar morphology present in the stomach. In several steps, similar to the intestine, the primitive epithelial cell lining transforms into the complex glandular structure of the mature stomach (Grosse et al. 2011). In contrast to humans where the gland formation and differentiation of functional cell types occur in the fetal state, in mice, the maturation of the gastric glands and epithelial cells take place postnatal in the first weeks after birth (Stein et al. 1983; Keeley and Samuelson 2010). Studies in chick embryos have revealed that an interplay of BMP, Wnt5a, sonic hedgehog (Shh) and Notch regulate the gland formation (McCracken and Wells 2017). For instance, Shin et al. (2006) have demonstrated that the inhibition of FGF10 in chick embryos impaired the gland formation. The overexpression of BMP2 in the underlying mesenchyme increased the number of gastric glands, while gland formation was inhibited by ectopic expression of the BMP antagonist Noggin (Narita et al. 2000).

In summary, sound knowledge about the mechanisms of the anterior-posterior and proximal-distal patterning in embryogenesis and morphogenesis exist gained from studies in animal models. A complex network of tightly regulated, interacting transcription factors and growth factors drive the process of organ formation. However, the understanding of the stomach specification in humans especially the patterning of

the luminal-basal axis of the gastric glands is still poor and deficient mainly due to lack of reliable *in vitro* and *in vivo* models.

1.3. Signaling pathways

1.3.1. BMP signaling

Bone morphogenetic proteins (BMP) belong to the transforming growth factor β (TGFβ) superfamily, a broad group of signaling molecules that are involved in all processes of embryogenesis but also in adult tissue homeostasis. Besides BMPs the TGFβ superfamily includes TGFβ's, Nodal, activins, inhibins, lefty, growth differentiation factors (GDFs), glial derived neurotrophic factors (GDNFs) and anti-Müllerian hormone (AMH). About 15 BMPs are known which are clustered into groups based on similarities. In fact, these are BMP2/4, BMP5/6/7/8, BMP9/10, BMP3/11, BMP12/13/14 and BMP15. BMP1 is a metalloprotease and does not belong to the TGFβ superfamily. BMP's can signal through the canonical (Smad dependent) or non-canonical (Smad independent) signaling pathway (Figure 4). The canonical pathway is activated by ligand binding to type I and type II BMP receptors (BMPRI and BMPRII). Both types have serine/threonine kinase activity. BMP can bind to three BMPRI (BMPRIA or Alk3, BMPRIB or Alk6, and Alk2) and three BMPRII (BMPRIIB, ACTRIIA, ACTRIIB). Receptor binding initiates the formation of a heterotetrameric receptor complex composed of a BMPRI homodimer and a BMPRII homodimer while BMP ligands primarily bind to BMPRII and initiate downstream signaling. In the cytosol, Smad's are responsible for the signal transduction from the receptor to the nucleus. Upon BMP ligand-receptor binding the receptor BMPRI is phosphorylated and recruits and phosphorylates the receptor-regulated Smad (R-Smad). Three R-Smads are involved in BMP signaling: Smad1, Smad5 and Smad8 (Smad1/5/8) which associates further downstream to the co-mediator-Smad (C-Smad) Smad4. The complex translocates to the nucleus to initiate target gene transcription especially of the canonical target gene *DNA-binding protein inhibitor 1* (*ID1*). Smad6 and Smad7 are inhibitory Smad proteins and regulate the activity of the BMP signaling pathway via a negative feedback loop (Wang et al. 2014).

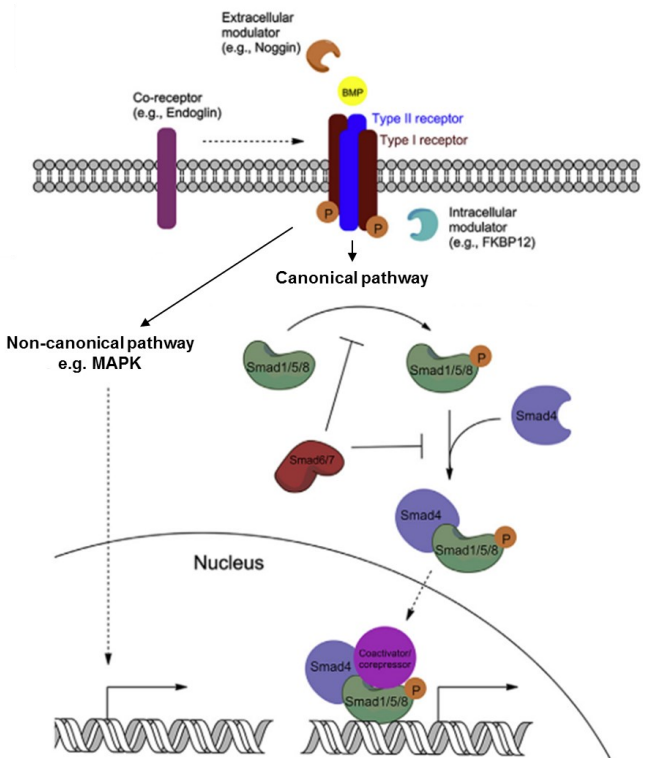

Figure 4: BMP signaling pathway. BMP ligands bind to type I and type II BMP receptors which form a heterotetrameric complex. Upon ligand binding, BMPRI is phosphorylated leading to recruitment and phosphorylation of Smad1/5/8. Smad4 associates with phosphorylated Smad1/5/8 and the complex translocates to the nucleus and functions as a transcription factor, initiating target gene transcription. The inhibitory Smad6 and Smad7 terminate the BMP signaling in a negative feedback loop. The figure was modified from Wang et al. (2014) (with permission from Elsevier, conveyed through CCC).

Additionally to the canonical pathway, different non-canonical pathways have been described to be activated by BMP. These are amongst other the MAPK pathway but also PI3K/Act pathway or Rho-GTPases. The activation of the MAPK pathway can regulate Smad activation (Derynck and Zhang 2003).

The BMP signaling pathway is influenced, modulated and regulated through interaction with multiple signaling pathways e.g. Hedgehog, Wnt/β-Catenin or Notch signaling pathway (Rahman et al. 2015). Three groups of antagonists can be distinguished which either block BMP directly e.g. Noggin, Gremlin1 or compete for receptor binding as receptor antagonists e.g. inhibin or complex the mature BMP protein.

In general, BMPs are involved in cell proliferation, differentiation, and apoptosis and are essential during all stages of development and embryogenesis e.g. in body axis patterning, bone and cartilage formation but also in the morphogenesis of the gastrointestinal tract and several other organs. Mutations or knockouts (examined mainly in mice) in components of the signaling pathway are mostly lethal or lead to severe malformations and abnormalities (Wang et al. 2014). A mutation in the BMP receptor BMPR1A is connected with the development of juvenile polyposis increasing in parallel the risk for gastrointestinal cancer development (Howe et al. 2001). Comparable to TGFβ, BMPs also have a bi-directional role in cancer progression and show both tumor-promoting and tumor-suppressive functions depending on the context (Ehata et al. 2013). In xenograft mouse models, for instance, it was shown that BMP2 and BMP4 have tumor-suppressive effects on diffuse-type gastric carcinoma cells (Shirai et al. 2011). The tumor-promoting effect instead was described by Katsuno et al. (2008) *in vitro* and *in vivo* in the xenograft mouse model. Here, the authors demonstrated that the metastasis of breast cancer into the bone is promoted by BMP2. Thus, in this context BMPs are also possible targets for cancer therapies to reduce metastasis (Owens et al. 2014).

1.3.2. WNT signaling

Wnt signaling molecules are an evolutionarily conserved group of growth factors acting in a paracrine way on neighboring cells and are involved in cell proliferation, differentiation, and stemness during embryogenesis but also in adult tissue homeostasis. Nineteen Wnt ligands are known which activate either the canonical or the non-canonical Wnt pathway. The canonical Wnt pathway also referred to as Wnt/β-Catenin pathway is well characterized but little is known about the non-canonical Wnt signaling pathway which is independent of β-Catenin. So far it is known that the non-canonical Wnt signaling pathway signals via small GTPases regulating cell movement, polarity and Ca^{2+} homeostasis (Steinhart and Angers 2018).

The canonical Wnt pathway (see Figure 5) is activated by binding of Wnt ligands to a Frizzled (FZD) receptor which forms a heterodimer with the Wnt co-receptor LRP5 or

LRP6 (LRP5/6) upon Wnt binding. In the absence of Wnt, a destruction complex consisting of Axin, APC, and GSK3 bind and permanently phosphorylate β-Catenin which leads to constant proteasomal degradation of β-Catenin. The binding of Wnt to FZD/LRP5/6 induces the binding of Dishevelled (Dsh) to FZD in the cytoplasm and conformational changes in the receptors. These changes lead to inhibition of GSK3 in the destruction complex and the stabilization of β-Catenin. β-Catenin, in turn, translocates to the nucleus where it binds to TCF/LEF and activates transcription of Wnt regulated genes like *Axin2* or *LGR5*. Agonists like R-spondin proteins can enhance the Wnt signaling, but cannot activate the Wnt signaling pathway in the absence of Wnt. R-spondins (RSPO1-RSPO4) interact with the LGR receptor (LGR4-6) and induce the complex formation of LGR with ZNRF3/RNF43 which inhibits the degradation of the Wnt receptor FZD (Clevers, Loh, and Nusse 2014).

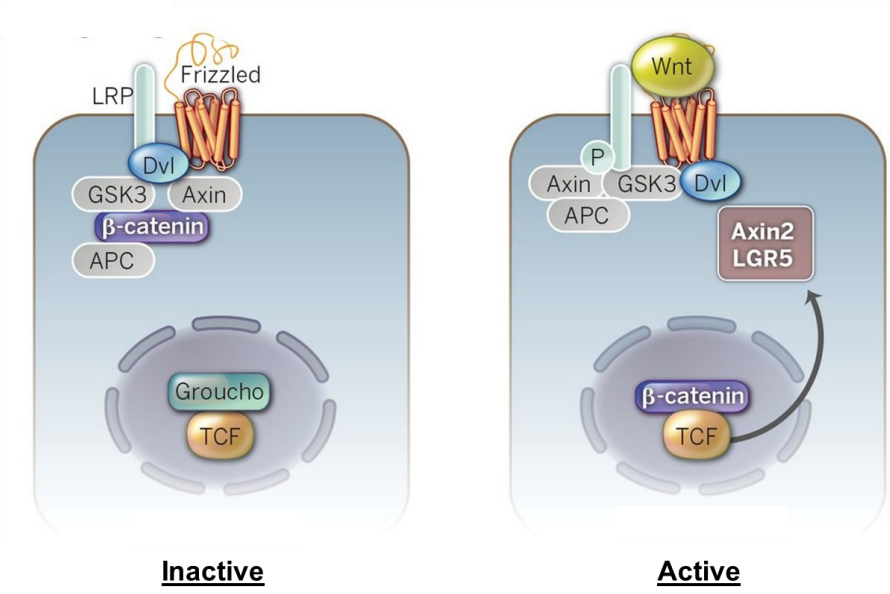

Figure 5: The canonical Wnt signaling pathway. In the inactive state (left) β-Catenin is bound in the Axin-APC-GSK3 destruction complex and is phosphorylated and constantly degraded. The binding of Wnt ligands to the Frizzled receptor and LRP co-receptor activates the Wnt/β-Catenin signaling pathway (right). Due to conformational changes upon Wnt binding LRP inhibits GSK3 of the destruction complex leading to stabilization of β-Catenin. β-Catenin translocates to the nucleus, binds to the transcription factor TCF/LEF and induces the transcription of Wnt target genes. The figure was adapted from Clevers, Loh, and Nusse (2014) (Reprinted with permission from AAAS).

The activity of the Wnt signaling pathway is terminated by several negative-feedback loops like ZNFR3 and RNF43 which ubiquitinate constantly FZD, leading to cell-surface degradation of the Wnt receptor. Dickkopf-1 (DKK1) is a further antagonist that competes with Wnt for LRP5/6 binding. Other inhibitors like Wnt inhibitory factor (WIF) or secreted frizzled proteins (sFRPs) bind directly to the Wnt ligands and prevent the receptor-ligand interaction (Steinhart and Angers 2018).

Wnt signaling plays an important role throughout the whole life of an organism. During embryonic development, the Wnt signaling determines the axis patterning of the embryo and the organs (Steinhart and Angers 2018). In the adult organism Wnt signaling fuels the stem cell niche in many tissues for self-renewal e.g. in the small intestine (Barker et al. 2007; van Es et al. 2012) or skin (Lim et al. 2013). Thus, mutations in the Wnt pathway are associated with several diseases i.e. cancer. Especially APC loss-of-function mutations are described in colorectal cancers (The Cancer Genome Atlas et al. 2012).

1.3.3. EGFR signaling

The epidermal growth factor receptor (EGFR) is part of the ErbB family and belongs to the superfamily of receptor tyrosine kinases. Beside EGFR/HER1/ErbB1 the ErbB family includes three further members: ErbB2/HER2/Neu, EbrB3/HER3, and ErbB4/HER4. The EGFR signaling pathway is involved in cell proliferation, differentiation, apoptosis and migration and plays also a crucial role in cancer progression and tumorigenesis. The pathway activation is initiated through ligand binding to the receptor. In total ten ligands are known to bind to the ErbB receptors while EGF, TGFα, and amphiregulin (AREG) bind specifically to EGFR. Betacellulin (BTC), heparin-binding EGF (HB-EGF) and epiregulin (EPGN) are further specific ligands of EGFR but also bind to ErbB4. Finally, four neuregulins (NRG1-4) are known, binding to ErbB3 and ErbB4. So far no ligand for ErbB2 was found and this receptor type rather functions as co-receptor during pathway activation. Although EGF, TGFα, and AREG bind exclusively to EGFR, they do not provoke the same cellular response. Upon ligand binding to EGFR, the receptor forms either a homodimer with

another EGFR or a heterodimer preferentially with ErbB2. Receptor dimerization activates the intrinsic tyrosine kinase and cross-phosphorylation of the cytoplasmic receptor tail occurs, initiating the recruitment of signaling molecules that have Src homology 2 (SH2) or phosphotyrosine binding (PTB) domain. In the following, the bound or interacting effector proteins activate downstream signaling cascades of Ras/Raf/MEK/ERK, phosphoinositide-3 kinase (PI3K)/AKT, JAK/STAT and phospholipase C (PLC)/protein kinase C (PKC) signaling pathway (Seshacharyulu et al. 2012; Zeng and Harris 2014). After receptor activation through ligand binding, the receptor dimer is internalized by clathrin-mediated endocytosis for receptor recycling or degradation. However, stimulation of downstream signaling cascades by the activated receptor also occurs in endosomes. In the endosome, the receptor is dephosphorylated and the ligand dissociates from the receptor due to the acidic pH of the endosomal lumen. The receptor is either recycled and transported back to the plasma membrane or is ubiquitylated and degraded in lysosomes (Lemmon and Schlessinger 2010). The duration of the pathway activation and the signal strength is determined also by the binding affinity of the ligand to the receptor. While the affinity of EGF to EGFR is very strong, thus prevent the dissociation of ligand and receptor in the endosome because of pH resistance and lead to receptor degradation, TGFα-EGFR binding instead is pH sensitive, resulting in fast dissociation of ligand and receptor in the endosome and recycling of the receptor (French et al. 1995). Amongst others, Wu et al. (2012) analyzed the location-specific EGFR signaling and showed that EGFR signaling activated at the plasma membrane as well as in the endosome lead to downstream activation of ERK. However, it induced different regulation of downstream transcription factors c-jun and c-fos and substrates ELK1 and RSK, demonstrating the diversity of the signaling pathway and the biological response not only regulated by the specific ligand but also by the localization of the receptor.

EGFR signaling is not only involved in embryo development starting already as early as fertilization and implantation but also in adult tissue homeostasis and the self-renewal of adult stem cells. Thus, mutations in components of the EGFR signaling pathway especially in the receptor are embryonically lethal. Mutations in the EGFR ligands instead are not fatal but induce developmental defects (Zeng and Harris 2014). Especially primary cell cultures like organoids rely on permanent supply with EGF to

maintain the regeneration capacity and longevity of the stem cells which was first shown by Sato et al. (2011) for the intestine and later by several groups for other organs.

Due to the important role of EGFR in the regulation of cell proliferation, differentiation, survival, and motility it implies that EGFR signaling components are prone to be involved in cancer progression and tumor development. Indeed mutations in EGFR (effect mainly trafficking of the receptor) or overexpression of EGFR and ligands, leading to permanent activation of the EGFR signaling pathway are found in several cancers like non-small cell lung cancer (NSCLC), head and neck cancer, glioblastoma, colorectal cancer or breast cancer (reviewed in Normanno et al. (2006)).

1.4. Culture systems of primary cells

1.4.1. 2D cell culture systems

Different *in vitro* culture models have been established in the last decades to analyze and understand biological processes of different organs under homeostatic and pathologic conditions in the human body including the gastrointestinal tract. Aim of all these models is to mimic the *in vivo* situation as close as possible, giving an alternative to *in vivo* animal models. Every model has advantages and disadvantages which need to be evaluated before their application to test a hypothesis. The simplest approach is the cultivation of cells in two dimensions (2D) using either cell lines or primary cells. Most of the established cell lines originate from tumors and can be cultivated over a long period of time on plastic or glass surface. Moreover, they are robust, cost-effective, and easy to handle and manipulate genetically. However, these cell lines comprise all the mutations and defects in their genome similar to the primary tumor they are derived from and therefore represent already a diseased state. Thus, the biological response of cell lines to certain stimuli or behavior under homeostatic conditions might be different from the *in vivo* situation due to altered metabolism and defects in certain signaling pathways (up- or downregulation). Nevertheless, cancer cell lines are still a valuable tool for cancer drug screenings and research on potential therapeutic targets. The

cultivation of primary cells from non-cancerous material *in vitro* instead is challenging as they show a very limited lifespan and undergo replicative senescence after a few passages due to telomere shortening (Campisi 1997; Cristofalo et al. 2004). Primary cells can be immortalized to overcome the limited lifespan. Commonly used methods are the transduction with viral compounds like the oncoprotein SV 40 large T antigen from polyomavirus SV40 or the E6/E7 protein from human papilloma virus (Münger et al. 1989; Steinberg and Defendi 1983; Jha et al. 1998; Daya-Grosjean et al. 1984; Hawley-Nelson et al. 1989; Hudson et al. 1990; Willey et al. 1991). However, these immortalization strategies influence p53 and retinoblastoma (Rb) tumor suppressor pathways. Another approach uses the overexpression of the human telomerase reverse transcriptase protein (hTERT) in primary cells, but some cell types especially epithelial cells fail to be immortalized by hTERT and rather undergo apoptosis (Lee, Choi, and Ouellette 2004). The conditional reprogramming of cells (CRC) is a further method to achieve indefinite growth in primary cells. Therefore, primary epithelial cells are cultivated on irradiated fibroblast feeder cells and treated with a Rho kinase inhibitor leading to prolonged lifespan without affecting the genome (Chapman et al. 2010; Liu et al. 2012). The CRC method is a 2D cultivation strategy which is limited to reflect the *in vivo* state because the complexity of the tissue, the anatomy and physiology get lost in the planar 2D culture. Cells cultivated in 2D show an unnatural polarization, loss of differentiated phenotype, altered response to pharmaceutical agents and oversaturation with nutrients due to the extended cell surface (Caliari and Burdick 2016).

1.4.2. 3D cell culture systems

In vivo epithelial cells are embedded in a complex three-dimensional (3D) architecture with defined and intricate cell-cell and cell-extracellular matrix contacts and are surrounded by a defined microenvironment which is lacking in all 2D culture models. Thus, 3D culture systems are an improvement as they mimic the *in vivo* conditions more accurately. First attempts of 3D tissue cultures used explanted organ slices which were placed on a porous membrane or in a collagen bed and cultivated under air-liquid interface conditions. This organotypic culture preserves the cytoarchitecture and the different cell types of the original tissue and is mainly applied to studies on brain physiology (Pampaloni, Reynaud, and Stelzer 2007).

In the last decades, different 3D cell culture systems were developed to resemble the *in vivo* situation *in vitro,* which can be broadly classified into scaffold-free or scaffold-dependent culture systems. Scaffold-free systems rely on the natural tendency of cells to form multicellular aggregates so-called spheroids. The scaffold of scaffold-based systems represents the complex network built by the ECM *in vivo* and is of synthetic or biological material in these systems (Pampaloni, Reynaud, and Stelzer 2007; Knight and Przyborski 2015). Although the spheroid models of the scaffold-free systems might be appropriate for tumor research as they reflect the heterogeneity of the tumor mass, they still do not fully recapitulate the polarized architecture of *in vivo* tissue structures like in the gastrointestinal tract or other organs. Especially epithelial cells depend on a scaffold and need the structural support by the ECM as it provides the spatial orientation for apical-basal polarization which ensures a proper function of the epithelial cells (Watt and Huck 2013). The ECM is a complex network composed of collagens, proteoglycans, hyaluronic acid, laminin, and fibronectin. This complexity is difficult to reproduce *in vitro* but commercially available products are nowadays able to mimic the ECM or elements of it (Justice, Badr, and Felder 2009). Matrigel is an extract from Engelbreth–Holm–Swarm (EHS) mouse sarcoma tumors that resembles the composition of the basement membrane. It is composed primarily of laminin, type IV collagen, and entactin, with various other constituents including proteoglycans and growth factors (Kleinman and Martin 2005).

The development of the organoid cultivation model by the Clever's group (Sato et al. 2009) was a breakthrough in terms of culturing primary epithelial cells nearly indefinitely and simultaneously mimicking tissue architecture, cell-type composition and self-renewal dynamics *in vitro.* Organoids are mini-organs grown from either pluripotent stem cells (induced pluripotent stem cells (iPSC) or embryonic stem cells (ESC)) or organ-specific adult stem cells and consist of organ-specific cell-types which self-organize in a 3D structure and thereby reflecting the epithelial organization *in vitro* (Kretzschmar and Clevers 2016). In the murine small intestine *Lgr5* expressing stem cells are located in the crypt base and are responsible for steady self-renewal and repopulation of the crypt (Barker et al. 2007). Sato et al. (2009) isolated single crypts containing adult stem cells or sorted single *Lgr5*+ stem cells from mice and seeded them in the ECM substitute Matrigel. The basic cultivation medium was supplemented with

mitogens and growth factors supporting the stem cell niche like WNT3A, the Wnt pathway agonist R-spondin (RSPO) 1, EGF and the BMP antagonist Noggin. With this approach, the authors achieved the formation of spheroids/organoids due to stem cell proliferation, consisting of a polarized epithelial monolayer with an apical side facing the lumen and the basal side aligned with Matrigel and the culture medium. The crypt-like structures were composed of all cell types present in the small intestinal crypt *in vivo.* Further progress was made when Spence et al. (2011) showed the generation of intestinal organoids from iPSC demonstrating the same developmental fate as *in vivo* during organogenesis. Besides murine organoids also human organoids were established for the intestine from PSC's (McCracken et al. 2011) as well as isolated crypts (Sato et al. 2011). Since then organoid cultures for a wide range of organs including stomach (Barker et al. 2010; McCracken et al. 2014; Schlaermann et al. 2014; Bartfeld et al. 2015), kidney (Xia et al. 2014; Morizane et al. 2015; Takasato et al. 2015), liver (Huch, Dorrell, et al. 2013; Huch et al. 2015), pancreas (Huch, Bonfanti, et al. 2013), brain (Lancaster et al. 2013), esophagus (DeWard, Cramer, and Lagasse 2014), fallopian tube (Kessler et al. 2015) and lung (Rock et al. 2009), among others were established. Human stomach organoids (gastric organoids) can be generated either from isolated glands harboring adult stem cells (Schlaermann et al. 2014; Bartfeld et al. 2015) or by differentiation from PSC's (McCracken et al. 2014). Likewise intestinal organoids, gastric organoids depend on permanent WNT supply to maintain stem cell activity (Barker et al. 2010). The cultivation medium was further defined to improve the lifespan of the organoid cultures. The medium of gastric organoids is supplemented with WNT3A, RSPO1, EGF and Noggin, FGF10, B27, N2, nicotinamide (NIC), gastrin, TGFβ inhibitor A-83-01 which inhibits Alk4/5/7, and rho-associated coiled-coil forming protein serine/threonine kinase (ROCK) Y-27632. This cultivation medium supports the gastric organoid culture and extended the lifespan from several months up to more than one year (Schlaermann et al. 2014; Bartfeld et al. 2015). Gastric organoids consist of a polarized epithelial monolayer with the apical side facing the lumen and the basal side aligning with the environment. Both, antral and corpus organoids show the same morphology and both can be differentiated into MUC5AC positive foveolar lineage by the withdrawal of WNT3A and RSPO1 from the cultivation medium. While undifferentiated MUC6 dominated organoids have a perfect round shape, differentiated organoids show a folded morphology with budding structures. Although antral

organoids are composed of all cell types present in the gland *in vivo*, corpus organoids lack important cell types like parietal cells or show a much lower abundance of chief cells than present *in vivo*. Thus, corpus organoids are not a perfect representation of the *in vivo* situation (Schlaermann et al. 2014).

Besides their application to answer fundamental questions of organ development, stem cell biology, and tissue regeneration, organoids are used to model diseases like cancer, chronic diseases, and study pathophysiologic conditions like infections with viruses, bacteria or parasites (Dutta and Clevers 2017). Due to the apical-basal polarization with the apical side inside, extracellular pathogens like *Helicobacter pylori* need to be injected into the lumen to mimic the *in vivo* route of infection (Bartfeld et al. 2015). For infections with intracellular pathogens, for instance, with *Salmonella* or *Chlamydia,* another method is used in which the organoids are segregated into fragments or single cells and then incubated with the infectious agent (Kessler et al. 2019; Forbester et al. 2015). However, especially the injection technique e.g. for *H. pylori* is low-throughput due to the time-consuming procedures.

Although organoids are a valuable 3D culture system recapitulating the *in vivo* situation of the organ of origin, a major drawback of this model is the lack of complexity. *In vivo* epithelial cells are in close contact and communicate with other cell types like immune cells, endothelial cells, and stromal cells especially under physiologic and pathophysiologic conditions. Organoids are rather primitive as they are only composed of epithelial cells. Thus, an effort is made to further improve and engineer the organoid system using for instance co-culture or transplantation into immunocompromised mice. Nevertheless, organoid cultures are heterogeneous and show high variability. Hence, it is attempted to standardize and better control organoid cultures with the aim to reduce variability e.g. by using chemically defined 3D hydrogels (Holloway, Capeling, and Spence 2019). Regardless of the total lifespan of an organoid culture that can last more than one year, the lifespan of one passage is rather short spanning from seven to ten days. Thus, the organoid model is not applicable for long-term *in vitro* studies.

The Kuo laboratory (Ootani et al. 2009) developed another 3D culture method to generate murine intestinal organoids. The authors applied a combination of an air-liquid interface (ALI) culture and a 3D culture matrix and recapitulated the cellular

myofibroblast architecture and the stem cell niche dependencies on Wnt and Notch pathway activation. They used a transwell filter system filled with two layers of collagen and seeded minced tissue pieces only in the upper collagen layer. The tissue fragments were exposed to air and the outer dish was filled with Ham's F12 / 20 % FCS medium to create an air-liquid interface. These culture conditions induced the formation of 3D structured organoids composed of a polarized epithelial monolayer with apical-basal orientation. Besides the proliferative activity, all cell lineages were detected in this model, thus recapitulating the *in vivo* situation accurately. Nevertheless, the authors stated that the long-term culture is only achieved by taking neonatal tissue as starting material. This 3D culture method was also applied to and established for the glandular stomach of mice using again only neonatal tissue (Katano et al. 2013) and a detailed protocol applicable for the whole gastrointestinal tract was published a few years ago (Li, Ootani, and Kuo 2016). Recently, Katano et al. (2015) extended the air-liquid interface gastric organoid culture and included mesenchymal myofibroblasts in the collagen layers of the set-up. They observed that the fibroblasts supported the formation of organoids and sustained proliferation and differentiation of the epithelial cells concluding that fibroblasts have a positive impact on the stem cell niche.

However, the ALI culture method was applied by the Kuo laboratory in other studies before; in this work, Ootani et al. (2000) demonstrated that gastric surface mucus cells GSM06 induce and preserve the mature differentiated phenotype when they are cultured on a collagen layer on a trans-well filter under air-liquid interface conditions. Control cultures without ALI condition resembled pre-pit cells and showed an immature phenotype. In a follow-up study, Ootani et al. (2003) performed the ALI culture with murine primary gastric epithelial cells seeded on a fibroblast-containing collagen gel layer. ALI condition resulted in a highly polarized epithelium and the fibroblastic support induced differentiation of the epithelial cells towards mature gastric surface mucus cells expressing MUC5AC. However, the model was only used for mouse primary cells and the applicability to human primary cells remains open. Moreover, the conducted studies using ALI did not give insights about the longevity of the culture. Finally, the mechanism inducing the foveolar differentiation in this model is not explored.

1.5. *Helicobacter pylori*

1.5.1. History, prevalence, and transmission

The human gastric pathogen *Helicobacter pylori* colonizes the stomach and shares a 100 000-year old history with its human host. Together with the modern human being, *H. pylori* spread from East Africa around the world approximately 58 000 years ago (Linz et al. 2007). In 1984 Berry Marshall and Robin Warren discovered and characterized *H. pylori* in human gastric biopsies and were awarded in 2005 with the Noble Prize in physiology and medicine for the link of gastritis to be caused by *H. pylori* (Marshall and Warren 1984; Marshall et al. 1985). The bacterium descended from the genus *Campylobacter* and was named as such until Goodwin, McCullough, and Boehm (1989) classified and renamed into *Helicobacter pylori*. *H. pylori* is the causing agent for gastric disorders like gastritis which evolves asymptomatic in most of the cases and a chronic infection can induce peptic ulcer disease (10-20 %), distal gastric adenocarcinoma (1-2 %), and gastric mucosal-associated lymphoid tissue (MALT) lymphoma (< 1 %) (Bauer and Meyer 2011). Due to its strong correlation with gastric cancer, *H. pylori* was declared in 1994 by the International Agency for Research on Cancer as class I human carcinogen (Parsonnet et al. 1991; IARC 1994). Although showing a declining incidence rate, gastric cancer is the fourth most common cancer worldwide and the second leading cause of cancer-related death after lung cancer, with 75 % of the cases attributable to *H. pylori* (de Martel, Forman, and Plummer 2013; de Martel et al. 2012). The development of gastric cancer is sequelae of steps that are described by Correa's cascade (Figure 6), always starting from chronic gastritis due to persistent inflammation as the major cause of gastric cancer. Chronic gastritis develops further into multifocal atrophic gastritis, intestinal metaplasia, dysplasia and finally into invasive adenocarcinoma and gastric cancer (Correa and Piazuelo 2012; Correa et al. 1975).

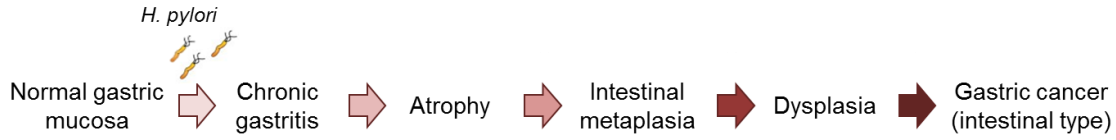

Figure 6: Schematic representation of *H. pylori*-induced Correa's cascade. The infection of the normal gastric mucosa with *H. pylori* induces chronic gastritis which consecutively develops further into atrophy, intestinal metaplasia, dysplasia, and intestinal-type gastric cancer. Bacteria are not detected anymore in the stage of intestinal metaplasia. The figure was adapted and modified from Correa and Piazuelo (2012).

Overall about 50 % of the world's population is infected with *H. pylori* while the prevalence is higher in developing countries (80 %) e.g. Saudi Arabia, India and Vietnam than in industrialized countries (< 40 %) due to lower socioeconomic statuses like housing conditions and hygiene. Infections are mostly acquired during childhood and can persist, if not treated through the whole lifetime of the host (Peek and Blaser 2002; Hooi et al. 2017). Nevertheless, only a minority of *H. pylori* infections lead to gastric cancer, but an infection increases the risk significantly (Peek and Blaser 2002). The transmission of *H. pylori* is still not fully understood. Most probably *H. pylori* are transmitted via the gastro-oral or fecal-oral route from human to human, but also transmitted through contaminated food and water was reported (Bauer and Meyer 2011). The treatment for *H. pylori* eradication is a standard triple therapy consisting of a proton pump inhibitor, clarithromycin and amoxicillin or metronidazole, but the efficacy of this treatment is decreasing because of *H. pylori* resistance against the antibiotics clarithromycin as well as metronidazole (Papastergiou, Georgopoulos, and Karatapanis 2014). Due to the co-evolution of the pathogen and the human host, *H. pylori* is highly adapted to its host to develop a persistent infection.

1.5.2. Biology of *H. pylori*

Helicobacter pylori is a Gram-negative, spiral-shaped bacteria with two to six unipolar flagella which allow the high motility of this bacterium, required for the penetration of the thick mucus layer (Goodwin, McCullough, and Boehm 1989; Suerbaum, Josenhans,

and Labigne 1993). Besides the spiral shape, also a coccoid form occurs which was described to be a non-replicative form of *H. pylori* and an early stage of cell death (Kusters et al. 1997). *H. pylori* requires microaerophilic growth conditions at neutral pH and to overcome the acidic pH of the stomach *H. pylori* expresses urease to neutralize the low pH in the microenvironment (Kusters, van Vliet, and Kuipers 2006). Interestingly, only 20 % of *H. pylori* in the gastric mucosa adhere to epithelial cells. Different autotransporter proteins, so-called adhesins like BabA, SabA, OipA or HopZ are expressed by *H. pylori* and mediate the adhesion to the epithelial cell surface (Bauer and Meyer 2011). *H. pylori* are equipped with a panel of virulence factors. Amongst others, these are the vacuolating toxin A (VacA) and the *cag* pathogenicity island (*cag*PAI) encoding the effector protein cytotoxin-associated gene A (CagA). Both VacA and CagA are strongly associated with the development of gastric cancer and peptic ulcer disease (Cover and Blaser 2009). Only 60-70 % of the western *H. pylori* strains harbor *cag*PAI compared to almost 100 % occurrence in Asian strains (Bauer and Meyer 2011). The *cag* pathogenicity island not only encodes CagA but also a Type IV secretion system (T4SS) to inject CagA into the cytoplasm of the host cell. The oncogenic feature of CagA was shown *in vivo* in mice and zebrafish where the expression of the protein alone induced the development of gastric adenocarcinoma (Ohnishi et al. 2008; Neal et al. 2013). In the cytosol, CagA is phosphorylated by host cell tyrosine kinases (c-Src and c-Abl) at the EPIYA (Glu-Pro-Ile-Tyr-Ala) motif (Mueller et al. 2012). The phosphorylation leads further to the activation of multiple host signaling pathways regulating inflammation, cell proliferation or inhibition of apoptosis (Backert and Blaser 2016). *In vitro* phosphorylated CagA activates the host phosphatase SHP2 inducing a cell elongation also described as the hummingbird phenotype (Higashi et al. 2002). The pore-forming toxin VacA is expressed in all *H. pylori* strains with allelic variations, determining the cytotoxic severity. The induced vacuolation in the host cell has effects on endocytic compartments and mitochondria by triggering the apoptotic cascade. Besides epithelial cells, VacA has also an influence on immune cells which can be immunostimulatory or immunosuppressive (Kim and Blanke 2012). Furthermore, *H. pylori* are able to escape the host immune response by depleting cholesterol from the host cell membrane and thereby prevent the activation of the pro-inflammatory interferon γ (INFG) signaling pathway (Morey et al. 2018).

1.6. Aim of the study

The human gastric mucosa is a complex structure organized in gastric units, referred to as glands formed by the epithelium, the *lamina propria* with gastric stromal cells and the *muscularis mucosae* a layer of myofibroblasts. The gastric units are populated by spatially distributed specialized cells with distinct functions, including parietal cells, chief cells, and foveolar cells, all deriving from a common stem cell progenitor. The cell-type composition of the gastric glands changes along the proximal-distal axis of the stomach, with oxyntic glands in the corpus and mucus glands in the antrum. From other tissues such as the intestine, it is known that the stromal cells surrounding the crypt communicate and interact with the adjacent epithelium, and recent studies revealed similar interactions between stroma and epithelium in the gastric mucosa, although the knowledge is still limited. Thanks to lineage tracing experiments in mice there is an increasing understanding of the stem cell niche in the gastric mucosa, however very little is known about the differentiation dynamics and the niche factors guiding the differentiation of stem cells into the specialized cells types. Most of the obtained data about the physiology and the patterning of the gut were generated in mice; therefore the transferability of the observations to the human physiology is still uncertain. 3D culture models as represented by organoids constitute a promising alternative to murine experimentation for understanding the complex biology of epithelial cells. A major drawback, however, is the short growth period of a single passage as organoids which is a disadvantage regarding the performance of long-term studies and the assessment of tissue homeostasis. In this thesis, it was aimed to establish an alternative long-lived *in vitro* culture model of human gastric primary cells that enables long-term cultivation based on the preservation of the stem cells to study tissue homeostasis as well as the study of the responses to an infection with the pathogen *Helicobacter pylori*.

Accordingly, the presented work is structured in three parts:

The objective of part I is to develop a stable and reliable *in vitro* culture model for human primary gastric epithelial cells that represent the *in vivo* situation and would thus allow analyzing the mucosal homeostasis under physiologic conditions. This part was done in collaboration with Dr. Francesco Boccellato. The herein developed “mucosoid

culture" model was successfully applied in part II to understand the luminal-basal axis patterning of the corpus gland. Accordingly, the differentiation dynamics and signaling niche factors of the oxyntic gland inducing the differentiation of the three major specialized cell types' foveolar cells, parietal cells, and chief cells were explored. The results obtained *in vitro* could further be validated *ex vivo* and *in situ* using human tissue specimens.

The focus of part III was on analyzing the communication between human gastric stromal cells of the *lamina propria* and gastric epithelial cells. Therefore human primary stromal cells were to be isolated from the same tissue as the gastric epithelial cells in order to establish a co-culture model of both cell types using the mucosoid culture model. The intention of this work was to obtain an understanding of the paracrine communication of stromal cells with epithelial cells under physiologic conditions but also under pathophysiologic conditions during the course of an infection with *Helicobacter pylori* and to assess whether stromal cells contribute to the inflammatory response against epithelial infection.

2.MATERIALS AND METHODS

2.1. Material

2.1.1. Human material

All human materials used in this thesis are listed in Table 1. Received patient samples were pseudonymized.

Table 1: Human material

All gastric sleeves were donated by patients negative for *H. pylori.* f: female, m: male.

Patient	Sex	Age	Region	Primary cells
hGAT16	m	34	Antrum	EPC, GSC
hGAT18	f	50	Antrum	EPC, GSC
hGAT20	f	45	Antrum	EPC
hGAT23	f	55	Antrum/Corpus	EPC
hGAT24	m	47	Antrum/Corpus	EPC, GSC
hGAT26	f	69	Antrum/Corpus	EPC

2.1.2. Cell lines

Table 2: Cell lines

Strain	Description	Source
L-WNT3A	mouse fibroblasts; cells secrete biologically active WNT3A protein, selection marker G418; Medium: DMEM, 10 % FCS hi, 1 mM Na-Pyruvat, 2 mM L-Glutamin, 0.4 mg/ml G418	Clevers Lab, Netherlands/Utrecht; ATCC® CRL-2647TM; Departmental collection #C-0705
293T HA Rspo1-Fc	Human; 293T cell line stably transfected to express murine RSPO1 with an N-terminal HA epitope tag and fused to a C-terminal murine IgG2a Fc fragment; Medium: DMEM (10% FCS, 2 mM L-Glutamin, 1 mM Na-Pyruvat)	Clevers Lab, Netherlands/Utrecht; Departmental collection #C-0005

293T WntR	human; Lentiviral transformed 293 T cells with Wnt GFP reporter (7TCF/LEF),Stability integrated expression plasmid with cherry marker (infection) and inducible GFP (Wnt dependent); Medium: DMEM/Ham`s F12+10 % FCS	Clevers Lab, Netherlands/Utrecht; Departmental collection #C-0001

2.1.3. Bacterial Strain

Table 3: Bacterial strain

Strain	Departmental collection No.	Resistance
H. pylori P12 WT	P511	Vancomycin

2.1.4. Chemicals and Reagents

Table 4: Chemicals and reagents

Reagent	Supplier
1x DPBS without Ca/Mg	Gibco, Life Technologies
A-83-01 (TGFβ inhibitor)	Calbiochem (616454)
Acetic acid (glacial)	Roth
Acridine orange	Sigma
Advanced DMEM/F12	Invitrogen (12634-028)
Ammonium persulfate	Merck
Amphotericin B	Thermo Fisher Scientific
B27 supplement 50x	Invitrogen (17504044)
Bacto Brain Heart Infusion (BHI)	BD Bioscience
BMP4	Gibco
Boric acid	Roth
Bovine collagen type IV	Gibco (A10644-01)
Bovine serum albumin (BSA), Fraction V	Life Technologies
Bromophenol blue	Biomol
ChillProtec Buffer	Biochrom
Chloroform	Merck

CryoSFM	Promocell (C-29910)
Dapi	Roche
Di-sodiumhydrogenphosphate (Na_2HPO_4)	Merck
DL-Dithiotreitol (DTT)	Applichem, Sigma-Aldrich D0632
DMSO	Merck
DNA loading dye 6x	Thermo Fisher Scientific
Draq5	Thermo Fisher Scientific
D-Sorbitol	ICN-Biochemicals
EDTA	Roth
Eosin Y solution (1 % aqueous solution)	Roth
Ethanol	Merck
Ethidiumbromide	Sigma
Fetal calf serum (FCS), heat inactivated	Biochrom
GC Agar Base	Remel
Gelatine	Merck
Gentamycin	Gibco
GlutaMax 100x	Invitrogen (35050-038)
Glutaraldehyde	Electron Microscopy Science
Glycerol	Roth
Glycine	Biomol
Hepes 1 M	Invitrogen (15630-056)
HistoGel™	Thermo Fisher Scientific
Histamine base	Sigma
Horse serum inactivated	Thermo Fisher Scientific
Human (Leu15-) Gastrin	Sigma (G9145)
Human EGF	Invitrogen Biosource (PHG0311)
Human FGF-10, recombinant	Peprotech (100-26-25)
Human Noggin	Peprotech (120-10C)
Iodoacetamide	Sigma-Aldrich I6125
Isopropanol	Merck
Matrigel, phenolred-free	BD (356231)
Mayer’s hematoxylin solution	Roth
Methanol	Merck
Mowiol 40-88	Sigma
N2 supplement 100x	Invitrogen (17502048)

N-acetyl-L-cysteine	Sigma Aldrich (A9165-5G)
Nicotinamide	Sigma (N0636)
Nuclease-free water	Thermo Fisher Scientific
Nystatin	MP Biomedicals
Osmiumtetroxide	Polyscience
PageRuler plus prestained protein ladder	Thermo Fisher Scientific
Paraffin	Roth
para-Formaldehyde (pFA)	Fluka
PD0325901 (MEK inhibitor, MEKi)	Sigma
Penicillin/Streptomycin (Pen/Strep)	Invitrogen (15140-122)
Polybed	Polyscience
Potassium chloride	Merck
Potassium-dihydrogen-phosphate (KH_2PO_4)	Merck
Restore™ Western Blot Stripping buffer	Thermo Fisher Scientific
Roti®-Histokitt	Roth
RSPO1 conditioned medium	In-house preparation
Sodium chloride	Roth
Sodium azide	Sigma Aldrich
Sodiumdodecylsulfate (SDS)	Serva
Spectra Multicolor High Range Protein Ladder	Thermo Fisher Scientific
Sucrose/Saccharose	Roth
Tannic acid	Merck
Target Retrieval	Dako
Tetramethylenediamide (TEMED)	Carl Roth
Trimethoprim	Sigma Aldrich
Tris base	Applichem
Triton X-100	Roth
TRIzol Reagent	Ambion
TrypLE	Gibco (12604021)
Trypsin/EDTA	Thermo Fisher Scientific
Tween-20	Merck
Uranylacetate	Electron Microscopy Sciences
Vancomycin	MP Biomedicals
Western Lightning Plus ECL	PerkinElmer
WNT3A conditioned medium	In-house preparation

Xylol	Roth
Y-27632 (ROCK Inhibitor)	Sigma (Y0503)
Zeocin	Invitrogen
β-mercaptoethanol	Roth

2.1.5. Buffer, solutions and media

Table 5: Composition of Adv++ and Adv+++ medium

Component	Adv++	Adv+++
Advanced DMEM/F12	+	+
GlutaMax (100 x)	1 x	1 x
HEPES (1 M)	12 mM	12 mM
FCS	5 %	10 %

Table 6: Primary epithelial cell culture medium

Component	Organoid culture	Mucosoid culture
WNT3A conditioned medium	50 % (v/v)	50 % (v/v)
RSPO1 conditioned medium	25 % (v/v)	25 % (v/v)
Adv++	ad 100 %	ad 100 %
B27	2 % (v/v)	2 % (v/v)
N2	1 % (v/v)	1 % (v/v)
Nicotinamide	15 mM	15 mM
N-Acetylcysteine	1.25 mM (*)	-
Human EGF	20 ng/mL	20 ng/mL
Human FGF10	150 ng/mL	150 ng/mL
Human Noggin	150 ng/mL	150 ng/mL
Human (Leu) Gastrin	10 nM	10 nM
A-83-01 (TGFβ inhibitor)	1 µM	1 µM
Y-27632 (ROCK Inhibitor)	7.5 µM / 1,5 µM (*)	7.5 µM / 1.5 µM (*)
Pen/Strep	100 U/mL	100 U/mL

(*) reduced to 1.5 µM three days after passaging/after ALI start

Table 7: Primary stromal cell medium

Component	Final Concentration
Adv++	-
FCS	10 % (v/v)
Y-27632 (ROCK Inhibitor)	7.5 µM
Pen/Strep	100 U/mL

Table 8: Differentiation media for corpus mucosoid cultures to induce secretory cell lineage differentiation.
Mucosoid culture medium is the basis for all differentiation media. Changes in the concentration of basic components are indicated.

Component	Noggin	EGF	PD0325901	BMP4
Medium 1	-	+	-	-
Medium 2	5 ng/mL	+	-	-
Medium 3	50 ng/mL	+	-	-
Medium 4	+	+	-	-
Medium 5	-	-	-	-
Medium 6	5 ng/mL	-	-	-
Medium 7	50 ng/mL	-	-	-
Medium 8	+	-	-	-
Medium 9	-	+	2 µM	-
Medium 10	-	+	2 µM	50 ng/mL

Table 9: General buffer and solutions

Name	Components	Solvent
1 x Chelating solution (fresh)	5 x Chelating solution	dilute 1:5
	DL-Dithiotreitol (DTT)	2.6 nM
	EDTA (pH 8.0)	10 mM
	ad H_2O	
10 x PBS	NaCl	1.37 M
	KCl	27 mM
	Na_2HPO_4	100 mM
	KH_2PO_4	18 mM
	in H_2O	

10 x TBS	Tris	20 mM
	NaCl	140 mM
	Ad H_2O pH 7.5	
2 x Laemmli buffer	SDS (Stock 10 % (w/v))	4 %
	Glycerol	20 %
	Tris-HCl (pH 6.8)	120 mM
	Bromphenol blue	0.02 %
	β-mercaptoethanol	5 %
	in H_2O	
5 x Chelating Solution	Na_2HPO_4	28 nM
	KH_2PO_4	40 nM
	NaCl	480 nM
	KCl	8 nM KCl
	Sucrose	220 nM
	D-Sorbitol	274 nM
	in H_2O	
ChillProtec buffer	Pen/Strep	1 %
(supplemented)	Gentamycin	50 µg/mL
	Amphotericin B	1.25 µg/mL
	in ChillProtec buffer	
Collagen coating solution	bovine collagen type IV	10 µg/cm^2
	in acetic acid	0.02 M
GC agar plates	Horse serum (inactivated)	10 %
	Vitamin mix	1 %
	Vancomycin	10 µg/mL
	Nystatin	1 µg/mL
	Trimethoprim	5 µg/mL
H. pylori freezing medium	FCS	10 %
	Glycerol	20 %
	in BHI	
IF Blocking solution	BSA in 1x PBS	5 %
	OR	
	Donkey serum	5 %
	FCS	1 %
	in 1x PBS	

Paraformaldehyde 4 %	Para-Formaldehyde 1 x PBS at 60°C pH 7.4	4 % (w/v); 40 g/L
SDS resolving gel buffer	Tris-HCl ad H_2O pH 6.8	0.5 M
SDS running buffer	248 mM Tris base 1,52 M Glycin 1 % SDS ad H_2O pH 8.3	248 mM 1.52 M 1 %
SDS stacking gel buffer	Tris-HCl ad H_2O pH 8.8	1.5 M
TBE	Tris base Boric acid EDTA	1 M 1 M 0.02 M
TBS-T	TBS Tween-20	1x 0.1 %
WB blocking solution	BSA in TBS-T	3 %
Western blot transfer buffer	For 10x: Tris 1,90 M Glycin For 1x: add Methanol	 250 mM 1.90 M dilute 1:10 20 % (v/v)
Whole mount IF blocking solution	Donkey serum TritonX-100 in 1x PBS	5 % 0,3 %

2.1.6. Kits

Table 10: Kits

Name	Application	Supplier
Tetro cDNA synthesis kit	Reverse transcription of RNA in complementary DNA (cDNA)	Bioline
SensiMix™ SYBR® Hi-ROX kit	RT-qPCR with cDNA template	Bioline
GeneJET RNA purification kit	RNA isolation kit	Thermo Fisher Scientific
RNAScope® 2.5 HD Reagent Kit-RED	*In situ* hybridization of human corpus tissue	ACD bio techne

2.1.7. Arrays

Table 11: Arrays

Name	Application	Supplier
Agilent SurePrint G3 Custom Gene Expression Microarray 8 x 60K	Gene expression microarray	Agilent; custom design based on Agilent SurePrint G3 v2, defined by Dr. Hans Mollenkopf (MPIIB)
Quantibody® Human IL-1 Family Cytokine Array Q1	Quantification of IL1β protein in the supernatant	RayBiotech
Quantibody® Human Th1/Th2 Array Q1 Kit	Quantification of cytokines in the supernatant	RayBiotech

2.1.8. Primer

Table 12: Primer. All primers were designed using the online tool NCBI Primer-BLAST and PrimerBank (MGH-PGA), purchased from Sigma or Eurofins and diluted to 20 µM. F: Forward; R: Reverse.

Gene	Name	Sequence 5'→3'
ATP4B	ATP4B_F	TGGGTGTGGATCAGCCTGTA
	ATP4B_R	CTGGTCTTGGTAGTCCGGTG
BARX1	BARX1_F	TTCCACGCCGGACAGAATAGA
	BARX1_R	AGTAAGCTGCTCGCTCGTTG

C1orf43	C1orf43_F	GGTGAATGTCGTGCTGGTG
	C1orf43_R	GGGATCTCAGAGGTACGAATGG
CD44	CD44_F	AGCACCATTTCAACCACACC
	CD44_R	GCAGTGGTGCCATTTCTGTC
CDH1	CDH1_F	TACCCTGGTGGTTCAAGCTG
	CDH1_R	CCTGACCCTTGTACGTGGTG
CHGA	CHGA_F	CCAAGGAGAGGGCACATCAG
	CHGA_R	TCTTCCACCGCCTCTTTCAG
CSF2	CSF2_F	TCCTGAACCTGAGTAGAGACAC
	CSF2_R	TGCTGCTTGTAGTGGCTGG
CTNNB	CTNNB_F	AGCAATTTGTGGAGGGGGTC
	CTNNB_R	AGCAGCTGCACAAACAATGG
CXCL12	CXCL12_F	ATTCTCAACACTCCAAACTGTGC
	CXCL12_R	ACTTTAGCTTCGGGTCAATGC
CXCL8	IL8_F	ACACTGCGCCAACACAGAAAT
	IL8_R	ATTGCATCTGGCAACCCTACA
DKK1	DKK1_F	CCTTGAACTCGGTTCTCAATTCC
	DKK1_R	CAATGGTCTGGTACTTATTCCCG
DKK2	DKK2_F	CTCACAGATCGGCAGTTCG
	DKK2_R	ATGCCAGTCCTTGGTACATGC
DKK3	DKK3_F1	AGGACACGCAGCACAAATTG
	DKK3_R1	CCAGTCTGGTTGTTGGTTATCTT
DKK3	DKK3_F2	ACGAGTGCATCATCGACGAG
	DKK3_R2	GCAGTCCCTCTGGTTGTCAC
DKK4	DKK4_F	ACGGACTGCAATACCAGAAAG
	DKK4_R	CGTTCACACAGAGTGTCCCAG
DKKL1	DKKL1_F	CTCTACCCTGGTGATCCCCTC
	DKKL1_R	CGAAGCAGGTTACCTTTCAGGA
EPCAM	EPCAM_F	GCTGGCCGTAAACTGCTTTG
	EPCAM_R	ACATTTGGCAGCCAGCTTTG
GAPDH	GAPDH_F	GGTATCGTGGAAGGACTCATGAC
	GAPDH_R	ATGCCAGTGAGCTTCCCGTTCAG
GIF	GIF_F	CCCAGAGTTCATGCTCCGTT
	GIF_R	ATCAGGATGCTGGGGTTTGG
ID1	ID1_F	GTGCTGCTCTACGACATGAAC

	ID1_R	CTTCAGCGACACAAGATGCG
IL18	IL18_F	TCGGGAAGAGGAAAGGAACC
	IL18_R	AGCCATCTTTATTCCTGCGACAA
IL1β	IL1b_F	ATGATGGCTTATTACAGTGGCAA
	IL1b_R	GTCGGAGATTCGTAGCTGGA
IL23A	IL23A_F	CTCAGGGACAACAGTCAGTTC
	IL23A_R	ACAGGGCTATCAGGGAGCA
IL6	IL6_F	ACTCACCTCTTCAGAACGAATTG
	IL6_R	CCATCTTTGGAAGGTTCAGGTTG
KRT18	KRT18_F	TTCTGGGGGCATGAGCTTCAC
	KRT18_R	GCGCCTGCATAGACGCTG
KRT19	KRT19_F	GTCACAGCTGAGCATGAAAGC
	KRT19_R	AGCTGGGCTTCAATACCGC
KRT8	KRT8_F	GCTGGCCGTAAACTGCTTTG
	KRT8_R	ACATTTGGCAGCCAGCTTTG
LGR5	LGR5_F	CTCCCAGGTCTGGTGTGTTG
	LGR5_R	GCTCGCAATGACAGTGTGTG
MIST1 (bHLHA15)	MIST1_F	CGGATGCACAAGCTAAATAACG
	MIST1_R	GCCGTCAGCGATTTGATGTAG
MUC5AC	MUC5AC_F	GGAGGTGCCCACTTCTCAAC
	MUC5AC_R	CTTCAGGCAGGTCTCGCTG
MUC6	MUC6_F	CAGCTCAACAAGGTGTGTGC
	MUC6_R	TGGGGAAAGGTCTCCTCGTA
PGC	PGC_F	TGTCTTTGGGGGTGTGGATAG
	PGC_R	ATGAGGAACTCTTCAATGCCAATC
sFRP1	sFRP1_F	ACGTGGGCTACAAGAAGATGG
	sFRP1_R	CAGCGACACGGGTAGATGG
sFRP2	sFRP2_F	ACGTGGGCTACAAGAAGATGG
	sFRP2_R	CAGCGACACGGGTAGATGG
sFRP3	sFRP3_F	ACACAGACTTACAGGGCTTGAT
	sFRP3_R	GAGCCCATACTCATCAAGTACCG
sFRP4	sFRP4_F	CCTGGAACATCACGCGGAT
	sFRP4_R	CGGCTTGATAGGGTCGTGC
sFRP5	sFRP5_F	AGGAGTACGACTACTATGGCTG
	sFRP5_R	GGTCGGCAGGGATGTCAAG

TNFα	TNF_F	TCCCCAGGGACCTCTCTCTA
	TNF_R	GAGGGTTTGCTACAACATGGG
USAG1	USAG1_F	GCCATCAGAGATGTATTTGGTGG
	USAG1_R	GTGCTCCCTAACTGGATTGGA
WIF1	WIF1_F	TCTCCAAACACCTCAAAATGCT
	WIF1_R	GACACTCGCAGATGCGTCT

2.1.9. Antibodies

Table 13: Primary antibodies

Target	Host	Reactivity	Application (Dilution)	Supplier, Clone/Cat#
ATP4B	Mouse	Human	IF (1:100)	Abcam, 2G11
CagA (b-300)	Rabbit	*H. pylori*	WB (1:1 000)	Santa Cruz, sc25766
CagA (bK-20)	Goat	*H. pylori*	IF (1:100)	Santa Cruz, sc-48128
CHGA	Rabbit	Human	IF (1:100)	Abcam, ab15160
E-Cadherin	Mouse	Human	WB (1:1 000)/ IF (1:100)	BD Bioscience, 610181
Ki67	Mouse	Human	IF (1:100)	Cell Signaling, 805
Ki67	Rabbit	Human	IF (1:100)	Cell Signaling, D2H10
MUC5AC	Mouse	Human	IF (1:100)	Abcam, 45M1/ab3649
MUC6	Rabbit	Human	IF (1:100)	Sigma, 4588/SAB4301182
Noggin	Mouse	Human	IF (1:100)	Santa Cruz, 2C10/sc-293439
Occludin	Mouse	Human	IF (1:100)	Invitrogen, OC-3F10
PGC	Sheep	Human	IF (1:100)	Abcam, ab9013
PGC	Rabbit	Human	IF (1:100)	Sigma, HPA031718
pTyrosin (PY99)	Mouse	Human	WB (1:1 000)	Santa Cruz, sc-7020
Vimentin	Rabbit	Human	WB (1:1 000)	Cell Signaling, D21H3/#5741
β-Actin	Mouse	Human	WB (1:10 000)	Sigma, AC-15
β-Catenin	Rabbit	Human	IF (1:100)	Sigma, C2206

Table 14: Secondary antibodies and antibody conjugates

Target	Host	Reactivity	Labeling/conjugation	Application (Dilution)	Supplier
Actin		Phalloidin	AlexaFluor 647	IF (1:40)	MoBiTech
Actin		Phalloidin	AlexaFluor 568	IF (1:40)	MoBiTech
IgG	Sheep	Mouse	HRP	WB (1:5 000-15 000)	GE Healthcare
IgG	Donkey	Rabbit	HRP	WB (1:5 000-15 000)	GE Healthcare
IgG (H+L)	Donkey	Rabbit	Cy3	IF (1:500)	Dianova
IgG (H+L)	Donkey	Rabbit	AlexaFluor 488	IF (1:500)	Dianova
IgG (H+L)	Donkey	Mouse	Cy3	IF (1:500)	Dianova
IgG (H+L)	Donkey	Mouse	AlexaFluor 488	IF (1:500)	Dianova
IgG (H+L)	Donkey	Mouse	AlexaFluor 647	IF (1:500)	Dianova
IgG (H+L)	Donkey	Sheep	Cy2	IF (1:500)	Dianova
IgG (H+L)	Donkey	Goat	Cy3	IF (1:500)	Dianova
IgG (H+L)	Goat	Rabbit	AlexaFluor 488	IF (1:500)	Dianova
IgG (H+L)	Goat	Rabbit	12 nm gold particles	Immunogold	Jackson Immuno Research
IgG (H+L)	Goat	Mouse	AlexaFluor 488	IF (1:500)	Dianova
IgG (H+L)	Goat	Mouse	12 nm gold particles	Immunogold	Jackson Immuno Research

2.1.10. RNAScope probes

Table 15: *in situ* hybridization probes

Target	Reactivity	#Cat	Supplier
BMP2	Human	430641	ACD Bio techne
BMP4	Human	454301	ACD Bio techne
DapB	Bacteria (negative control)	310043	ACD Bio techne
EGF	Human	606771	ACD Bio techne
POLR2a	Human (positive control)	310451	ACD Bio techne
TGFα	Human	313131	ACD Bio techne

2.1.11. Consumables

Table 16: Consumables

Name	Application	Supplier
0.5-2.0 mL tubes	General	Sarstedt
6- /24-well plates	Primary cell culture	TPP
Acclaim C18 PepMap RSLC column	LC-MS/MS	Thermo Fisher Scientific
Coverslips	IF	Marienfeld
Falcon tubes (5/50 mL)	General	Sarstedt
Filter tips	RNA and primary cell work	Thermo Scientific
Hyperfilm ECL	Western Blot	Amersham Bioscience
Microcon YM-30 kDa centrifugal filter units	LC-MS/MS	Merck Millipore
Microscope slides	IF	Marienfeld
MilliCell® Cell culture inserts (0.4 µm / 12 mm)	Primary cell culture	Merck Millipore
Mini-PROTEAN TGX Gels 4-15 %	Western Blot	Bio-Rad
Paraffin wax embedding cassette	Sample embedding	Carl Roth
PCR tubes	cDNA synthesis	Sarstedt
PCR® microplate	RT-qPCR	Axygen
Pipette tips (200/1000µL)	Pipetting	Sarstedt
Platemax® Ultra Clear Sealing Film	RT-qPCR	Axygen
Polyvinylidene fluoride (PVDF) membrane	Western Blot	Perkin Elmer
Serological pipettes	Primary cell culture	Sarstedt
Superfrost slides	*In situ* hybridization	Thermo Fisher Scientific
T75 culture flask	Stromal cell culture	TPP

2.1.12. Lab instrumentation

Table 17: Lab instrumentation

Name	Application	Supplier
Agilent 2100 Bioanalyzer	Quality control of RNA	Agilent Technologies
AP-250	Paraffin embedding console	Microm
Balances	Weighing	Sartorius
Dionex UltiMate 3000 RSLC nano system	MS	Thermo Fisher Scientific
Eppendorf centrifuge 5417C	Microbiology	Eppendorf
Eppendorf centrifuge 5417R	RNA isolation	Eppendorf
Eppendorf centrifuge 5810R	Primary cell culture	Eppendorf
Film developer Optimax 2010	Development of Western Blots	Protec
Forma Series II water-jacketed CO_2 incubator	Microbiology	Thermo Scientific
G2565CA high-resolution laser microarray scanner	Microarray scanner	Agilent Technologies
Gel imaging System GeneGenius	Gel electrophoresis	Syngene
GeneAmp® PCR System 9700	PCR	AB Applied Biosystems
Hera Safe Cell 150	Primary cell incubator	Thermo Scientific
Heraeus Hera Safe	Microbiology laminar flow box	Thermo Scientific
IX50-S8F inverted microscope	Light microscopy	Olympus
Leo 906E transmission electron microscope	Transmission electron microscopy	Zeiss
Microconcentrator 5301	MS sample preparation	Eppendorf
Mini Trans-Blot® Cell	Western Blot	Bio-Rad
Mini-PROTEAN tetra cell	SDS-PAGE/Western Blot	Bio-Rad
Mini-PROTEAN© Tetra Handcast Systems	SDS-PAGE	Bio-Rad
Nalgene Mr.Frosty	Freezing of primary cell stocks	
NanoDrop 1000 UV-Vis spectrophotometer	RNA concentration measurement	paq lab Biotechnologies
pH meter	pH measurement and adjustment	Mettler-Toledo
PowerPac™ HC	Power supply	Bio-Rad

QExactive Plus mass spectrometer	MS	Thermo Fisher Scientific
RMC MTX/CRX cryo-ultramicrotome	Sectioning of samples for electron microscopy	Boeckeler Instruments Inc.
Rotation Manual Microtome	Sectioning of samples	Leica
Safe2020	Primary cell culture laminar flow box	Thermo Scientific
ScanR Inverted Microscope	Automated microscopy	Olympus
Shaking platform 3006	Sample agitation	GFL
StepOnePlus Real-time PCR system	RT-qPCR	AB Applied Biosystems
TCS SP-8	Confocal microscopy	Leica Microsystems
Thermomixer comfort	Boiling of protein samples	Eppendorf
TP1020 tissue processor	Sample dehydration and paraffinization	Leica
Waterbath 1083	Pre-warming of samples, medium	GFL

2.1.13. Software and databases

Table 18: Software and databases

Name	Application	Supplier
Excel 2016	Data processing	Microsoft
GraphPad Prism v7	Data processing	GraphPad
Illustrator CS4	Image processing	Adobe
ImageJ	Image processing	Fiji/Open source
Leica LasX	Image acquisition	Leica Microsystems CMS GmbH
NCBI	Biological database	https://www.ncbi.nlm.nih.gov/
PowerPoint 2016	Presentation	Microsoft
Primerbank	Primer design tool	https://pga.mgh.harvard.edu/primerbank/
ScanR Aquisition	Automated microscopy	Olympus
StepOne Software v2.3	RT-qPCR analysis	Thermo Fisher Scientific
USCS	Primer design tool	https://genome.ucsc.edu/
ZEN 2.3 (blue edition)	Image processing	Carl Zeiss Microscopy GmbH
MaxQant Version 1.626	MS data analysis	Max Planck Institute for Biochemistry

2.2. Methods

2.2.1. Cell culture and primary cell culture

2.2.1.1. Human material

Human gastric tissue material was obtained from the Clinic for General, Visceral, and Oncologic Surgery, Department of Obesity and Metabolic Surgery located in the Helios Clinic, Berlin-Buch and the Charité Centre for Obesity and Metabolic Surgery located in Charité University Medicine, Berlin, Germany. The tissue originated from the greater curvature of the human stomach and was removed from the surgeon during gastric sleeve resection. The Ethics Commission of the Charité, Berlin (EA1/129/12) approved the scientific usage of the gastric material. The tissue material was stored in ChillProtec buffer until further processing.

2.2.1.2. Isolation of Gastric Primary Cells from human tissue

2.2.1.2.1. Preparation of human tissue material for cell isolation

A 2 x 2 cm piece of human tissue sample was cleaned from blood by washing with cold PBS supplemented with 100 U/mL Streptomycin/Penicillin, 1.25 µg/mL Amphotericin and 50 µg/mL Gentamycin. Muscles, adipose tissue, and blood vessels were removed. Tissue samples from gastric sleeve resection consist of the three main parts of the human stomach: fundus, corpus, and antrum. These three parts were distinguished by their macroscopic characteristics and separated for cell isolation. Tissue pieces were kept in PBS until further processing.

2.2.1.2.2. Isolation of Gastric Primary Epithelial Cells and Stromal Cells

The isolation protocol for epithelial cells and stromal cells are the same in the first steps: After cleaning the tissue sample from muscle, adipose tissue, and blood vessels the tissue sample was minced into small pieces (1 mm^3), transferred into a 50 mL-falcon

tube and washed with 25 mL PBS by vortexing to remove fat tissue. After tissue pieces precipitate, the washing step was repeated until the supernatant was clear.

For epithelial cells:

Tissue pieces were incubated in 45 mL chelating solution for 20 min at 37°C under constant agitation. The supernatant was discarded and tissue pieces were transferred to a sterile petri dish while excessive liquid was removed. Gastric glands were released from the tissue by gentle squeezing of the pieces with a sterile glass slide. Pieces and extracted gastric glands were collected with 3 mL cold Adv+++ in a 15 mL falcon tube. The glass slide and petri dish were washed with 3 mL cold Adv+++ and pooled with the tissue pieces in the 15 mL falcon tube. Pieces were further disrupted by pipetting up and down to release gastric glands and epithelial cells. After tissue pieces settled by gravity, the supernatant was collected in a new 15 mL falcon tube. The procedure of pipetting and collection was repeated five times. 10 µl of final cell suspension were transferred to a glass slide and inspected under the microscope to count the number of gastric glands. The cell suspension was centrifuged (300 x g, 5 min, 4°C) and the pellet was washed three times with cold Adv++. The supernatant was removed and the cell pellet was resuspended in Matrigel (300 isolated glands / 40 µL Matrigel) on ice. A drop of 40 µL Matrigel – epithelial cell mixture was placed per well in a pre-warmed 24-well plate and incubated for 30 min at 37°C until Matrigel polymerized. 500 µL of 3D media were added per well and cultures were kept at 37°C, 5 % CO_2 in a humidified incubator.

For stromal cells:

Tissue pieces were incubated in 45 mL chelating solution for 45 min at 37°C under constant shaking. Chelating solution was removed, media supplemented with FCS (Adv+++) was added to inactivate the chelating solution and centrifuged (300 x g, 5 min, 4°C). Supernatant was removed, 2 mL Trypsin/EDTA were added and incubated in a water bath for 20 min at 37°C. Trypsin/EDTA was inactivated by adding 15 mL Adv+++, followed by a centrifugation step (300 x g, 5 min, 4°C). Supernatant was exchanged with fresh 15 mL Adv+++ and tissue pieces were shortly vortexed. After big tissue pieces settled by gravity, supernatant with tissue fragments was collected in a new 50 mL falcon tube. Supernatant with tissue fragments and the tube with big pieces were centrifuged (300 x g, 5min, 4°C). Supernatant in both conditions was removed,

cell pellets were resuspended in 2 mL GSC media and seeded in one well of a 6-well plate. Cells were incubated for one week without medium change at 37°C, 5 % CO_2 cell incubator, until cells have attached to the plastic and started growing, forming microcolonies.

2.2.1.3. Cultivation of Gastric Primary Cells

2.2.1.3.1. Organoid cultivation

Organoids are cultivated in Matrigel. In preparation for the segregation of organoids, Matrigel needs to be thawed on ice and kept at 4°C and a 24-well plate has to be pre-warmed at 37°C. Medium was removed from organoids. Matrigel drop with organoids was dissolved with 1 mL cold media Adv++ or PBS per well. Up to 6 wells with organoids were collected in a 15 mL falcon tube. Wells were washed with 1-2 mL cold Adv++ or PBS and pooled in the same falcon tube. Tubes were gently vortexed to dissolve Matrigel. Sample was centrifuged (300 x g, 5 min, 4°C) and supernatant was removed. Cell pellet was resuspended in 1 mL TrypLE. Organoids were sheared with a narrowed Pasteur pipette (max. eight times) and incubated for 10 min at 37°C. Shearing with the Pasteur pipette was repeated. TrypLE was inactivated by adding 6 mL Adv+++. Cell suspension was centrifuged (300 x g, 5 min, 37 °C) and cell pellet was washed with Adv++, followed by centrifugation. Cell pellet was kept on ice and resuspended in Matrigel. 30 000 cells/50 µl Matrigel drops were seeded in a 24-well-plate. Plate was stored at 37°C for 30 min until Matrigel drops have solidified. Wells were filled with 500 µL 3D culture media and organoids were incubated at 37°C, 5 % CO_2 in a cell incubator. Medium was changed every three days. Organoids were grown with an altered concentration of ROCK inhibitor (2,5 µl/mL) for the first three days after seeding.

2.2.1.3.2. Air-liquid interface cultivation – Mucosoid cultures

MilliCell® cell culture inserts (diameter 12 mm) with PCF membrane (0,4 µm pore size) were used for air-liquid interface cultivation of gastric primary epithelial cells. Filter membranes were coated with 12,5 µg/cm^2 bovine collagen Type IV dissolved in

0,02 M acetic acid in a volume of 100 µl/filter for 60 min at 37°C followed by washing with pre-warmed PBS. Epithelial cells were grown as organoids before first seeding on filter inserts and were further propagated by passaging the cells on the filters. Organoids were sheared to single-cell level following the protocol of organoid cultivation (2.2.1.3.1) without resuspending the final cell pellet in Matrigel. Cells were counted and $2*10^5$-$2,4*10^5$ cells were seeded in a volume of 200 µl of mucosoid cultivation medium per filter. 400 µL mucosoid cultivation medium were filled in the well below. Medium was supplemented with an increased concentration of 2,5 µl/mL ROCK inhibitor until the first medium change. Liquid in the filter insert was removed after three days and the air-liquid interface condition was started. Medium was changed every three days. For epithelial cell propagation medium was removed from the well. Filter inserts were washed twice with PBS. Trypsinization was done in two steps: 0,05 % Trypsin/EDTA were placed on the filter and the well below and incubated for 20 min at 37°C. Trypsin on the filter was collected in a 15 mL falcon tube and inactivated with 5 x volume Adv+++. Trypsinization step was repeated. Afterward, filter was washed with Adv+++ and pooled in the same falcon tube. Cell suspension was centrifuged (300 x g, 5 min, 4°C), cell pellet was washed with Adv+++, centrifuged and resuspended in mucosoid cultivation medium. $2*10^5$–$2,4*10^5$ cells were seeded on a new collagen-coated filter insert. Medium was filled in the well below. After three days air-liquid interface condition was started.

2.2.1.3.3. Primary gastric stromal cell cultivation

Primary gastric stromal cells were cultivated on plastic indefinitely but maximum up to 16 passages. For cell propagation, medium was removed, cells were washed with PBS, and incubated with 0,05 % Trypsin/EDTA for 10 min at 37°C. Trypsin/EDTA was inactivated by adding 5 x volume Adv+++. Cell suspension was collected in a 15 ml falcon tube. Culture flask/well was washed with Adv+++ and pooled with cell suspension, centrifuged (300 x g, 5 min, 4°C), resuspended in GSC cultivation medium and seeded in the desired cell number. In general stromal cells were passaged weekly in a ratio 1:4 – 1:5. For co-culture experiments, stromal cells were seeded in confluency with 60 000 cells per well in a 24-well plate.

2.2.1.3.4. Co-culture of epithelial cells and stromal cells

For the co-culture of epithelial cells with stromal cells, epithelial cells were grown for at least 10 days under air-liquid interface conditions (see 2.2.1.3.2). Stromal cells were cultivated as described in 2.2.1.3.3. One day before co-culture was started stromal cells were seeded in confluency with 60 000 cells per well in a 24-well plate in GSC medium and incubated at 37 °C, 5 % CO_2. After 24 hours medium on stromal cells was exchanged with 500 µl mucosoid culture medium and filter insert with epithelial cells was placed on top of the stromal cells. Cells were incubated at 37 °C, 5 % CO_2 cell incubator and co-culture was performed for seven days. Medium was changed by 50 % every two days.

2.2.1.4. Freezing and Thawing of Gastric Primary Cells

2.2.1.4.1. For primary gastric epithelial cells:

For preservation of gastric primary epithelial cells, cultivation of epithelial cells in organoid format was needed. Organoids were grown for 3 to 4 days after seeding until small organoids have formed. Matrigel drops of two to three wells were dissolved with cold Adv++ and collected in 15 mL falcon tube, centrifuged (300 x g, 4 min, 4 °C) and the cell pellet was resuspended in 500 µL freezing medium Cryo-SFM. Cell suspension was transferred into a cryo-vial and frozen in a Nalgene Mr. Frosty freezing container at -80°C. For long-term storage, epithelial cells vials were transferred into liquid nitrogen.

In preparation for thawing of primary epithelial cells, Matrigel was thawed and kept on ice and a 24-well plate was pre-warmed at 37°C. One vial with cryopreserved epithelial cells was thawed within two minutes at 37°C until only a small rest of frozen cells was left. Cells were resuspended in Adv++, transferred in a 15 mL-falcon tube and centrifuged (300 x g, 4 min, 4 °C). The cell pellet was resuspended in 100 – 150 µL Matrigel and cells were seeded in two to three wells of the pre-warmed 24-well plate. After Matrigel has solidified at 37°C, culture wells were filled with 500 µL organoid culture medium (supplemented with 2,5 µL/mL ROCK inhibitor for the first three days).

2.2.1.4.2. For primary gastric stromal cells:

For cryopreservation of GSC, cells were grown until 100 % confluency. Medium was removed, cells were washed with PBS and incubated with 0,05 % Trypsin/EDTA as described in GSC cultivation. Cell suspension was centrifuged (300 x g, 4 min, 4°C), cell pellet was washed with Adv+++ and after cell counting again centrifuged. Cell pellet was resuspended in 500 µl/1*10^6 cells Cryo-SFM and transferred into cryo-vials (500 µL per vial). Cryo-vials were stored in a Nalgene Mr. Frosty freezing container at -80°C for gentle freezing. For long-term storage stromal cell vials were transferred to liquid nitrogen.

To start stromal cell cultivation from frozen stocks, a cryo vial was placed at 37°C for app. 2 min until cells in cryo-SFM were nearly melted. Cells were resuspended in pre-warmed stromal cell medium and transferred into a culture flask (per 1*10^6 cells 1 x T75 culture flask) which was filled with stromal cell cultivation medium before. Cells were incubated at 37°C, 5 % CO_2 cell incubator.

2.2.1.5. Treatment of mucosoids to induce secretory cell lineage differentiation

Primary gastric epithelial cells were grown as mucosoid cultures for a minimum of two weeks before treatments were started to induce differentiation.

Foveolar cell differentiation was induced in antrum and corpus mucosoids by depletion of WNT3A and RSPO1 from the medium for seven days as described for organoids before (Bartfeld et al. 2015; Schlaermann et al. 2014). Medium was changed every three days by 50 %.

For secretory cell lineage differentiation, corpus mucosoids were treated with differentiation medium (see 2.1.5 Table 8) for twelve days with 50 % medium change every three days. Briefly, mucosoids were treated with different concentrations of Noggin (0-150 ng/mL) in the presence or absence of EGF. In further conditions, Noggin was depleted from the medium and 2 µM PD0325901 (Sigma) were added in the presence or absence of 50 ng/mL BMP4 (Gibco).

Corpus mucosoids treated with medium depleted from Noggin and supplemented with PD0325901 (2 µM) and BMP4 (50 ng/mL) were further stimulated with Histamine (1 mM, Sigma) to activate gastric acid secretion.

2.2.1.6. Monitor of acid production by parietal cells using Acridine Orange

Corpus mucosoids were grown for 13 days in regular medium followed by two weeks treatment with 50 ng/mL of BMP4 and removal of Noggin and EGF. Corpus epithelial cells on filters were pre-incubated with 1 µm Acridine Orange (AO) for 15 min. The filter was cut out of the insert and mounted with the cells facing the glass on an IBIDI chamber with 400 µl of media (the same with AO). A coverslip was put on top. Images were taken with 25 x (Glycerol) for 10 min to stabilize the filter and avoid movements. A solution of 10 µl of 5 mM Histamin in medium was applied on the border of the coverslip while imaging. Fluorescence of Acridine Orange was excited at 488 nm (3-4 %) and images were collected in a time series (image recording every 10 sec) at 500–550 nm and 600–650 nm. Pinhole was opened at 180-190 AU. Images were analyzed by ImageJ and corrected for (X-Y) drifts of the sample. Images were generated by averaging the signal from nine time points (90 sec).

2.2.1.7. Production of WNT3A and RSPO1 conditioned medium

WNT3A and RSPO1 conditioned media were produced with two stable cell lines provided by the Clevers group, Utrecht, Netherlands. L Wnt-3A cells (ATCC® CRL-2647™), 293T HA Rspo1-Fc cells or L cells (ATCC® CRL-2648™) were quickly thawed and seeded in T75 cell culture flasks in DMEM/F12 +10 %FCS, +1 mM Na-pyruvate, +2 mM L-Glutamine. Cells were passaged at confluency using Trypsin/EDTA and seeded in a ratio of 1:20 in new culture flasks. WNT3A and RSPO1 producing cells were selected with Zeocin (final concentration: 125 µg/mL, Invitrogen). After five days the medium was removed and fresh medium with only 5 % FCS was added. The supernatant was collected after five days and fresh medium was added. Another five days later the 2nd supernatant was collected. Both supernatants were centrifuged (1 200-1 500 x g, 10 min, RT) and sterile filtered. The first and second supernatants were mixed, aliquoted and stored at -20°C. The Wnt activity of the conditioned medium was

determined using a Wnt reporter cell line (293T WntR) which is transfected with a 7 TCF/LEF promoter-binding site driving the expression of GFP upon Wnt pathway activation. Both conditioned supernatants (WNT3A and RSPO1) were added for 24 h to 293T WntR test cells seeded on a poly-L-lysine coated 48-well. Cells were fixed for 20 min with 4 % pFA and stained with Hoechst. The number of green cells divided by the number of nuclei representing the "activated cells" was determined automatically from images acquired with an automated microscope (Olympus Soft Imaging Solutions). L cells are the parental cell line of the L Wnt-3A cells and were used to control for Wnt-independent effects.

2.2.1.8. WNT activation reporter assay

239T WntR cells were transfected with a vector containing 7 TCF/LEF binding sites driving the expression of GFP. Cells were seeded on a poly-L-lysine-coated 48-well plate and exposed to a constant amount of WNT3A (50 %) and an increasing ratio of GSC CM : DMEM (0:100 to 100:0) to test for the presence of Wnt activators or inhibitors derived from the gastric stromal cells. The percentage of GFP positive cells was normalized against the total number of nuclei (Olympus Soft Imaging Solutions).

2.2.2. Bacterial Cell Culture

2.2.2.1. Cryo-preservation of *Helicobacter pylori*

Helicobacter pylori strain was plated from the general departmental collection on the respective GC agar plates. Bacteria culture was expanded over two passages by daily re-plating on new GC agar plates. Bacteria colonies were collected with a swap and resuspended in BHI supplemented with 10 % FCS (heat-inactivated), 20 % Glycerol (86 %), Vancomycin (10 µg/ml), Nystatin (10 µg/ml) and Trimethoprim (5 µg/mL) and aliquots were stored at -80°C.

2.2.2.2. Cultivation of *Helicobacter pylori* for infection

One aliquoted vial of *H. pylori* was thawed and 50 µl of bacteria suspension were plated on the corresponding culture plates. Bacteria plates were incubated under microaerophilic conditions with 5 % O_2 at 37°C for three days. Bacteria were harvested in pre-warmed BHI and Optical Density (OD) of a 1:10-dilution was measured at 550 nm. Bacteria suspension with $OD_{550\,nm} = 1$ was prepared, plated in dilutions of 400 µl, 200 µl, 100 µl, and 50 µl on culture plates respectively and incubated for 24 hours under microaerophilic conditions. Part of each plated dilution was resuspended in pre-warmed BHI and 3 µl of bacteria suspension were transferred on a glass slide and mixed with 12 µl BHI. Bacteria motility was determined under the microscope by the following ranking:

Table 19: Motility scoring for *H. pylori*

Motility Score	Interpretation
0	Coccoid shape, no movement
+	Rod and coccoid shape, little movement
++	Rod shape, twisting motion, little transversal motion
+++	Rod shape, spacious motion with many transversal motions

Bacteria dilution with the highest motility score (++ to +++) was used to prepare a bacteria suspension with $OD_{550\,nm} = 1$ in BHI and plated in dilutions of 400 µl, 200 µl, 100 µl, and 50 µl. Bacteria plates were incubated for 24 hours under microaerophilic conditions. Motility check was repeated the next day as described above. Dilution with the highest motility (minimum ++) was used to prepare a bacteria suspension with $OD_{550\,nm} = 1$ which corresponds to a bacteria load of $1*10^8$ bacteria/mL. Epithelial cells were infected with a multiplicity of infection (MOI) of 50 to 100. Mucus on top of epithelial cells was removed and cells were washed twice with PBS. Bacteria were applied in a volume of 30 µl PBS on the apical side of the epithelial cells. Infection was performed for two hours to three days.

2.2.3. RNA and DNA techniques

2.2.3.1. RNA isolation from gastric primary cells

RNA was isolated from primary cells in a two-step procedure, combining two protocols. First, cells were lysed with 500 µl TRIzol for RNA isolation. For mucosoid cultures, the filter was cut out from the insert and directly put into TRIzol. Stromal cells were incubated with TRIzol for two minutes and cell lysate was transferred into 1.5 mL tube. TRIzol samples were snap-frozen at -80°C and thawed again. In the following, 170 µL chloroform were added to the sample and the samples was vigorously vortexed, incubated for 3 min at RT and centrifuged (16 000 x g, 15 min, 4°C). The upper aqueous phase was transferred to a new 1.5 mL tube and same volume of isopropanol was added. The tube was inverted six times and incubated for 10 min at RT. The solution was transferred to an RNA isolation column (GeneJET RNA purification kit, Thermo Scientific). Further protocol was followed the manufacture instructions. Briefly, the column was centrifuged (12 000 x g, 1 min, RT), flow-through was discarded; column was washed with wash buffer I and centrifuged, followed by two wash steps with wash buffer II. RNA was eluted from the column with 40 µL nuclease-free water. RNA concentration was measured using the NanoDrop1000 UV-Vis spectrophotometer. RNA sample was stored at -20°C until further use.

2.2.3.2. cDNA synthesis from RNA

Isolated RNA was transcribed into first-strand complementary DNA (cDNA) using the Tetro™ cDNA synthesis kit from Bioline. The reverse transcription was performed following the manufacturer's protocol. All steps were performed under nuclease-free conditions. In brief, cDNA synthesis was performed in a reaction volume of 20 µL. Depending on the RNA concentration, 100 to 200 ng were used as input in a maximum volume of 12 µL. A Mastermix was prepared containing dNTP’s, Random Hexamer Primer, 5 x RT buffer, Ribo Safe RNase inhibitor, and Reverse Transcriptase. Per reaction 8 µL Mastermix were combined with the RNA in a 0.2 mL reaction tube. The following polymerase chain reaction (PCR) protocol was performed to generate cDNA:

Table 20: Reverse Transcription PCR setting

Temperature	Time
25°C	10 min
45°C	30 min
85°C	5 min
4°C	∞

Final cDNA was diluted up to ten times with nuclease-free water and stored at -20°C until further use.

2.2.3.3. Polymerase chain reaction (PCR) and agarose gel electrophoresis

The polymerase chain reaction (PCR) serves to copy and amplify a specific DNA segment using primers that are specific and complementary to the DNA target region. Each PCR consists of three major steps: denaturation, annealing, and elongation. In the first step, the DNA and primers were denaturated into single strands followed by annealing of the primers to the DNA target region. After primer binding, the DNA polymerase elongates the new DNA strand complementary to the DNA segment. This 3-step cycle is repeated multiple times. To analyze the expression of Wnt antagonists in gastric stromal cells, RNA of stromal cells was reverse transcribed as described in 2.2.3.2 and cDNA was used to perform the PCR. For the PCR the *Taq* DNA polymerase and the corresponding 10 x Standard *Taq* Reaction Buffer were used. All steps were done under nuclease-free conditions. One reaction was performed in 25 µL reaction volume, consisting of 24 µL Mastermix and 1 µL cDNA. The composition for one reaction is summarized in Table 21 below. A Primer-mix of forward and reverse primer with a concentration of 20 µM respectively, was prepared in nuclease-free water.

Table 21: Composition of one PCR reaction

Component	Volume
10x Standard *Taq* Reaction buffer	2,5 µL
10 mM dNTPs	0,5 µL
Taq DNA polymerase	0,125 µL
Primer-mix (20 µM)	1 µL
Nuclease-free H_2O	19,87 µL
cDNA	1 µL

Mastermix and cDNA were combined in PCR tube, gently vortexed and centrifuged for 10 sec in a mini centrifuge. The PCR was performed with the following setting:

Table 22: Programm setting of the PCR cycler

Temperature	Time	Cycles	Step
94°C	3 min	1	Initial denaturation
94°C	30 sec	35	Denaturation
56°C	30 sec		Annealing
72°C	30 sec		Elongation
72°C	3min	1	

Afterward, an agarose gel electrophoresis was performed to separate the DNA fragments by size. A 2 % (w/v) agarose gel was prepared by dissolving agarose powder (Biozym) in 1 x TBE buffer through short boiling in a microwave. Ethidium bromide (EtBr) was added to the agarose solution (app. 2 µL per 100 mL agarose solution). EtBr intercalates with the DNA and fluoresces under UV light thus enabling the visualization of DNA. The agarose solution was poured into a gel chamber (BioRad) with a comb. In the following 10 µL of the PCR product were mixed with 2 µL 6x DNA loading buffer and loaded onto the solidified agarose gel. A molecular weight ladder was added (GeneRuler™ 1kb DNA ladder) to the gel and electrophoresis was run at 100 V for app. one hour. The gel was analyzed under UV light and a picture was taken for result documentation.

2.2.3.4. Quantitative real-time polymerase chain reaction (RT-PCR)

The quantitative real-time polymerase chain reaction (RT-PCR) is a method to estimate the relative mRNA expression of a gene of interest (GOI) and is based on the measurement of a fluorescence signal during the elongation phase of the PCR. Primers designed specifically for the gene of interest bind to the template DNA and elongate the complementary DNA strand. The fluorescence dye SYBR Green I binds to the big groove of double-stranded DNA which is present in the elongation phase of the PCR. The DNA-SYBR Green-complex absorbs blue light at a wavelength of 494 nm and emits light with a wavelength of 521 nm. The fluorescence signal is detected during the elongation phase. The intensity of the fluorescence signal is proportional to the amount of double-stranded DNA. After the PCR is completed, a melting curve analysis is performed to ensure the purity of the PCR product and the quality of the primers and the product. Negative control with water is included to avoid false-positive results. For the RT-PCR the kit SensiMix® Hi-ROX from Bioline was used. SensiMix® is a ready-to-use reaction mix containing the DNA polymerase, the fluorescence dye SYBR Green, dNTP's for elongation, reaction buffer and magnesium. All steps were done under nuclease-free conditions. One reaction was performed in 20 µL reaction volume, consisting of 17 µL Mastermix and 3 µL cDNA. The composition for one reaction is summarized in Table 24. A primer-mix of forward and reverse primer with a concentration of 20 µM respectively, was prepared in nuclease-free water. Mastermix and cDNA were combined in a 96-well-PCR-plate. The plate was covered with the provided foil and centrifuged for 30 sec at 1000 x g. Each reaction was measured in triplicate. The RT-PCR was performed with the following setting:

Table 23: Programm setting of the RT-PCR cycler

Temperature	Time	Cycles	Step
95°C	10 min	1	Initial denaturation and activation of polymerase
95°C	10 sec	40	Denaturation
63°C	15 sec		Annealing
72°C	20 sec		Elongation and detection
95°C	10 sec	1	Denaturation
65-95°C	5 sec per 0,5°C	1	Melting curve analysis

Table 24: Composition of one RT-PCR reaction

Component	Volume
2x SensiMix®	10 µL
Primer-Mix (20 µM)	0,5 µL
Nuclease-free H_2O	6,5 µL
cDNA	3 µL

The data analysis was done using the ΔC_t method which gives a relative quantification of a GOI by normalization on a housekeeping gene (HKG). In this thesis, HKG's GAPDH and C1orf43 were used. The ΔC_t value was calculated with the following formula:

$$\Delta Ct = Ct(GOI) - Ct(HKG)$$

For further normalization on an internal control within one sample set the $\Delta\Delta C_t$ and relative quantity (RQ) were calculated:

$$\Delta\Delta Ct = \Delta Ct(Treated) - \Delta Ct(Control)$$

$$RQ = 2^{-\Delta\Delta Ct}$$

2.2.3.5. *In situ* hybridization – RNAscope

In situ hybridization is a method to detect and localize a specific RNA sequence in e.g. tissue using labeled complementary RNA or modified nucleic acid strands (probes). Here, *in situ* hybridization was applied to human stomach tissue. For the *in situ* hybridization, the RNAScope® 2.5 HD Reagent Kit-RED from ACD was used following the manufacturer's protocol while the incubation time in "target retrieval reagent", peroxidase and AMP5 were adapted to the tissue. In brief, slides were baked in a dry oven at 60°C for 60 min to melt paraffin. Under a fume hood slides were incubated twice for 5 min at RT in fresh xylene and twice for 2 min in fresh 100 % ethanol for deparaffinization. After air-drying completely, the slides were incubated with

RNAscope hydrogen peroxide for 10 min at RT and washed twice with distilled water. Slides were transferred to pre-heated 1x target retrieval reagent and boiled for 17 min at 98 – 102°C, followed by 5 min washing in distilled water and once in 100 % ethanol. A barrier was drawn around each sample with an Immedge hydrophobic barrier pen and slides were dried overnight at RT. Dried slides were placed in a HybEZ slide rack and sections were incubated with RNAscope Protease Plus for 22 min at 40°C and washed twice for 2 min in distilled water. Probes and 50x wash buffer had to be pre-warmed to 40°C before use. Pre-warmed probe was hybridized to sample for 2 h at 40°C. Slides were washed twice for 2 min in 1x wash buffer. Next, slides were incubated with AMP1 (30 min, 40°C), AMP2 (15 min, 40°C), AMP3 (30 min, 40°C) and AMP4 (15 min, 40°C). Between each AMP-step slides were washed with 1x wash buffer twice for 2 min. Then, slides were incubated with AMP5 for 45 min at RT, washed twice for 2 min in 1x wash buffer and incubated with AMP6 for 15 min at RT and finally washed twice for 2 min with 1x wash buffer. For signal detection, RED working solution was prepared directly prior to use by mixing RED B with RED A in a 1:60 ratio. Sections were incubated for 10 min at RT with RED working solution. Next, slides were washed twice in distilled water. Sections were incubated in 50 % Hematoxylin for 5 min at RT, followed by washing in distilled water and short incubation in 0.02 % ammonia water until sections turn blue. Sections were washed with water and dried at 60°C. Before mounting, sections were shortly dipped in fresh xylene and finally mounted with EcoMount by dropping mounting medium on the tissue and cover it with a coverslip, avoiding air bubbles.

Analysis of RNAscope data

Images of the *in situ* hybridization samples were recorded with an Axion Scan.Z1 microscope (Zeiss) by the MPIIB core facility Microscopy (Dr. Volker Brinkmann). The images were processed with the software ZEN 2.3 (blue edition) and Fiji ImageJ. The latter was used to count the number of signal spots of the whole image and per defined region. Therefore the tools ‘colour deconvolution’, ‘threshold’ and ‘analyze particles’ were used. The whole image of the gland was divided into top, middle and base. Top and base were defined by a square with a height of 90-110 µm which was measured from the top of the

gland (defined as “top”) and from the bottom where the gland started (defined as “base”) as shown in the scheme below (Figure 7).

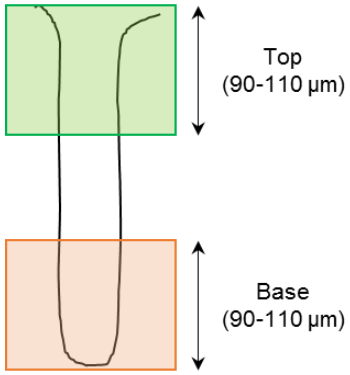

Figure 7: Scheme of the gastric gland with the determination of the regions' "top" and "base" for the analysis of *in situ* hybridization samples. Whole gland images were analyzed in ImageJ. “Top” and “base” were defined by drawing a square with 90-110 µm in height.

2.2.3.6. Microarray Analysis

Microarray experiments were performed in three biological replicates as single-color hybridization on custom whole-genome human 8x60K Agilent arrays (Design ID 048908) according to the manufacturer’s instructions and Agilent Feature Extraction software used to obtain probe intensities. Single-color hybridization allowed multiple comparisons in subsequent analysis. RNA isolation from TRIzol samples and all subsequent steps including Bioanalyzer, labeling, hybridization, and scanning were performed by the MPIIB core facility Microarray (Dr. Hans Mollenkopf). For the microarray analysis mucosoid cultures and mucosoids co-cultured with stromal cells (see 2.2.1.3.4) were infected with *H. pylori* (see 2.2.2.2) for three days. Non-infected counterparts served as controls and were also hybridized. Filters with mucosoid cultures and stromal cells were dissolved in 1 ml TRIzol, respectively and RNA was isolated as per the manufacturer’s protocol. Quantity of RNA was measured using NanoDrop1000 UV-Vis spectrophotometer and quality was assessed by Agilent 2100 Bioanalyzer with an RNA Nano 6000 microfluidics kit (Agilent Technologies). RNA labeling was performed using the Agilent One-Color Low Input Quick Amp Labeling Kit according to the supplier’s protocol. In brief, mRNA was reverse transcribed with oligo dT-T7-

promoter primer and amplified and labeled with T7 RNA polymerase and Cyanine 3-CTP. Labeled and fragmented cDNA was hybridized to the arrays and scanning was performed according to the manufacturer's protocol with 3 µm resolution using the Agilent high-resolution laser microarray scanner. Scan data were extracted with the Image Analysis/Feature Extraction software G2567AA v. A.11.5.1.1 (Agilent Technologies) using default settings and the GE1_1105_Oct12 (single color) extraction protocol. The single-color raw data files were background corrected, quantile normalized and further processed and analyzed for differential gene expression using R (R Core Team 2013) and the associated BioConductor package LIMMA (Ritchie et al. 2015) by Dr. Hilmar Berger. Microarray gene expression comparisons between groups were performed using paired tests between conditions.

Gene expression microarray data (txt files and QC report) generated in this thesis is provided in the electronic appendix file EA.1, thereby only GSC relevant data (txt files) are considered.

2.2.3.7. Gene set enrichment analysis

Differential gene expression between antrum and corpus mucosoids of three biological replicates was determined using a moderated paired t-test, and resulting p-values were adjusted using the Benjamini-Hochberg false discovery rate (FDR) algorithm. Antrum and corpus signatures were defined from previously published gastric biopsy microarray experiments (Nookaew et al. 2013), applying a threshold of $|logFC| > 1$ and FDR < 5 %. Gene set enrichment analysis (GSEA) with these signatures was performed on genes pre-ranked by t-score between antrum and corpus and with standard settings with 5 000 permutations. For the selection of leading-edge genes determined by GSEA of antrum vs corpus, a threshold of $|logFC| > 0.6$ and $p < 0.05$ was applied. Log2 fold changes between corpus and antrum biopsies and corpus and antrum mucosoids were computed independently for both data sets. The GSEA analysis in this thesis was performed in collaboration with Dr. Kristin Fritsche and underlying data is to be found in the respective PhD thesis of Dr. Kristin Fritsche.

2.2.4. Immunohistochemistry and Microscopy

2.2.4.1. Fixation and paraffinization of gastric tissue and mucosoid cultures

Tissue or filters with epithelial cells from mucosoid cultures were fixed overnight in 4 % paraformaldehyde (pFA) at 4°C and washed with PBS. Filters were further embedded orthogonally in Histogel (HG-4000-144) inside a casting mold. Tissue sample or Histogel block with embedded filter were paraffinized overnight in a Leica TP1020 tissue processor which performed automatic dehydration with the following steps: 70 % ethanol (2 h), 80 % ethanol (2 h), 90 % ethanol (2 h), 96 % ethanol (2 h), isopropanol (2 h), xylene (2x 2 h), and paraffin (2x 2 h). The paraffin blocks are generated inside a metal casting mold on a paraffin embedding console (Microm). From pre-cooled paraffin blocks, thin sections (5-10 µm) were cut with a paraffin rotation microtome (Microm) and transferred to glass slides.

2.2.4.2. De-paraffinization

For de-paraffinization of the sections, slides were incubated twice in xylene for 10 min respectively, twice in 100 % ethanol for 2 min respectively, followed by two minutes incubation steps in 95 % ethanol, 70 % ethanol, 50 % ethanol and twice in tap water. Slides were transferred to a slide chamber with pre-heated antigen retrieval solution (Gibco) and incubated for 30 min in a 100°C water bath and 20 min at RT to cool down the slides. Slides were washed for 5 min under running tab water. Water was exchanged with PBS.

2.2.4.3. Hematoxylin & Eosin staining (H&E)

Hematoxylin and eosin staining are used to visualize the various structures of histologic sections. Hematoxylin stains nuclear DNA while with eosin cytoplasmic compartments

are stained. De-paraffinized sections of mucosoid cultures were covered with Mayer's Hematoxylin solution (Roth) and incubated for 15 min at RT. The slides were rinsed shortly with ddH_2O, followed by 5x 3 min rinsing under running tab water and finally 2 min rinsing with ddH_2O. In the following, the sections were covered with Eosin Y solution (1 % aqueous, Roth) and incubated for 10 min at RT. Finally, the slides were rinsed for 1 min with ddH_2O and embedded using Roti®-Histokitt.

2.2.4.4. Immunofluorescence labeling of paraffin sections

Immunofluorescence (IF) is a method to visualize proteins by labeling the target protein in two steps with a specific primary antibody and a fluorescence dye coupled secondary antibody. De-paraffinized sections were encircled with PapPen (biozol #CED-MU12) to prevent the running down of liquid. Sections were incubated for 60 min at RT in a humidified chamber with IF blocking solution to block unspecific binding sites and avoid unspecific background signals. Blocking solution was removed and primary antibody was added on the section and incubated for 90 min at RT for mucosoid cultures or overnight at 4°C for tissue sections in a humidified chamber. Slides with sections were washed 3x 5 min in PBS. Sections were incubated with immunofluorescence labeled secondary antibody, nuclei dye and cytoskeleton dye, light protected in a humidified chamber for 60 – 120 min at RT. Slides were washed in PBS (3x 5 min), followed by water once. Sections were embedded with mowiol and stored light protected at 4°C. Sections were imaged, using the Leica TSP8 confocal microscope.

2.2.4.5. Whole Mount Immunofluorescence

Whole Mount Immunofluorescence is a method in which part of the filter of mucosoid culture insert is used to visualize a target protein by fluorescence antibody labeling. In comparison to immunofluorescence staining of filter sections which gives a vertical view on the cell monolayer, the whole mount staining serves a top view on the cells and allows analyzing a greater amount of cells. For whole mount immunofluorescence staining, one-quarter of a mucosoid culture filter with epithelial cells is needed. The filter was fixed with 4 % pFA for 20 min at RT, followed by 10 min incubation in pre-

cooled methanol at -20°C. Filter was washed twice in PBS and unspecific binding sites of the cells on the filter were blocked by incubating the filter in 50 µL whole mount IF blocking solution for 60 min at RT in a humidified chamber. Afterward, filter was incubated with primary antibody (overnight, 4°C), washed five times in PBS and incubated light protected with fluorescence-labeled secondary antibody, nuclei dye, and cytoskeleton dye for 120 min at RT in a humidified chamber. Filter was embedded on a glass slide with mowiol and stored light protected. Samples were imaged at Leica TSP8 confocal microscope.

2.2.4.6. Confocal Microscopy and image analysis

After IF or H&E staining, images were recorded at the confocal microscope with a 10x, 20x or 40x oil objective using the Leica TCS SP-8 confocal microscope (Leica Microsystems GmbH) and the corresponding Leica software (Leica Microsystems GmbH). Afterward, images were further processed and analyzed using Fiji ImageJ (open source). This software was also used for cell and particle counting and measurement of cell height.

2.2.4.7. Transmission Electron Microscopy

Transmission electron microscopy (TEM) is a method serving for the fine structural analysis of cells. Mucosoid culture cells were fixed with 2.5 % glutaraldehyde (GA) in PBS and post-fixed with 0.5 % Osmium-tetroxide, contrasted with Uranyl-acetate and tannic acid, dehydrated in a graded ethanol series, and infiltrated in Polybed (Polysciences). Cut out pieces of the filters were stacked in flat embedding molds with Polybed. After polymerization, specimens were cut at 60 nm and contrasted with lead citrate. Specimens were analyzed in a Leo 906E transmission electron microscope (Zeiss, Oberkochen. DE) equipped with a side-mounted digital camera (Morada, SIS-Olympus, Münster, DE). The sample preparation after fixation, image aquistion, and analysis were performed by Dr. Christian Goosmann from the MPIIB core facility Microsopy.

2.2.4.8. Cryo-Immunogold Electron Microscopy

Mucosoid culture samples were fixed with 4 % pFA and 0.05 % GA in PBS and filter membrane was cut into 1 mm wide streaks. The filter membrane pieces were gelatin-embedded and infiltrated with 2.3 M sucrose according to the method described (P.J.Peters 2006). Ultrathin sections were cut at -95°C with an RMC MTX/CRX cryo-ultramicrotome (Boeckeler Instruments Inc., Tucson AZ, USA) transferred to carbon- and pioloform-coated EM-grids and blocked with 0.3 % BSA, 0.01 M glycine, 3 % CWFG in PBS. The sections were incubated with appropriate dilutions in the same buffer of rabbit polyclonal antibody directed against PGC (see Table 13) or mouse antibody directed against ATP4B (see Table 13). Secondary antibody-incubations were carried out with goat-anti-rabbit (or mouse) antibodies coupled to 12 nm gold particles (Jackson Immuno Research, West Grove, PA, USA). Specimens were then contrasted and embedded with uranyl-acetate/methyl-cellulose following the method described (Slot et al. 1991) and analyzed in a Leo 912AB transmission electron microscope (Zeiss, Oberkochen, Germany) at 120 kV acceleration voltage. Micrograph-mosaics were scanned using a bottom mount Cantega digital camera (SIS, Münster, Germany) with ImageSP software from TRS (Tröndle, Moorenweis, Germany). Annotation of gold particles was performed with Fiji Image J (Schindelin et al. 2012; Schneider, Rasband, and Eliceiri 2012) software using the 'Gold Digger' Macro (Sjollema and Giepmans Oct. 24, 2016). The sample preparation after fixation, image aquistion, and analysis were performed by Dr. Christian Goosmann from the MPIIB core facility Microsopy.

2.2.5. Protein biochemistry

2.2.5.1. SDS-PAGE

Sodium-dodecylsulfate polyacrylamide gel electrophoresis (SDS-PAGE) serves to separate proteins by their molecular weight in an electric field. SDS is an anionic detergent that binds to the protein surface masking the charge of the protein and covers the protein with a negative charge. Thus, the protein moves in an electric field to the anode. The speed of movement depends on the size of the protein: the smaller the

protein, the faster it moves through the gel. Before the protein sample was loaded onto the SDS gel the proteins were denaturated with 2x Laemmlibuffer containing β-mercaptoethanol and heated for 5 min at 95°C. SDS gel consisted of a separating gel and a collecting gel having a lower percentage of polyacrylamide and served to concentrate the sample. As a protein marker, prestained PageRuler™ was used. The electrophoresis was run with a constant voltage of 120 V for 90 min.

2.2.5.2. Western Blot Analysis

Proteins that were separated in an SDS-PAGE were transferred on a polyvinylidene difluoride (PVDF) membrane by electrophoresis and target proteins were immunologically detected. For the protein transfer, the wet blot method was used. Due to the global negative charge of the denaturated proteins in the SDS-PAGE, the proteins move to the positive pole in an electric field, thereby proteins were 1:1 horizontally transferred from the SDS gel onto the PVDF membrane. On the anode side of the cassette, one sponge and two Whatman paper wetted in transfer buffer were placed, followed by the PVDF membrane which was activated with methanol for 1 min, washed with water and incubated with transfer buffer before. On top of the membrane, the SDS gel was placed, which was shortly incubated in transfer buffer before, followed by two Whatman paper and a sponge, both wetted with transfer buffer. The cassette was closed and placed in the electrophoresis chamber, filled with transfer buffer. The transfer was run overnight at 4°C with a constant voltage of 20 V per membrane/gel-sandwich. Free binding sites were blocked on the membrane with WB blocking solution for 1 h at RT to avoid unspecific antibody reaction. Membrane was incubated in primary antibody for 90 min at RT or overnight at 4°C, depending on the antibody and washed three times with TBS-Tween 20 (TBS-T). Next, the membrane was incubated with a horseradish peroxidase-coupled secondary antibody for 60 min at RT and washed three times with TBS-T and finally once with TBS. Target protein on the membrane was detected and developed on X-ray film after incubation of the membrane with a two-component ECL solution for 3 min in the dark. The ECL solution was prepared directly prior to use by mixing both components Enhanced Luminal Reagent Plus and Oxidizing Reagent Plus in a 1:1 ratio.

2.2.5.3. Mass spectrometry

Mass spectrometry (MS) is an analytical method to determine the mass-to-charge (m/z) ratio of ionized molecules in a sample. The output is a mass spectrum that blots the m/z ratios against their intensities. Here, this method was used to analyze the protein composition of mucus produced by mucosoid cultures. The sample preparation and LC-MS/MS analysis were performed by Monika Schmid from the MPIIB core facility Mass spectrometry.

2.2.5.3.1. Sample preparation

The mucus samples were prepared according to the FASP method (Wisniewski et al. 2009) and following modifications (Rodriguez-Pineiro et al. 2013). Samples were diluted with 200 µl 6 M guanidinium hydrochloride in 0.1 M Tris/HCl pH 8.5 (GuHCl) and 20 µL of 5 protein standard mixture (10 pmol/protein) were added. Cysteines were reduced by adding 30 µl 0.1 M DTT (Sigma-Aldrich D0632) at 60°C for 20 min and samples were transferred into Microcon YM-30 kDa centrifugal filter units. After each step filter units were centrifuged at 10 000 x rpm for 10 to 15 min at RT. 200 µL 6 M GuHCl were added and samples were alkylated with 100 µL 0,05 M iodoacetamide (IAA, Sigma-Aldrich I6125) in 6 M GuHCl at RT for 20 min in the dark. After washing twice with 100 µL 6 M GuHCl and twice with 100 µL 50 mM ammonium bicarbonate (ABC) the proteins were digested with 0.2 µg sequencing-grade modified trypsin (Promega V5111) in 40 µL 50 mM ABC overnight at 37°C with agitation (Thermomixer 500 rpm). In a new collection tube, samples were washed twice with 40 µL 50 mM ABC followed by acidification with TFA to 0.5% (vol/vol). ABC was evaporated by adding 50 µL 60 % acetonitrile/0.1 % TFA and dried at 45°C (Microconcetrator 5301, Eppendorf).

2.2.5.3.2. LC-MS/MS Analysis

The peptides were analyzed using a QExactive Plus mass spectrometer (Thermo Fisher Scientific) coupled online to a Dionex UltiMate 3000 RSLC nano system (Thermo Fisher Scientific). After solubilization in 90 µl 2 % (v/v) acetonitrile/0.1 % TFA, 5 µL of each sample was loaded on a C18 PepMap 100 trap column (300 µm x 5mm; 5 µm

particle size 100 Å pore size; Thermo Fisher Scientific) at a flow rate of 20 µL/min 2 % (v/v) acetonitrile/water containing 0.1% TFA for pre-concentration. Separation was performed using an Acclaim C18 PepMap RSLC column (75µm x 250 mm; 2 µm particle size 100 Å pore size; Thermo Fisher Scientific) at a flow rate of 300 nL/min. HPLC solvent A was 0.1 % (v/v) FA and peptides were eluted from the column using HPLC solvent B 80 % (v/v) acetonitrile/0.1 % FA starting from 3 %, increasing to 40 % in 85 min, and to 98 % in 5 min. The peptides were analyzed in data-dependent acquisition mode that alternated between one MS scan and 10 MS/MS scans for the most abundant precursor ions. MS scans were acquired over a mass range of m/z 350–1600 and resolution was set to 70 000. Peptides were fragmented using HCD at 27 % normalized collision energy and measured in the orbitrap at a resolution of 17 500.

2.2.5.3.3. Protein identification

Proteins were identified and quantified using the MaxQuant software (Version 1.626) (Cox and Mann 2008; Tyanova, Temu, and Cox 2016) searching against the SwissProt human sequence database (released 2018_11, 20 412 entries). Searches were performed using the following parameters: max. missed cleavages 2; variable modifications Oxidation (M); Acetyl (Protein N-term); pyro-Glu (Gln) and carbamidomethylation of cysteines as fixed modification. The FDR was set to 0.01 for proteins, peptides, and modified sites.

MaxQuant data analysis results are provided in the electronic appendix EA.2.

2.2.5.4. Cytokine Array (Quantibody®)

Quantibody® (Raybiotech) cytokine arrays are commercially available multiplex ELISA systems based on a glass slide antibody array that allow simultaneous measurement of multiple cytokines. For this assay, the conditioned media of (1) GSC co-cultured mucosoids infected with *H. pylori* for three days, (2) non-infected counterpart and (3) mucosoids cultured without stromal cells infected and (4) non-infected were used. 160 µL conditioned medium of each condition was collected, centrifuged (1 000 x g, 2 min) and 150 µL were diluted 1:1 with sample diluent of the Quantibody® array kit. The protocol provided by the supplier was followed. Briefly,

glass slide was equilibrated in the plastic bag for 30 min at RT followed by air desiccation for two hours at RT. For blocking 100 µl Sample Diluent were added into each well and incubated for 30 min at RT (gentle rocking). The cytokine standard mix dilution series (STD1-7: 200µl Sample Diluent + 100µL Std, negative control) was prepared. After removing the Sample Diluent with a vacuum pump from the wells, 100 µL of standard cytokines or samples were added and incubated for 2 h. Array was washed 5x 5 min with 150 µL 1x Wash Buffer I and 2x 5 min with 150 µL 1x Wash Buffer II both at RT (gentle rocking). The primary antibody was added (80 µL/well) and incubated overnight at 4°C. After washing (5x 5 min 150 µL Wash buffer I, 2x 5 min 150 µL Wash buffer II) the secondary Cy3-antibody was applied (80 µL/well) and incubated overnight at 4°C. Array was washed 5x 5 min with 150 µl 1x Wash Buffer I at RT. The device was disassembled; slide was placed in the slide washer filled with 1x Wash Buffer I and washed with gentle shaking at RT for 15 min followed by washing with 1x Wash Buffer II for 5min. The liquid was decanted and vessel was centrifuged 3 min, 200 x g to dry the slide. The array was imaged with Agilent high-resolution laser microarray scanner (5 µm resolution). Afterward, data was extracted by Dr. Hans Mollenkopf and analyzed with the supplier's analyzing software.

2.2.6. Statistics

Statistical analysis of the data was done using the software GraphPad Prism 7.03. If not otherwise stated, the results are presented either as mean ± SD (standard deviation) or as median with 95 % CI and min and max values. Data sets were compared as indicated using either the unpaired or paired Student's t-test. A p value ≤ 0.05 was considered as statistically significant.

3.RESULTS

3.1. Development of the mucosoid culture model

3.1.1. Mucosoid cultures resemble the *in vivo* situation

Human sleeve resections from obese patients were used to isolate primary epithelial cells. The tissue was provided by the clinical collaborators Prof. Dr. Jürgen Ordemann (Helios Clinic, Berlin Buch) and Dr. Christian Denecke (Charité, Berlin) under the ethical approval EA1/129/12.

Each tissue sample was dissected from the greater curvature and comprised the three main parts of the stomach: fundus, corpus, and antrum. The fundus was marked for orientation reasons by the surgeon. Figure 8A depicts schematically, the anatomical subdivision of the human stomach with the resection side, while in Figure 8B a corresponding and representative image of the gastric tissue sample before processing for epithelial cell isolation is shown. Epithelial cells were isolated from corpus and antrum of the tissue material and either grown first as organoids or directly seeded on a collagen-coated polycarbonate filter membrane of a trans-well insert fitting into a 24-well plate. A cultivation scheme of the mucosoids is shown in Figure 8C. As mentioned, the epithelial cells were seeded on the filter membrane in the primary epithelial cell culture medium. After three days, medium on top of the cells was removed and air-liquid interface (ALI) condition was started, maintaining nutrients supply only from the basal vessel. This ALI culture technique induced polarization of the epithelial cells.

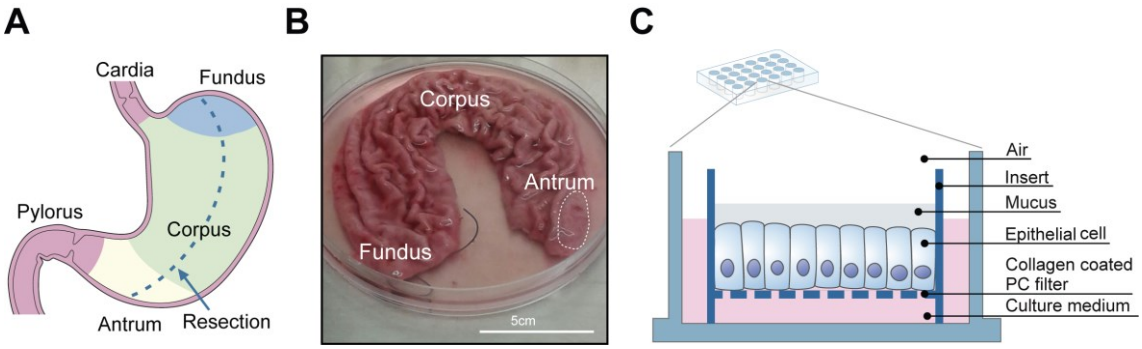

Figure 8: Primary stomach material and schematic representation of the mucosoid culture. (A) Schematic representation of the stomach with the tissue resection side labeled with a dotted line. (B) Stomach tissue piece before processing. The three main parts fundus, corpus, and antrum (white dashed line) are labeled. Scale bar: 5 cm (C) Schematic representation of the structure of the trans-well filter system of the mucosoid culture.

The development of the polarized monolayer over time is shown in Figure 9. Paraffinized sections of mucosoids were labeled using IF against the epithelial cell marker E-Cadherin and the nuclei. E-Cadherin is expressed only basolaterally and not on the apical side of polarized cells. One day after seeding (Figure 9A) epithelial cells showed a loose and unorganized 2D structure with an initial height of 6.8 µm. Three days after seeding and before the air-liquid interface was started the epithelial cells proliferated, became taller (10.2 µm) and built a sealed monolayer (Figure 9B). The cells still did not develop in height and E-Cadherin labeling was present all around the cell membrane. One day after ALI was started epithelial cells began to straighten and further increased in height (11.9 µm; Figure 9C). The polarization became more obvious after five days of air-liquid interface (Figure 9D). The E-Cadherin labeling was mainly present basolaterally and the nuclei were located on the basal side of the cells. After ten days in ALI, the epithelial monolayer was fully polarized with a height of 15.6 µm (Figure 9E). The E-Cadherin staining was exclusively present basolaterally and the nuclei were located on the basal side.

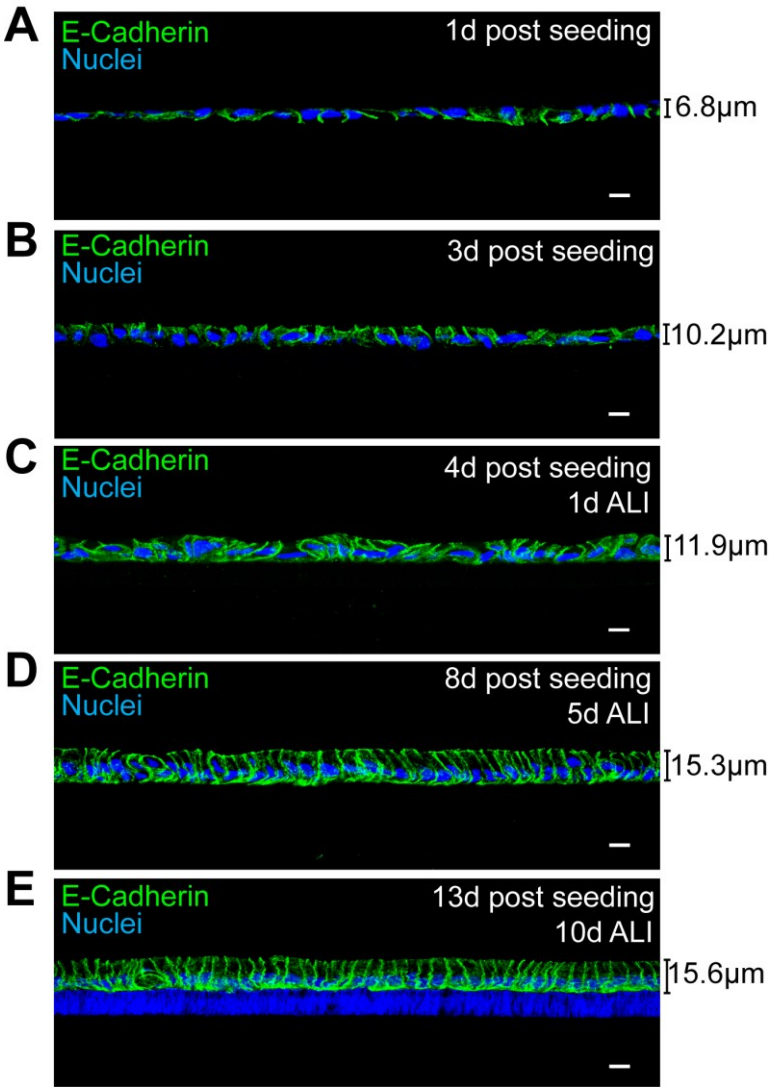

Figure 9: Development of the polarized epithelial monolayer over time. Primary gastric epithelial cells from two distinct patient samples were seeded on collagen-coated filter inserts and growth of the cells was followed for 13 days after seeding. Confocal micrographs of paraffinized filter sections of mucosoids fluorescently labeled with antibodies against epithelial marker E-Cadherin (green) and counterstain of nuclei with dye Draq5 (blue). The height of the cell layer was measured in ImageJ (Measure tool) and is depicted next to the micrograph. Cell growth was analyzed (A) one day after seeding, height 6.8 µm (B) three days post-seeding, height 10.2 µm (C) one day after ALI condition was started, height 11.9 µm (D) five days in ALI (equal to eight days post-seeding), height 15.3 µm and (E) ten days after ALI was started (13 days post-seeding), height 15.6 µm. Over time epithelial cells became a fully polarized monolayer with E-Cadherin labeling on the basolateral side with increasing height. Scale bar: 10 µm.

The polarization of the mucosoid culture was further confirmed by H&E staining of a paraffin section of the mucosoids fixed ten days after ALI was started (Figure 10A). The *in vitro* polarized monolayer reflected the same phenotype as observed in the

stomach: The nuclei were located at the basal side of the cells; the apical side faced the lumen where mucus was accumulated (see Figure 13 with MUC6 IF staining) and the basal side faced the filter, where nutrients and growth factors were taken up. Furthermore, the epithelial cells of the monolayer were sealed on their apical side by tight junctions as shown by the presence of tight junction marker occludin revealed by IF (Figure 10B).

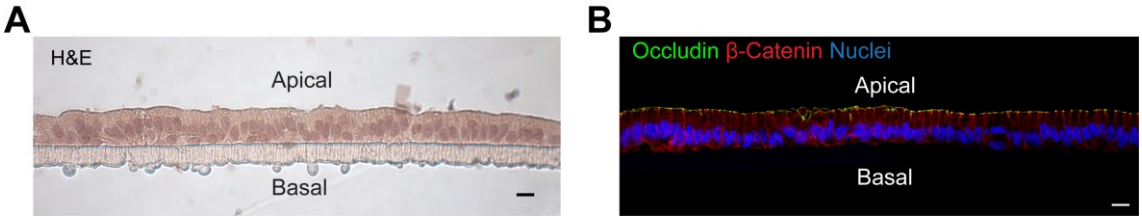

Figure 10: Mucosoid cultures show typical characteristics of a polarized monolayer present in the human stomach. (A) Microscopic graph of H&E staining of a paraffinized section of a mucosoid culture after ten days in ALI showed a polarized cell monolayer. H&E staining and image recording were performed by Dr. Francesco Boccellato. (B) The epithelial monolayer is sealed on the apical side by tight junctions demonstrated through IF labeling against tight junction marker protein occludin (green). Epithelial cells were visualized with an antibody against β-Catenin and nuclei were counterstained with dye Draq5. The image was recorded at a confocal microscope. Scale bar: 10 µm.

A further characteristic of the mucosoid culture was longevity; epithelial cells were kept for up to two months in mucosoid cultures with regular medium change but without passaging. To prove whether the cells were still capable to proliferate, sustain and regenerate, filter sections of two weeks, one month and two months old mucosoid cultures were labeled by IF against the proliferation marker Ki67 (Figure 11A-C). Obtained results show that after two months Ki67 positive epithelial cells were still detected and organized in a polarized monolayer indicating the sustained proliferative capacity and the longevity of this model system. Moreover, 1.5 months old mucosoids were segregated and single cells were seeded in Matrigel to test whether the epithelial cells preserve their regenerative capacity and re-grow into organoids assuming that only stem cells can do this. Obtained results demonstrated that mucosoids were able to re-grow into organoids confirming that the cells retain intact their regenerative capacity (Figure 11D).

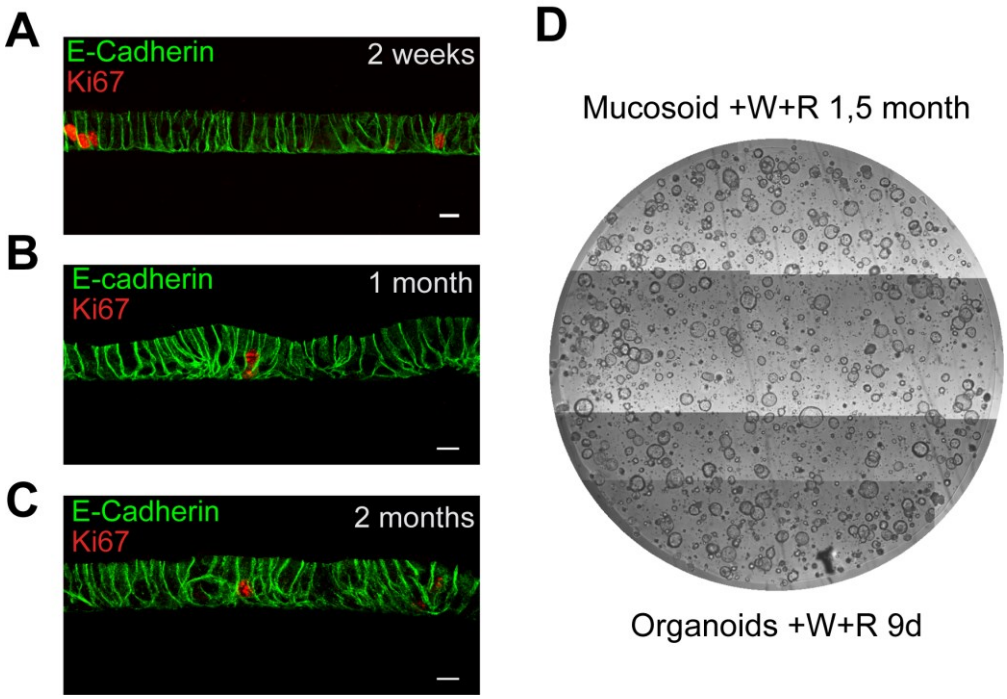

Figure 11: Mucosoid cultures are long-living and can be re-grown into organoids. Confocal micrographs of mucosoids cultured for (A) two weeks, (B) one month or (C) two months showing IF labeling with antibodies against the proliferation marker Ki67 (red) and E-Cadherin (green). Scale bar: 10 µm. (D) Regenerative capacity was further tested by trypsinizing 1.5 months old mucosoids to break up the monolayer into single cells. Single cells were seeded in Matrigel and growing of organoids was monitored nine days after seeding. A representative image of a technical triplicate is shown.

In the following, the longevity of the mucosoid cultures was tested. Therefore mucosoids from two patient samples were regularly segregated and monitored over eight months. Mucosoids of different passages were analyzed by IF against E-Cadherin after ten days in ALI when full polarization should be established. IF images in Figure 12 A and B show that polarity and height of the cells are maintained as the E-Cadherin was identical over time indicating the stability of the mucosoid culture. In addition, also mRNA expression levels of epithelial stemness marker (Figure 12C), epithelial cell marker (Figure 12D) and gland cell type marker (Figure 12E) were found to be similar at each passage. This shows that the regenerative capacity of the mucosoid cultures remains intact with time and that the epithelial identity of the cells and their differentiation capacity remains constant through the regenerative steps.

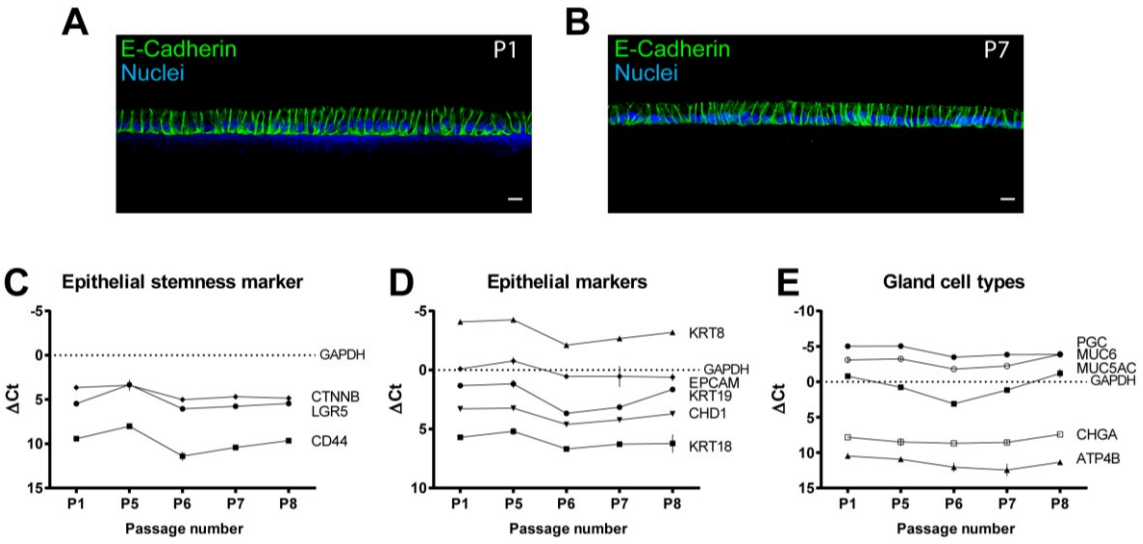

Figure 12: Mucosoid cultures show stable longevity through propagation keeping their characteristic features. Epithelial cells were grown in mucosoid cultures and were propagated by re-seeding on a new trans-well filter insert every four weeks for a total of eight months confirming the longevity of this culture model. Representative confocal micrographs of paraffinized filter section of mucosoids in (A) passage 1 (P1) and (B) passage 7 (P7) labeled by IF against E-Cadherin (green) and nuclei were counterstained with Draq5 (blue). Scale bar: 10 µm (C-E) qRT-PCR analysis for mRNA expression levels of (C) epithelial stemness marker genes, (D) epithelial marker genes and (E) gland cell types genes of passages P1, P5, P6, P7, and P8. Mucosoids from two patients (two biological replicates) were analyzed. Representative graphs from one replicate are shown. RT-PCR analysis was done by Dr. Francesco Boccellato.

The gastric gland comprises different cell types with specific functions like two different types of mucus-secreting cells, hormone-producing endocrine cells and digestive enzyme secreting chief cells. It was proven whether these cell types were also found in the mucosoids reflecting *in vitro* the heterogeneity found *in vivo* in the stomach. Therefore, paraffin sections of mucosoid filters were labeled by IF for foveolar cell marker mucin 5AC (MUC5AC), mucus gland cell marker mucin 6 (MUC6), enterochromaffin cell marker chromogranin A (CHGA) and chief cell marker pepsinogen C (PGC). Results are depicted in Figure 13 and demonstrate that mucosoids were strongly positive for MUC6 (Figure 13B) and showed only low MUC5AC expression (Figure 13A). CHGA labeling showed a strong signal in only few cells per section (Figure 13C) while the labeling appeared on the basal side characteristic for this cell type, which is responsible for the secretion of hormones into the bloodstream. PGC

labeling was very rare and was located on the apical side where PGC is secreted to the lumen also *in vivo* (Figure 13D).

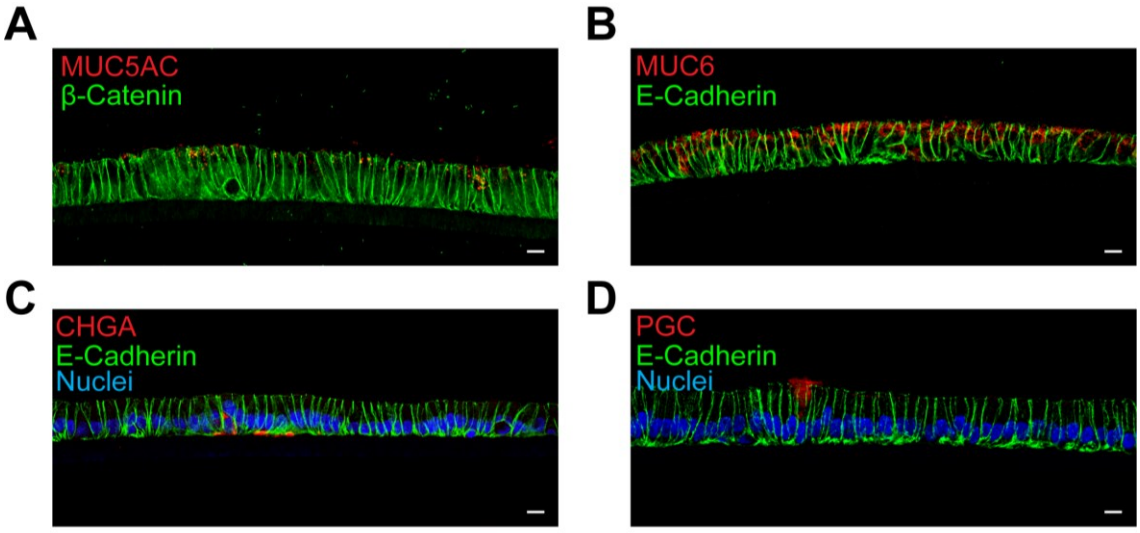

Figure 13: Mucosoid cultures comprise the cell types of the stomach gland *in vivo.* Representative confocal images of paraffinized sections of mucosoid cultures labeled by IF against different cell type marker: (A) pit cell marker MUC5AC (red); (B) mucus gland cell marker MUC6 (red); (C) endocrine cell marker CHGA (red); (D) chief cell marker PGC (red). Epithelial cells were visualized using an antibody against E-Cadherin (B,C,D, green) or β-Catenin (A, green). Nuclei were stained with dye Draq5. Scale bar: 10 µm.

3.1.2. WNT and RSPO influence foveolar differentiation in antral mucosoids

In the murine antrum, the stem cells are located in the base of the gland expressing the stem cell marker *Lgr5* (Barker et al. 2010). This stem cell population repopulates the entire gland through proliferation and migration up to the pit forming the foveolar lineage. *Lgr5* is a target gene of the Wnt signaling pathway and mediates Wnt pathway activation. Thus, the stem cell niche depends on WNT and the co-activator R-spondin. *In vitro,* this situation is mimicked by permanent supplementation of the cultivation medium with recombinant WNT3A (+W) and R-spondin (RSPO) 1 (+R). Consequently, it was tested which influence the Wnt pathway has in mucosoids and thereby on human gastric cells.

The activation of the Wnt pathway leads to the release and translocation of β-Catenin from the cytoplasm into the nucleus. IF labeling against β-Catenin in +W+R mucosoid cultures showed clearly the localization of β-Catenin in the nuclei of the cells confirming the active Wnt pathway (Figure 14B). In comparison, the cultivation of mucosoid cultures without WNT and RSPO1 (-W-R) for seven days led to inactivation of the Wnt pathway resulting in restraint of β-Catenin in the cytoplasm and especially at the plasma membrane (Figure 14A). Moreover, the inactivation of the Wnt pathway in -W-R mucosoid cultures significantly abolished the mRNA expression of the Wnt target gene *LGR5* (Figure 14C).

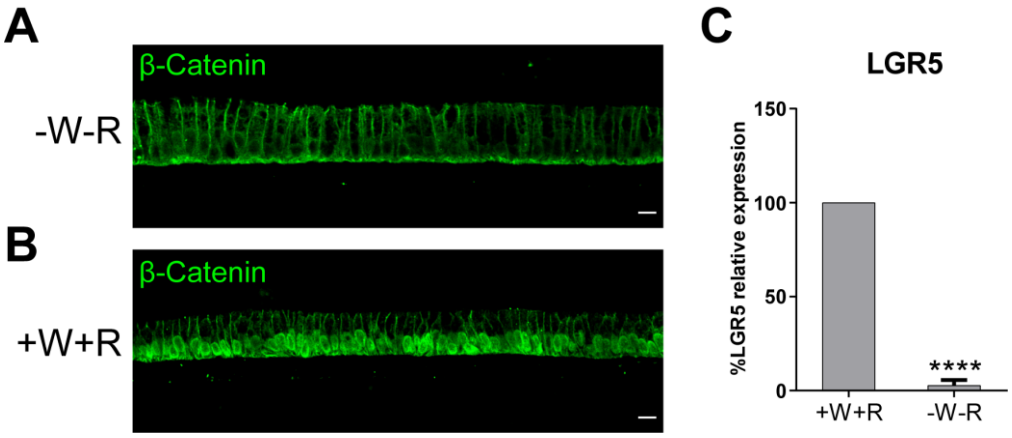

Figure 14: Inactivation of the Wnt pathway in mucosoid cultures restraint β-Catenin in the cytoplasm and reduced *LGR5* expression. (A-B) Representative confocal micrographs of paraffinized filter sections of mucosoids cultured with (+W+R, B) or without WNT and RSPO1 (-W-R, A) for seven days fluorescently labeled against β-Catenin (green). The experiment was done with two biological replicates originating from two patient samples. Scale bar: 10 µm. (C) mRNA expression analysis of WNT target gene *LGR5* in +W+R and -W-R mucosoid cultures. RT-PCR analysis was performed by Dr. Francesco Boccellato. Summary of three biological replicates calculated as mean ± SD. Unpaired Student's t-test, ****, $p < 0.0001$.

In the antrum, the proliferative zone is found in the sub-foveolar compartment just below the pit region in the gastric mucosa. This is confirmed by IF labeling for the proliferation marker Ki67 in human antral tissue (Figure 15C). In mucosoid cultures deprived from WNT3A and RSPO1 (-W-R) increased levels of proliferation marker Ki67 were observed (Figure 15B) compared to +W+R mucosoid cultures (Figure 15A). Along with the significantly higher proliferation rate in -W-R mucosoid cultures

(Figure 15D) the cells of -W-R mucosoid cultures showed an increase in cell height (32 µm in -W-R compared to 19 µm in +W+R) (Figure 15 A-B) and higher density of cells, displayed as the number of nuclei per 100 µm (Figure 15E).

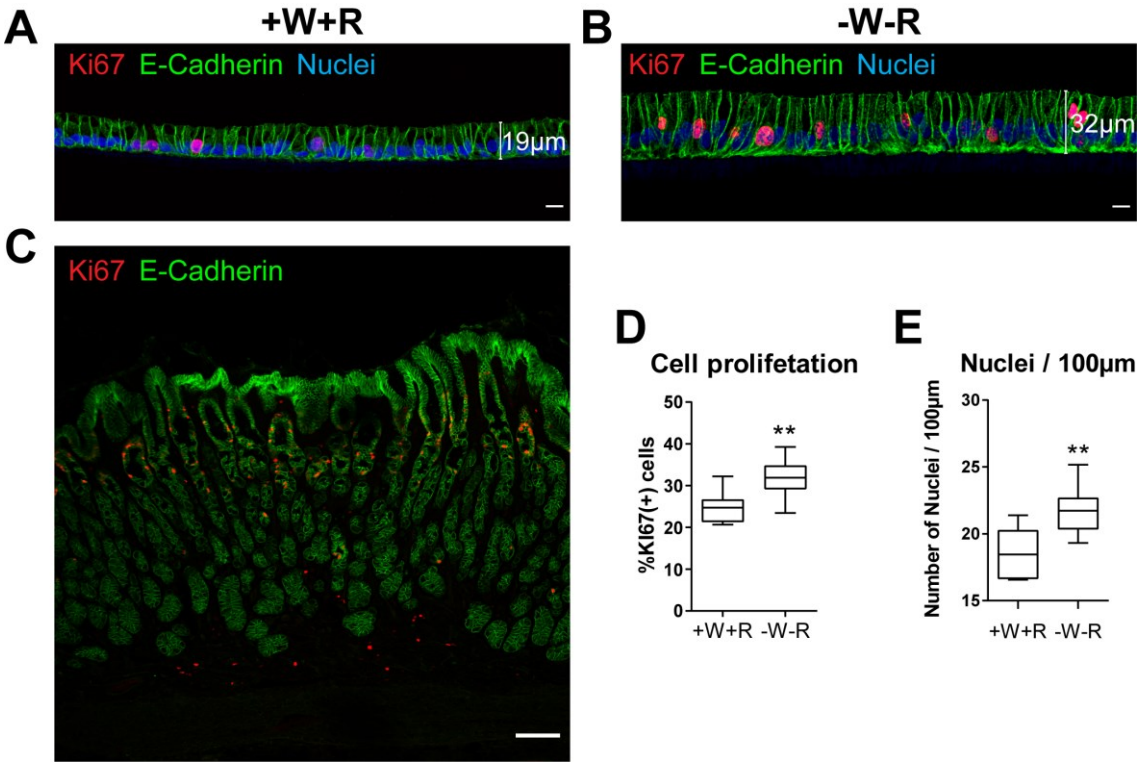

Figure 15: Inactivation of the Wnt pathway induced a higher proliferation rate in mucosoid cultures. Two or three biological replicates of mucosoid cultures were cultivated without WNT3A and RSPO1 for seven days. (A,B) Confocal images of paraffinized sections of (A) +W+R control and (B) -W-R mucosoid cultures labeled using IF against Ki67 (red) and E-Cadherin (green). The height of the epithelial monolayer was measured with ImageJ by drawing a bar from the basal to the apical side and using the "measure" tool of the program. Scale bar: 10 µm (C) Tissue section from human antrum was labeled by IF against Ki67 (red) revealing the proliferative zone in the antral gland to be located in the sub-foveolar region. Scale bar: 100 µm (D) Number of Ki67 positive nuclei in +W+R and -W-R mucosoid cultures were counted on eight sections per condition (n>400) and displayed as % of the average total cell number per section. (E) The total number of cells per 100 µm was enumerated from eight sections (n>400) in +W+R and -W-R condition. Unpaired Student's t-test **, $p < 0.01$. Data in (D) and (E) were generated by Dr. Francesco Boccellato.

As foveolar cells were represented in low abundance in the mucosoids under culture conditions including WNT3A and RSPO1 it was analyzed if lack of these Wnt pathway activators could induce differentiation into the foveolar lineage by depriving these

factors of the mucosoids cultivation cocktail. The effects of the treatments were analyzed through IF of filter sections for pit cell marker MUC5AC and mucus gland marker MUC6. Additionally, the mRNA expression level of both mucins *MUC6* and *MUC5AC* were analyzed with RT-PCR.

Obtained results (Figure 16) demonstrate that under normal +W+R condition, epithelial cells mainly express MUC6 (Figure 16A) and showed only low expression of MUC5AC (Figure 16B). The removal of both, WNT3A and RSPO1 for seven days switched the mucin pattern; -W-R cultured epithelial cells showed no MUC6 labeling (Figure 16C) and were only positive for MUC5AC (Figure 16D) indicating foveolar differentiation. The results obtained by analyzing mRNA expressions confirmed the IF results: *MUC6* mRNA expression levels were completely abolished in -W-R condition while *MUC5AC* mRNA expression was significantly upregulated compared to the +W+R control.

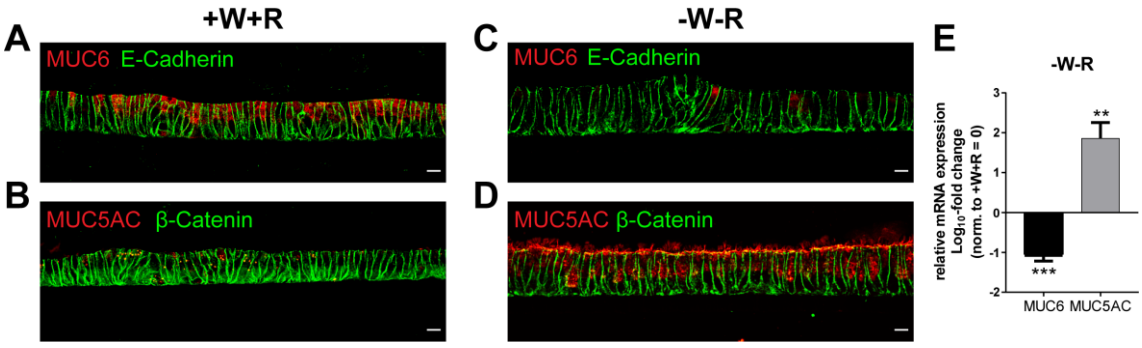

Figure 16: Removal of WNT3A and RSPO1 induced foveolar differentiation in epithelial cells. Mucosoids were cultured in the presence of WNT3A and RSPO1 (+W+R) or in the absence of both factors (-W-R) for seven days. (A-D) IF labeling of paraffinized sections against (A,C) MUC6 (red) and (B,D) MUC5AC (red) was performed. Epithelial cells were labeled with E-Cadherin or β-Catenin. Confocal images show one out of three biological replicates. Scale bar: 10 µm (E) mRNA expression levels of *MUC6* and *MUC5AC* were analyzed using RT-PCR (done by Dr. Francesco Boccellato) from -W-R mucosoid cultures and normalized to +W+R mucosoid cultures. Data represents the summary of three biological replicates from three patient samples depicted as mean ± SD. Unpaired Student's t-test **, $p < 0.01$; ***, $p < 0.001$.

Moreover removal of only RSPO1 (Figure 17 A-B) or only WNT3A (Figure 17 C-D) for seven days from the cultivation medium induced partial foveolar differentiation observed by positive IF labeling against MUC6 (Figure 17 A and C) and MUC5AC (Figure 17 B and D) under these conditions.

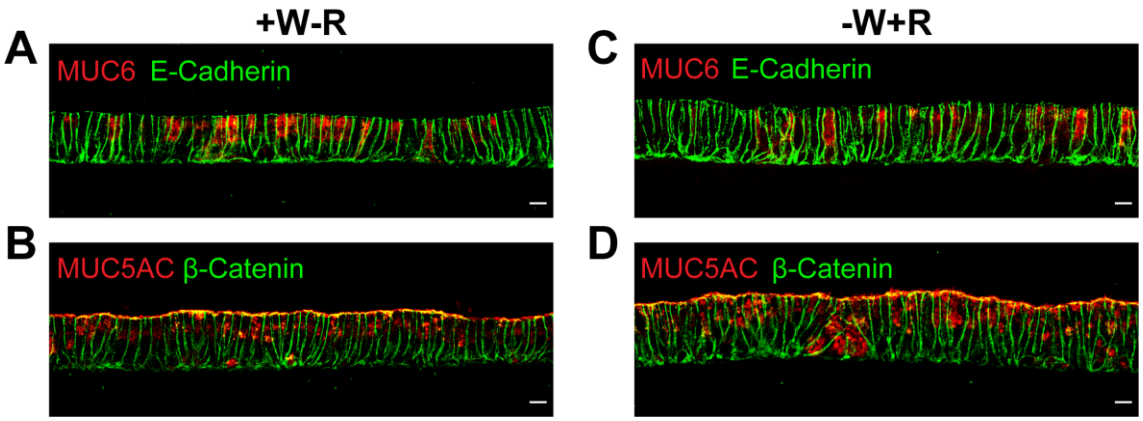

Figure 17: Removal of either RSPO1 or WNT3A from the cultivation medium induced partial foveolar differentiation in mucosoid cultures. Three biological replicates of mucosoids were cultivated either (A,B) without RSPO1 or (C,D) without WNT3A for seven days. Representative confocal images show IF labeling of paraffinized sections of mucosoids of each condition against (A,C) MUC6 (red) or (B,D) MUC5AC (red). E-Cadherin and β-Catenin respectively were used to visualize the epithelial cells. Scale bar: 10 µm.

Next, it was investigated whether the differentiation status of epithelial cells in mucosoids was reversible or permanent. Therefore, mucosoids were deprived from WNT3A and RSPO1 for 12 days followed by recovery in full medium (+W+R) for 12 days. +W+R mucosoid cultures served as a control as well as -W-R mucosoid cultures deprived from WNT3A and RSPO1 for a total of 30 days. As a read-out, the organoid forming capacity was analyzed by seeding the same number of single cells from mucosoid cultures in Matrigel. Obtained results showed that the differentiation of mucosoids into foveolar lineage was terminal (Figure 18). While single cells from +W+R mucosoid cultures showed very high organoid formation capacity (Figure 18, left panel) the opposite was observed for mucosoids deprived from WNT3A/RSPO1 for a total of 30 days. Here, no organoids were formed (Figure 18, right panel) confirming indirectly the loss of stem cells due to the significant reduction in *LGR5* expression as shown before. The restoration of WNT3A and RSPO1 resulted in the formation of only

very few organoids. Thus, the differentiation process was not reversible because foveolar cells, obtained by removal of WNT3A and RSPO1 were not able to regenerate even when WNT3A and RSPO1 were restored (Figure 18, middle panel) indicating a point of no return in the differentiation process when the Wnt pathway was inactivated.

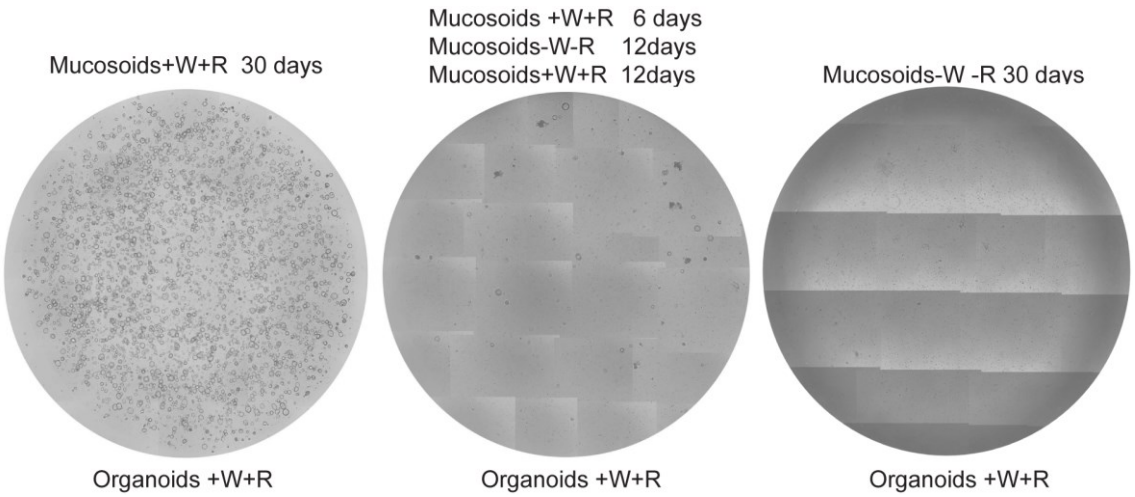

Figure 18: Foveolar differentiation of mucosoids was permanent and not reversible. Mucosoids treated with either +W+R for 30 days (left panel) or -W-R for 12 days followed by recovery in +W+R medium for 12 days (middle panel) or -W-R for 30 days (right panel) were trypsinized and 30 000 single cells were seeded in Matrigel in technical triplicates per condition to analyze the ability to grow into organoids. Seeded cells were cultivated in full medium supplemented with W/R for ten days and images of whole Matrigel drops were recorded.

3.2. Differentiation dynamics of the oxyntic gland

3.2.1. Characterization of human corpus tissue

The human corpus gland is differently structured compared to the antral gland as described in the introduction of this thesis (see 1.1.2). Corpus glands are deeper and harbor more types of cells of a secretory type like digestive enzyme-secreting chief cells, gastric acid-producing parietal cells and two major types of mucus-secreting cells. Very little is known about the differentiation dynamics of the different secretory cell types especially parietal cells and chief cells. Karam and Leblond (1993a) suggested that proliferative cells are located in the sub-foveolar and isthmus region of the corpus gland, proven by nucleotide incorporation experiments. Thus, first the localization of the proliferative zone was confirmed in human corpus tissue using IF labeling with an antibody against the proliferation marker Ki67 (Figure 19). Confocal images showed that Ki67 positive cells were only present in the sub-foveolar and isthmus region, close to and overlapping with a region that is described to be the stem cell compartment of the corpus gland in the murine model (Han et al. 2019).

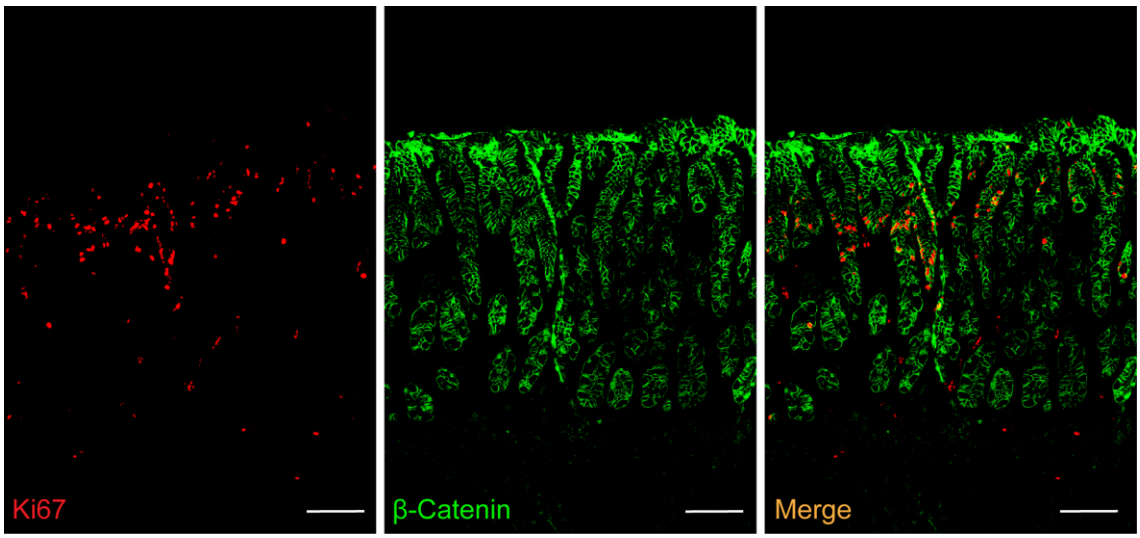

Figure 19: Localization of the proliferative zone in the corpus gland. Confocal micrographs of a human corpus tissue section fluorescently labeled against the proliferation marker Ki67 (red). Epithelial cells were visualized using an antibody against β-Catenin (green). Scale bar: 100 µm.

Two main types of mucus-producing cells are present in the gastric gland: mucin MUC5AC producing foveolar/pit cells and MUC6 secreting mucous neck cells. The latter are described to be the progenitors of chief cells in mice that arise through transdifferentiation (Karam and Leblond 1993c; Ramsey et al. 2007). IF labeling of corpus tissue sections against the pit cell marker MUC5AC and the mucous neck cell marker MUC6 (Figure 20) revealed that both compartments were strictly separated and not overlapping. MUC5AC positive cells were only detected in the foveolar region, while MUC6 positive mucous neck cells were only present below the foveolar and the isthmus, mainly in the neck but very few also in the base of the corpus gland.

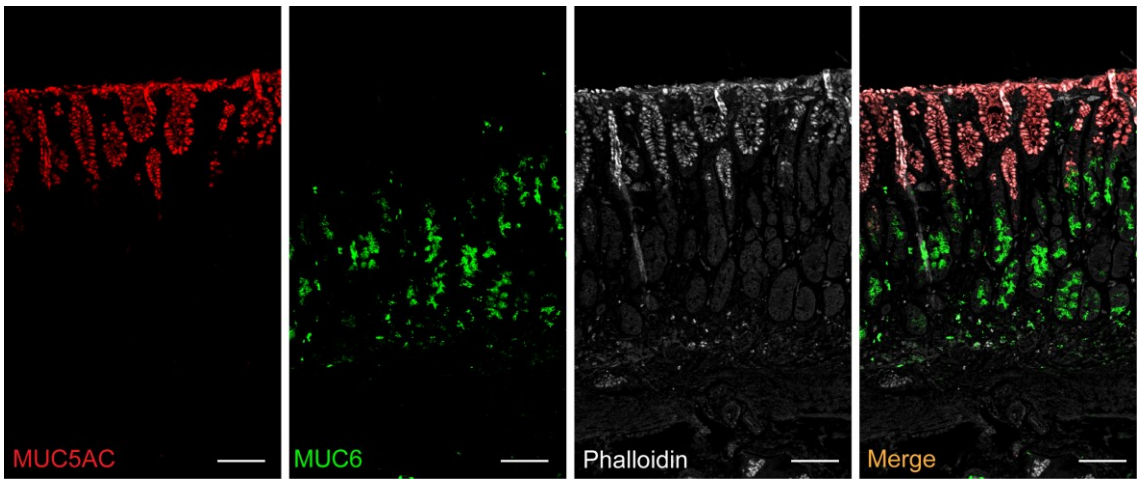

Figure 20: Localization of MUC5AC secreting foveolar cells and MUC6 secreting mucus neck cells. Confocal micrographs of human corpus tissue sections labeled by IF against MUC5AC (red) and MUC6 (green). Phalloidin (white) was used to visualize the cells. Scale bar: 100 µm.

Chief cells as well as parietal cells are the most characteristic cell types of the corpus gland and ensure the function of the entire stomach, the secretion of digestive enzymes and production of gastric acid. The localization of both cell types was of high importance to further explore the differentiation dynamics and niche factors of these cell types. IF staining of chief cells using the marker PGC for labeling revealed a high abundance of PGC+ chief cells in the base and the neck region of the gland (Figure 21A). Gastric acid-producing parietal cells are large in size and have a very characteristic triangular shape. IF labeling of parietal cells in human corpus tissue using

an antibody against the H^+/K^+ ATPase β-subunit (ATP4B) of the proton pump (Figure 21B) showed that parietal cells were distributed throughout the gland except for the outer pit region. Moreover, parietal cells were less present in the base of the gland where mainly chief cells were located.

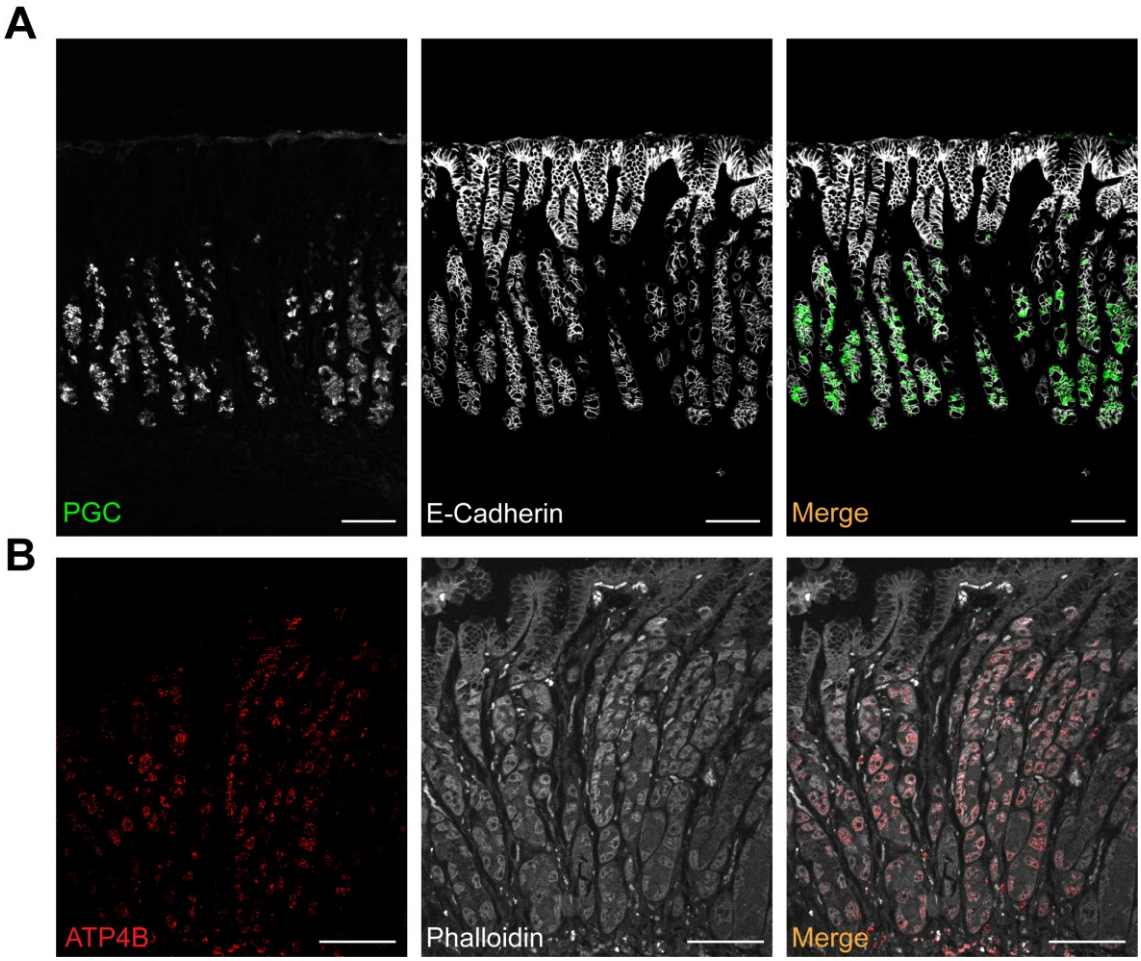

Figure 21: Localization of chief cells and parietal cells in human corpus tissue. (A) Confocal micrographs of corpus tissue sections showing chief cells by IF labeling using a specific antibody against PGC (green). Epithelial cells were visualized using an antibody against E-Cadherin (white). (B) Confocal micrograph representing parietal cells labeled by IF against the H+/K+ ATPase β-subunit of the proton pump (ATP4B, red). Cells were visualized by Phalloidin (white). Scale bar: 100 µm.

3.2.2. Corpus derived mucosoids are different from antrum derived mucosoids but lack important *in vivo* characteristics

Mucosoid cultures of corpus epithelial cells were generated following the same protocol used for antral mucosoid cultures. Corpus epithelial cells formed a fully sealed, polarized monolayer after ten days in ALI and accumulated mucus on the apical side as it was observed in antral mucosoids. A departmental co-worker Dr. Kristin Fritsche analyzed in her PhD thesis the similarities, commonalities, and differences of fundus, corpus, and antrum using mucosoid cultures and compared the matching efficiency and similarities of corpus mucosoid cultures and antral mucosoid cultures with the *in vivo* counterpart. The data in the following Figure 22 was generated in collaboration with Dr. Kristin Fritsche and is used in this thesis with her agreement. The direct comparison of antral and corpus mucosoids for regional specific genes revealed that clear difference between antral and corpus derived mucosoids exists (Figure 22 C). Antrum specific genes like gastrin (*GAST*) and *CDX2* were significantly higher expressed in antral mucosoid cultures compared to corpus mucosoids. Corpus specific genes like *IRX2* or ghrelin instead are completely down-regulated (*IRX2*) or not expressed (*ghrelin*) in antral mucosoids. Furthermore, gene set enrichment analyses (GSEA) of antral and corpus derived mucosoids were performed using the biopsy dataset from Nookaew et al. (2013) as a reference. The results demonstrated significant enrichment of antrum and corpus specific genes in the respective mucosoid culture indicating that the *in vitro* cultures maintained their antrum or corpus identity respectively. The GSEA comparison of antrum vs corpus (Figure 22A) showed a strong enrichment of antral genes in antral mucosoids, matching, with a high score (NES = 2.5), the differential expression of antrum vs corpus biopsies calculated from public dataset. Interestingly, the GSEA comparison of corpus vs antrum revealed instead that the corpus mucosoids showed a lower enrichment score (NES = 1.3) when compared to the same GSEA comparison of the respective biopsies (Figure 22B). Although a clear difference between antrum and corpus derived mucosoid cultures was shown, data for the comparison of corpus with antrum biopsies and corpus with antral mucosoids regarding the expression of parietal cell-specific genes revealed a lack of parietal cells in corpus derived mucosoids (Figure 22D). Typical parietal cell genes like the subunits of the H^+/K^+ ATPase proton pump (*ATP4A*, *ATP4B*) or the gastric intrinsic factor (*GIF*) were highly expressed in

corpus biopsies (Figure 22D in_vivo) but not in corpus mucosoids (Figure 22D in_vitro) indicating a lack of this important cell type *in vitro* and a non-optimal matching with the *in vivo* situation.

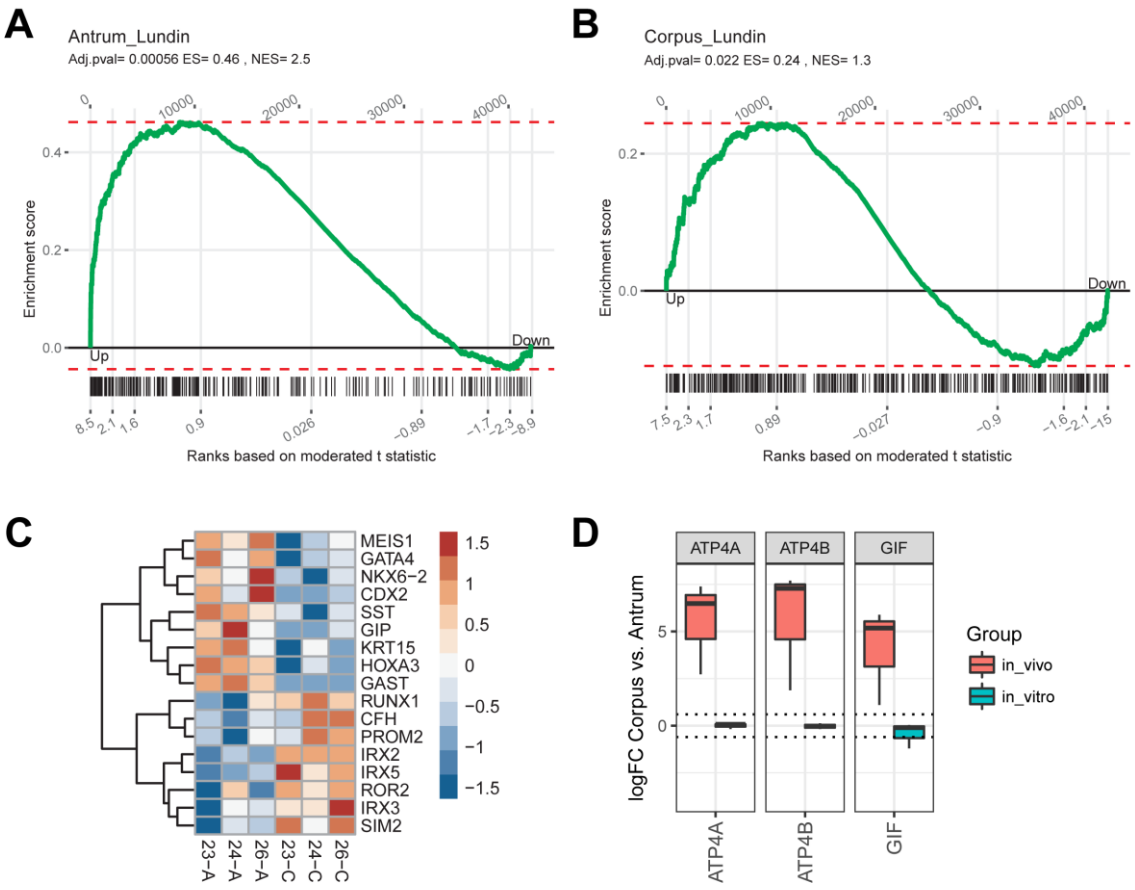

Figure 22: Corpus derived mucosoids are different from antrum derived mucosoids but do not fit the *in vivo* situation. (A-B) GSEA of differentially expressed genes in (A) antrum vs corpus and (B) corpus vs antrum derived mucosoid cultures determined by microarray analysis of three biological replicates and correlated with publicly available gene expression data from antrum vs corpus biopsies (Nookaew et al. 2013). (C) Heatmapt of significantly up- and downregulated genes in antrum vs corpus mucosoid cultures ($p<0.05$). (D) Boxplot of parietal cell markers that are upregulated in the public corpus vs antrum biopsies microarray data set (in_vivo, red) but not regulated when comparing corpus vs antrum derived mucosoid cultures (in_vitro, cyan). ES: enrichment score; NES: normalized enrichment score. The GSEA analysis and data visualization were performed by Dr. Kristin Fritsche.

3.2.3. Mapping of morphogens in the human corpus gland

In the mature intestine BMPs were found to be expressed in the villi (small intestine) and top of the crypts (colon), while Wnt pathway agonists are expressed in the crypt base inducing cell proliferation and supporting the stem cell niche. It was shown that BMPs counteract and modulate the Wnt/β-Catenin activity and the proliferation of stem cells in the crypt base thereby inducing cell differentiation along the crypt-villus axis (He et al. 2004; Auclair et al. 2007). Thus, the impact of BMP in the stomach was of interest and the localization of the two BMP pathway agonists BMP4 and BMP2 was analyzed in human corpus tissue using *in situ* hybridization with gene-specific RNA probes. Obtained results demonstrate that both morphogens BMP4, as well as BMP2, were mainly expressed by epithelial cells but also by stromal cells in the *lamina propria* (Figure 23). The distributions of BMP2 (Figure 23C) and BMP4 (Figure 23A) expression were higher in the foveolae/isthmus region and significantly lower in the gland base (Figure 23B and D).

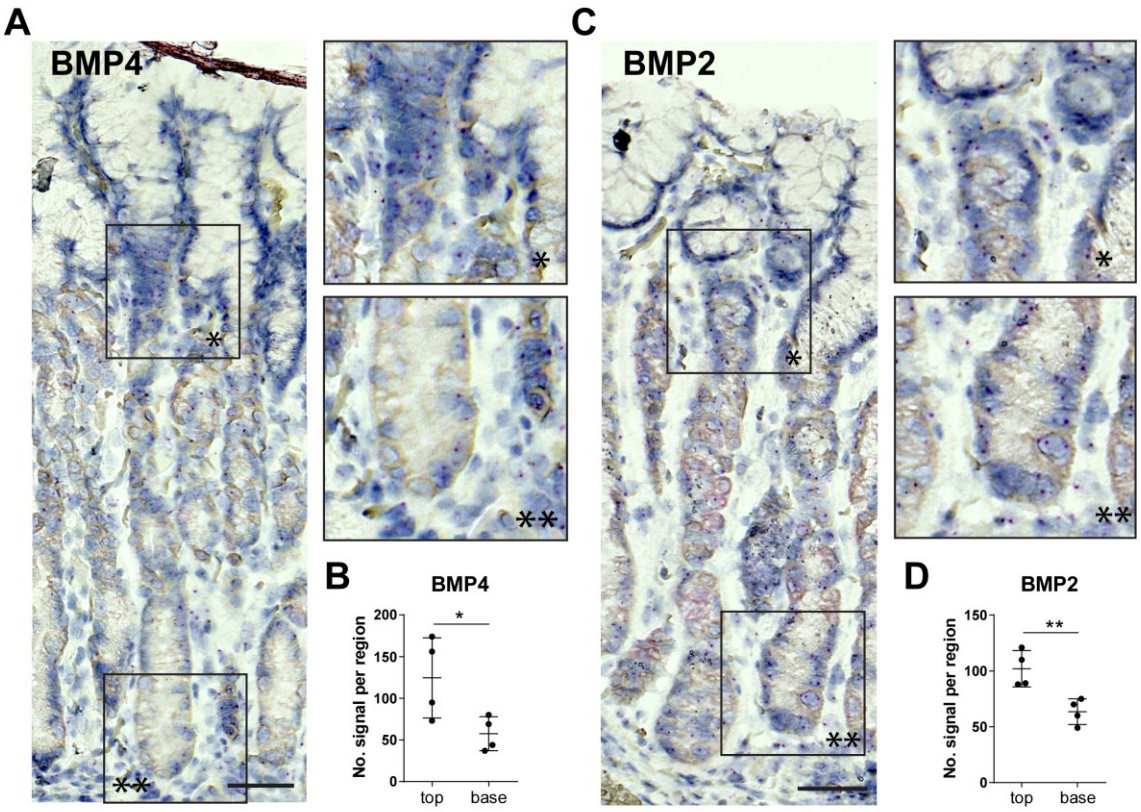

Figure 23: BMP4 and BMP2 showed higher expression in the pit region than in the base. Representative micrographs of RNA *in situ* hybridization of human corpus tissue using specific RNA probes for (A) BMP4 and (C) BMP2. The enlargements on the right are showing details of the isthmus (*) and base (**) of the gland. Scale bar: 50 µm. (B, D) Quantification of the signal spots per region divided in top and base for (B) BMP4 and (D) BMP2. Four microscopic images (technical replicates) of the whole gland from pit to base from two distinct patient samples were used for quantification respectively. Data shows results from one patient with the mean ± SD (error bars). Analysis was performed in ImageJ using the tools 'colour deconvolution', 'threshold' and 'analyze particles'. Top and base were defined by a square with a height of 90-110 µm which was measured from the top of the gland (defined as "top") and from the bottom where the gland started (defined as "base"). Unpaired Student's t-test of technical replicates, *, $p < 0.05$; **, $p < 0.01$.

The BMP pathway activity is regulated by antagonists like Noggin, gremlin or chordin-like to protect for instance the stem cell niche from BMP (Kosinski et al. 2007). Although in mice Noggin could only be detected in traces in the gut (He et al. 2004), the localization of this potent BMP antagonist was assessed in the human corpus tissue through IF labeling using a specific antibody (Figure 24). Interestingly, Noggin was detected in stromal cells of the *muscularis mucosae* right below the base of the gland and the *lamina propria* surrounding the base region but was not expressed by epithelial

cells as the Noggin labeling was not overlapping with epithelial cell labeling (β-Catenin). Due to the very specific localization of Noggin, a gradient of BMP activation is expected that is higher in the pit region and decreased towards the base of the gland.

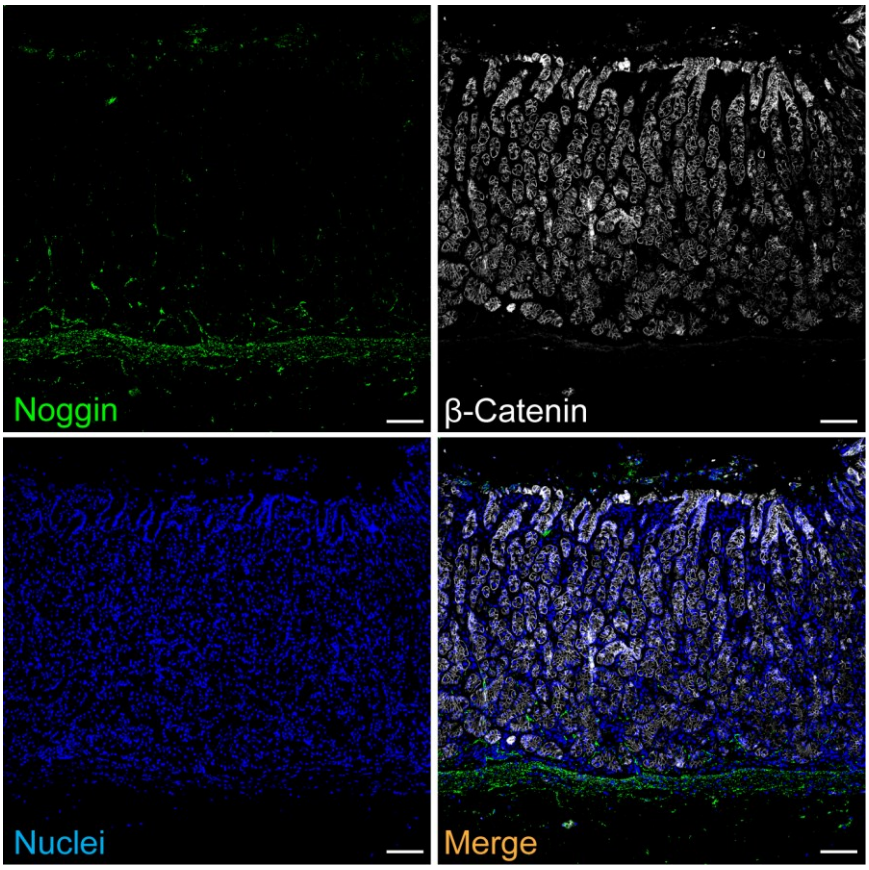

Figure 24: Noggin is expressed by *muscularis mucosae* cells below the base of gastric glands. Representative confocal micrographs of a human corpus tissue section labeled by IF against Noggin (green), epithelial marker β-Catenin (white) and nuclei staining with Dapi (blue). Scale bar: 100 µm.

Next, the localization of EGF and its homolog TGFα were assessed using *in situ* hybridization of human corpus tissue. EGF is a trigger of proliferation, supporting the stem cell niche and makes it indispensable for *in vitro* culture of primary epithelial cells of the gut (Sato et al. 2009; Sato and Clevers 2013). In contrast, chief cells, as well as parietal cells, show very low proliferative capacity suggesting that a co-localization of these cell types and the mitogens is unlikely. Obtained results (Figure 25) showed that EGF and TGFα are significantly higher expressed in the foveolae and isthmus region

than in the base of the gland generating a decreasing gradient of EGF and TGFα respectively from the pit to the base of the gland.

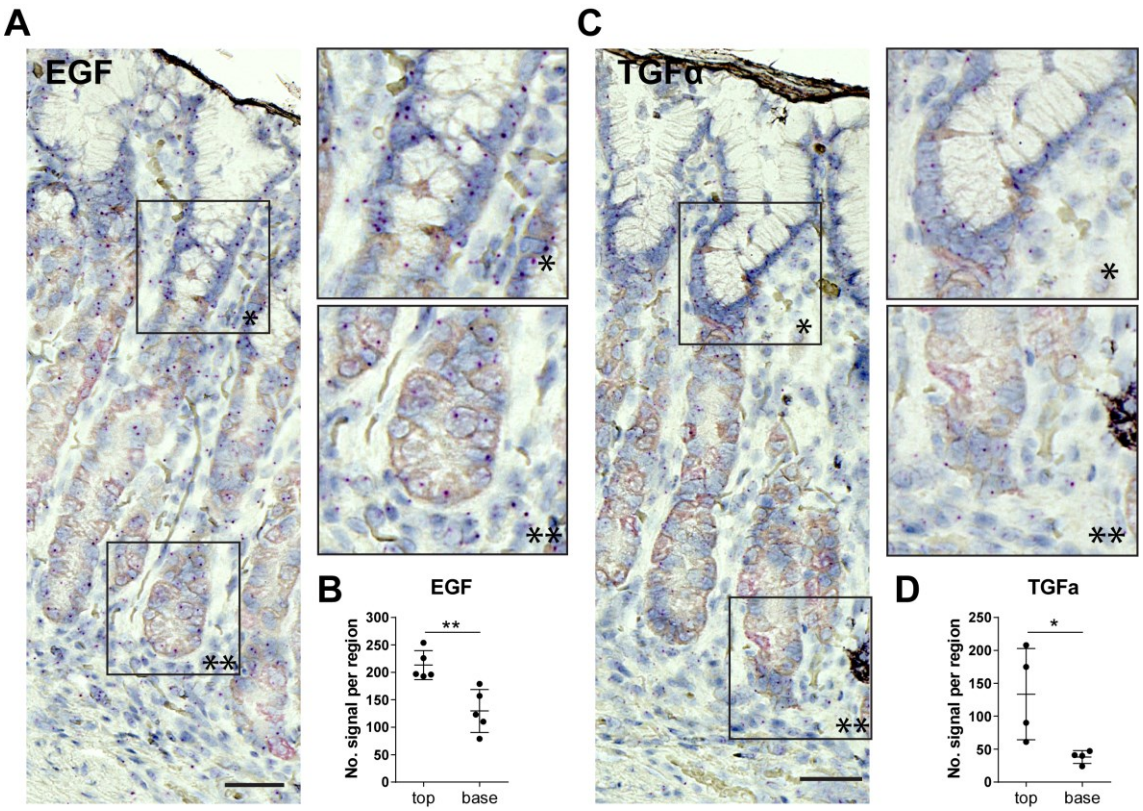

Figure 25: EGF and TGFα showed significantly higher expression in the pit region than in the base. Representative micrographs of RNA *in situ* hybridization of human corpus tissue using specific RNA probes for (A) EGF and (C) TGFα. The enlargements on the right are showing details of the isthmus (*) and base (**) of the gland. Scale bar: 50 µm. (B,D) Quantification of the signal spots per region divided into top and base for (B) EGF and (D) TGFα. Four microscopic images (technical replicates) displaying the whole gland from pit to the base from two distinct patient samples were used for quantification respectively. Data show representative results from one patient with mean ± SD (error bars). The analysis was performed in ImageJ using the tools 'colour deconvolution', 'threshold' and 'analyze particles'. Top and base were defined by a square with a height of 90-110 µm which was measured from the top of the gland (defined as "top") and from the bottom where the gland started (defined as "base"). Unpaired Student's t-test of technical replicates, *, $p < 0.05$; **, $p < 0.01$.

3.2.4. BMP and EGF play important roles in foveolar differentiation in the corpus gland

An active Wnt pathway is crucial for maintaining the stemness in antral mucosoid cultures and is ensured by supplementing the culture medium with recombinant WNT3A and RSPO1. The removal of WNT3A and RSPO1 from the cultivation medium induced foveolar differentiation in antral mucosoid cultures characterized by the switch in the mucin profile from MUC6 to MUC5AC (see Figure 16). An identical experiment was performed with corpus mucosoid cultures to investigate the dynamics of the foveolar differentiation in the corpus gastric gland. Therefore, corpus mucosoids were deprived from WNT3A and RSPO1 (-W-R) and compared to +W+R corpus mucosoids. IF labeling against the mucus neck cell marker MUC6 (Figure 26A and B) and the pit cell marker MUC5AC (Figure 26 C and D) revealed that +W+R mucosoids showed a strong signal for MUC6 and were negative for MUC5AC, while -W-R mucosoids showed the opposite. These -W-R mucosoid cultures were negative for MUC6 but highly positive for MUC5AC indicating that they have acquired the phenotype of foveolar cells. Additionally, the mRNA expression levels of *MUC6* and *MUC5AC* were analyzed and results confirmed the mucin expression pattern observed in IF (Figure 26E). *MUC6* mRNA expression was significantly down-regulated in -W-R mucosoid cultures, whereas the mRNA expression of *MUC5AC* was significantly up-regulated. These observations indicate that the foveolar differentiation in corpus mucosoids is regulated by WNT3A and RSPO1.

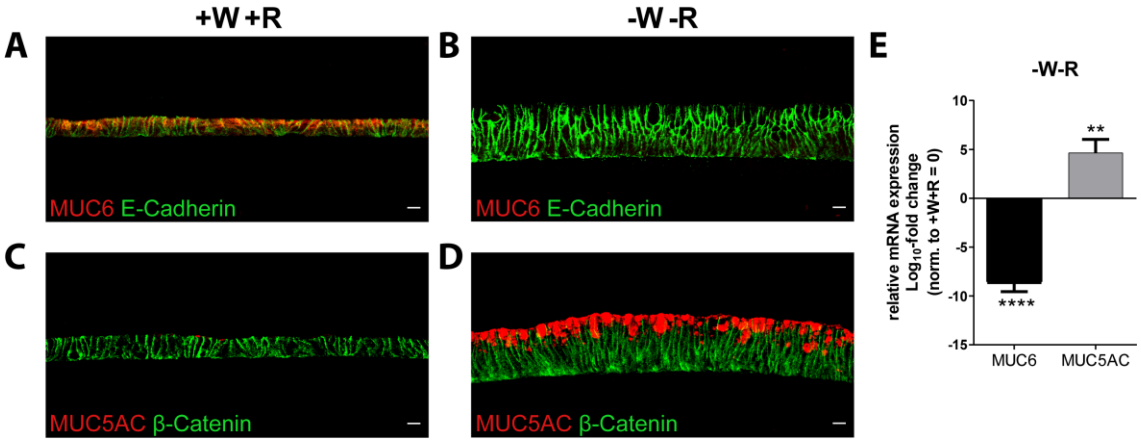

Figure 26: Removal of WNT3A and RSPO1 induced foveolar differentiation in corpus mucosoid cultures. Corpus mucosoid cultures of three different patient samples were grown either in the presence of W/R (+W+R) or absence of W/R (-W-R) for seven days. (A-D) Confocal micrographs of paraffinized sections were fluorescently labeled against (A,B) MUC6 or (C,D) MUC5AC. One representative image of one patient sample is shown for each condition. Scale bar: 10 µm. (E) RT-PCR analysis of *MUC6* and *MUC5AC* mRNA expression levels in +W+R and -W-R mucosoid cultures from three biological replicates derived from three patient samples shown as mean ± SD normalized to +W+R. Unpaired Student's t-test, **, $p < 0.01$; ****, $p < 0.0001$.

Next, the influence of the BMP pathway on foveolar differentiation was tested. As previously mentioned in the intestine BMP induces epithelial cell differentiation which is inhibited by BMP antagonists secreted by stromal cells surrounding the stem cell niche to protect the Wnt-dependent stem cells (Auclair et al. 2007) Thus, BMP could also be an important niche factor for the foveolar differentiation in the stomach.

Epithelial cells were a source of BMP4 as the *in situ* hybridization data showed (see Figure 23A). To maintain the longevity of the gastric primary cell culture the cultivation cocktail is constantly supplemented with Noggin, a strong antagonist of BMP4. If epithelial cells secrete BMP's *in vitro* the Noggin in the cultivation medium would prevent any action of intrinsic BMP. Thus, corpus mucosoids were deprived from Noggin for 12 days and mRNA expression level of the BMP target gene *ID1* was analyzed as a readout for an active BMP pathway (Figure 27A). The depletion of Noggin indeed significantly increased the mRNA expression level of *ID1* indicating an active BMP pathway through intrinsic BMP stimulation in epithelial cells in the absence of Noggin.

The Wnt pathway is fully active in corpus mucosoid cultures due to constant supplementation of the medium with WNT3A and RSPO1. If the intrinsic BMP has an influence on the Wnt pathway, this would result in changes in Wnt target gene expression. Hence, the mRNA expression level of *LGR5,* as a Wnt target gene was assessed in mucosoid cultures deprived from Noggin (Figure 27B). *LGR5* mRNA expression was significantly reduced in the absence of Noggin, indicating that the intrinsic BMP had an inhibitory effect on the Wnt pathway. Inactivation of the Wnt pathway induced foveolar differentiation in corpus mucosoids, consequently the mRNA expression level of the foveolar cell marker *MUC5AC* was analyzed together with the mRNA expression level of *MUC6* (Figure 27B) in Noggin deprived mucosoids. Obtained results demonstrate a significant decrease in *MUC6* mRNA expression and a significant increase in *MUC5AC* mRNA expression in Noggin deprived mucosoid cultures indicating a foveolar differentiation driven by intrinsic BMP.

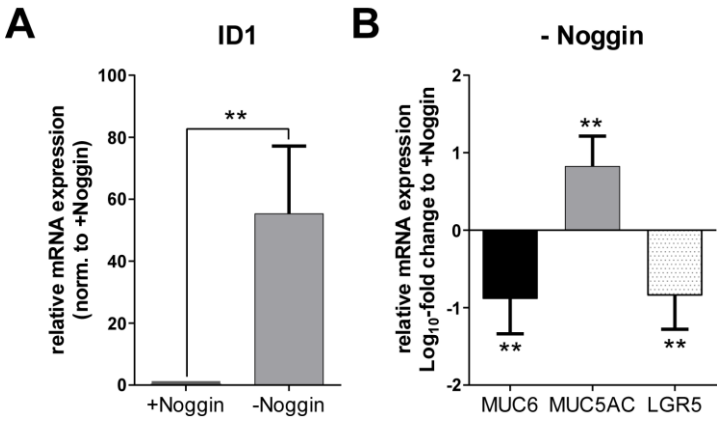

Figure 27: Depletion of Noggin leads to activation of the BMP pathway in corpus mucosoid cultures and foveolar differentiation. Corpus mucosoid cultures of two different patient samples with a total of four to six replicates were cultivated either in the presence of Noggin (+Noggin) or without Noggin (-Noggin) for 12 days. (A) mRNA expression level of *ID1* was analyzed by RT-PCR. Data show the mean ± SD. (B) RT-PCR analysis of the mRNA expression levels of *MUC6, MUC5AC* and *LGR5,* shown as mean ± SD and normalized to +Noggin condition (=0). Paired Student's t-test, **, $p < 0.01$.

Next, the role of EGF in foveolar differentiation was assessed as the *in situ* data suggested a gradient from pit to base and higher expression of EGF in the foveolar region. First, the depletion of EGF from the cultivation medium was tested either in the

presence or absence of Noggin. *LGR5*, *MUC5AC,* and *MUC6* mRNA expression levels were analyzed by RT-PCR (Figure 28) and the results indicated a significant dependency of foveolar cells on EGF. Only in the presence of EGF and the simultaneous absence of Noggin a significant increase in *MUC5AC* (Figure 28B) expression was observed. In parallel *MUC6* (Figure 28C) and *LGR5* (Figure 28A) expression were significantly down-regulated under this condition. Thus, foveolar differentiation not only depends on BMP but also on the presence of EGF.

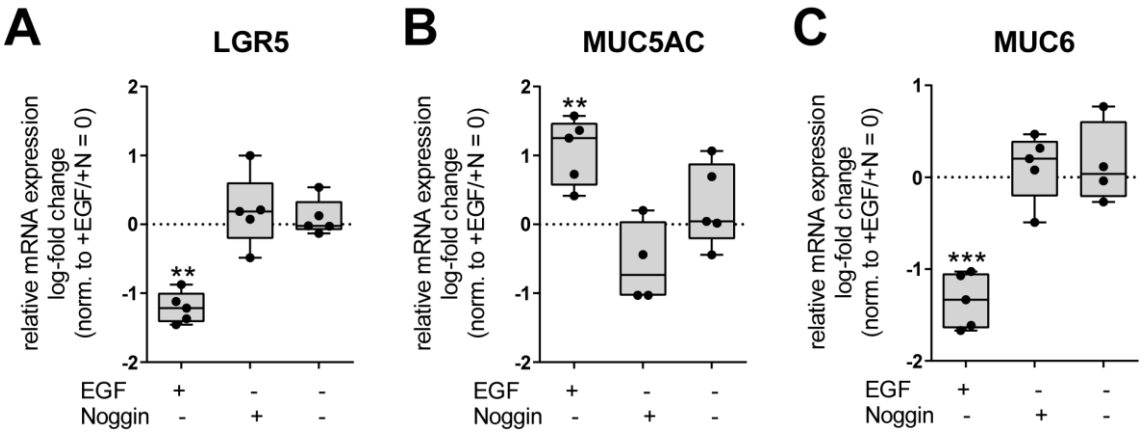

Figure 28: Influence of EGF on foveolar differentiation in corpus mucosoids. Corpus mucosoid cultures of two different patient samples with a total of five replicates were cultivated in the presence or absence of Noggin or EGF or both for 12 days. RT-PCR was performed to analyze the mRNA expression levels of (A) *LGR5,* (B) *MUC5AC* and (C) *MUC6.* Data is summarized in boxplots showing the median with 95 % CI. Error bars: min and max values. Data were normalized to +EGF/+Noggin (+N) condition (=0). Paired Student's t-test, **, $p < 0.01$; ***, $p < 0.001$.

Normal mucosoid cultures are propagated in the presence of high concentrations (150 ng/mL) of Noggin. To investigate the threshold of Noggin on BMP pathway inhibition, corpus mucosoids were cultivated with an increasing amount of Noggin in either the presence or absence of EGF and RT-PCR was performed to analyze the mRNA expression levels of *ID1*, *LGR5*, *MUC5AC,* and *MUC6* (Figure 29). Obtained results demonstrate that Noggin concentrations higher than 5 ng/mL blocked the BMP pathway because no mRNA expression of the BMP target gene *ID1* (Figure 29A) was detected. In parallel upregulation of the *MUC5AC* mRNA expression (Figure 29C) implying foveolar differentiation and downregulation of *LGR5* mRNA expression

(Figure 29B) were only observed for low Noggin concentration or in its absence. Additionally, the supplementation with EGF was a strict requirement. Without EGF no induction of *MUC5AC* was detected regardless of the withdrawal of Noggin. Similar observations were made for *LGR5* mRNA expression. Only in the presence of EGF, the increasing BMP inhibition with Noggin resulted in a decrease of *LGR5* mRNA expression. The expression of *MUC6* mRNA followed the same tendency and was directly proportional to the Noggin concentration (Figure 29D).

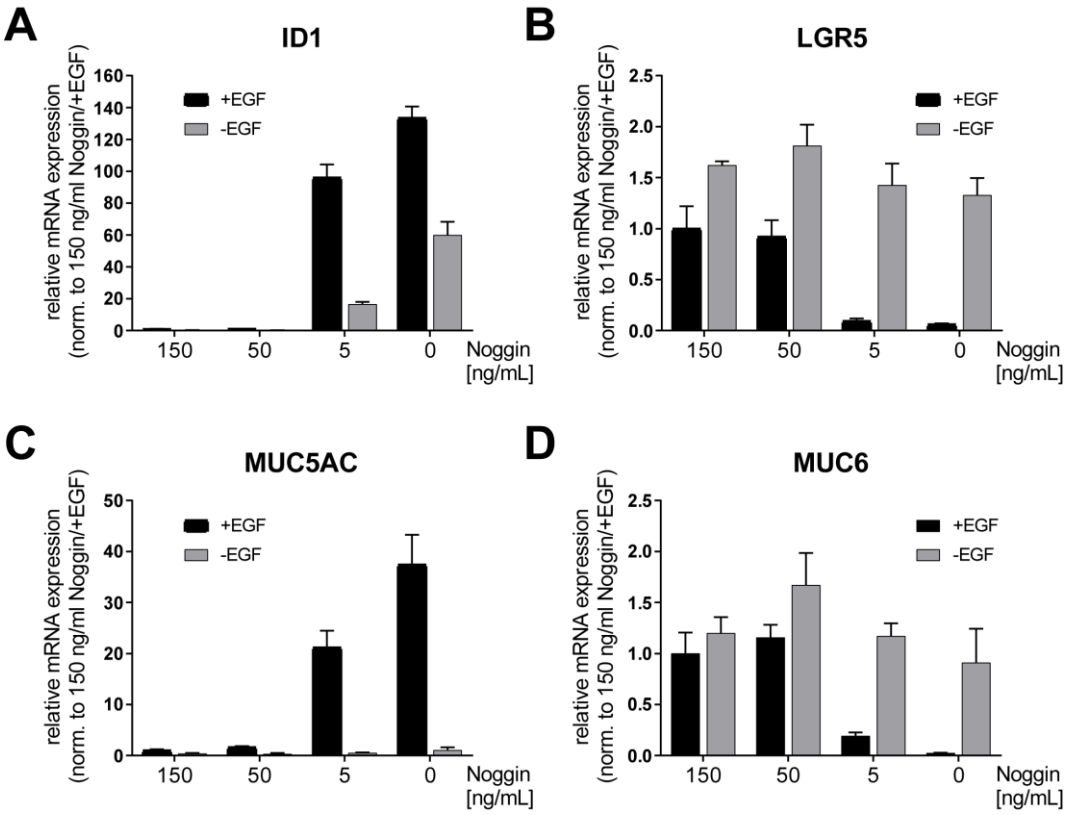

Figure 29: Foveolar differentiation highly depends on EGF and the BMP concentration. Corpus mucosoid cultures of two different patient samples (two replicates) were cultivated in the presence or absence of EGF and different concentrations of Noggin (0-150 ng/mL) for 12 days. mRNA expression levels of (A) *ID1,* (B) *LGR5*, (C) *MUC5AC,* and (D) *MUC6* were analyzed by RT-PCR. Representative data from one patient are shown. Error bars represent min and max values of technical triplicate.

EGF activates the EGFR-MEK-ERK-signaling pathway through binding to the EGF receptor (EGFR), inducing proliferation. To confirm whether EGF signals through the EGFR-MEK-ERK cascade to induce foveolar differentiation a downstream inhibitor for

MEK (PD0325901, MEKi) was applied on Noggin deprived corpus mucosoids to block the effect of EGF. RT-PCR analysis for the mRNA expression levels of *MUC5AC, MUC6,* and *LGR5* (Figure 30A) revealed that *MUC5AC* mRNA expression was significantly abolished in +MEKi condition confirming that EGF signals through the EGFR-MEK-ERK pathway and that the treatment with MEKi prevent foveolar cell differentiation. Concurrently the mRNA expression levels of *MUC6* and *LGR5* were significantly altered in +MEKi condition indicating the habitation of mucus neck cells in this culture. Furthermore, the abundances of MUC5AC (Figure 30B) and MUC6 (Figure 30C) in the accumulated mucus were assessed using mass spectrometry (MS). Previously shown results for MUC5AC from RT-PCR were confirmed in MS analysis (No statistical analysis was performed due to too little number of replicates.): MUC5AC was completely reduced in +MEKi condition however the abundance of MUC6 did not change. In mice, Trefoil factor (TFF) 1 is secreted by pit cells and can be used as a further marker of foveolar cells (Karam, Tomasetto, and Rio 2004). The MS analysis of the mucus revealed that MEKi treated mucosoids showed a lower abundance of TFF1 and in three out of four replicates TFF1 was not detected anymore (Figure 30D) confirming that under this condition no pit cells arise.

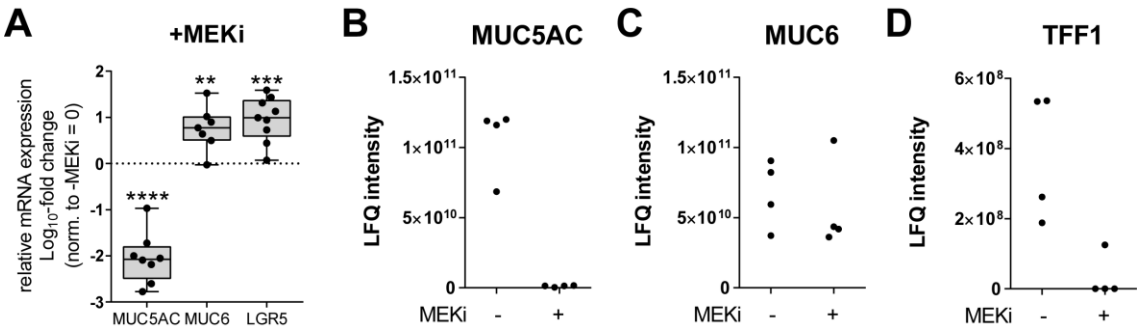

Figure 30: Inhibition of EGF signaling pathway with MEKi blocked foveolar differentiation. (A) RT-PCR analyses of the mRNA expression levels of *MUC5AC, MUC6,* and *LGR5*. Boxplots show median with 95 % CI and error bars represent min and max values of seven to nine biological replicates from two distinct patient samples. Data were normalized to non-treated, Noggin deprived control (-MEKi = 0). Paired Student's t-test, **, $p < 0.01$; ***, $p < 0.001$; ****, $p < 0.0001$. (B-D) MS analysis of mucus from Noggin deprived non-treated or MEKi treated corpus mucosoid cultures after 12 days of treatment. The abundance of (B) MUC5AC, (C) MUC6 and (D) TFF1 are displayed in a dot plot. Data shows values of single measurements of four biological replicates from two distinct patient samples. LFQ: label-free quantification. The sample preparation and LC-MS/MS analysis were performed by Monika Schmid from the MPIIB core facility Mass spectrometry.

3.2.5. EGF regulates chief cell differentiation through MAPK pathway

Chief cells are a characteristic cell type of the corpus gland and are essential for the secretion of digestive enzymes like pepsinogen and lipase. EGF and Noggin are important supplements for the cultivation of gastric primary cells to ensure the longevity of the mucosoid cultures. As chief cells are fully differentiated, long-living and rarely proliferating, it was of interest to test whether the inhibition of proliferation was involved in the differentiation process of chief cells. EGF is a prominent morphogen inducing proliferation in target cells via the EGFR-MAPK pathway (Zeng and Harris 2014). To stop proliferation in corpus mucosoid cultures and abolish the effect of EGF on the epithelial cells, EGF was depleted from the cultivation cocktail for 12 days. Along with EGF, Noggin was removed in part of the sample set as well to test the effect of intrinsic BMP on chief cell differentiation. The analysis of the mRNA expression levels of chief cell marker genes *PGC* and *MIST1* (Figure 31) revealed that depletion of EGF induced chief cell differentiation in vitro marked by a significant increase in *PGC* mRNA expression (Figure 31A). The removal of Noggin had an additional positive effect on the induction of *PGC* indicating a role of intrinsic BMP on the differentiation of chief cells. The results of the mRNA expression level of *MIST1* (Figure 31B) were not consistent but showed a trend similar to *PGC* with increased expression in the absence of EGF and Noggin. The removal of Noggin alone did not have an effect on chief cell marker mRNA expression.

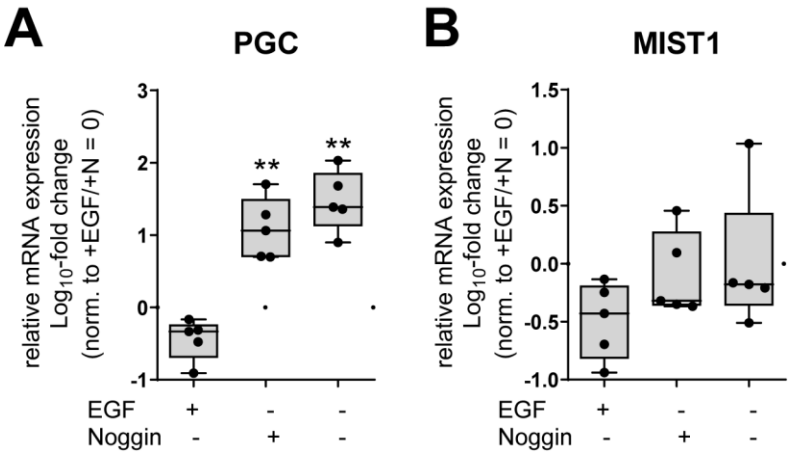

Figure 31: Depletion of EGF promoted chief cell differentiation. Corpus mucosoid cultures of five biological replicates of two different patient samples were either deprived from Noggin or EGF or both for 12 days. mRNA expression levels of chief cell marker (A) *PGC* and (B) *MIST1* were analyzed by RT-PCR. Data in boxplots represent median with 95 % CI. Error bars represent min and max values. Data were normalized to +EGF/+Noggin (+N) control (=0). Paired Student's t-test, **, $p < 0.01$.

To further confirm the role of EGF and thereby proliferation and intrinsic BMP on chief cell differentiation corpus mucosoids were treated with an increasing amount of Noggin to regulate the intrinsic BMP concentration either in the presence or absence of EGF. The results for *PGC* shown in Figure 32A indicate that the dynamic of chief cell differentiation highly depends on the absence of EGF. The Noggin concentration was secondary in the differentiation process. The data implies that the chief cell differentiation is not affected by low BMP signaling. The changes in the mRNA expression of *MIST1* (Figure 32B) were not as prominent as for *PGC*, but the data indicate that *MIST1* mRNA expression was induced only in the absence of EGF, independent of Noggin.

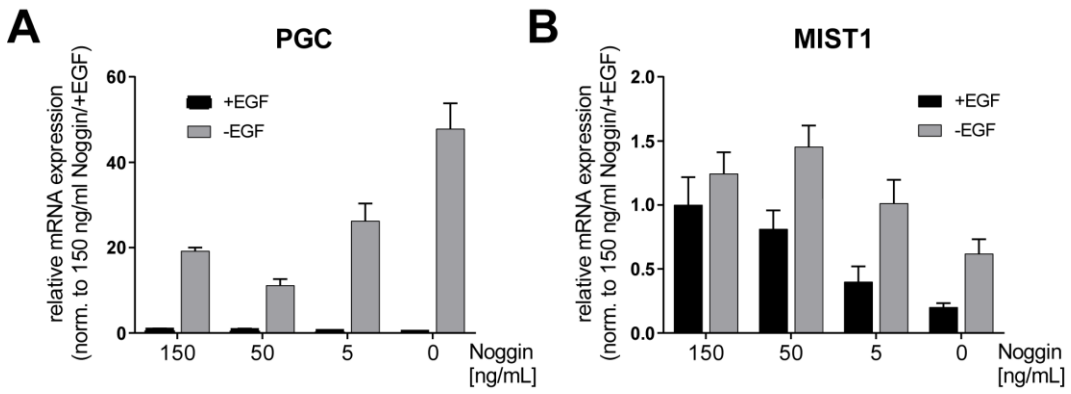

Figure 32: Absence of EGF is crucial for chief cell differentiation. Corpus mucosoid cultures of two different patient samples (two replicates) were cultivated in the presence or absence of EGF and different concentrations of Noggin (0-150 ng/mL) for 12 days. mRNA expression level of (A) *PGC* and (B) *MIST1* were analyzed by RT-PCR. Representative data from one patient are shown. Error bars represent min and max values of technical triplicate.

Moreover, the downstream inhibitor for MEK (PD0325901, MEKi) was applied on corpus mucosoids instead of EGF removal to abolish proliferation and the effect of EGF and to confirm whether the EGFR-MEK-ERK pathway also plays a role in the chief cell differentiation. As the removal of EGF together with the depletion of Noggin showed the highest increase in chief cell marker genes (see Figure 31) all subsequent experiments were done with depletion of Noggin from the cultivation medium to provoke intrinsic BMP activation. The depletion of Noggin alone did not have an effect on chief cell differentiation, thus Noggin deprived mucosoids were used as control. Additionally, corpus mucosoids were treated with extrinsic BMP4 (50 ng/mL) to test which effect a high dose of BMP4 had on the chief cell differentiation. The results depicted in Figure 33 showed a significant up-regulation of *MIST1* (Figure 33B) in +MEKi condition. The stimulation with extrinsic BMP4 instead impaired *MIST1* mRNA expression and thereby the chief cell differentiation. Similar and even stronger observations were made for *PGC* (Figure 33A): The inhibition of the EGFR pathway with MEKi strongly induced *PGC* mRNA expression with high significance while extrinsic BMP4 blocked and impaired the *PGC* mRNA expression and thereby chief cell differentiation.

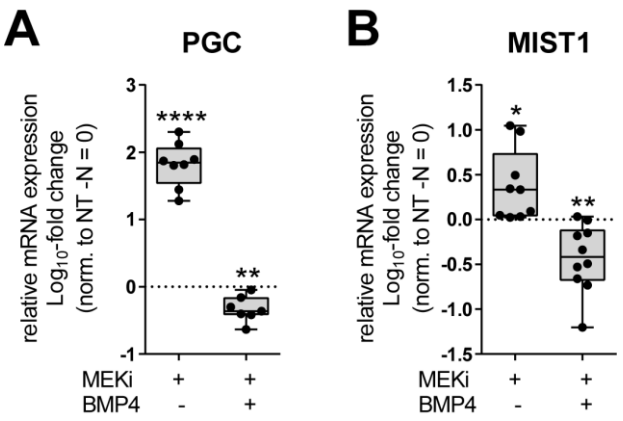

Figure 33: Inhibition of the EGFR-MAPK pathway induced chief cell differentiation, while a high concentration of BMP4 inhibited the differentiation. Seven to ten biological replicates of two different patient samples of corpus mucosoid cultures were treated with MEKi for 12 days, preventing a downstream activation of the EGF receptor pathway. A further sample set was treated with MEKi and BMP4 (50 ng/mL) for 12 days. RT-PCR was performed to analyze the mRNA expression levels of (A) *PGC* and (B) *MIST1*. Data represent the median with 95 % CI. Error bars: min and max values. Data were normalized to non-treated, Noggin deprived control (NT –N =0). Paired Student's t-test, *, $p < 0.05$; **, $p < 0.01$; ****, $p < 0.0001$.

The differentiation towards chief cells through inhibition of the EGF signaling pathway was further confirmed on protein level by whole mount IF labeling against PGC (Figure 34). While in non-treated samples (Figure 34A) only very few PGC positive cells were detected, a significant increase of PGC positive cells was observed in MEKi treated samples (Figure 34B). The number of PGC positive cells was determined in both conditions (Figure 34C), confirming the significantly higher number of PGC+ cells in +MEKi condition [+16.8 ± 6.7 %].

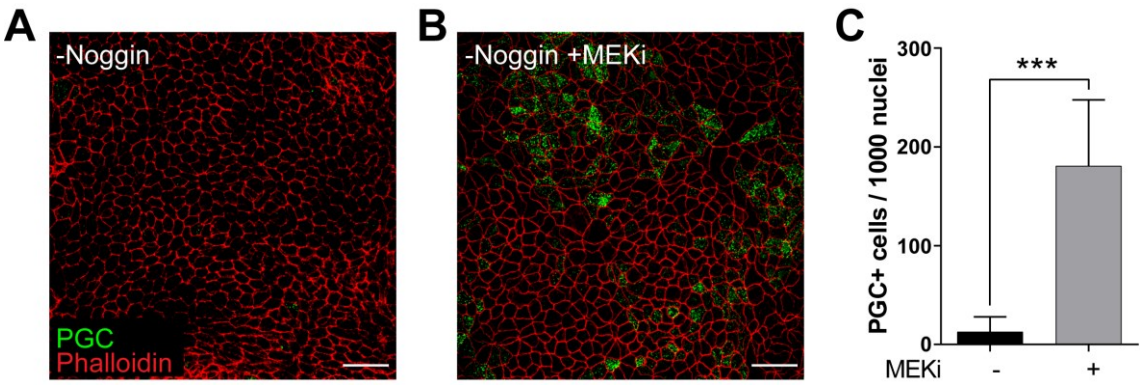

Figure 34: IF labeling against PGC confirmed a significant increase in chief cells when the EGFR pathway was inhibited. Corpus mucosoid cultures were treated with MEKi for 12 days and whole mount IF labeling was performed using a PGC (green) specific antibody. (A,B) Only very few PGC positive cells were detected in (A) control corpus mucosoid culture samples while in (B) MEKi treated samples patches of PGC positive cells were observed. Scale bar: 25 µm. (C) The number of PGC positive cells per field was counted and displayed as mean ± SD of number of PGC+ cells per 1000 nuclei. For analysis, five images (technical replicates) were randomly recorded and were used for counting and calculation. Unpaired Student's t-test of technical replicates, *** $p < 0.001$.

Furthermore, MEKi treated mucosoid cultures were investigated by electron microscopy to analyze the chief cell phenotype in these mucosoids. Obtained results (Figure 35) confirmed the presence of chief cells in MEKi treated mucosoid cultures. Two chief cells are displayed in the representative image in Figure 35A, which showed an accumulation of typical secretory granules with high electron density containing digestive (pro-) enzymes on the apical side of the epithelial cells, which were not detected in non-treated controls (data not shown). Finally, immunogold labeling against PGC (Figure 35B) of putative chief cell culture definitely confirmed the presence of PGC in the secretory granules of chief cells located on the apical side of the cell.

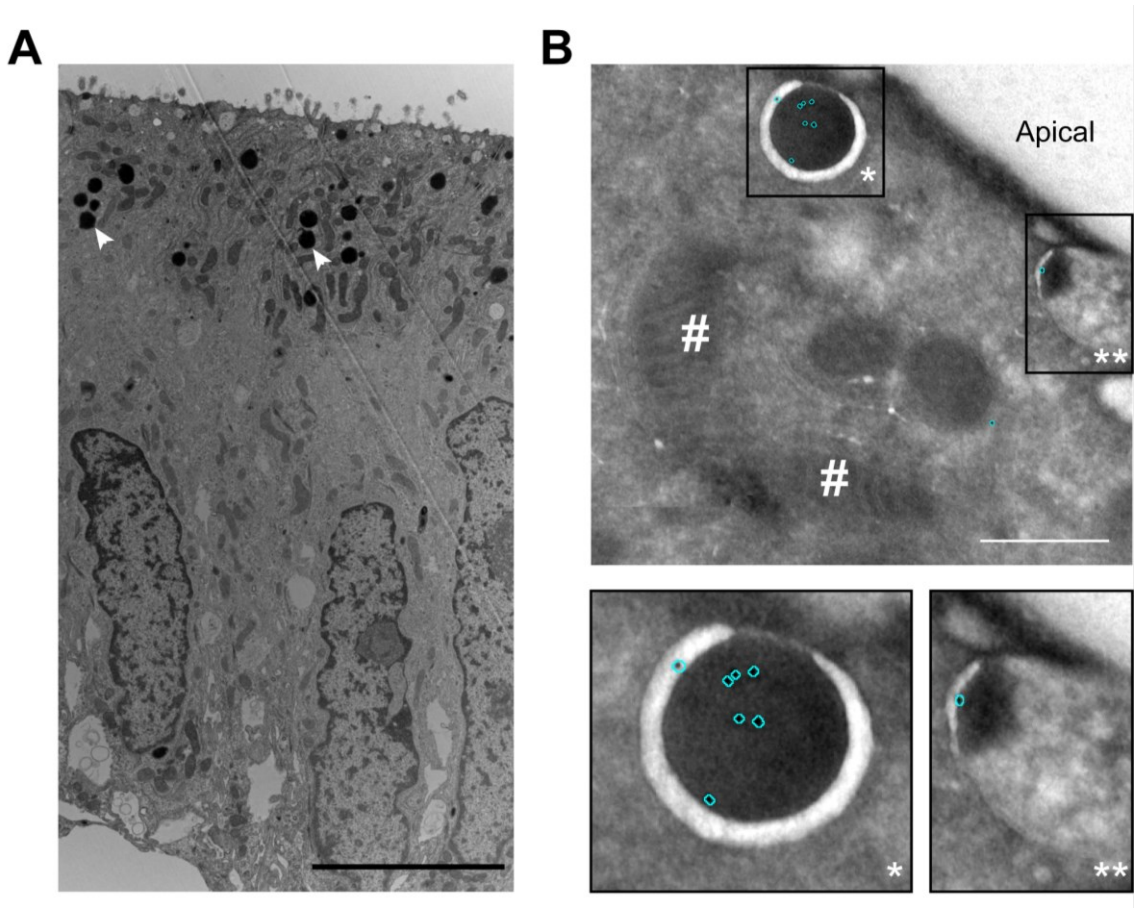

Figure 35: Electron microscopic images of chief cells after 12 days of treatment with MEKi. Corpus mucosoid cultures were treated with MEKi for 12 days to induce chief cell differentiation (A) Representative TEM micrograph shows two chief cells with secretory granules on the apical side (white arrowhead). Scale bar: 5 µm. (B) Representative TEM micrograph close-up of a chief cell in which PGC was labeled by immunogold (cyan circles) showing the localization of PGC in a secretory granule on the apical side (*) and in a brighter vesicle (V) which might transform into a secretory granule (**). V: Vesicle; #: mitochondrion. Scale bar: 500 nm. All samples were processed and TEM images were recorded by Dr. Christian Goosmann from the MPIIB core facility Microscopy.

Along with the induction of chief cell differentiation in mucosoid cultures through the administration of MEKi, a significant reduction in the mucus volume accumulated on the apical side was observed in these samples (Figure 36A). Also the functionality of the chief cells was assessed using MS to analyze the accumulated mucus. Chief cells are responsible for the secretion of digestive enzymes like lipase and PGC. If the differentiated chief cells were functional, these two enzymes should be secreted in the mucus and should be detected in the MS analysis. Obtained results revealed some accumulation of PGC (three out of four replicates, Figure 36B) in the mucus of MEKi

treated mucosoid cultures although the increase was only tendencially suggesting that PGC might not been secreted constitutively. Lipase was only detected in one out of four replicates and only in MEKi treated mucosoid (data not shown).

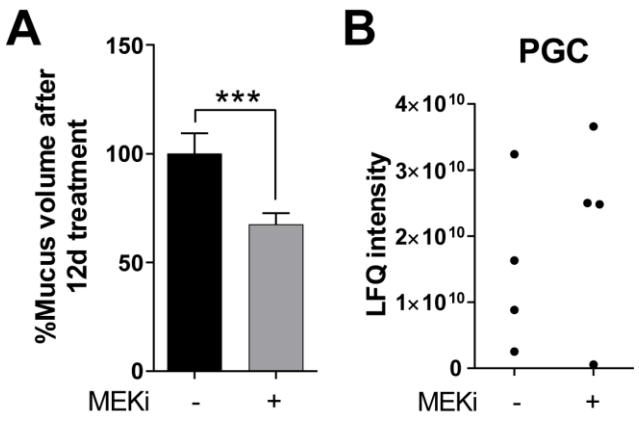

Figure 36: MEKi treated corpus mucosoids accumulated less mucus and showed PGC secretion. Corpus mucosoids were depleted from Noggin and treated with MEKi for 12 days. Non-treated, but Noggin deprived samples served as control. (A) Total mucus volume was measured after 12 days of treatment. Graph shows mean ± SD of three biological replicates. Unpaired Student's t-test, ***, $p < 0.001$. (B) MS analysis of mucus from non-treated or MEKi treated corpus mucosoid cultures after 12 days of treatment. The abundance of PGC is displayed in a dot plot. Data shows values of single measurements of four biological replicates from two distinct patient samples. LFQ: label-free quantification. The sample preparation and LC-MS/MS analysis were performed by Monika Schmid from the MPIIB core facility Mass spectrometry.

3.2.6. Inhibition of proliferation together with BMP4 guide parietal cell differentiation

Besides chief cells also the differentiation dynamics of parietal cells were of high interest. Under standard culture conditions, parietal cells could only rarely be observed *in vitro*. The influence of BMP4 on the differentiation of parietal cells was described before (McCracken et al. 2017). The results obtained so far indicated an intrinsic BMP activation when Noggin was removed from the cultivation cocktail. Parietal cells are terminally differentiated, long-living cells that do not proliferate anymore. Thus, to obtain parietal cells *in vitro* the proliferation of the mucosoid culture had to be inhibited and the same approaches as for the chief cells were used.

First, the influence of EGF and intrinsic BMP were tested by subsequent removal of EGF or Noggin (to activate intrinsic BMP pathway) or both from the cultivation medium. RT-PCR analysis for human parietal cell marker genes *GIF* (Figure 37B) and *ATP4B* (Figure 37A) revealed that *GIF* mRNA expression was significantly increased only in EGF deprived mucosoids. The highest alteration of *GIF* mRNA expression was achieved when both EGF and Noggin were removed from the cultivation medium. However, the results for the mRNA expression level of *ATP4B* (Figure 37A) were not as conclusive as for *GIF.* Only minor changes were detected for *ATP4B.* Results suggest that EGF had a major impact on *ATP4B* mRNA expression because a significant upregulation was observed for EGF deprived mucosoids. The additional removal of Noggin did not change the mRNA expression of *ATP4B*. Obtained data suggest that EGF removal and thereby abolished proliferation was not enough to induce parietal cell differentiation.

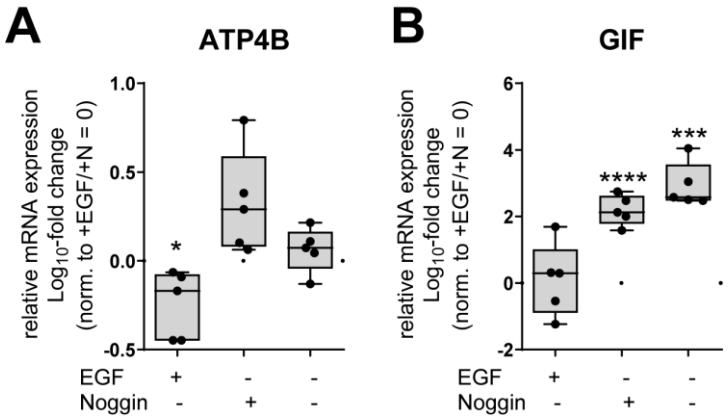

Figure 37: EGF is involved in parietal cell differentiation. Corpus mucosoid cultures of five biological replicates of two different patient samples were either deprived from Noggin or EGF or both for 12 days. mRNA expression levels of parietal cell marker (A) *ATP4B* and (B) *GIF* were analyzed by RT-PCR. Data were summarized in boxplots representing the median with 95 % CI. Error bars: min and max values. Data were normalized to +EGF/+Noggin (+N) control (=0). Paired Student's t-test, *, $p < 0.05$; ***, $p < 0.001$; ****, $p < 0.0001$.

The role of intrinsic BMP in combination with EGF driven proliferation was further assessed by treating mucosoids with increasing concentrations of Noggin to titrate the intrinsic BMP concentration either in the presence or absence of EGF. Obtained results

in Figure 38 demonstrate that EGF is crucial in parietal cell differentiation and BMP plays a secondary role as for chief cells. Again only in the absence of EGF an induction on mRNA level of parietal cell marker *GIF* (Figure 38B) was observed revealing that abolition of EGFR pathway activity is needed. Although the highest increase in *GIF* mRNA level was observed when Noggin and EGF were removed from the cultivation medium, this trend was not confirmed for *ATP4B* mRNA expression (Figure 38A). In general *ATP4B* mRNA levels were more inconsistent and data obtained show induction of *ATP4B* with medium-high Noggin concentration (50 ng/mL) in the absence of EGF. However, the data still indicates that EGF removal is crucial for parietal cell differentiation.

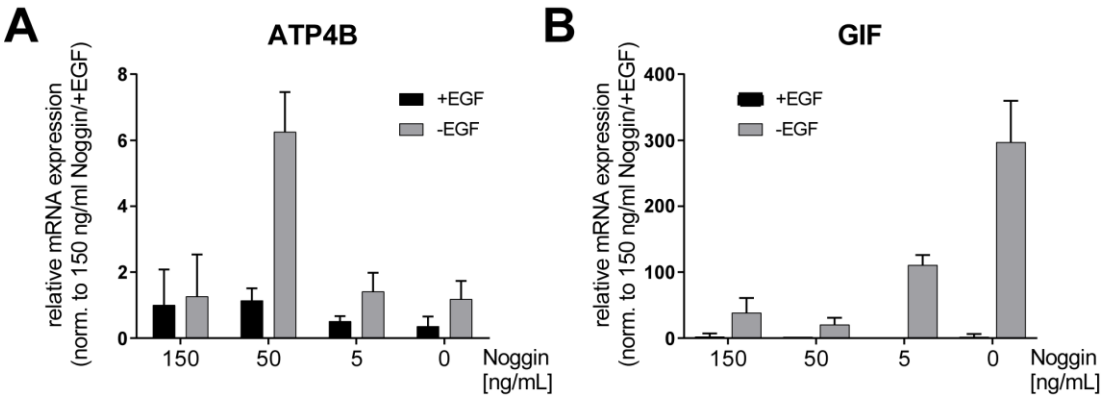

Figure 38: Regulation of intrinsic BMP concentration by administration of increasing Noggin concentration. Corpus mucosoid cultures of two different patient samples (two replicates) were cultivated in the presence or absence of EGF and different concentrations of Noggin (0-150 ng/mL) for 12 days. mRNA expression level of (A) *ATP4B* and (B) *GIF* were analyzed by RT-PCR. Representative data from one patient are shown. Error bars represent min and max values of technical triplicate.

It was shown for chief cells that inhibition of the EGFR-MEK-ERK pathway with MEKi attained similar results as the removal of EGF from the cultivation medium. Thus, mucosoids were treated with MEKi in all conditions except the non-treated control to inhibit the EGFR signaling pathway. For activation of the intrinsic BMP, Noggin was depleted in all conditions including the control. Previous results indicated that intrinsic BMP concentrations might not be sufficient to induce parietal cell differentiation. Moreover, McCracken et al. (2017) achieved differentiation towards

parietal cells from pluripotent stem cells by administration of a high concentration of BMP4 (50 ng/mL). Thus, corpus mucosoids were treated with BMP4 (50 ng/mL) to analyze the effect of a high concentration of BMP4 on parietal cell differentiation. The release of gastric acid from parietal cells is induced by histamine stimulation. Finally, BMP4 treated mucosoid cultures were stimulated with a single shot of histamine for 30 min prior to analysis.

First, corpus mucosoids were treated as described and RT-PCRs were performed to analyze the mRNA expression levels of the parietal cell marker genes *ATP4B* and *GIF*. Obtained results (Figure 39) demonstrate that similar to EGF removal the inhibition of proliferation by MEKi together with intrinsic BMP due to depletion of Noggin already induced *GIF* mRNA expression (Figure 39B). Although additional treatment with BMP4 significantly increased *GIF* mRNA expression as well, the magnitude was significantly lower than in +MEKi condition. The stimulation with histamine did not have an impact on *GIF* mRNA expression. The mRNA expression of *ATP4B* (Figure 39A) was significantly altered in all conditions but the highest induction was obtained in histamine stimulated BMP4 treated samples. These results suggest that inhibition of proliferation by MEKi is the driving force of parietal cell differentiation. The treatment with BMP4 and stimulation with histamine further pushes parietal cell differentiation as the mRNA expression data of *ATP4B* revealed.

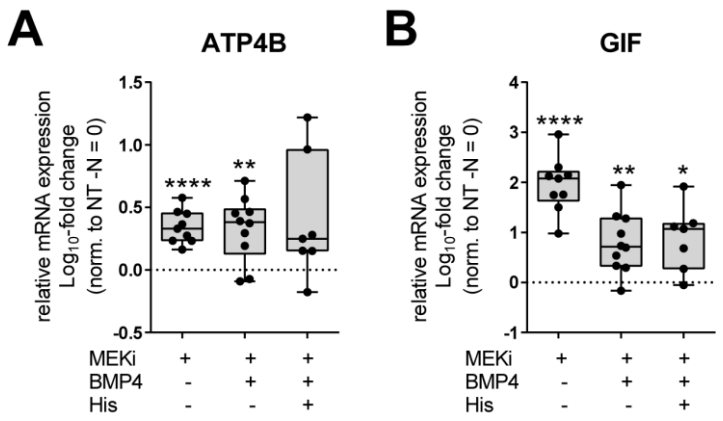

Figure 39: Intrinsic BMP as well as extrinsic BMP4 induced parietal cell differentiation, which is additionally stimulated by histamine. Corpus mucosoid cultures were treated with MEKi or MEKi/BMP4 (50 ng/mL) for 12 days. A third sample set was treated for 12 days with MEKi/BMP4 (50 ng/mL) and stimulated with histamine (1 mM) for 30min. RT-PCRs were performed to analyze the mRNA expression levels of parietal cell marker genes (A) *ATP4B* and (B) *GIF*. Boxplots depict median with 95 % CI of seven to ten biological replicates derived from two patient samples. Error bars represent min and max values. Data were normalized to non-treated, Noggin deprived control (NT –N =0). His: Histamine. Paired Student's t-test, *, $p < 0.05$; **, $p < 0.01$; ****. $p < 0.0001$.

Next, the RNA based results were confirmed on protein level by whole mount IF staining against ATP4B. Representative confocal images of all tested conditions are displayed in Figure 40 A-D. Again BMP4 treated mucosoid cultures were additionally stimulated with histamine. IF labeling against ATP4B showed that only a few parietal cells were detected in –Noggin condition (Figure 40A), serving as a control. Although an induction was observed in MEKi treated samples on mRNA level for *ATP4B*, almost no parietal cells were detected under this condition (Figure 40B). In comparison, a high number of ATP4B positive cells was detected in BMP4 treated mucosoid cultures and even more in histamine stimulated samples (Figure 40C and D). The number of ATP4B positive cells was determined in every condition, confirming the significantly higher number of ATP4B positive cells in BMP4 [+13.9 ± 4.9 %] and BMP4 + Histamine [+28.9 ± 9.1 %] conditions (Figure 40E). Furthermore, the stimulation with histamine induced the release of gastric acid from parietal cells. This process was visualized by administration of the pH-sensitive dye Acridine Orange to the parietal cell-enriched mucosoid culture. The cells were monitored over time by life cell imaging microscopy. Due to its pH-sensitivity, Acridine Orange appears orange when it gets in contact with acidic compartments; thereby the punctual release of gastric acid became visible. A

hyper stack of the recorded images is shown in Figure 40F, which showed an increase in Acridine Orange turn over in histamine stimulated samples that is conterminous with an increase in the gastric acid release. Very few orange spots were detected in the unstimulated control representing a spontaneous release of gastric acid. The obtained results demonstrate the functionality of the gained parietal cells.

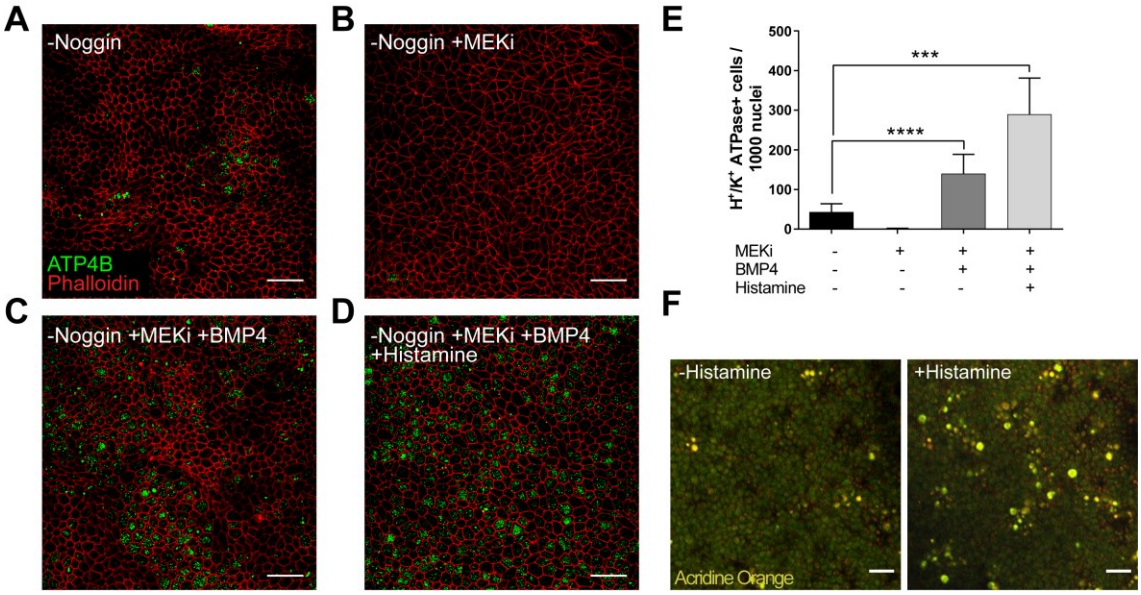

Figure 40: Extrinsic BMP4 and stimulation with histamine induced differentiation into functional parietal cells. (A-D) Representative confocal images of whole mount IF labeling against ATP4B (green) in (A) control, (B) +MEKi treated, (C) +MEKi/BMP4 (50 ng/mL) treated and (D) +MEKi/BMP4 (50 ng/mL) treated and +Histamine (1 mM, 30 min) stimulated corpus mucosoid cultures. All samples were treated for 12 days. Scale bar: 25 µm. (E) Quantification of ATP4B positive cells in all four conditions. Four to five confocal images (technical replicates) per condition were randomly recorded and ATP4B positive cells were counted per field. Data represent the mean ± SD of ATP4B+ cells per 1000 nuclei. Unpaired Student's t-test of technical replicates, ***, $p < 0.001$; ****, $p < 0.0001$. (F) Hyperstack from life cell image movie of corpus mucosoid cultures, treated with BMP4 (50 ng/mL) and stimulated either with +Histamine (5 mM, right panel) or left unstimulated (-Histamine, left panel). In both conditions, cells were pre-incubated with the pH-sensitive dye Acridine Orange (1 µM, 15 min) and living cells were recorded over time. Acridine Orange changed the color in an acidic environment. This experiment was performed by Dr. Francesco Boccellato in collaboration with Dr. Volker Brinkmann from the MPIIB core facility Microscopy. Scale bar: 25 µm.

Finally, the BMP4 treated and histamine stimulated mucosoid cultures were analyzed in transmission electron microscopy to prove the characteristic phenotype of parietal cells including the triangular shape and the presence of canaliculi. A representative image of a parietal cell is depicted in Figure 41A. The typical triangular shape of the parietal cells was not found in any processed sample set. However, other very characteristic features of parietal cells were detected. Accumulation of mitochondria on the apical side of the parietal cell was observed which are needed for energy availability and delivery during the active gastric acid transport to the lumen. Along with this finding, also tubular structures most likely canaliculi were found close to the mitochondria on the apical side. The identity of parietal cells and the putative canaliculi were further confirmed by immunogold labeling against ATP4B. Obtained results (Figure 41B) demonstrate that immunogold particles were mainly detected in the canalicular and tubulovesicular structures on the apical side of the cells, in close proximity to mitochondria. Both observations definitely confirmed the presence of parietal cells in the mucosoid culture achieved by inhibition of the EGFR-MAPK pathway and treatment with a high dose of BMP4. One reason for the missing triangular shape could be a space problem of the cells on the filter insert as this cell type is very large and the space on the filter membrane was limited.

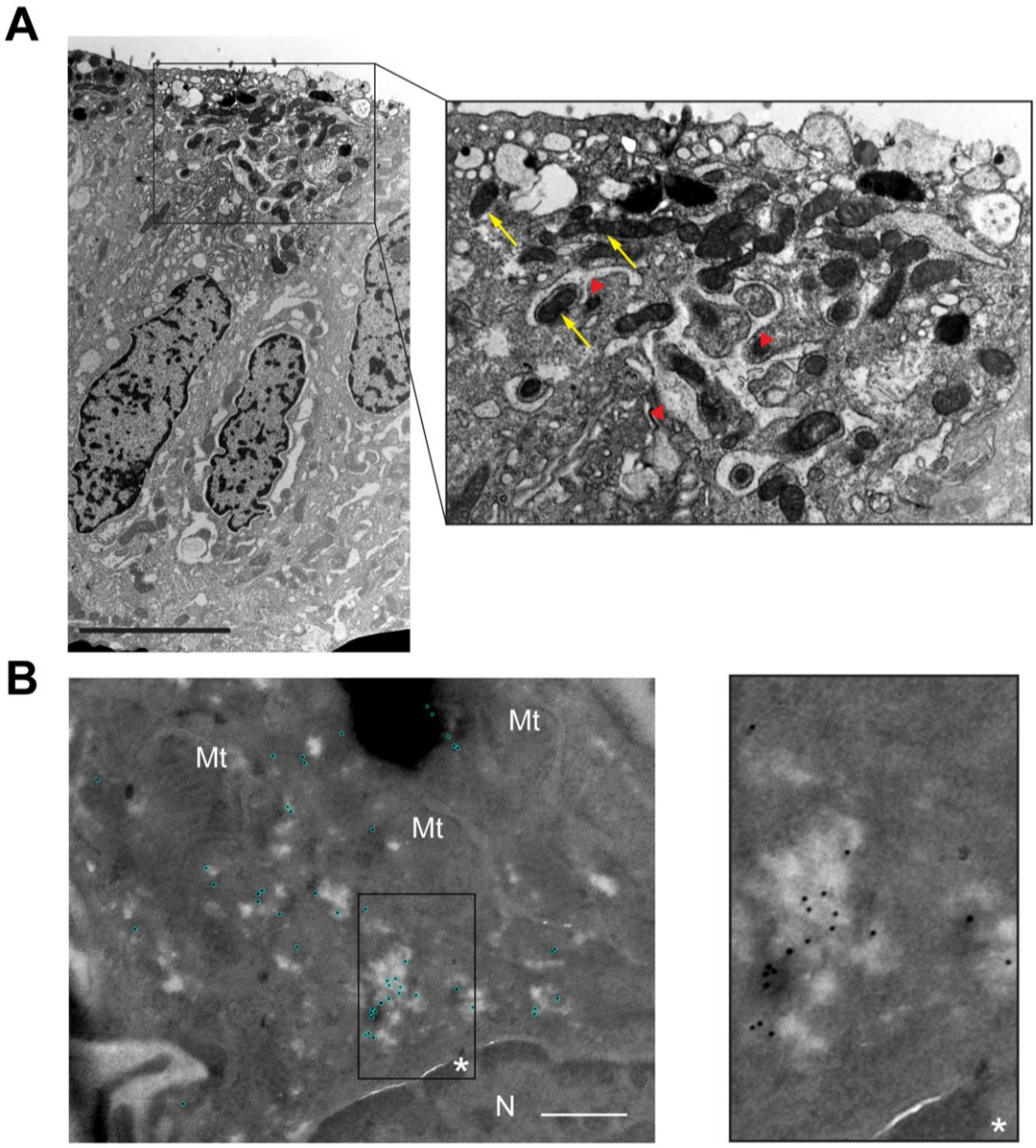

Figure 41: Electron microscopic image of a parietal cell. Corpus mucosoid cultures deprived from Noggin and treated with MEKi and BMP4 (50 ng/mL) for 12 days and stimulated with histamine (1 mM, 30 min) were fixed (A) in 2.5 % GA and processed for electron microscopy or (B) fixed in 2 % pFA/0.05 % GA for sucrose embedding and labeling with immunogold using an antibody against ATP4B. Sample processing and electron microscopy were performed by Dr. Christian Goosmann from the MPIIB core facility Microscopy. (A) Representative TEM image of a parietal cell with the accumulation of mitochondria (zoom-in: yellow arrows) on the apical side intercalating with tubulovesicles and canaliculi (zoom-in: red arrowheads). Scale bar: 5 µm. (B) Representative electron micrograph of a parietal cells in which ATP4B was labeled by immunogold showing localization of ATP4B in canaliculi on the apical side of the cell (black dots marked with cyan circles, left panel) and a zoom-in (black dots, right panel, *) showing concentration of labeled ATP4B in canalicular structure. Scale bar: 500 nm. N: nucleus, Mt: mitochondrion.

3.3. Communication between epithelium and stroma

3.3.1. Isolation of a human gastric stromal cell population from the *lamina propria*

Gastric stromal cells (GSC) were isolated from the *lamina propria*, surrounding and separating the gastric glands (Figure 42A), of human gastric tissue and cultured on plastic showing an elongated cell shape typical of fibroblasts (Figure 42B). Below the lamina propria there is a thin muscle layer that separates the mucosa from the submucosa. This consists of myofibroblasts forming the so-called *lamina muscularis mucosae* (Figure 42A). The herein cultivated GSCs originate only from the *lamina propria*. The *muscularis mucosae* was removed during the isolation process to receive only stromal cells from the *lamina propria* compartment. Isolation and cultivation of fibroblasts from the *muscularis mucosae* were also successful, but will not be included and discussed in this work.

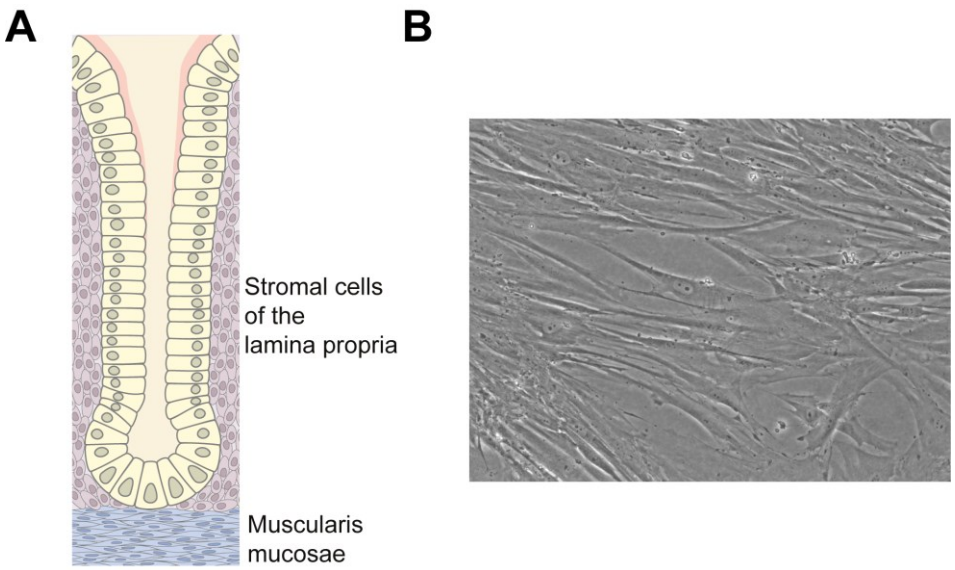

Figure 42: Stromal cells were isolated from the *lamina propria* of human gastric tissue and show typical fibroblast phenotype. (A) Schematic depiction of the gastric gland with the surrounding stromal cells of the *lamina propria* and *muscularis mucosae*. Only stromal cells from the *lamina propria* were isolated from human gastric antral tissue. (B) Isolated antral stromal cells grow on plastic and show typical fibroblast phenotype.

After isolation, GSC were analyzed to confirm their mesenchymal origin and the absence of epithelial cell (EPC) contamination. A western blot analysis was performed using antibodies against the stromal cell marker vimentin and the epithelial cell marker E-Cadherin (Figure 43). GSCs were only positive for vimentin and negative for E-Cadherin. On the other hand, the results for EPC showed that these cells were only positive for the epithelial cell marker E-Cadherin but negative for vimentin. Hence, both cell type cultures were pure and neither had contamination of EPCs in GSC culture nor GSC in EPC culture.

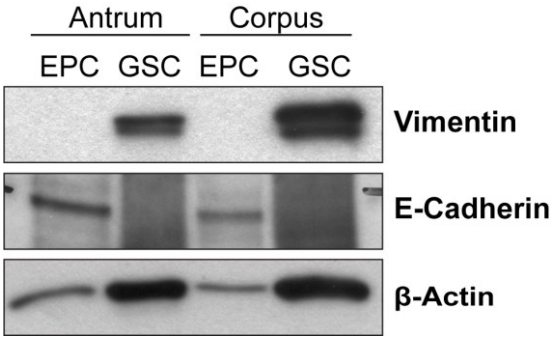

Figure 43: Western Blot analysis for E-Cadherin and vimentin to test the purity of epithelial cell and stromal cell culture. Protein cell lysates of EPC and GSC from antrum and corpus were separated in SDS-PAGE and labeled with antibodies against the stromal cell marker vimentin and the epithelial cell marker E-Cadherin in western blot. β-Actin was used as a housekeeping protein.

Isolated GSCs from antrum were used to establish a co-culture system in mucosoid cultures to explore the communication signaling between stromal and epithelial cells. Figure 44 displays schematically the structure of the co-culture system. Stromal cells were seeded at 100% confluency ($0.6*10^5$ cells/well) in a 24-well plate. Co-culture started 24 hours after seeding. Therefore, the filter insert with epithelial cells, grown in ALI conditions for 14 days, was carefully placed on top of the GSC. This co-culture system was cultivated with mucosoid culture medium for seven days, with bi-weekly replacement of 50 % of the culture medium volume.

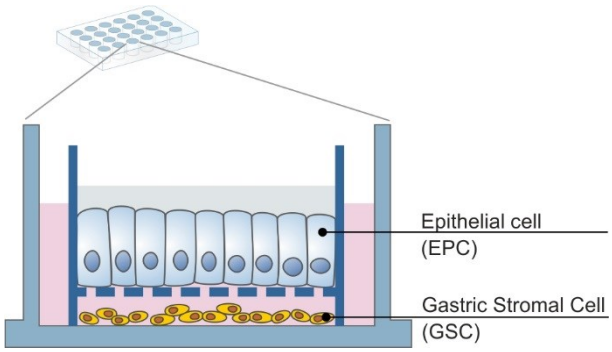

Figure 44: Schematic representation of the co-culture system of gastric primary epithelial cells and stromal cells. $0.6*10^5$ GSCs were seeded in a 24-well plate with GSC medium 24 hours prior to start the co-culture. The cultivation medium was changed to mucosoid culture medium. The filter insert with EPC was carefully placed on top of the GSC. The distance between both compartments was app. 1 mm.

3.3.2. Gastric stromal cells induce differentiation in epithelial cells by blocking the Wnt/β-Catenin pathway

Previous studies in mice suggested that stromal cells have an impact on the differentiation of embryonic epithelial cells toward foveolar cells (Katano et al. 2015; Ootani et al. 2000). To understand the impact of human GSCs on human gastric EPCs these two cell types were co-cultured with the mucosoid system as described above. As shown in this work before, the foveolar differentiation is regulated by the Wnt pathway (see section 3.1.2). Inactivation of the Wnt pathway through the removal of WNT3A and RSPO1 from the culture medium induced foveolar differentiation. To analyze if stromal cells influence the epithelial Wnt pathway, the localization of the transcription factor β-Catenin (that controls Wnt target genes) was determined by IF labeling in co-cultured mucosoids and respective +W+R and -W-R controls (Figure 45). When the Wnt pathway was active (+W+R condition) β-Catenin was located in the nuclei (Figure 45B). Conversely, the IF staining for β-Catenin showed that in the presence of GSC (Figure 45C), β-Catenin was exclusively located in the cytoplasm of epithelial cells like in -W-R condition (Figure 45A), indicating a de-activation of the epithelial Wnt signaling pathway when epithelial cells were co-cultured in the presence of stromal cells.

Further, the expression level of the Wnt target gene *LGR5* was analyzed by RT-PCR (Figure 45D) and found to be significantly reduced in epithelial cells when they were

co-cultured with GSCs although the reduction was not as pronounced as in the -W-R control, indicating a partial inhibitory effect. To analyze whether secreted factors from GSC were responsible for the decrease of *LGR5* mRNA expression, mucosoids were treated with 50 % GSC conditioned medium (GSC CM) for seven days. The GSC CM was able to reduce *LGR5* mRNA expression similar to the presence of the GSC in co-culture, confirming that GSCs secrete Wnt/β-Catenin soluble inhibitors in the medium.

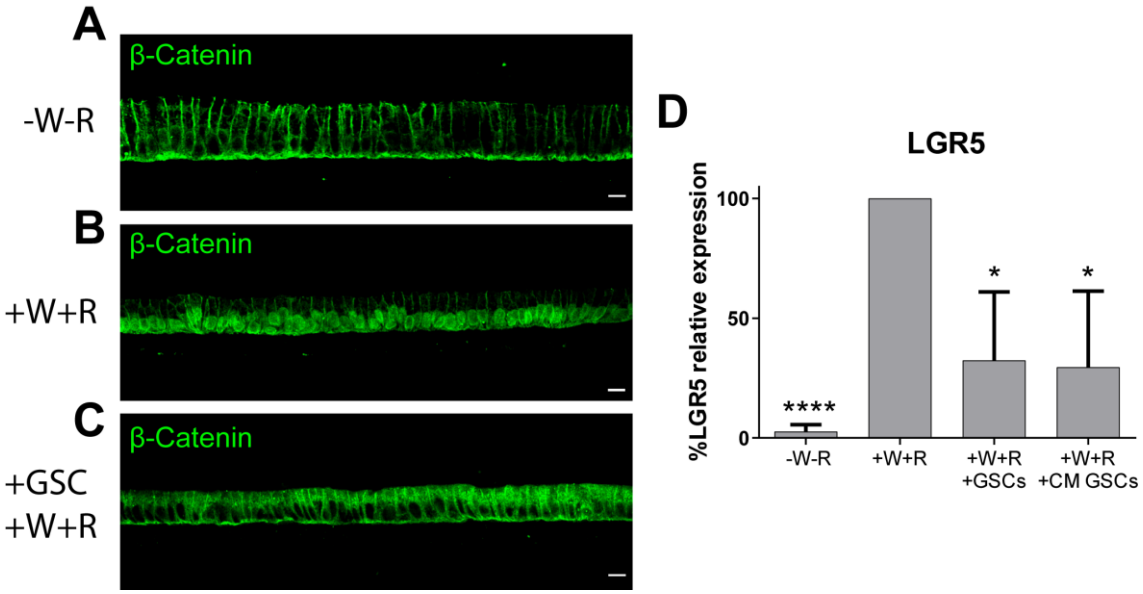

Figure 45: Secreted GSC factors inactivate the Wnt pathway in EPC. Three biological replicates of EPC from two different patients were co-cultured with the corresponding GSC for seven days. +W+R mucosoids and -W-R mucosoids were used as controls. (A-C) Representative confocal images of (A) -W-R mucosoids, (B) +W+R mucosoids and (C) GSC co-cultured mucosoids fluorescently labeled against β-Catenin. Scale bar: 10 µm (D) Analysis of mRNA expression level of *LGR5* by RT-PCR in +W+R condition, -W-R condition, +GSC co-cultured mucosoids, and mucosoids treated for seven days with GSC CM. Data are shown as mean ± SD. Unpaired Student's t-test, *, $p < 0.05$; ****, $p < 0.0001$. CM: conditioned medium.

Next, to test the active concentration of Wnt/β-Catenin soluble inhibitors in GSC conditioned medium, it was titrated against recombinant WNT3A and the mix was tested on L-WNT3A-GFP reporter cells. In this cell line, GFP is expressed under the control of seven consecutive T-cell factor (TCF) promoter elements. In the presence of WNT3A, the cells express GFP in a Wnt concentration dependent manner. When cells were treated with 50 % WNT3A solution (produced as a conditioned medium from the

cell line L-WNT3A; for details of the supernatant production see section 2.2.1.7 of material and methods) a strong GFP reporter signal was detected (Figure 46A). The combination of WNT3A supernatant with an increasing amount of GSC CM reduced the GFP signal in a concentration dependent manner. (Figure 46B).

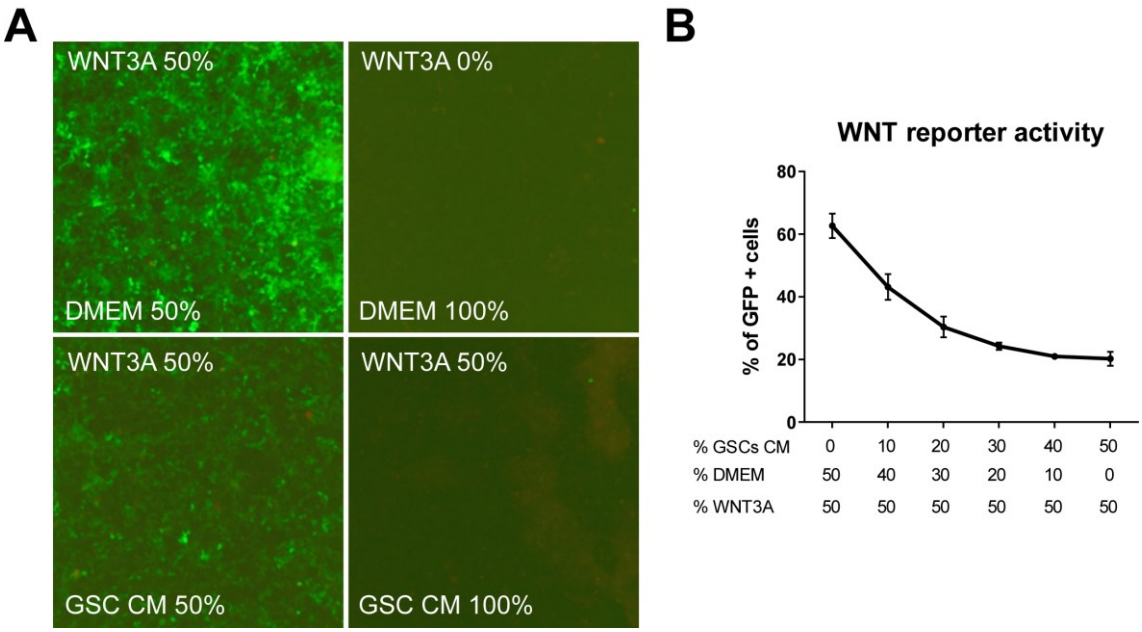

Figure 46: GSCs inhibit GFP signal expression in WNT3A reporter cell line in concentration dependent manner. (A) WNT3A reporter cell line was incubated with either 50 % WNT3A/50 % DMEM to fully activate GFP expression (upper left panel) or 0 % WNT3A/100 % DMEM as negative control (upper right panel) or 50 % WNT3A/50 % GSC CM (lower left panel) or 50 % WNT3A/100 % GSC CM (lower right panel). GFP signal was recorded at the automated microscope. (B) WNT3A reporter activity was assessed by measuring the percentage of GFP positive cells. The reporter cell line was activated with a constant concentration of 50 % WNT3A while the concentration of GSC CM was increased.

As these results indicate the presence of soluble Wnt inhibitors secreted by the GSCs, the expression of Wnt inhibitors Dickkopf (*DKK*) *1*, *DKK2*, *DKK3*, and *DKK4*, and secreted frizzled-related protein (*sFRP*) *1*, *sFRP2*, *sFRP3*, and *sFRP4* in GSC was analyzed by PCR. Furthermore, also the expression of the Wnt pathway inhibitors Dickkopf like acrosomal protein (*DKKL1*), sclerostin domain containing protein 1 (*USAG1*), Wnt inhibitory factor 1 (*WIF1*) and Homeobox protein BarH-like 1 (*BARX1*) were tested by PCR. The results in Figure 47 show that *sFRP1*, *DKK1*, and *DKK3* were

strongly expressed in GSCs. Additionally, low expression of *sFRP3*, *sFRP4* and *DKK2* were also detected. The Wnt pathway inhibitors *sFRP2*, *DKK4*, *DKKL1*, *USAG1*, and *WIF1* instead were not expressed in stromal cells.

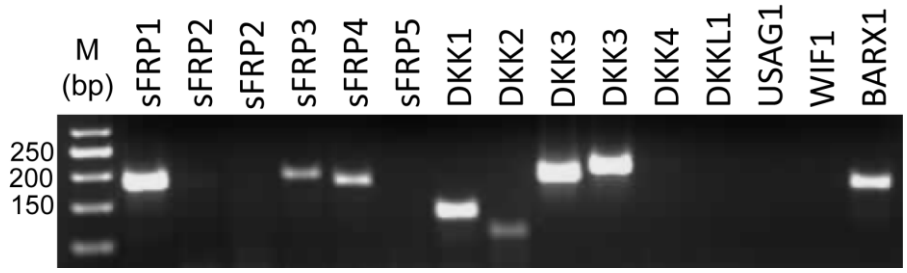

Figure 47: GSCs express different Wnt pathway inhibitors. DNA from GSC was isolated and PCR was performed to analyze the expression of Wnt inhibitors *sFRP1-4*, *DKK1-4*, *DKKL1*, *USAG1*, *WIF1* and *BARX1* using specific primers. M: marker, bp: base pair.

In mucosoids, the foveolar differentiation can be monitored by the switch from MUC6 to MUC5AC expression induced by removal of WNT3A and RSPO1 from the cultivation cocktail. As stromal cells impair the Wnt pathway activation of epithelial cells, it was tested if the epithelial cells were undergoing differentiation. GSC co-cultured mucosoids were analyzed for MUC5AC expression by IF labeling (Figure 48) using -W-R mucosoids and +W+R mucosoids as controls. The co-culture with GSC induced an intermediate expression of the foveolar differentiation marker MUC5AC (Figure 48C) indicating that some cells were induced to differentiate.

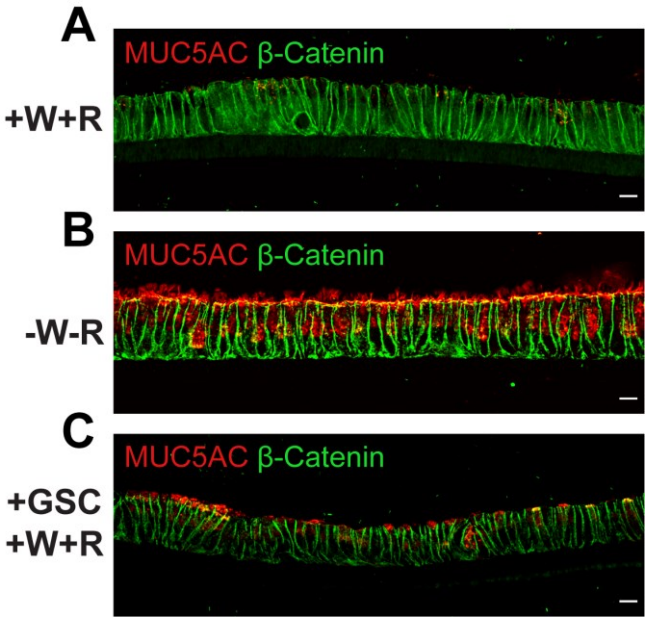

Figure 48: GSCs induce partial foveolar differentiation in epithelial cells. Confocal images of (A) +W+R mucosoids, (B) -W-R mucosoids and (C) GSC co-cultured mucosoids, fluorescently labeled against MUC5AC (red) to analyze the status of foveolar differentiation. IF labeling against β-Catenin was used to visualize epithelial cells. Scale bar: 10 µm.

3.3.3. Infection of epithelial cells with *H. pylori* induced an inflammatory response in stromal cells

The co-cultivation of gastric stromal cells with the epithelial counterpart reconstituted the gastric mucosa *in vitro*. As the results have shown, stromal cells influence the epithelial monolayer under homeostatic conditions. Thus, it was of interest to investigate also the interplay and communication of these two cell populations under pathophysiologic conditions i.e. acute *H. pylori* infection. The human pathogen *H. pylori* colonize and infect epithelial cells mainly in the antrum of the human stomach. This bacterium is equipped with the Type IV secretion system (T4SS) that translocate with an injection the virulence factor CagA into the host cells. The phosphorylation of CagA (pCagA) inside the host cell and the consequent detection of pCagA (PY99) in epithelial cells is, therefore, a hallmark of a successful *H. pylori* infection. Hence, antral mucosoid cultures were infected with *H. pylori* strain P12 for three days to prove the susceptibility of this culture model for infection studies. Confocal images of infected mucosoid cultures immunolabeled with an antibody against CagA (red) showed different groups of bacteria (Figure 49A) which either have not

adhered to the epithelial cells yet (Figure 49A*) or were attached to the epithelial surface (Figure 49A**). The western blot analysis of pCagA (PY99) in infected mucosoid cultures and non-infected control showed the detection of pCagA (PY99) in infected mucosoid culture (Figure 49B) similarly as in the positive control of the same cells infected in 2D but not in the non-infected control.

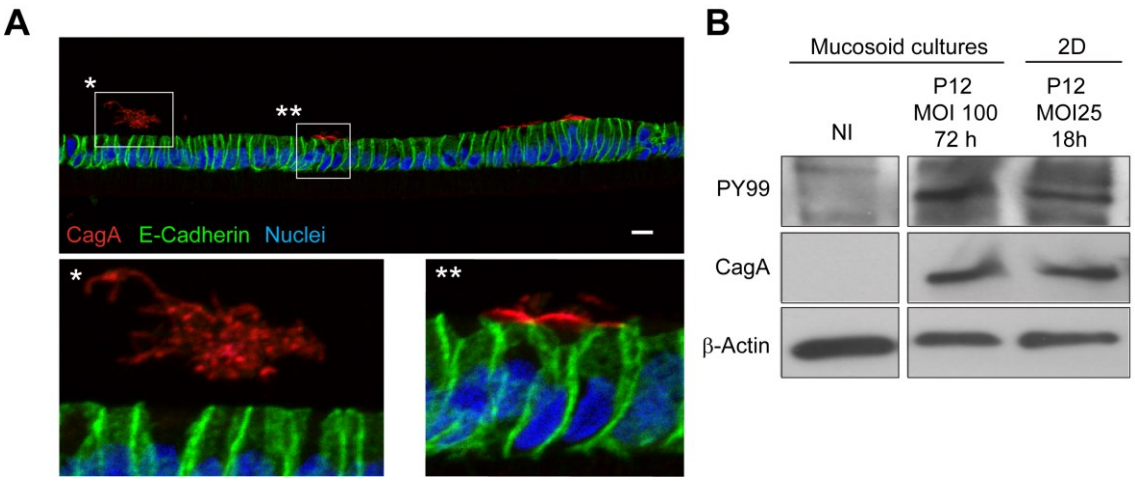

Figure 49: *H. pylori* attached to the epithelial surface and translocated CagA into the host cell. (A) Antral mucosoid cultures infected with isogenic *H. pylori* P12 (MOI 100) for 72 hours were labeled by IF against *H. pylori* CagA (red) to visualize bacteria and epithelial cell marker E-Cadherin (green). Enlarged images below show groups of bacteria that (*) have not yet adhered to the epithelial cells or (**) attached to the epithelial surface. Scale bar: 10 µm. (B) Western Blot analysis of pCagA detected with an antibody against PY99 (phosphorylated CagA) and total CagA in cell lysates of non-infected mucosoid culture (left lane), antral mucosoid culture infected with P12 at MOI 100 for 72 hours (middle lane) and the same cells seeded planar in 2D on collagen-coated plastic and infected with P12 at MOI 25 for 18 hours (right lane).

As the mucosoid cultures are responsive to stromal cells under physiological conditions and also to infection with *H. pylori* the next step was to explore the impact of infection in the communication between epithelial and stromal cells by differential gene profiling. For this purpose, epithelial cells of mucosoids alone or co-cultured with GSC were infected with *H. pylori* strain P12 (MOI 100) for three days as depicted in the schematic in Figure 50.

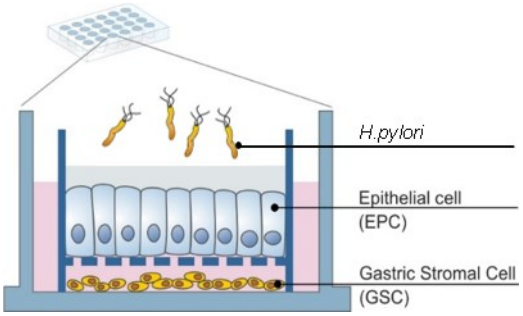

Figure 50: Schematic representation of the *H. pylori* infection of co-cultured mucosoids. Only EPCs were in contact with bacteria.

Differential gene expression of the infected cultures and co-cultures was analyzed by microarray and the gene expression was compared to their non-infected mucosoid culture and co-culture counterparts. The differential gene expression of the co-cultured GSC from this experiment was also analyzed in parallel. In general obtained results shown in Figure 51A revealed that the infection of EPCs with *H. pylori* induced the expression of NFκB target genes in mucosoids as well as in co-cultured mucosoids. Most of the analyzed NFκB target genes were similarly regulated in both EPC cultures, although co-cultured mucosoids showed a stronger induction for certain genes like interleukin (*IL*) *11*, *IL15, IL18, CXCL3, CXCL5, CXCL8* (*IL8*) or tumor necrosis factor (*TNF*) (Figure 51A). A small panel of genes was differently regulated in co-cultured mucosoids compared to mucosoids alone i.e. *CSF2* (colony stimulating factor 2), *IL11* (interleukin 11), *IL1RN* (interleukin 1 receptor antagonist), *IGFBP1* (insulin growth factor binding protein 1), *MMP1* (matrix metalloproteinase 1), *IL1A* (interleukin 1 alpha) and *IL1B* (interleukin 1 beta, *IL1β*). Selected candidates of the gene profiling were further validated by RT-PCR using the same RNA as for the microarray. RT-PCR analysis results revealed that *IL1β* (Figure 51B) indeed is higher expressed in infected co-cultured mucosoids. For *CSF2* (Figure 51C) instead, the differences observed in the gene profiling were not confirmed. Furthermore, mRNA expression levels of *IL8* (Figure 51D) and *TNFα* (Figure 51E) were analyzed and showed higher induction in *H. pylori* infected co-cultured mucosoids, confirming the differences observed in the gene profiling in Figure 51A.

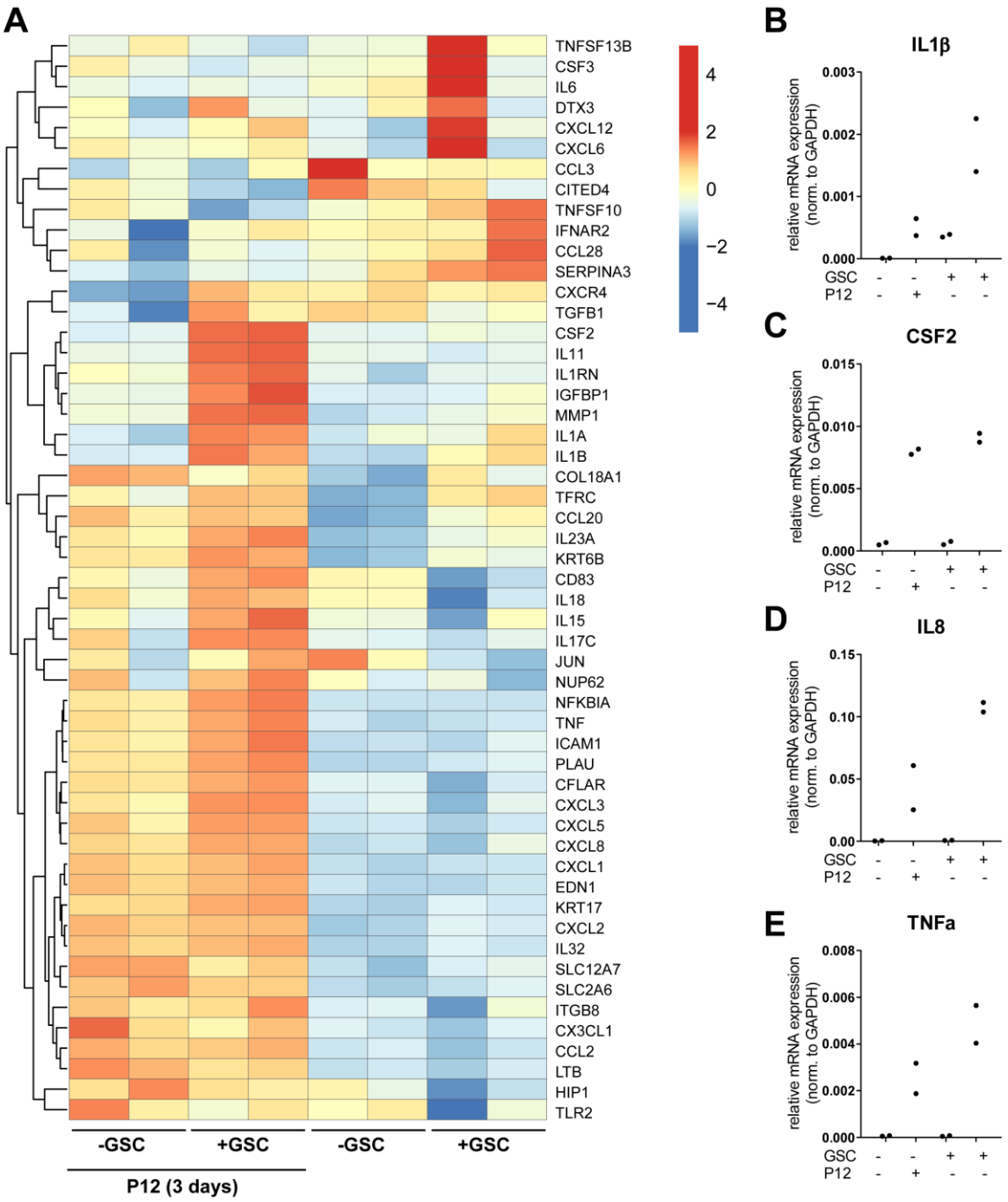

Figure 51: *H. pylori* infection induced an early NFκB driven immune response in epithelial cells independent of GSC co-culture. Mucosoids alone (-GSC) or co-cultured with GSC for seven days (+GSC) were infected for three days with *H. pylori* (MOI 100; P12 (3days)). Non-infected counterparts were used as controls. (A) RNA from two biological replicates per group was used to perform microarray analysis. Displayed are the gene expression levels (Log_{10} fold change) of target genes of the NFκB signaling pathway in EPCs. Microarray data processing and visualization as a heat map were performed by Dr. Hilmar Berger. (B-E) RT-PCR analyses were performed to validate observations from microarray using the RNA from the two biological replicates of each group. mRNA expression levels of (B) *IL1β*, (C) *CSF2*, (D) *IL8* and (E) *TNFα* were determined using specific primers. The mRNA expression was normalized to the housekeeping gene *GAPDH*.

The differential gene expression of corresponding GSC of non-infected and *H. pylori* infected mucosoids was also analyzed in the microarray. In Figure 52A an overview of regulated NFκB pathway target genes in GSCs is displayed in a heat map. The infection of EPCs induced an NFκB driven immune response also in GSCs. A panel of cytokines and chemokines especially *IL1β, IL6, CXCL8* (*IL8*), was upregulated in GSCs upon epithelial infection indicating paracrine signaling between epithelium and stroma. To validate the obtained differential gene expression data for selected candidates, RT-PCR analyses were performed to determine the mRNA expression levels of *IL6, IL1β, IL8* (Figure 52B), *CXCL12* and *IL18* (Figure 52C). The results demonstrate that specifically *IL1β* is highly induced in GSC when EPCs were infected with *H. pylori.* The upregulation of *IL8* and *IL6* was confirmed by RT-PCR, but the induction was lower compared to *IL1β* (Figure 52B). The mRNA expression level of *CXCL12* was analyzed as the microarray data revealed that *CXCL12* is downregulated in GSCs during infection. RT-PCR data did not confirm this observation because the *CXCL12* mRNA expression did not change between non-infected and infected samples (Figure 52C). *IL18* instead was upregulated in GSC during infection confirming the microarray data.

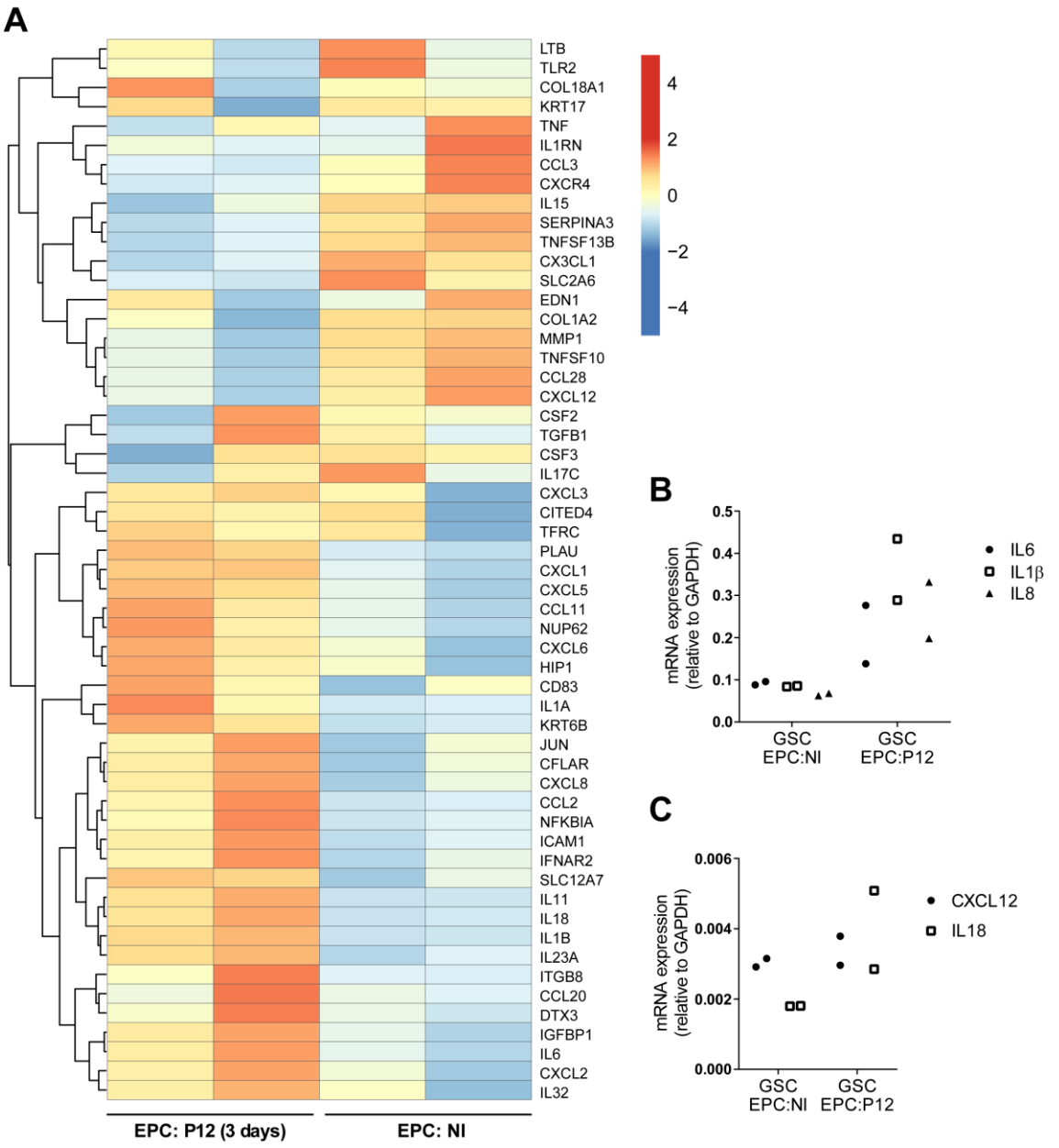

Figure 52: GSCs respond to the *H. pylori* infection of overlaying EPCs. Co-cultured mucosoids were infected for three days with *H. pylori* (MOI 100; EPC: P12 (3days)). Non-infected counterparts served as control (EPC: NI). (A) RNA from GSCs from two biological replicates per group was used to perform microarray analysis. Displayed are the gene expression levels (Log_{10} fold change) of target genes of the NFκB signaling pathway in GSCs. Microarray data processing and visualization as a heat map were performed by Dr. Hilmar Berger. (B-C) RT-PCR analyses were performed to validate observations from microarray using the RNA from the two biological replicates of each group. mRNA expression levels of (B) *IL6, IL1β* and *IL8* and (C) *CXCL12* and *IL18* were determined using specific primers. The mRNA expression levels were normalized to the housekeeping gene *GAPDH*.

In summary infection of co-cultured epithelial cells led to higher expression in a selected panel of NFκB target genes, while a small subset of NFκB target genes was only specifically induced in co-cultured mucosoids against infection. Furthermore, gastric stromal cells actively participate in the modulation of the immune response by inducing the expression of inflammatory cytokines specifically *IL1β, IL6*, and *IL8*.

Infection with *H. pylori* for analyzing the differential gene expression was performed for three days. It was shown in cell lines that the NFκB subunit p65 translocation from the cytoplasm into the nucleus is oscillating during *H. pylori* infection (Bartfeld et al. 2010) subsequently it is expected that also the NFκB p65 target gene expression should follow this trend. Thus, a time course of infection was performed over 36 hours to analyze eventual changes in cytokine induction. The mRNA expression level of *IL8* was chosen as readout and was analyzed in epithelial cells as well as in stromal cells using RT-PCR (Figure 53). Results showed that the *IL8* mRNA expression level peaked first 12 hours post-infection (hpi) in epithelial cells (Figure 53A) with declining expression levels at 24 hpi followed by a second peak after 36 hpi. However, in stromal cells (Figure 53B), the highest *IL8* mRNA expression was observed after 24 hpi, 12 hours later than in epithelial cells indicating that the stroma starts the inflammatory response obviously after the epithelium.

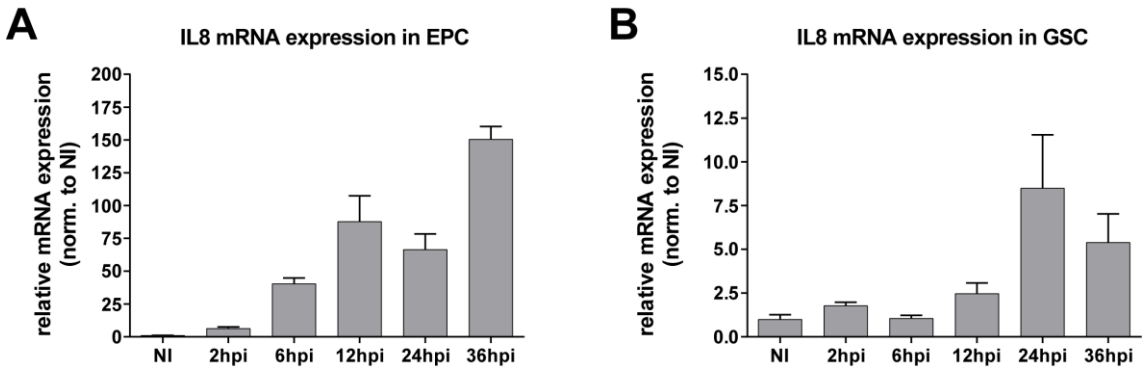

Figure 53: Time course of IL8 mRNA expression in EPC and GSC after *H. pylori* infection of co-cultured mucosoids. Mucosoids were co-cultured with GSC for seven days and epithelial cells were infected with *H. pylori* (MOI 50) for 2 h, 6 h, 12 h, 24 h, and 36 h. Non-infected (NI) co-cultured mucosoids served as a control. RT-PCR analyses of *IL8* mRNA expression were performed for the different time points of infection in (A) EPCs and in (B) corresponding GSC. Data were normalized to NI control respectively and are depicted as fold change. Experiment was done once. Error bars represent min and max values of technical triplicate NI: non-infected; hpi: hours post-infection.

The following experiments were done using an infection time of 24 hours to be able to detect both epithelial and stromal immune responses. Besides *IL8*, the mRNA expression level of the cytokines *IL1β* and *IL6* were analyzed in stromal cells, 24 hours after *H. pylori* infection of co-cultured epithelial cells as these were the strongest hits in the microarray analysis.

Results shown in Figure 54 demonstrate that especially mRNA expression level of *IL1β* (Figure 54A) was upregulated with high statistical significance. For *IL6* (Figure 54A) and *IL8* (Figure 54A), also an increase in mRNA expression level was observed. To confirm the results a semi-quantitative cytokine array for IL1β and IL6 was performed using the culture medium 24 hours after infection. The supernatant was centrifuged to remove cell debris prior to the cytokine array. Results revealed that epithelial cells alone did not produce IL1β (Figure 54B). Only in the presence of stromal cells, IL1β was detected in the supernatant, while the amount was dependent on the bacterial load; the stronger the infection, the higher the IL1β response. For infection with an MOI 25, the IL1β concentration was lower than for infection with MOI 100. No IL1β was detected in the non-infected control. These results confirm that the stromal cells are the main source of IL1β and not the epithelial cells. Comparable results were observed in the IL6 cytokine array (Figure 54C). Here as well only in the presence of stromal cells, IL6 was detected in the supernatant. The IL6 concentration did not change with increasing MOI suggesting that the maximal threshold was attained or the system was saturated. Interestingly, also in the supernatant of the non-infected GSC co-cultured control, a high IL6 concentration was detected that was not present in the supernatant of neither non-infected nor infected epithelial cells alone. Again these results strongly confirm that stromal cells were the producer of IL6 and secreted IL6 also under non-infected, homeostatic condition.

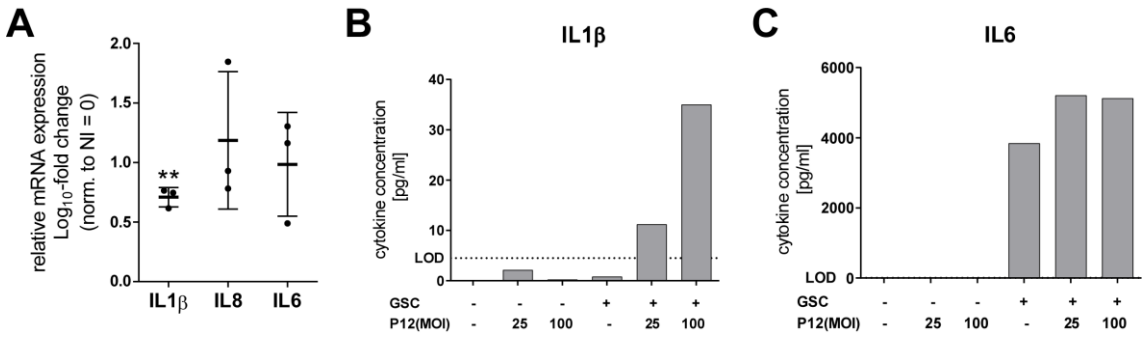

Figure 54: EPC infection induced a strong immune response in GSC. Mucosoid cultures co-cultured with GSCs were infected with *H. pylori* (MOI 50) for 24 hours. (A) RT-PCR analyses of mRNA expression levels of *IL1β*, *IL6* and *IL8* in GSC were performed in three biological replicates calculated as mean ± SD. Paired Student's t-test. **, $p < 0.01$. (B-C) Mucosoids and co-cultured mucosoids were infected with *H. pylori* (MOI25 and MOI100) and culture medium was used for semi-quantitative cytokine array of (B) IL1β and (C) IL6. Culture medium from non-infected culture and co-culture counterparts were used as controls. The experiment was done once. LOD: limit of detection.

4. DISCUSSION

4.1. Development of the mucosoid culture model

Experimental animals and especially genetically modified mice have revealed to be a valuable tool to analyze and understand the biology behind physiological and pathophysiological processes however the transferability of the results to humans has often been argued due to the obvious morphological and genetic differences between these two species. In the last decade, thanks to advancements in stem cell research, it became possible to cultivate human tissue and to propagate this indefinitely by maintaining the stem cells *in vitro*. These cultures are known as organoids and this new cultivation method is paving the way to understand relevant processes of human biology as well as to understand the response of patient-specific cells. However, organoids are a type of batch culture that requires disaggregation and re-seeding every 7 to 10 days (typical passage time). This limitation reduces the time for experimental observations to phenomena that occur during the passage time. Albeit, organoids show an apical-basal polarization a further limitation for their application is the orientation of the apical side which faces the lumen. In fact, this is a limitation for infection studies because to mimic the natural route of infection it is necessary to break the barrier integrity by injecting pathogens into the lumen or disaggregate the organoids. In this thesis, the first example of a stem cell-based human epithelial homeostatic culture that maintains the same stem cell potential of the organoids is presented but they grow indefinitely on a 2D porous surface. Due to the longevity of this culture, this method can be used for the cost-efficient expansion of large amounts of primary cells for experimental purpose and it allows implementation of long-term studies.

The first part of this work aimed to develop this *in vitro* culture model for human gastric primary cells that mimic the biology of epithelial barriers *in vitro* and is suitable for analysis of epithelial homeostasis and infections. Primary gastric epithelial cells were seeded on a porous membrane of a transwell filter insert and cultivated under air-liquid interface conditions. The air-liquid interface technology was adopted from airway

epithelial culture (Gray et al. 1996; Ghio et al. 2013) and the power of this cultivation method is that of forcing the cells of absorbing the nutrients only on their basal side and therefore it enhances distinct apical vs basal features promoting cell polarization. The establishment of this culture takes longer compared to the organoids of the same epithelial origin (Schlaermann et al. 2014). In fact, it takes ten days for the complete polarization. Due to the high similarity with the gastric mucosa, the polarized monolayer *in vitro* culture was named mucosoid culture (short mucosoid). Mucosoid cultures are still able to proliferate even two months after seeding. This long period indicates a permanent cell turnover while the polarized monolayer structure is maintained. This observation implies the presence of long-living stem cells that sustain and constantly regenerate the epithelial monolayer. Furthermore, the longevity of one passage points out that this *in vitro* culture model is suitable for long-term experiments. Comparable with gastric organoids, mucosoids can be segregated and propagated over months with a stable epithelial phenotype and stem cell marker expression. Moreover, the mucosoids harbor the same cell types which populate the antral gland *in vivo* – mucus gland cells, chromogranin A positive enteroendocrine cells, PGC expressing cells. This indicates that the stem cells are retaining the capability to differentiate into all the gastric epithelial lineages present in the antrum. Under the standard growing condition, the mucosoid culture is dominated by MUC6 mucus-secreting cells, while MUC5AC positive pit cells are not or very rarely expressed. The data confirmed that the composition and proportion of the cell types are constant over time and are not influenced during culture propagation. Therefore under standard growing condition the mucosoids represent the intra-glandular epithelium that produces the moistening mucin MUC6 and it includes stem cells. In the small intestine and colon *Lgr5* positive cells were identified as stem cells, responsible for the repopulation of the entire crypt (Barker et al. 2007). *In vitro* experiments conducted by Sato et al. (2009) demonstrated that organoids generated by *Lgr5*+ stem cells highly depend on the activation of the Wnt/β-Catenin signaling pathway. This can be obtained *in vitro* by the supplementation of WNT3A. Similar to the intestinal epithelium also the stem cell niche of the antrum of the gastric epithelium in mice is populated by *Lgr5*+ stem cells which are able to regenerate the entire gastric gland (Barker et al. 2010). Opposite to the intestine, the gastric murine organoids require RSPO in addition to WNT for the Wnt/β-Catenin signaling pathway activation (Barker et al. 2010). Likewise, also the stem cells of the

human stomach depend on WNT and RSPO for stem cell-based regeneration of the epithelium (Schlaermann et al. 2014; Bartfeld et al. 2015). The cultivation of organoids without WNT3A and RSPO1 induce the differentiation of the epithelial cells into foveolar phenotype dominant for MUC5AC (Bartfeld et al. 2015; Schlaermann et al. 2014). The composition of the mucosoid cultivation medium is similar to the one of the gastric organoids. Thus, also for the mucosoid, WNT3A and RSPO1 are essential for the maintenance of the stem cell population *in vitro.* Removal of either WNT3A or RSPO1 or both from the cultivation medium led to a restraint of β-Catenin in the cytoplasm in proximity to the cell membrane and the differentiation of the epithelial cells into foveolar cell type marked by the expression of MUC5AC. Along with the induced foveolar differentiation, the epithelial cells lose their regeneration capacity indicating that the foveolar lineage is probably an endpoint of differentiation. As these cells are located in the lumen of the stomach they are probably shed out of the epithelium and replaced by new cells. Further, the experiment in this thesis indicates that this lineage might not participate in any regenerative program of the gastric gland. Interestingly it was observed that the differentiation into foveolar cells is accompanied by an increase in cell proliferation. The proliferation zone of the antral gland is located sub-foveolar and it is also known as the trans-amplifying compartment. Hence, the detection of foveolar cells and proliferating cells together rather indicate a mixed population of cells from the trans-amplifying compartment and terminally differentiated pit cells. The foveolar cells might derive directly from the differentiation of mucus gland cells (MUC6 positive) or the mucus gland cells first differentiate into cells of the proliferative compartment and subsequentially to foveolar cells. As the position of the stem cells in the human stomach antrum is not known and the differentiation dynamics are still largely unknown, future studies should focus on the use of specific markers to perform lineage tracing *in vitro* by using genetically modified human mucosoids. Such systems should include an inducible Cre reporting system under the control of a lineage-specific promoter: by providing different stimulation to the mucosoids (for example removal of WNT3A and RSPO1) it would be possible to understand if the foveolar cells derive from the transit-amplifying compartment or from the MUC6 cells. Although the mucosoids can differentiate, the distribution of the cells in the monolayer is random due to the lack of a 3D scaffold. It is foreseeable that bioengineering cellular scaffolding technology combined with the regenerative and differentiation power of the mucosoid

will enable the construction of epithelial monolayers folded into gland, where cells might locate at the different positions as in the gastric gland *in situ*.

The herein developed mucosoid culture is a valid *in vitro* culture model for human gastric primary cells allowing a wide range of investigations. The simple switch from mucus gland to surface mucus-secreting cells allows the analysis of cell-specific responses. The apical-basal polarization facilitates the analysis of transport processes in gastric epithelial cells. Compared to organoids the apical side of mucosoids is easily accessible, thus mucosoid cultures are prone to be a valuable tool for pathophysiologic studies like infections or toxic agents. The mucosoid culture model could be further applied to grow pathological conditions of the gastric mucosa like atrophy, intestinal metaplasia or gastric cancer to explore cellular responses, genetic changes or even to perform patient-specific research and to test individual chemotherapy. Thus, it is conceivable to use mucosoid cultures for drug screens and in personalized medicine. A further advantage of the mucosoid culture is the constant accumulation of mucus on the apical side of the epithelial cells inaugurating the possibility to conduct in-depth mucus research. Moreover, mucosoids pave the way to study mucosal drug delivery transport in an *in vitro* system which considers the natural mucosal barrier that is neglected in most cell-based models.

4.2. Differentiation niche factors of the oxyntic gland

The oxyntic gland of the corpus has a more complex structure and harbors more types of specialized cells than the antral gland. Besides mucus-secreting cells and endocrine cells, corpus glands are populated by chief cells and parietal cells. Most of the knowledge is based on mouse studies where genetic tracing is possible. Especially the stem cell compartment of the corpus is poorly understood due to a missing stem cell marker. Lineage tracing experiments in mice revealed that differently to the antrum, in the corpus two stem cell compartments exist: one is localized in the isthmus of the gland, responsible for the fast regeneration of the oxyntic gland and a second stem cell population is located in the base of the gland which are chief cells that are activated upon damage and function as reserve/quiescent stem cells (Han et al. 2019; Leushacke et al. 2017; Stange et al. 2013). Important cell types of the oxyntic gland namely chief cells and parietal cells are either underrepresented or not present at all in organoids (Schlaermann et al. 2014; Bartfeld et al. 2015) which make this *in vitro* model inappropriate to study the physiology of the corpus gland. Chief and parietal cells are long-living (Karam and Leblond 1993a) and their differentiation process might take longer than the life of an organoid passage, explaining the lack of these cells in such cultures. Insights in the anterior-posterior patterning process of the stomach into fundus/corpus and antrum were given by differentiation studies using pluripotent stem cells to grow fundic and antral organoids, respectively and thereby demonstrated the importance of the canonical Wnt/β-Catenin pathway in the developmental fate of fundus and antrum (McCracken et al. 2017; McCracken et al. 2014). Although some understanding exists about the anterior-posterior patterning, the luminal-basal axis patterning of the gastric gland is less known. Especially the differentiation dynamics of foveolar cells, chief cells, and parietal cells are poorly understood due to lack of an appropriate model. The organoid model is limited because of the short lifespan (7-10 days) of one organoid passage making it impossible to study processes of long-living cell populations like chief cells and parietal cells that last longer than an organoid lifespan. The mucosoid culture represents a better model for long term studies as the epithelial cells are stable and long-living for up to two months in the same dish. Corpus epithelial cells were grown on transwell filter inserts following the same protocol

established for antral epithelial cells. To characterize the corpus mucosoids and antral mucosoids, gene expression profiles of both cultures were compared among themselves and with respect to *in vivo* data. The presented data showed that antral mucosoids and corpus mucosoids match the *in vivo* biopsy differential gene expression data, respectively, but the correlation of corpus mucosoids with corpus biopsies was less pronounced than for the antrum counterparts. This observation already indicated that corpus mucosoids lack certain characteristics of corpus tissue *in vivo.* The comparison of the gene expression profile of antrum and corpus mucosoids showed high similarities, but decisive differences were detected in significant genes. Besides *CDX2*, *GAST*, and *SST* which are exclusive markers for antral epithelial cells, differential expression in transcription factors and homeobox genes (e.g. *GATA4, IRX2,3,5*,) was observed that are involved in the patterning of the corpus and antrum during stomach development (McCracken et al. 2017; Mori et al. 2018; Jacobsen et al. 2002). Notably, other genes expressed by corpus specific cell types like parietal cells were not expressed in corpus mucosoids per se. Like organoids, corpus mucosoids harbor none or only very few specialized cell types like parietal cells and chief cells under standard growing culture conditions which favor the longevity of the stem cell population. Notwithstanding, this finding made the mucosoid culture an attractive model to study the differentiation dynamics in the oxyntic gland.

Chief and parietal cells are spatially distributed in the corpus gland but not overlapping with the foveolar cell compartment in the pit region suggesting an underlying mechanism that distinguishes the compartmentalization of foveolar cells from chief and parietal cells. Proliferative cells were only found in the sub-foveolar region as previously shown (Karam and Leblond 1993a) and confirmed in this thesis with human tissue specimens. The Wnt signaling pathway plays an important role during embryonic development (anterior-posterior patterning) but also in adult tissue homeostasis especially in the maintenance and support of the stem cell (reviewed in Kretzschmar and Clevers (2017)). However, the spatially different response is not correlated with different localization of the Wnt ligands and Wnt agonists across the gland, beside RSPO3 which is expressed by cells from the *muscularis mucosae* (Sigal et al. 2015; Sigal et al. 2017). It was suggested that BMP could be the counteracting effector of Wnt (Ye et al. 2018). In the small intestine, the adjacent organ to the stomach, the stem cells

in the crypt base are fueled by WNT and cell differentiation along the crypt-villus axis is regulated by an opposing BMP gradient generated in the villi and active BMP signaling represses the stem cell activity in the crypt base (Auclair et al. 2007; He et al. 2004; Kosinski et al. 2007; Qi et al. 2017). Thus, it was of high interest whether in the stomach BMP pathway agonists are distributed in the same manner. In the presented work, BMP2 and BMP4 were found to be mainly expressed in the isthmus of the corpus gland while the BMP antagonist Noggin was detected in myofibroblasts of the *muscularis mucosae* below the corpus gland. The expression pattern of BMP and Noggin are in line with the findings in the colon crypt suggested by Kosinski et al. (2007). The authors found BMP expression (except BMP4) in the luminal part of murine colon crypts, while myofibroblasts in proximity to the crypt base express BMP antagonists to inhibit the action of BMP in the microenvironment of the stem cells. However, the authors did not find Noggin but gremlin and chordin-like to be expressed by the myofibroblasts as BMP antagonists. While Kosinski et al. (2007) did not observe Noggin expression in the gut, He et al. (2004) reported Noggin expression under lacZ knock-in conditions, but only in traces at gene level and not as protein. Overall both studies found BMP antagonist expression in murine myofibroblasts close to the crypt base similar to the herein detected Noggin expression in the human *muscularis mucosae*. Noggin plays a major role in the regulation of BMP activity, especially during development. The knock-out of Noggin in mice leads for instance to strong skeletal malformations probably to altered activity of BMP (Brunet et al. 1998). Nonetheless, the expression of Noggin in the murine gut is not conclusive from the literature. The present thesis instead shows the definite expression of Noggin in human tissue, highlighting a major difference between humans and the mouse model. Still, the BMP/Noggin interaction does not seem to be sufficient to regulate the differentiation fate in the corpus gland especially of the foveolar compartment. The proliferation zone is located in the sub-foveolar and isthmus region of the gland as shown in this work. Mitogens that promote proliferation are for instance EGF and its homolog TGFα. The first, EGF, is an indispensable supplement for the successful propagation of human gastrointestinal organoids as already concluded in the first organoid cultures by Sato et al. (2009). EGF might trigger the proliferation in the gastric gland through binding to EGFR and downstream activation of the MAPK pathway. The mapping of EGF in the human corpus tissue revealed a higher expression of this morphogen in the foveolar and

isthmus region suggesting that EGF might play a role in the differentiation dynamics. If assuming that stem cells are located in the isthmus also in humans, this population would face active BMP and EGF signaling concluded by the morphogen mapping in this thesis. Noggin would only have a minor effect on the stem cell compartment and none on foveolar cells. Chief cells and parietal cells are slow cycling or not proliferating. These characteristics suggest that both cell types migrate away from the proliferation trigger EGF which fit with the spatial segregation of chief and parietal cells in the corpus gland. The herein presented results indicate that EGF is crucial for foveolar differentiation together with an active BMP signaling pathway. Also *in vitro* epithelial cells are a source of BMP because the BMP signaling pathway has shown to be active in the absence of Noggin. The differentiation towards MUC5AC expressing foveolar cells was induced by active BMP and EGF signaling although WNT3A and RSPO1 were present. Previously it was shown in this work that the withdrawal of WNT3A/RSPO1 induced the differentiation into foveolar phenotype in antrum as well as in corpus epithelial cells *in vitro*. This condition of a complete absence of WNT and RSPO *in vivo* is very unlikely and not physiological, thus the foveolar differentiation rather seems to be regulated by locally active EGF and BMP signaling which is also reflected in the composition of the apical secretome (mucus). MUC5AC and TFF1 were absent when the EGFR signaling pathway was inhibited. In the literature (Goldenring et al. 1996) it was described that the overexpression of TGFα, a homolog of EGF that also binds to EGFR, induces hyperplasia of foveolar cells, supporting the drawn conclusion, while other cell types were not affected in this mouse model.

While EGF is essential for foveolar cell differentiation it is necessary to be absent in the differentiation process of chief cells and parietal cells. Both cell types only arise in the absence of EGF suggesting that EGF is the discriminating factor that determines the differentiation fate. Cells that are responsive to EGF are directed to foveolar differentiation while cells that are less or not responsive to EGF or do not receive the EGF signal are guided to chief cell and parietal cell fate. Active BMP signaling seems to play a secondary role in the differentiation process of chief cells and parietal cells. The obtained data suggest that chief cells are less sensitive to active BMP signaling, but excessive BMP stimulation clearly inhibits the chief cell differentiation. In cell lines it was proposed that an active MAPK pathway might have an inhibitory effect on BMP

signaling pathway at the level of Smad1: EGF/FGF activated ERK phosphorylates Smad1 at a position that inhibits the nuclear accumulation of Smad1 (Kretzschmar, Doody, and Massagu 1997; Sapkota et al. 2007). Consequently, it is also possible that EGF has an additional inhibitory effect on intrinsic BMP signaling and withdrawal of EGF leads to further stimulation of BMP. However, this hypothesis can be rejected as the BMP target gene expression of *ID1* was higher in the presence of EGF than in the absence. Hence, the observed chief cell differentiation was a direct effect of EGF removal and not an indirect effect through possible unblocking of the BMP pathway. The EGFR signaling through the MAPK pathway was confirmed using a MEK inhibitor and similar observations were made regarding the differentiation of chief cells: only if the MAPK pathway was blocked chief cell differentiation occurred. Of note, chief cell culture conditions (+MEKi) lead to reduced accumulation of mucus on epithelial cells which is plausible as mature chief cells do not secrete mucus. Furhtermore, the analysis of the apical secretome showed some accumulation of PGC in the gained chief cell culture but the secretion might not be constitutive. In the future, further focus should be given on the analysis of the regulation of the EGF signaling: Do chief cells simply not receive the EGF signal during downward migration and maturation or are EGF inhibitors involved in this process? The origin of chief cells is still poorly understood; do they develop through trans-differentiation from mucus neck cells as described in rodent models (Huh et al. 2010; Gomez-Santos et al. 2017)? Interestingly, it was reported that parietal cells might influence the differentiation of chief cells but the mechanisms are unknown (Bredemeyer et al. 2009). Thus, the analysis of the origin of chief cell and the interaction with parietal cells could be addressed by the mucosoid model considering the results about the differentiation dynamics presented in this thesis. In future studies, it would be of interest to explore the plasticity of chief cells as they were described to serve as reserve stem cell population in the mouse corpus gland (Stange et al. 2013; Leushacke et al. 2017). Leushacke and colleagues showed that induced cell damage activated the stem cell capacity of chief cells; however, the repopulation of the murine gland was a slow process. Ultimately, the same approach could be applied to chief cells in mucosoid cultures.

The differentiation process of parietal cells was already addressed by McCracken et al. (2017) who developed fundic organoids from human PSC and gained also parietal cells

in vitro by applying a cocktail of high dose BMP4 and MEK inhibitor. Why the authors used an inhibitor for the MAPK pathway is not explained but the administration of BMP4 as an effector for parietal cell differentiation was already suggested before. The ablation of the BMP signal in the microenvironment of parietal cells by induced expression of BMP antagonist Noggin leads to a loss of parietal cells in mice (Shinohara et al. 2010) which indicates the dependency of the parietal cell population on BMP. Results obtained in this thesis showed that similar to chief cells, parietal cell differentiation was only achieved when the EGFR pathway was inactive either by the absence of EGF or by inhibition of the downstream pathway with MEK inhibitor. This phenomenon explains the usage of a MEK inhibitor by McCracken and colleagues because the inactivation of the EGFR pathway is necessary to gain secretory cell lineage differentiation. It was suggested before in *in vitro* studies with isolated canine parietal cells that BMP4 has a stimulatory effect on H^+/K^+ ATPase expression (Nitsche et al. 2007) indicating that also mature parietal cells depend on active BMP signaling. While on gene expression level it seems that intrinsic BMP activation together with EGF removal or EGFR pathway inhibition is sufficient for parietal cell differentiation this observation was not translated on protein level. Here, only with extrinsic BMP4 administration the parietal cell marker ATP4B could be detected on protein level. Furthermore, it is likely that the stimulation of the gastric acid release by histamine has an additional positive effect on the protein expression of the proton pump. In early studies, it was described that EGF has a negative effect on the histamine stimulated acid release in isolated gastric glands from rabbits (Dembiński et al. 1986), but the authors worked with freshly isolated gastric glands in suspension which do not recapitulate the *in vivo* situation and the administered EGF concentration which induced the described effect was rather high. Low EGF concentrations did not have an effect on the gastric acid release. This and related studies imply that EGF influences parietal cells as it was also shown in this thesis although the focus of this work lay in the impact of EGF in the differentiation process of parietal cells and not on their functionality. In future studies, it needs to be examined which role BMP2 in the differentiation process might play as it is expressed in the isthmus of the corpus gland like BMP4 confirmed by *in situ* hybridization. Initial experiments conducted in the department by colleagues indicated that BMP2 did not induce parietal cell differentiation.

Further, it needs to be explored which importance the gastric intrinsic factor (GIF) during parietal cell differentiation has. Is GIF a marker for mature parietal cells like the proton pump or is GIF expressed already early during differentiation? In this thesis, the expression of GIF is rather independent of BMP. Interestingly, in mice GIF is a marker for chief cells but was found to be expressed in humans by parietal cells, a major difference between those two species. In future studies, it needs to be further dissected if GIF is an exclusive marker for parietal cells or if it is expressed by both chief and parietal cells or if it is a common immature progenitor marker. The mouse model is not appropriate to test the hypothesis due to the different expression of GIF in chief cells. Thus, the mucosoid culture model should be adapted for this analysis and human corpus tissue should be evaluated for chief cells, parietal cells (using another marker than GIF) and GIF in parallel. Although McCracken et al. (2017) could already detect and show parietal cells in the fundic organoid culture a major improvement of the here presented work is first the differentiation of functional parietal cells from an adult stem cell culture; second, the number of parietal cells in the mucosoids was comparable to *in vivo* data (Helander, Leth, and Olbe 1986) consequently an enrichment of parietal cells *in vitro* with adult human primary epithelial cells was achieved matching physiological conditions. The ultrastructural shape of the parietal cell population was not found as described in the literature (Karam 1993). The typical triangular shape could not be detected *in vitro* probably due to space problems of the epithelial cells as they are seeded in almost confluency on the transwell filter insert for the mucosoid culture. After four to five weeks in ALI culture about one million epithelial cells, tightly packed in the polarized monolayer are attached to the filter membrane. Thus, large cell types like parietal cells can hardly occupy the needed space. Nonetheless, other very characteristic parietal cell structures were observed like canaliculi and tubulovesicles and an elevated amount of mitochondria concentrated on the apical side of the cell close to the canaliculi (Karam 1993).

In summary, the here presented work showed the successful differentiation of foveolar, chief and parietal cells highlighting the importance of the EGFR pathway in controlling cell differentiation. Foveolar cells are committed to active EGF signaling combined with BMP while chief and parietal cells only arise when the EGF pathway is inactive determining EGF as an important differentiation niche factor. BMP4 and its antagonist

Noggin seem to shape the differentiation fate of the different secretory cell types of the corpus gland in a secondary role. Figure 55 represents a schematic summary of the findings and proposes a model for the differentiation dynamics of the oxyntic gland. How the inactivation of the EGF pathway occurs *in vivo* need to be further elucidated. The fate decision switch between chief cells and parietal cells remains less clear, as these two cell types are intermingled in the corpus gland. Notably, it was shown very early that parietal cells in the base of the gland are less responsive to gastric acid release stimuli than parietal cells in the isthmus and neck region (Coulton and Firth 1988). Later it was suggested that parietal cells migrate down to the base of the gland during aging and these parietal cells in the gland base might be nonfunctional anymore or have other function than acid release (Karam, Yao, and Forte 1997) before they undergo apoptosis and are shed out of the gland revealing that active BMP signaling at this place may not be needed. The herein developed mucosoid culture enriched for chief or parietal or foveolar cells raises the great advantage and unique opportunity to analyze these specialized cell types respectively *in vitro*, for instance, their inflammatory response on pathological stimuli. So far parietal and chief cells could only be analyzed either *in vivo* or by isolating these cell types from biopsies, with a very limited lifespan in culture. It is of high importance to understand the differentiation niche factors that guide the luminal-basal axis patterning as deregulations in this complex network can be probably connected to pathophysiological conditions like infection or the development of gastric cancer. An altered morphogen response against *H. pylori* infection was recently shown by Sigal et al. (2017). The authors observed that *H. pylori* infected mice have an increased expression of RSPO3 in the antral *muscularis mucosae* to activate *Axin2*+ stem cells leading to hyperproliferation and gland hyperplasia maybe to shed out bacteria from the gland. This study indicates that signaling molecules normally involved in the maintenance of homeostatic conditions are influenced and modulated under pathophysiologic conditions. In corpus glands *H. pylori* inhibit acid secretion (Jablonowski et al. 1994; Saha et al. 2010) and is connected with loss of parietal cells (oxyntic atrophy) and SPEM development (Neu et al. 2002; Wang et al. 1998; Goldenring and Nam 2010). The second type of atrophic gastritis in the corpus (do not exist in the antrum) is the autoimmune metaplastic atrophic gastritis (AMAG or AIG). This AIG leads to loss of parietal cells due to autoantibody reaction in which cytotoxic T cells recognize the H^+/K^+ ATPase on parietal cells (Minalyan et al. 2017). However,

AIG differs from *H. pylori* induced oxyntic atrophic gastritis in clinical and morphological aspects (Venerito et al. 2016) and how *H. pylori* perturbs the homeostasis of parietal cells and the progress of SPEM is still poorly understood. It could well be that *H. pylori* do not only induce apoptosis in parietal cells as suggested by Neu et al. (2002) but rather disturb directly or indirectly (maybe through inflammatory processes or signaling crosstalk) underlying mechanisms like the EGFR pathway that control the differentiation of specialized cells like parietal and chief cells. Hence, the parietal cells and finally also chief cells are lost because new parietal and chief cells do not arise due to deregulated differentiation signals and TFF2 positive mucus cells can expand leading to the development of SPEM. This hypothesis needs to be proven by analyzing the expression of the morphogens (*EGF*, *BMP4*, *Noggin*) involved in foveolar, chief and parietal cell differentiation explored in this work, in different states of the Correa's cascade like *H. pylori* induced chronic gastritis, atrophic gastritis/SPEM and possibly also intestinal metaplasia and gastric cancer. Unfortunately, SPEM is not distinguishable in patients macroscopically and is rather classified as atrophy. Indications are given by some studies which demonstrated that *H. pylori* influence the EGFR pathway. It was shown that *H. pylori* induce an upregulation of EGFR in gastric cancer cell lines *in vitro* (Keates et al. 2007) to probably inhibit apoptosis (Yan et al. 2009). Elevated levels of EGF and EGFR were also reported in patients with chronic gastritis induced by *H. pylori* which were normalized to basal level after *H. pylori* eradication (Wong et al. 2001; Jurkowska et al. 2014). Assuming that *H. pylori* alter the EGFR pathway this would induce an expansion of foveolar cells causing foveolar hyperplasia at the expense of chief cells and parietal cells as both cell types absolutely need the absence of EGF to differentiate. The foveolar hyperplasia would lead to a shed out of bacteria from the gastric gland rather indirectly due to altered foveolar differentiation fate than a direct defense mechanism by the epithelial cells. First experiments by colleagues in the department indicate an increase of EGF in atrophic samples concurrently with chief and parietal cell marker decrease. In general EGFR and its ligands were found to be elevated in many carcinoma types also in gastric cancer and were connected with poor prognosis, thus making this pathway an important target for cancer therapy (reviewed in Normanno et al. (2006)). Oppositely, Nam et al. (2009) showed that in mice the knockout of Amphiregulin (AREG), an EGF-like molecule binding and activating the EGFR pathway like EGF, lead to the

development of SPEM that progressed into intestinal metaplasia. This thesis highlights the important role of EGF in the gastric epithelium homeostasis and it suggests that the regulation of this factor and of the signaling cascade that it provokes through the EGFR plays a major role in the changes of tissue morphology observed during disease progression to gastric cancer.

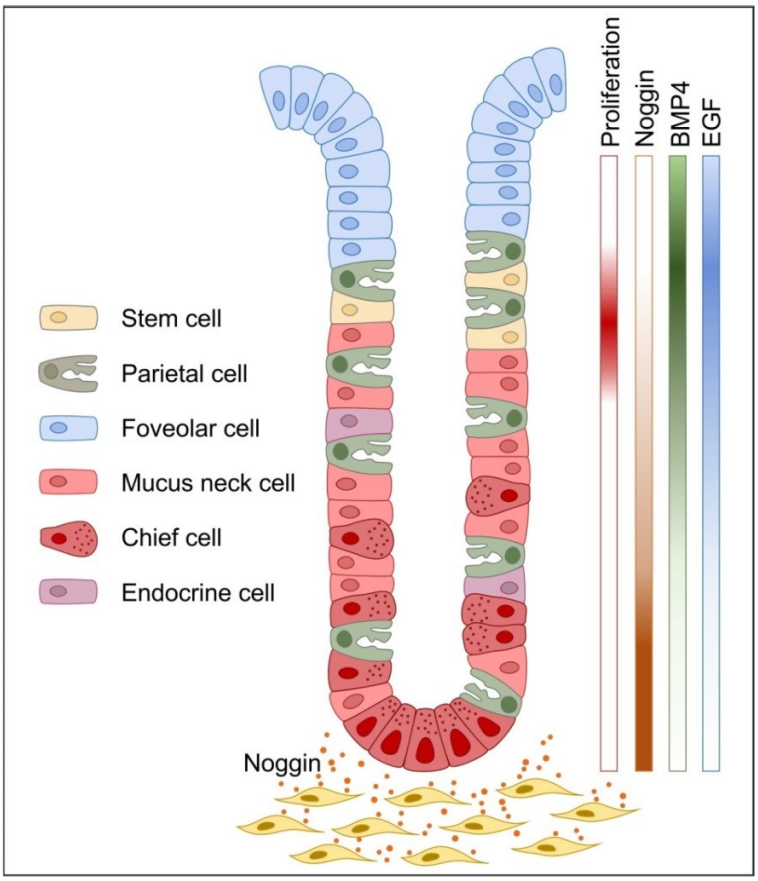

Figure 55: Proposed model for involved processes in the luminal-basal axis patterning of the oxyntic gland. The scheme represents the oxyntic gland populated with different specialized cell types and assuming that also in humans' fast-regenerating stem cells (yellow) are located in the isthmus region. Foveolar cells (blue) are present in the pit region, while parietal cells (green) populate the isthmus, neck and rarely also the base of the gland. Chief cells (dark red with dots) are mainly located in the base and the neck region and mucus neck cells (bright red) are present mainly in the isthmus and neck, more rarely in the base. The proliferation zone is located in the isthmus and sub-foveolar region. EGF and BMP4 signaling pathways are involved in the differentiation dynamics of foveolar, chief, and parietal cells. A gradient of BMP4 and EGF exists from the isthmus to the base of the gland. The BMP4 effect is counteracted by the antagonist Noggin which is expressed by stromal cells below the gastric gland. Foveolar differentiation highly depends on active EGF and BMP signaling while chief and parietal cells only arise when the EGF pathway is inactive. BMP4 favors parietal cell fate, while high BMP4 concentrations block chief cell differentiation. The scheme was developed in collaboration with Diane Schad.

4.3. Communication between stroma and epithelium

Stromal cells are a layer of fibroblast-like cells underneath every epithelial layer: their role is to produce the extracellular matrix for the structural support of the organ but they are also classified as non-professional antigen-presenting cells with immunomodulatory function. The interaction of the stroma with the adjacent epithelium starts as early as embryogenesis and continues in adults to maintain tissue homeostasis. Little is known about the communication between the stromal cells of the *lamina propria* and the epithelium and in this thesis, this interaction is studied for stomach cells using the mucosoid cultures.

Human primary gastric stromal cells (GSCs) were isolated from the same specimen as the gastric epithelial cells and successfully cultivated for long time *in vitro*. To analyze the paracrine cross-signaling between stromal cells and the epithelial counterpart the mucosoid culture model was used and co-culture of both cell types was performed, recapitulating the *in vivo* situation. The supportive effect of fibroblasts on epithelial cells was known and used before in the so-called feeder cell cultures; here epithelial cells are seeded on a confluent layer of growth-arrested but metabolically active fibroblasts. The feeder cells improve the epithelial cell viability and proliferation by providing ECM components and growth factors which are replaced by synthetic components like Matrigel in organoid cultures. However, feeder cell cultures are not considered as co-cultures because only one cell type in this system is proliferating while in co-cultures both cell types need to be proliferative (summarized in Llames et al. (2015)). Ootani et al. (2003) described that the co-cultivation of gastric epithelial cells of newborn mice with gastric fibroblasts induced foveolar differentiation in epithelial cells but the underlying mechanism, how the fibroblasts induced epithelial differentiation into foveolar phenotype remained unclear. Still, this indication together with the herein presented results in section 3.1.2, that removal of WNT3A and RSPO1 from the cultivation medium induced foveolar differentiation in mucosoids led to the hypothesis that stromal cells influence the canonical Wnt pathway in epithelial cells resulting in foveolar differentiation. The results in section 3.3.2 confirmed that gastric

stromal cells impair the Wnt/β-Catenin pathway through active secretion of different Wnt pathway inhibitors which either block the Wnt receptor LRP5/6 like DKK1 or prevent the Wnt ligand from receptor binding like sFRP1 and sFRP4. As a consequence, the expression of the Wnt signaling pathway target gene *LGR5* was significantly downregulated. Similarly, DKK1 and DKK3 were exhibited to be expressed in the murine antrum likewise DKK4 which in contrast was not detected in human stromal cells (Sigal et al. 2017). Of note Sigal et al. (2017) also reported that Wnt ligands are expressed throughout the stomach tissue. Active Wnt signaling instead is only detected in the gland base and the Wnt activity is regulated by RSPO3 secreted by stromal cells below the gland. However, stromal Wnt inhibitors might restrict the Wnt activity in the luminal part of the gland to provide the microniche for the differentiation of foveolar cells. Although the Wnt/β-Catenin pathway was markedly inhibited in epithelial cells by GSCs only part of the epithelial cells was positive for MUC5AC and differentiate into foveolar cells. Likewise in the mucosoid the spatial resolution of the single niche factors is lost thus it is possible to hypothesize that as in the mouse, the soluble WNT inhibitors are produced by distinct stromal cells of the *lamina propria* in a specific position. As those Wnt inhibitors are soluble their effect might be local and therefore induce the differentiation only where they are produced. This implies that the stromal cells might be different and that similarly to the epithelium they can differentiate into lineages and different subpopulations exist. Single-cell RNA sequencing would provide relevant information about possible subpopulations. With this technique, cells are clustered by joint characteristics as it was shown for the colon where different stromal subsets were identified (Kinchen et al. 2018). Ultimately, if different stroma subsets exist within the *lamina propria* they should be distinguishable and can be further characterized and mapped back to their site of origin along the luminal-basal axis of the gastric gland. Indications for the heterogeneity of the stromal cells were found in the murine intestine and reported for instance by Stzepourginski et al. (2017) who identified a $CD34^+$ stromal cell subpopulation in close vicinity to the crypt base where *Lgr5*+ stem cells are located to be responsible for the secretion of RSPO1 and BMP antagonist Gremlin 1 to maintain the stem cell niche and inhibit BMP signaling. BMPs, in turn, are higher expressed in the top of the crypt to probably guide intestinal epithelial cell differentiation (Kosinski et al. 2007). In the murine antrum, it was shown that fibroblasts in proximity to the stem cells in the gland base express RSPO3 and maintain

thereby the niche (Sigal et al. 2017) but a further characterization of these stroma cells is still missing. Likewise, human stromal cells from the *muscularis mucosae* which were also isolated and cultivated *in vitro*, but were not discussed in this thesis, were positively tested for the expression of RSPO3, indicating that comparable mechanism might exist in the human antrum as in the murine antrum. As discussed before for the corpus (see section 4.2), foveolar differentiation requires the activation of EGFR and BMP signaling pathway. Although the Antrum has less parietal and chief cells and the gland is, therefore, shorter in size it is plausible that EGF and BMP are also expressed in the antrum gland and that together with the WNT inhibitors might contribute the foveolar differentiation. This study together with others is unravelling the role of multiple signaling pathways that contribute to the gastric epithelium homeostasis and differentiation and it predicts that by mapping all these signals into the human tissue *in situ* might reveal fine details of how the cell fate is governed in the gland.

After confirming that the stroma signals to the epithelium it has been verified if this condition could be perturbed after infection with *H. pylori*. Successful infection of the mucosoids with *H. pylori* was confirmed by detecting the phosphorylation of CagA as this bacterial virulence factor is injected into the host cells and phosphorylated by a host kinase and by visualizing attached bacteria on the epithelial surface of an infected mucosoid culture. Furthermore, the infection induced an acute NFκB driven immune response in epithelial cells even after three days of infection emphasizing the benefits of using this tool for long-term infection studies. To characterize the role of stromal cells against infection, the gene expression profile of infected mucosoids and co-cultured mucosoids and their non-infected counterparts were compared in a microarray analysis. Epithelial cells co-culture with their stromal counterpart show a difference in the expression of pro-inflammatory genes after infection compared to the epithelium alone. Although the expression of a panel of NFκB target genes was induced in infected mucosoids, the alteration for a subset of NFκB target genes (e.g. *CXCL8*, *CXCL5* or *TNF*) was higher in infected co-cultured mucosoids, thus indicating that stromal cells actively enhance the epithelial response against infection. Notably, a small set of NFκB target genes was differently regulated and only induced in infected co-cultured mucosoids including *IL1β*, *IL1α*, *IL18*, and *MMP1*. This observation suggests that

stromal cells modulate and activate the production of specific cytokines in epithelial cells.

Simultaneously, the comparison of the gene expression profile of corresponding GSC (infected vs non-infected epithelial counterpart) indicated a strong inflammatory response in GSCs when epithelial cells were infected. Specifically *IL1β*, *IL6*, and *IL8* were induced in GSC upon infection and interestingly the *IL1β* response was higher in GSCs compared to EPCs validating that stromal cells have a strong immunomodulatory capability. Also in other tissues like the colonic mucosa, it was reported that a subpopulation of $CD90^+$ stromal cells reacts actively to bacterial infection with the expression of IL1 family cytokines (Owens et al. 2013). In contrast to the referred study in which stromal cells were directly infected with *Salmonella*, the gastric stromal cells were not in contact with *H. pylori.* The activation was exclusively through paracrine signaling with infected epithelial cells emphasizing active intercellular communication. Interestingly, gene expression profiles of -W-R mucosoids, which exhibit complete foveolar phenotype, compared to +W+R mucosoids, both infected with *H. pylori* showed that foveolar cells have a lower inflammatory response than undifferentiated epithelial cells (data was generated by Dr. Francesco Boccellato and is part of the publication Boccellato et al. (2018)). Co-cultured epithelial cells instead are partially differentiated but show enhanced NFκB dependent transcriptional signature after infection with *H. pylori,* compared with the epithelium infected without stroma. This apparent contradiction could be attributed to the additional pro-inflammatory promoting effect of the stromal cells on the epithelial cells, most probably due to their secreted cytokines which affect the epithelial cells and enhance the epithelial immune response independent of the differentiation state. Notably, the stromal response is induced after the epithelial response against the infection suggesting that the inflammatory cascade follows a logical sequence of events: first epithelial cells are activated and secrete cytokines which induce downstream an immune response in stromal cells. The stromal cytokines in turn probably intensify the epithelial cytokine expression proposing that the communication is bi-directional. It was reported before that epithelial cells secrete chemokines and cytokines against *H. pylori* infection which attract mesenchymal stromal cells (isolated from bone marrow) to migrate to the site of infection to induce tissue repair (Ferrand et al. 2011). This phenomenon could not be observed in the herein

used *in vitro* model because of the co-culture setting (both cell types were adherent and the pore size of the filter membrane was too small and did not allow the migration of any cell) but the time-shifted response of the stromal cells after the epithelial response implies that stromal cells are directly targeted and stimulated by the epithelial cells.

In addition, stromal cytokines could activate and recruit immune cells to the site of infection. The co-culture of stromal cells and epithelial cells recapitulates the gastric mucosa *in vivo* and the infection with *H. pylori* demonstrated the active communication between both compartments. Still, the model has limitations because only part of the complex interaction network of the gastric mucosa is reproduced. As previously mentioned stromal cells are a heterogeneous population of cells with specific characteristics depending on the geographical positioning and the cell identity. The heterogeneity of the stromal cells is neither considered in the analysis of the communication against infection and as discussed earlier for homeostatic condition this should be the focus of future research. Along with the generation of different microniches by epithelial and stromal cells due to their functional compartmentalization along the luminal-basal axis, immune cells are also highly diverse and are distributed accordingly to the microniches. Like stromal and epithelial cells, immune cells also actively communicate with adjacent cell types in the tissue, especially during inflammation. Depending on the surrounding immune cell subset the stromal cells are instructed to secrete a panel of cytokines and vice versa. Under homeostatic conditions, stromal cells probably suppress the immune response and promote the development of regulatory T cells (Pinchuk et al. 2011). It is likely that activated stromal cells and also epithelial cells during *H. pylori* infection induce the activation of different immune cells. Among others, these could be tissue-resident innate lymphoid cells (ILC) like ILC3 which respond to bacterial infection. The focus and interest on tissue-resident immune cells as a first reactive cell population in place on pathophysiological conditions rather than migrating lymphoid tissue immune cells raised in the last decade however almost nothing is known in the gastric mucosa. In the intestinal mucosa instead, ILC3's are well-described key players in antimicrobial defense (reviewed in Geremia and Arancibia-Cárcamo (2017)). Buonocore et al. (2010) firstly described ILC3's which are activated by IL23 and secrete upon activation of the cytokines IL17 and IL22. Interestingly, also IL1β was found to induce the differentiation of ILC1 into

ILC3 (Bernink et al. 2015) which suggests a connection of the herein detected stromal produced IL1β against *H. pylori* infection with downstream processes regulating the inflammatory response. Furthermore, also IL6 was suggested to influence the cytokine production in ILC3 in the intestine during inflammation (Powell et al. 2015) proposing another target site of the stromal produced IL6 against *H. pylori* infection. Hence, it needs to be examined if the stromal produced cytokines IL1β and IL6 are activators of ILC3's also in the gastric mucosa and future studies should include immune cells specifically ILC3 from the human gastric mucosa in the mucosoid co-culture together with stromal cells to analyze whether similar mechanisms as in the intestine are valid. Alternatively, the co-culture could also be performed only with immune cells instead of stromal cells to decipher the communication between the epithelium and specific immune cells *in vitro*. Beside ILC3's also other immune cells like Th17 cells were reported to be activated from stromal cells upon *H. pylori* infection (Pinchuk et al. 2013).

In summary, the work in this thesis shows that stromal and epithelial cells of the gastric mucosa actively communicate and regulate epithelial cell homeostasis as well as acute inflammation responses. Stromal cells might take the role of a mediator under pathologic conditions between the epithelial cells as the first line of defense against damage and injury and putatively the immune system as an effector to regulate and control inflammation. Notably, they are not only transferring the signal from the epithelium to the immune cells as the data suggested but actively and offensively react and instruct the adjacent epithelial cells to enhance their immune response probably to recruit more immune cells but maybe also to enforce microbial peptide secretion and defense mechanisms to fight the bacterial invasion. The communication works in both directions from the epithelium to the stroma and vice versa. The mucosoid cultures are a suitable model to study the interaction between these two cell populations and further experiments are needed to understand the effectiveness of this communication especially in controlling bacterial infection. Herein presented results set the base for future investigations aiming to shed further light into the complex interaction network of different cell types of the gastric mucosa. The herein performed co-culture was without cell-cell contact between the two cell types aiming to analyze the paracrine intercellular communication between stroma and epithelium. In future studies, this

model could be adapted to perform co-cultures in which both epithelial and stromal cells are in contact to explore the signaling based on cell-cell contact and whether the gene expression profiles change due to the vicinity of both cell types. Moreover, the co-culture could be expanded and other cell types of the *lamina propria* like immune cells should be included to receive further insights into the interesting and very complex interaction network of the gastric mucosa.

5. CONCLUSION

The work presented in this thesis showed the successful establishment and application of a stem cell driven *in vitro* culture for human primary gastric epithelial cells to study tissue homeostasis and response to infections. The herein developed mucosoid culture model recapitulates the *in vivo* situation of the antral gastric gland and mimics the biology of the epithelial barrier *in vitro*. Indeed, the polarized monolayer harbors the same specialized cell types that are found in the human antral gland and represent the intra-glandular part under standard growing conditions. Due to its longevity mucosoid cultures can be applied for long-term studies. It was further shown that an active Wnt/β-Catenin pathway is essential for antral stem cells and abrogation of the Wnt/β-Catenin pathway induced foveolar differentiation.

The mucosoid culture model was further used to explore the niche factors that are involved in the differentiation dynamics of the corpus gland. Under normal culture conditions corpus mucosoids lack important specialized cell types like in the organoid model but the long-living and stable epithelial cells of the mucosoid culture made it an appropriate model to study long-term processes like the differentiation of parietal and chief cells. The collected *in vitro* data perfectly coincided with human specimens *in situ.* A further novelty of this study was the localization of Noggin in the *muscularis mucosae* antagonizing the BMP pathway. Likewise to antral mucosoids, foveolar differentiation in corpus mucosoids could be induced by inactivation of the Wnt/β-Catenin pathway however another mechanism could be more physiologic. It was demonstrated that EGF is indispensable for foveolar cell differentiation together with an active BMP pathway. Oppositely EGF is detrimental for the differentiation of chief cells and parietal cells. It remains less clear how the fate decision between both cell types occur as chief and parietal cells are intermingled in the gland but the collected data indicates that BMP could be the discriminating factor as high BMP concentrations are destructive for chief cells. The here presented results could be the basis for future investigations to understand pathophysiologic changes in the gastric mucosa like SPEM.

In summary the mucosoid culture is a suitable model for human primary gastric epithelial cells that allows a wide range of investigations and paves the way for multiple

applications. To get further insight into physiologic processes, mucosoids could be genetically manipulated to perform for instance lineage tracing. Furthermore, future studies should also focus on pathophysiologic conditions and infection. The mucosoid culture could be used to grow pathologic states of the gastric mucosa like atrophy, metaplasia or gastric cancer to explore cellular responses, genetic and phenotypic changes or to test individual chemotherapy. Moreover, the accumulation of mucus by the epithelial cells allows in depth mucus research.

In the third part of this study, the mucosoid culture model was applied for the co-culture of epithelial cells with GSC to analyze the communication between stroma and epithelium under physiologic conditions but also after infection with *H. pylori.* It was shown that stromal cells actively communicate with epithelial cells under physiologic conditions and against infection. During infection stromal cells are activated by paracrine stimuli from epithelial cells to produce cytokines and chemokines and they modulate in turn the inflammatory response in epithelial cells. In future studies the signaling between stroma and epithelium should be investigated in more detail considering also the immune system in the response to infections.

6. REFERENCES

Aggarwal, S., and M. F. Pittenger. 2005. 'Human mesenchymal stem cells modulate allogeneic immune cell responses', *Blood*, 105: 1815-22.

Al Menhali, A., T. M. Keeley, E. S. Demitrack, and L. C. Samuelson. 2017. 'Gastrin induces parathyroid hormone-like hormone expression in gastric parietal cells', *Am J Physiol Gastrointest Liver Physiol*, 312: G649-g57.

Ameri, J., A. Stahlberg, J. Pedersen, J. K. Johansson, M. M. Johannesson, I. Artner, and H. Semb. 2010. 'FGF2 specifies hESC-derived definitive endoderm into foregut/midgut cell lineages in a concentration-dependent manner', *Stem Cells*, 28: 45-56.

Aoki, T. O., N. B. David, G. Minchiotti, L. Saint-Etienne, T. Dickmeis, G. M. Persico, U. Strahle, P. Mourrain, and F. M. Rosa. 2002. 'Molecular integration of casanova in the Nodal signalling pathway controlling endoderm formation', *Development*, 129: 275-86.

Arnold, K., A. Sarkar, M. A. Yram, J. M. Polo, R. Bronson, S. Sengupta, M. Seandel, N. Geijsen, and K. Hochedlinger. 2011. 'Sox2(+) adult stem and progenitor cells are important for tissue regeneration and survival of mice', *Cell Stem Cell*, 9: 317-29.

Auclair, B. A., Y. D. Benoit, N. Rivard, Y. Mishina, and N. Perreault. 2007. 'Bone morphogenetic protein signaling is essential for terminal differentiation of the intestinal secretory cell lineage', *Gastroenterology*, 133: 887-96.

Augello, A., R. Tasso, S. M. Negrini, A. Amateis, F. Indiveri, R. Cancedda, and G. Pennesi. 2005. 'Bone marrow mesenchymal progenitor cells inhibit lymphocyte proliferation by activation of the programmed death 1 pathway', *Eur J Immunol*, 35: 1482-90.

Backert, Steffen, and Martin J. Blaser. 2016. 'The Role of CagA in the Gastric Biology of Helicobacter pylori', *Cancer Res*, 76: 4028.

Barker, N., M. Huch, P. Kujala, M. van de Wetering, H. J. Snippert, J. H. van Es, T. Sato, D. E. Stange, H. Begthel, M. van den Born, E. Danenberg, S. van den Brink, J. Korving, A. Abo, P. J. Peters, N. Wright, R. Poulsom, and H. Clevers. 2010. 'Lgr5(+ve) stem cells drive self-renewal in the stomach and build long-lived gastric units in vitro', *Cell Stem Cell*, 6: 25-36.

Barker, N., J. H. van Es, J. Kuipers, P. Kujala, M. van den Born, M. Cozijnsen, A. Haegebarth, J. Korving, H. Begthel, P. J. Peters, and H. Clevers. 2007. 'Identification of stem cells in small intestine and colon by marker gene Lgr5', *Nature*, 449: 1003-7.

Bartfeld, S., T. Bayram, M. van de Wetering, M. Huch, H. Begthel, P. Kujala, R. Vries, P. J. Peters, and H. Clevers. 2015. 'In vitro expansion of human gastric epithelial stem cells and their responses to bacterial infection', *Gastroenterology*, 148: 126-36.e6.

Bartfeld, S., S. Hess, B. Bauer, N. Machuy, L. A. Ogilvie, J. Schuchhardt, and T. F. Meyer. 2010. 'High-throughput and single-cell imaging of NF-kappaB oscillations using monoclonal cell lines', *BMC Cell Biol*, 11: 21.

Bartman, A. E., M. P. Buisine, J. P. Aubert, G. A. Niehans, N. W. Toribara, Y. S. Kim, E. J. Kelly, J. E. Crabtree, and S. B. Ho. 1998. 'The MUC6 secretory mucin gene is expressed in a wide variety of epithelial tissues', *J Pathol*, 186: 398-405.

Bauer, Bianca, and Thomas F. Meyer. 2011. 'The Human Gastric Pathogen Helicobacter pylori and Its Association with Gastric Cancer and Ulcer Disease', *Ulcers*, 2011: 1-23.

Bayha, E., M. C. Jorgensen, P. Serup, and A. Grapin-Botton. 2009. 'Retinoic acid signaling organizes endodermal organ specification along the entire antero-posterior axis', *PLoS One*, 4: e5845.

Beauchamp, R. D., J. A. Barnard, C. M. McCutchen, J. A. Cherner, and R. J. Coffey, Jr. 1989. 'Localization of transforming growth factor alpha and its receptor in gastric mucosal cells. Implications for a regulatory role in acid secretion and mucosal renewal', *J Clin Invest*, 84: 1017-23.

Ben-Haim, N., C. Lu, M. Guzman-Ayala, L. Pescatore, D. Mesnard, M. Bischofberger, F. Naef, E. J. Robertson, and D. B. Constam. 2006. 'The nodal precursor acting via activin receptors induces mesoderm by maintaining a source of its convertases and BMP4', *Dev Cell*, 11: 313-23.

Bernardo, Maria Ester, and Willem E Fibbe. 2013. 'Mesenchymal Stromal Cells: Sensors and Switchers of Inflammation', *Cell Stem Cell*, 13: 392-402.

Bernink, J. H., L. Krabbendam, K. Germar, E. de Jong, K. Gronke, M. Kofoed-Nielsen, J. M. Munneke, M. D. Hazenberg, J. Villaudy, C. J. Buskens, W. A. Bemelman, A. Diefenbach, B. Blom, and H. Spits. 2015. 'Interleukin-12 and -23 Control Plasticity of CD127(+) Group 1 and Group 3 Innate Lymphoid Cells in the Intestinal Lamina Propria', *Immunity*, 43: 146-60.

Boccellato, F., S. Woelffling, A. Imai-Matsushima, G. Sanchez, C. Goosmann, M. Schmid, H. Berger, P. Morey, C. Denecke, J. Ordemann, and T. F. Meyer. 2018. 'Polarised epithelial monolayers of the gastric mucosa reveal insights into mucosal homeostasis and defence against infection', *Gut*.

Bredemeyer, A. J., J. H. Geahlen, V. G. Weis, W. J. Huh, B. H. Zinselmeyer, S. Srivatsan, M. J. Miller, A. S. Shaw, and J. C. Mills. 2009. 'The gastric epithelial progenitor cell niche and differentiation of the zymogenic (chief) cell lineage', *Dev Biol*, 325: 211-24.

Brunet, Lisa J., Jill A. McMahon, Andrew P. McMahon, and Richard M. Harland. 1998. 'Noggin, Cartilage Morphogenesis, and Joint Formation in the Mammalian Skeleton', *Science*, 280: 1455.

Buechler, Matthew B., and Shannon J. Turley. 2018. 'A short field guide to fibroblast function in immunity', *Semin Immunol*, 35: 48-58.

Buonocore, Sofia, Philip P. Ahern, Holm H. Uhlig, Ivaylo I. Ivanov, Dan R. Littman, Kevin J. Maloy, and Fiona Powrie. 2010. 'Innate lymphoid cells drive interleukin-23-dependent innate intestinal pathology', *Nature*, 464: 1371.

Caliari, Steven R., and Jason A. Burdick. 2016. 'A practical guide to hydrogels for cell culture', *Nature Methods*, 13: 405.

Campisi, J. 1997. 'The biology of replicative senescence', *Eur J Cancer*, 33: 703-9.

Chapman, S., X. Liu, C. Meyers, R. Schlegel, and A. A. McBride. 2010. 'Human keratinocytes are efficiently immortalized by a Rho kinase inhibitor', *J Clin Invest*, 120: 2619-26.

Choi, E., J. T. Roland, B. J. Barlow, R. O'Neal, A. E. Rich, K. T. Nam, C. Shi, and J. R. Goldenring. 2014. 'Cell lineage distribution atlas of the human stomach reveals heterogeneous gland populations in the gastric antrum', *Gut*, 63: 1711-20.

Clevers, Hans, Kyle M. Loh, and Roel Nusse. 2014. 'An integral program for tissue renewal and regeneration: Wnt signaling and stem cell control', *Science*, 346: 1248012.

Correa, P., W. Haenszel, C. Cuello, S. Tannenbaum, and M. Archer. 1975. 'A model for gastric cancer epidemiology', *Lancet*, 2: 58-60.

Correa, P., and M. B. Piazuelo. 2012. 'The gastric precancerous cascade', *J Dig Dis*, 13: 2-9.

Coulton, Gary R., and J. Anthony Firth. 1988. 'Effects of starvation, feeding, and time of day on the activity of proton transport adenosine triphosphatase in the parietal cells of the mouse gastric glands', *Anat Rec*, 222: 42-48.

Cover, Timothy L., and Martin J. Blaser. 2009. 'Helicobacter pylori in health and disease', *Gastroenterology*, 136: 1863-73.

Cox, J., and M. Mann. 2008. 'MaxQuant enables high peptide identification rates, individualized p.p.b.-range mass accuracies and proteome-wide protein quantification', *Nat Biotechnol*, 26: 1367-72.

Cristofalo, V. J., A. Lorenzini, R. G. Allen, C. Torres, and M. Tresini. 2004. 'Replicative senescence: a critical review', *Mech Ageing Dev*, 125: 827-48.

Daya-Grosjean, L., B. Azzarone, R. Maunoury, P. Zaech, G. Elia, S. Zaniratti, and A. Benedetto. 1984. 'SV40 immortalization of adult human mesenchymal cells from neuroretina. Biological, functional and molecular characterization', *Int J Cancer*, 33: 319-29.

De Bolos, C., M. Garrido, and F. X. Real. 1995. 'MUC6 apomucin shows a distinct normal tissue distribution that correlates with Lewis antigen expression in the human stomach', *Gastroenterology*, 109: 723-34.

de Martel, Catherine, Jacques Ferlay, Silvia Franceschi, Jérôme Vignat, Freddie Bray, David Forman, and Martyn Plummer. 2012. 'Global burden of cancers attributable to infections in 2008: a review and synthetic analysis', *The Lancet Oncology*, 13: 607-15.

de Martel, Catherine, David Forman, and Martyn Plummer. 2013. 'Gastric Cancer: Epidemiology and Risk Factors', *Gastroenterol Clin North Am*, 42: 219-40.

Dembiński, A., D. Drozdowicz, H. Gregory, S. J. Konturek, and Z. Warzecha. 1986. 'Inhibition of acid formation by epidermal growth factor in the isolated rabbit gastric glands', *The Journal of Physiology*, 378: 347-57.

Demitrack, Elise S., Gail B. Gifford, Theresa M. Keeley, Alexis J. Carulli, Kelli L. VanDussen, Dafydd Thomas, Thomas J. Giordano, Zhenyi Liu, Raphael Kopan, and Linda C. Samuelson. 2015. 'Notch signaling regulates gastric antral LGR5 stem cell function', *Embo j*, 34: 2522-36.

Derynck, Rik, and Ying E. Zhang. 2003. 'Smad-dependent and Smad-independent pathways in TGF-β family signalling', *Nature*, 425: 577-84.

Dessimoz, J., R. Opoka, J. J. Kordich, A. Grapin-Botton, and J. M. Wells. 2006. 'FGF signaling is necessary for establishing gut tube domains along the anterior-posterior axis in vivo', *Mech Dev*, 123: 42-55.

DeWard, Aaron D, Julie Cramer, and Eric Lagasse. 2014. 'Cellular Heterogeneity in the Mouse Esophagus Implicates the Presence of a Nonquiescent Epithelial Stem Cell Population', *Cell Reports*, 9: 701-11.

Di Nicola, M., C. Carlo-Stella, M. Magni, M. Milanesi, P. D. Longoni, P. Matteucci, S. Grisanti, and A. M. Gianni. 2002. 'Human bone marrow stromal cells suppress T-lymphocyte proliferation induced by cellular or nonspecific mitogenic stimuli', *Blood*, 99: 3838-43.

Dockray, G. J., A. Varro, and R. Dimaline. 1996. 'Gastric endocrine cells: gene expression, processing, and targeting of active products', *Physiol Rev*, 76: 767-98.

Dominici, M., K. Le Blanc, I. Mueller, I. Slaper-Cortenbach, F. Marini, D. Krause, R. Deans, A. Keating, Dj Prockop, and E. Horwitz. 2006. 'Minimal criteria for defining multipotent mesenchymal stromal cells. The International Society for Cellular Therapy position statement', *Cytotherapy*, 8: 315-7.

Dutta, D., and H. Clevers. 2017. 'Organoid culture systems to study host-pathogen interactions', *Curr Opin Immunol*, 48: 15-22.

Ehata, Shogo, Yuichiro Yokoyama, Kei Takahashi, and Kohei Miyazono. 2013. 'Bi-directional roles of bone morphogenetic proteins in cancer: Another molecular Jekyll and Hyde?', *Pathology International*, 63: 287-96.

Fedosov, Sergey N. 2012. 'Physiological and Molecular Aspects of Cobalamin Transport.' in Olaf Stanger (ed.), *Water Soluble Vitamins: Clinical Research and Future Application* (Springer Netherlands: Dordrecht).

Ferrand, J., P. Lehours, A. Schmid-Alliana, F. Megraud, and C. Varon. 2011. 'Helicobacter pylori infection of gastrointestinal epithelial cells in vitro induces mesenchymal stem cell migration through an NF-kappaB-dependent pathway', *PLoS One*, 6: e29007.

Forbester, J. L., D. Goulding, L. Vallier, N. Hannan, C. Hale, D. Pickard, S. Mukhopadhyay, and G. Dougan. 2015. 'Interaction of Salmonella enterica Serovar Typhimurium with Intestinal Organoids Derived from Human Induced Pluripotent Stem Cells', *Infect Immun*, 83: 2926-34.

French, Anthony R., Douglas K. Tadaki, Salil K. Niyogi, and Douglas A. Lauffenburger. 1995. 'Intracellular Trafficking of Epidermal Growth Factor Family Ligands Is Directly Influenced by the pH Sensitivity of the Receptor/Ligand Interaction', *Journal of Biological Chemistry*, 270: 4334-40.

Geremia, Alessandra, and Carolina V. Arancibia-Cárcamo. 2017. 'Innate Lymphoid Cells in Intestinal Inflammation', *Front Immunol*, 8: 1296-96.

Ghio, Andrew J., Lisa A. Dailey, Joleen M. Soukup, Jacqueline Stonehuerner, Judy H. Richards, and Robert B. Devlin. 2013. 'Growth of human bronchial epithelial cells at an air-liquid interface alters the response to particle exposure', *Particle and Fibre Toxicology*, 10: 25.

Goldenring, James R., and Ki Taek Nam. 2010. 'Oxyntic atrophy, metaplasia, and gastric cancer', *Progress in molecular biology and translational science*, 96: 117-31.

Goldenring, James R., Ki Taek Nam, Timothy C. Wang, Jason C. Mills, and Nicholas A. Wright. 2010. 'Spasmolytic Polypeptide-Expressing Metaplasia and Intestinal Metaplasia: Time for Reevaluation of Metaplasias and the Origins of Gastric Cancer', *Gastroenterology*, 138: 2207-10.e1.

Goldenring, James R., Gregory S. Ray, Carol J. Soroka, Jenetta Smith, Irvin M. Modlin, Katherine S. Meise, and Robert J. Coffey. 1996. 'Overexpression of transforming growth factor-α alters differentiation of gastric cell lineages', *Dig Dis Sci*, 41: 773-84.

Gomez-Santos, L., E. Alonso, L. Diaz-Flores, J. F. Madrid, and F. J. Saez. 2017. 'Transdifferentiation of mucous neck cells into chief cells in fundic gastric glands shown by GNA lectin histochemistry', *Tissue Cell*, 49: 746-50.

Goodwin, C. S., C. McCullough, and J. Boehm. 1989. 'Successful lyophilization of Campylobacter pylori and spiral organisms from the stomachs of animals', *Pathology*, 21: 227-9.

Gray, T. E., K. Guzman, C. W. Davis, L. H. Abdullah, and P. Nettesheim. 1996. 'Mucociliary differentiation of serially passaged normal human tracheobronchial

epithelial cells', *American Journal of Respiratory Cell and Molecular Biology*, 14: 104-12.

Gregorieff, A., D. Pinto, H. Begthel, O. Destree, M. Kielman, and H. Clevers. 2005. 'Expression pattern of Wnt signaling components in the adult intestine', *Gastroenterology*, 129: 626-38.

Grosse, A. S., M. F. Pressprich, L. B. Curley, K. L. Hamilton, B. Margolis, J. D. Hildebrand, and D. L. Gumucio. 2011. 'Cell dynamics in fetal intestinal epithelium: implications for intestinal growth and morphogenesis', *Development*, 138: 4423-32.

Hagos, E. G., and S. T. Dougan. 2007. 'Time-dependent patterning of the mesoderm and endoderm by Nodal signals in zebrafish', *BMC Dev Biol*, 7: 22.

Han, S., J. Fink, D. J. Jorg, E. Lee, M. K. Yum, L. Chatzeli, S. R. Merker, M. Josserand, T. Trendafilova, A. Andersson-Rolf, C. Dabrowska, H. Kim, R. Naumann, J. H. Lee, N. Sasaki, R. L. Mort, O. Basak, H. Clevers, D. E. Stange, A. Philpott, J. K. Kim, B. D. Simons, and B. K. Koo. 2019. 'Defining the Identity and Dynamics of Adult Gastric Isthmus Stem Cells', *Cell Stem Cell*, 25: 342-56.e7.

Hanby, A. M., R. Poulsom, S. Singh, G. Elia, R. E. Jeffery, and N. A. Wright. 1993. 'Spasmolytic polypeptide is a major antral peptide: distribution of the trefoil peptides human spasmolytic polypeptide and pS2 in the stomach', *Gastroenterology*, 105: 1110-6.

Hawley-Nelson, P., K. H. Vousden, N. L. Hubbert, D. R. Lowy, and J. T. Schiller. 1989. 'HPV16 E6 and E7 proteins cooperate to immortalize human foreskin keratinocytes', *Embo j*, 8: 3905-10.

He, X. C., J. Zhang, W. G. Tong, O. Tawfik, J. Ross, D. H. Scoville, Q. Tian, X. Zeng, X. He, L. M. Wiedemann, Y. Mishina, and L. Li. 2004. 'BMP signaling inhibits intestinal stem cell self-renewal through suppression of Wnt-beta-catenin signaling', *Nat Genet*, 36: 1117-21.

Helander, H. F., R. Leth, and L. Olbe. 1986. 'Stereological investigations on human gastric mucosa: I. Normal oxyntic mucosa', *Anat Rec*, 216: 373-80.

Higashi, Hideaki, Ryouhei Tsutsumi, Syuichi Muto, Toshiro Sugiyama, Takeshi Azuma, Masahiro Asaka, and Masanori Hatakeyama. 2002. 'SHP-2 Tyrosine Phosphatase as an Intracellular Target of Helicobacter pylori CagA Protein', *Science*, 295: 683.

Hoffmann, W. 2008. 'Regeneration of the gastric mucosa and its glands from stem cells', *Curr Med Chem*, 15: 3133-44.

———. 2015. 'Current Status on Stem Cells and Cancers of the Gastric Epithelium', *Int J Mol Sci*, 16: 19153-69.

Holloway, Emily M., Meghan M. Capeling, and Jason R. Spence. 2019. 'Biologically inspired approaches to enhance human organoid complexity', *Development*, 146: dev166173.

Hoogduijn, Martin J. 2015. 'Are mesenchymal stromal cells immune cells?', *Arthritis Research & Therapy*, 17: 88.

Hooi, J. K. Y., W. Y. Lai, W. K. Ng, M. M. Y. Suen, F. E. Underwood, D. Tanyingoh, P. Malfertheiner, D. Y. Graham, V. W. S. Wong, J. C. Y. Wu, F. K. L. Chan, J. J. Y. Sung, G. G. Kaplan, and S. C. Ng. 2017. 'Global Prevalence of Helicobacter pylori Infection: Systematic Review and Meta-Analysis', *Gastroenterology*, 153: 420-29.

Howe, J. R., J. L. Bair, M. G. Sayed, M. E. Anderson, F. A. Mitros, G. M. Petersen, V. E. Velculescu, G. Traverso, and B. Vogelstein. 2001. 'Germline mutations of the

gene encoding bone morphogenetic protein receptor 1A in juvenile polyposis', *Nat Genet*, 28: 184-7.

Huch, Meritxell, Paola Bonfanti, Sylvia F. Boj, Toshiro Sato, Cindy J. M. Loomans, Marc van de Wetering, Mozhdeh Sojoodi, Vivian S. W. Li, Jurian Schuijers, Ana Gracanin, Femke Ringnalda, Harry Begthel, Karien Hamer, Joyce Mulder, Johan H. van Es, Eelco de Koning, Robert G. J. Vries, Harry Heimberg, and Hans Clevers. 2013. 'Unlimited in vitro expansion of adult bi-potent pancreas progenitors through the Lgr5/R-spondin axis', *Embo j*, 32: 2708.

Huch, Meritxell, Craig Dorrell, Sylvia F. Boj, Johan H. van Es, Vivian S. W. Li, Marc van de Wetering, Toshiro Sato, Karien Hamer, Nobuo Sasaki, Milton J. Finegold, Annelise Haft, Robert G. Vries, Markus Grompe, and Hans Clevers. 2013. 'In vitro expansion of single Lgr5+ liver stem cells induced by Wnt-driven regeneration', *Nature*, 494: 247.

Huch, Meritxell, Helmuth Gehart, Ruben van Boxtel, Karien Hamer, Francis Blokzijl, Monique M A. Verstegen, Ewa Ellis, Martien van Wenum, Sabine A Fuchs, Joep de Ligt, Marc van de Wetering, Nobuo Sasaki, Susanne J Boers, Hans Kemperman, Jeroen de Jonge, Jan N M. Ijzermans, Edward E S. Nieuwenhuis, Ruurdtje Hoekstra, Stephen Strom, Robert R G. Vries, Luc J W. van der Laan, Edwin Cuppen, and Hans Clevers. 2015. 'Long-Term Culture of Genome-Stable Bipotent Stem Cells from Adult Human Liver', *Cell*, 160: 299-312.

Hudson, J. B., M. A. Bedell, D. J. McCance, and L. A. Laiminis. 1990. 'Immortalization and altered differentiation of human keratinocytes in vitro by the E6 and E7 open reading frames of human papillomavirus type 18', *J Virol*, 64: 519-26.

Huelsken, J., R. Vogel, V. Brinkmann, B. Erdmann, C. Birchmeier, and W. Birchmeier. 2000. 'Requirement for β-catenin in anterior-posterior axis formation in mice', *Journal of Cell Biology*, 148: 567-78.

Huh, Won Jae, Emel Esen, Jessica H. Geahlen, Andrew J. Bredemeyer, Ann–Hwee Lee, Guanglu Shi, Stephen F. Konieczny, Laurie H. Glimcher, and Jason C. Mills. 2010. 'XBP1 Controls Maturation of Gastric Zymogenic Cells by Induction of MIST1 and Expansion of the Rough Endoplasmic Reticulum', *Gastroenterology*, 139: 2038-49.

IARC. 1994. 'Schistosomes, Liver Flukes and *Helicobacter pylori*', *IARC Monographs on the Evaluation of Carcinogenic Risks to Humans.*, 61.

Itoh, K., H. Kataoka, M. Sasaki, S. Tanida, T. Oshima, N. Ogasawara, H. Ohara, H. Nakao, and T. Joh. 2006. 'Bone morphogenetic protein 2 induced differentiation toward superficial epithelial cells in the gastric mucosa', *J Gastroenterol*, 41: 1064-75.

Jablonowski, H., K. J. Hengels, N. Kraemer, G. Geis, W. Opferkuch, and G. Strohmeyer. 1994. 'Effects of Helicobacter pylori on histamine and carbachol stimulated acid secretion by human parietal cells', *Gut*, 35: 755.

Jacobsen, Christina M., Naoko Narita, Malgorzata Bielinska, Andrew J. Syder, Jeffrey I. Gordon, and David B. Wilson. 2002. 'Genetic Mosaic Analysis Reveals That GATA-4 Is Required for Proper Differentiation of Mouse Gastric Epithelium', *Developmental biology*, 241: 34-46.

Jain, R. N., and L. C. Samuelson. 2007. 'Transcriptional profiling of gastrin-regulated genes in mouse stomach', *Physiol Genomics*, 29: 1-12.

Jha, Krishna K., Satnam Banga, Vaseem Palejwala, and Harvey L. Ozer. 1998. 'SV40-Mediated Immortalization', *Exp Cell Res*, 245: 1-7.

Jurkowska, G., G. Piotrowska-Staworko, K. Guzinska-Ustymowicz, A. Kemona, A. Swidnicka-Siergiejko, W. Laszewicz, and A. Dabrowski. 2014. 'The impact of Helicobacter pylori on EGF, EGF receptor, and the c-erb-B2 expression', *Adv Med Sci*, 59: 221-6.

Justice, Bradley A., Nadia A. Badr, and Robin A. Felder. 2009. '3D cell culture opens new dimensions in cell-based assays', *Drug Discovery Today*, 14: 102-07.

Kageyama, T. 2002. 'Pepsinogens, progastricsins, and prochymosins: structure, function, evolution, and development', *Cell Mol Life Sci*, 59: 288-306.

Kalluri, R., and M. Zeisberg. 2006. 'Fibroblasts in cancer', *Nat Rev Cancer*, 6: 392-401.

Kalluri, Raghu. 2016. 'The biology and function of fibroblasts in cancer', *Nature Reviews Cancer*, 16: 582.

Kalluri, Raghu, and Robert A. Weinberg. 2009. 'The basics of epithelial-mesenchymal transition', *J Clin Invest*, 119: 1420-28.

Karam, S. M. 1993. 'Dynamics of epithelial cells in the corpus of the mouse stomach. IV. Bidirectional migration of parietal cells ending in their gradual degeneration and loss', *Anat Rec*, 236: 314-32.

———. 2010. 'A focus on parietal cells as a renewing cell population', *World J Gastroenterol*, 16: 538-46.

Karam, S. M., and C. P. Leblond. 1992. 'Identifying and counting epithelial cell types in the "corpus" of the mouse stomach', *Anat Rec*, 232: 231-46.

———. 1993a. 'Dynamics of epithelial cells in the corpus of the mouse stomach. I. Identification of proliferative cell types and pinpointing of the stem cell', *Anat Rec*, 236: 259-79.

———. 1993b. 'Dynamics of epithelial cells in the corpus of the mouse stomach. II. Outward migration of pit cells', *Anat Rec*, 236: 280-96.

———. 1993c. 'Dynamics of epithelial cells in the corpus of the mouse stomach. III. Inward migration of neck cells followed by progressive transformation into zymogenic cells', *Anat Rec*, 236: 297-313.

———. 1993d. 'Dynamics of epithelial cells in the corpus of the mouse stomach. V. Behavior of entero-endocrine and caveolated cells: general conclusions on cell kinetics in the oxyntic epithelium', *Anat Rec*, 236: 333-40.

Karam, S. M., C. Tomasetto, and M. C. Rio. 2004. 'Trefoil factor 1 is required for the commitment programme of mouse oxyntic epithelial progenitors', *Gut*, 53: 1408-15.

Karam, S. M., X. Yao, and J. G. Forte. 1997. 'Functional heterogeneity of parietal cells along the pig-gland axis', *American Journal of Physiology-Gastrointestinal and Liver Physiology*, 272: G161-G71.

Katano, T., A. Ootani, T. Mizoshita, S. Tanida, H. Tsukamoto, K. Ozeki, H. Kataoka, and T. Joh. 2015. 'Gastric mesenchymal myofibroblasts maintain stem cell activity and proliferation of murine gastric epithelium in vitro', *Am J Pathol*, 185: 798-807.

Katano, Takahito, Akifumi Ootani, Tsutomu Mizoshita, Satoshi Tanida, Hironobu Tsukamoto, Keiji Ozeki, Masahide Ebi, Yoshinori Mori, Hiromi Kataoka, Takeshi Kamiya, Shuji Toda, and Takashi Joh. 2013. 'Establishment of a long-term three-dimensional primary culture of mouse glandular stomach epithelial cells within the stem cell niche', *Biochem Biophys Res Commun*, 432: 558-63.

Katoh, Y., and M. Katoh. 2006. 'Hedgehog signaling pathway and gastrointestinal stem cell signaling network (review)', *Int J Mol Med*, 18: 1019-23.

Katsuno, Y., A. Hanyu, H. Kanda, Y. Ishikawa, F. Akiyama, T. Iwase, E. Ogata, S. Ehata, K. Miyazono, and T. Imamura. 2008. 'Bone morphogenetic protein

signaling enhances invasion and bone metastasis of breast cancer cells through Smad pathway', *Oncogene*, 27: 6322.

Keates, S., A. C. Keates, K. Katchar, R. M. Peek, Jr., and C. P. Kelly. 2007. 'Helicobacter pylori induces up-regulation of the epidermal growth factor receptor in AGS gastric epithelial cells', *J Infect Dis*, 196: 95-103.

Keeley, T. M., and L. C. Samuelson. 2010. 'Cytodifferentiation of the postnatal mouse stomach in normal and Huntingtin-interacting protein 1-related-deficient mice', *Am J Physiol Gastrointest Liver Physiol*, 299: G1241-51.

Kessler, M., K. Hoffmann, K. Fritsche, V. Brinkmann, H. J. Mollenkopf, O. Thieck, A. R. Teixeira da Costa, E. I. Braicu, J. Sehouli, M. Mangler, H. Berger, and T. F. Meyer. 2019. 'Chronic Chlamydia infection in human organoids increases stemness and promotes age-dependent CpG methylation', *Nat Commun*, 10: 1194.

Kessler, Mirjana, Karen Hoffmann, Volker Brinkmann, Oliver Thieck, Susan Jackisch, Benjamin Toelle, Hilmar Berger, Hans-Joachim Mollenkopf, Mandy Mangler, Jalid Sehouli, Christina Fotopoulou, and Thomas F. Meyer. 2015. 'The Notch and Wnt pathways regulate stemness and differentiation in human fallopian tube organoids', *Nature Communications*, 6: 8989.

Kikuchi, Y., H. Verkade, J. F. Reiter, C. H. Kim, A. B. Chitnis, A. Kuroiwa, and D. Y. Stainier. 2004. 'Notch signaling can regulate endoderm formation in zebrafish', *Dev Dyn*, 229: 756-62.

Kim, B. M., G. Buchner, I. Miletich, P. T. Sharpe, and R. A. Shivdasani. 2005. 'The stomach mesenchymal transcription factor Barx1 specifies gastric epithelial identity through inhibition of transient Wnt signaling', *Dev Cell*, 8: 611-22.

Kim, B. M., I. Miletich, J. Mao, A. P. McMahon, P. A. Sharpe, and R. A. Shivdasani. 2007. 'Independent functions and mechanisms for homeobox gene Barx1 in patterning mouse stomach and spleen', *Development*, 134: 3603-13.

Kim, Ik-Jung, and Steven R. Blanke. 2012. 'Remodeling the host environment: modulation of the gastric epithelium by the Helicobacter pylori vacuolating toxin (VacA)', *Front Cell Infect Microbiol*, 2: 37-37.

Kim, Tae-Hee, and Ramesh A. Shivdasani. 2016. 'Stomach development, stem cells and disease', *Development*, 143: 554.

Kinchen, James, Hannah H. Chen, Kaushal Parikh, Agne Antanaviciute, Marta Jagielowicz, David Fawkner-Corbett, Neil Ashley, Laura Cubitt, Esther Mellado-Gomez, Moustafa Attar, Eshita Sharma, Quin Wills, Rory Bowden, Felix C. Richter, David Ahern, Kamal D. Puri, Jill Henault, Francois Gervais, Hashem Koohy, and Alison Simmons. 2018. 'Structural Remodeling of the Human Colonic Mesenchyme in Inflammatory Bowel Disease', *Cell*, 175: 372-86.e17.

Kleinman, H. K., and G. R. Martin. 2005. 'Matrigel: basement membrane matrix with biological activity', *Semin Cancer Biol*, 15: 378-86.

Knight, Eleanor, and Stefan Przyborski. 2015. 'Advances in 3D cell culture technologies enabling tissue-like structures to be created in vitro', *Journal of anatomy*, 227: 746-56.

Kolf, Catherine M., Elizabeth Cho, and Rocky S. Tuan. 2007. 'Mesenchymal stromal cells. Biology of adult mesenchymal stem cells: regulation of niche, self-renewal and differentiation', *Arthritis Research & Therapy*, 9: 204-04.

Kosinski, Cynthia, Vivian S. W. Li, Annie S. Y. Chan, Ji Zhang, Coral Ho, Wai Yin Tsui, Tsun Leung Chan, Randy C. Mifflin, Don W. Powell, Siu Tsan Yuen, Suet Yi Leung, and Xin Chen. 2007. 'Gene expression patterns of human colon tops

and basal crypts and BMP antagonists as intestinal stem cell niche factors', *Proceedings of the National Academy of Sciences*, 104: 15418.

Kretzschmar, Kai, and Hans Clevers. 2016. 'Organoids: Modeling Development and the Stem Cell Niche in a Dish', *Developmental cell*, 38: 590-600.

———. 2017. 'Wnt/β-catenin signaling in adult mammalian epithelial stem cells', *Developmental biology*, 428: 273-82.

Kretzschmar, Marcus, Jacqueline Doody, and Joan Massagu. 1997. 'Opposing BMP and EGF signalling pathways converge on the TGF-β family mediator Smad1', *Nature*, 389: 618-22.

Kusters, J. G., M. M. Gerrits, J. A. Van Strijp, and C. M. Vandenbroucke-Grauls. 1997. 'Coccoid forms of Helicobacter pylori are the morphologic manifestation of cell death', *Infect Immun*, 65: 3672-79.

Kusters, J. G., A. H. van Vliet, and E. J. Kuipers. 2006. 'Pathogenesis of Helicobacter pylori infection', *Clin Microbiol Rev*, 19: 449-90.

Lancaster, Madeline A., Magdalena Renner, Carol-Anne Martin, Daniel Wenzel, Louise S. Bicknell, Matthew E. Hurles, Tessa Homfray, Josef M. Penninger, Andrew P. Jackson, and Juergen A. Knoblich. 2013. 'Cerebral organoids model human brain development and microcephaly', *Nature*, 501: 373.

Latorre, R., C. Sternini, R. De Giorgio, and B. Greenwood-Van Meerveld. 2016. 'Enteroendocrine cells: a review of their role in brain-gut communication', *Neurogastroenterology and motility : the official journal of the European Gastrointestinal Motility Society*, 28: 620-30.

Lee, K. M., K. H. Choi, and M. M. Ouellette. 2004. 'Use of exogenous hTERT to immortalize primary human cells', *Cytotechnology*, 45: 33-8.

Lemmon, Mark A., and Joseph Schlessinger. 2010. 'Cell signaling by receptor tyrosine kinases', *Cell*, 141: 1117-34.

Leushacke, M., A. Ng, J. Galle, M. Loeffler, and N. Barker. 2013. 'Lgr5(+) gastric stem cells divide symmetrically to effect epithelial homeostasis in the pylorus', *Cell Rep*, 5: 349-56.

Leushacke, M., S. H. Tan, A. Wong, Y. Swathi, A. Hajamohideen, L. T. Tan, J. Goh, E. Wong, Slij Denil, K. Murakami, and N. Barker. 2017. 'Lgr5-expressing chief cells drive epithelial regeneration and cancer in the oxyntic stomach', *Nat Cell Biol*, 19: 774-86.

Li, Q., S. M. Karam, and J. I. Gordon. 1996. 'Diphtheria toxin-mediated ablation of parietal cells in the stomach of transgenic mice', *J Biol Chem*, 271: 3671-6.

Li, X., A. Ootani, and C. Kuo. 2016. 'An Air-Liquid Interface Culture System for 3D Organoid Culture of Diverse Primary Gastrointestinal Tissues', *Methods Mol Biol*, 1422: 33-40.

Lim, Xinhong, Si Hui Tan, Winston Lian Chye Koh, Rosanna Man Wah Chau, Kelley S. Yan, Calvin J. Kuo, Renée van Amerongen, Allon Moshe Klein, and Roel Nusse. 2013. 'Interfollicular Epidermal Stem Cells Self-Renew via Autocrine Wnt Signaling', *Science*, 342: 1226.

Linz, B., F. Balloux, Y. Moodley, A. Manica, H. Liu, P. Roumagnac, D. Falush, C. Stamer, F. Prugnolle, S. W. van der Merwe, Y. Yamaoka, D. Y. Graham, E. Perez-Trallero, T. Wadstrom, S. Suerbaum, and M. Achtman. 2007. 'An African origin for the intimate association between humans and Helicobacter pylori', *Nature*, 445: 915-18.

Litingtung, Ying, Li Lei, Heiner Westphal, and Chin Chiang. 1998. 'Sonic hedgehog is essential to foregut development', *Nat Genet*, 20: 58-61.

Liu, X., V. Ory, S. Chapman, H. Yuan, C. Albanese, B. Kallakury, O. A. Timofeeva, C. Nealon, A. Dakic, V. Simic, B. R. Haddad, J. S. Rhim, A. Dritschilo, A. Riegel, A. McBride, and R. Schlegel. 2012. 'ROCK inhibitor and feeder cells induce the conditional reprogramming of epithelial cells', *Am J Pathol*, 180: 599-607.

Llames, Sara, Eva García-Pérez, Álvaro Meana, Fernando Larcher, and Marcela del Río. 2015. 'Feeder Layer Cell Actions and Applications', *Tissue engineering. Part B, Reviews*, 21: 345-53.

Lo, H. G., R. U. Jin, G. Sibbel, D. Liu, A. Karki, M. S. Joens, B. B. Madison, B. Zhang, V. Blanc, J. A. Fitzpatrick, N. O. Davidson, S. F. Konieczny, and J. C. Mills. 2017. 'A single transcription factor is sufficient to induce and maintain secretory cell architecture', *Genes Dev*, 31: 154-71.

Maloum, F., J. M. Allaire, J. Gagne-Sansfacon, E. Roy, K. Belleville, P. Sarret, J. Morisset, J. C. Carrier, Y. Mishina, K. H. Kaestner, and N. Perreault. 2011. 'Epithelial BMP signaling is required for proper specification of epithelial cell lineages and gastric endocrine cells', *Am J Physiol Gastrointest Liver Physiol*, 300: G1065-79.

Marshall, B. J., J. A. Armstrong, D. B. McGechie, and R. J. Glancy. 1985. 'Attempt to fulfil Koch's postulates for pyloric Campylobacter', *Med J Aust*, 142: 436-9.

Marshall, BarryJ, and J. Robin Warren. 1984. 'UNIDENTIFIED CURVED BACILLI IN THE STOMACH OF PATIENTS WITH GASTRITIS AND PEPTIC ULCERATION', *The Lancet*, 323: 1311-15.

Martini, Frederic, Michael J. Timmons, and Robert B. Tallitsch. 2012. *Human anatomy* (Pearson Benjamin Cummings: Boston).

Matsuo, J., S. Kimura, A. Yamamura, C. P. Koh, M. Z. Hossain, D. L. Heng, K. Kohu, D. C. Voon, H. Hiai, M. Unno, J. B. So, F. Zhu, S. Srivastava, M. Teh, K. G. Yeoh, M. Osato, and Y. Ito. 2017. 'Identification of Stem Cells in the Epithelium of the Stomach Corpus and Antrum of Mice', *Gastroenterology*, 152: 218-31.e14.

McCracken, K. W., E. Aihara, B. Martin, C. M. Crawford, T. Broda, J. Treguier, X. Zhang, J. M. Shannon, M. H. Montrose, and J. M. Wells. 2017. 'Wnt/beta-catenin promotes gastric fundus specification in mice and humans', *Nature*, 541: 182-87.

McCracken, K. W., J. C. Howell, J. M. Wells, and J. R. Spence. 2011. 'Generating human intestinal tissue from pluripotent stem cells in vitro', *Nat Protoc*, 6: 1920-8.

McCracken, Kyle W., Emily M. Cata, Calyn M. Crawford, Katie L. Sinagoga, Michael Schumacher, Briana E. Rockich, Yu-Hwai Tsai, Christopher N. Mayhew, Jason R. Spence, Yana Zavros, and James M. Wells. 2014. 'Modelling human development and disease in pluripotent stem-cell-derived gastric organoids', *Nature*, 516: 400-04.

McCracken, Kyle W., and James M. Wells. 2017. 'Mechanisms of embryonic stomach development', *Semin Cell Dev Biol*, 66: 36-42.

Minalyan, Artem, Jihane N. Benhammou, Aida Artashesyan, Michael S. Lewis, and Joseph R. Pisegna. 2017. 'Autoimmune atrophic gastritis: current perspectives', *Clinical and experimental gastroenterology*, 10: 19-27.

Morey, P., L. Pfannkuch, E. Pang, F. Boccellato, M. Sigal, A. Imai-Matsushima, V. Dyer, M. Koch, H. J. Mollenkopf, P. Schlaermann, and T. F. Meyer. 2018. 'Helicobacter pylori Depletes Cholesterol in Gastric Glands to Prevent Interferon Gamma Signaling and Escape the Inflammatory Response', *Gastroenterology*, 154: 1391-404.e9.

Mori, K., H. Nakamura, H. Kurooka, H. Miyachi, K. Tamada, M. Sugai, T. Takumi, and Y. Yokota. 2018. 'Id2 Determines Intestinal Identity through Repression of the Foregut Transcription Factor Irx5', *Mol Cell Biol*, 38.

Morizane, R., A. Q. Lam, B. S. Freedman, S. Kishi, M. T. Valerius, and J. V. Bonventre. 2015. 'Nephron organoids derived from human pluripotent stem cells model kidney development and injury', *Nat Biotechnol*, 33: 1193-200.

Mueller, D., N. Tegtmeyer, S. Brandt, Y. Yamaoka, E. De Poire, D. Sgouras, S. Wessler, J. Torres, A. Smolka, and S. Backert. 2012. 'c-Src and c-Abl kinases control hierarchic phosphorylation and function of the CagA effector protein in Western and East Asian Helicobacter pylori strains', *J Clin Invest*, 122: 1553-66.

Mueller, Scott N., and Ronald N. Germain. 2009. 'Stromal cell contributions to the homeostasis and functionality of the immune system', *Nature reviews. Immunology*, 9: 618-29.

Münger, K., W. C. Phelps, V. Bubb, P. M. Howley, and R. Schlegel. 1989. 'The E6 and E7 genes of the human papillomavirus type 16 together are necessary and sufficient for transformation of primary human keratinocytes', *Journal of Virology*, 63: 4417.

Nam, K. T., H. J. Lee, H. Mok, J. Romero-Gallo, J. E. Crowe, Jr., R. M. Peek, Jr., and J. R. Goldenring. 2009. 'Amphiregulin-deficient mice develop spasmolytic polypeptide expressing metaplasia and intestinal metaplasia', *Gastroenterology*, 136: 1288-96.

Narita, T., K. Saitoh, T. Kameda, A. Kuroiwa, M. Mizutani, C. Koike, H. Iba, and S. Yasugi. 2000. 'BMPs are necessary for stomach gland formation in the chicken embryo: a study using virally induced BMP-2 and Noggin expression', *Development*, 127: 981-8.

Neal, J. T., T. S. Peterson, M. L. Kent, and K. Guillemin. 2013. 'H. pylori virulence factor CagA increases intestinal cell proliferation by Wnt pathway activation in a transgenic zebrafish model', *Dis Model Mech*, 6: 802-10.

Neu, B., P. Randlkofer, M. Neuhofer, P. Voland, A. Mayerhofer, M. Gerhard, W. Schepp, and C. Prinz. 2002. 'Helicobacter pylori induces apoptosis of rat gastric parietal cells', *Am J Physiol Gastrointest Liver Physiol*, 283: G309-18.

Nitsche, H., S. Ramamoorthy, M. Sareban, N. Pausawasdi, and A. Todisco. 2007. 'Functional role of bone morphogenetic protein-4 in isolated canine parietal cells', *Am J Physiol Gastrointest Liver Physiol*, 293: G607-14.

Nookaew, I., K. Thorell, K. Worah, S. Wang, M. L. Hibberd, H. Sjovall, S. Pettersson, J. Nielsen, and S. B. Lundin. 2013. 'Transcriptome signatures in Helicobacter pylori-infected mucosa identifies acidic mammalian chitinase loss as a corpus atrophy marker', *BMC Med Genomics*, 6: 41.

Normanno, Nicola, Antonella De Luca, Caterina Bianco, Luigi Strizzi, Mario Mancino, Monica R. Maiello, Adele Carotenuto, Gianfranco De Feo, Francesco Caponigro, and David S. Salomon. 2006. 'Epidermal growth factor receptor (EGFR) signaling in cancer', *Gene*, 366: 2-16.

Nozaki, K., V. Weis, T. C. Wang, A. Falus, and J. R. Goldenring. 2009. 'Altered gastric chief cell lineage differentiation in histamine-deficient mice', *Am J Physiol Gastrointest Liver Physiol*, 296: G1211-20.

Ohnishi, N., H. Yuasa, S. Tanaka, H. Sawa, M. Miura, A. Matsui, H. Higashi, M. Musashi, K. Iwabuchi, M. Suzuki, G. Yamada, T. Azuma, and M. Hatakeyama. 2008. 'Transgenic expression of Helicobacter pylori CagA induces gastrointestinal and hematopoietic neoplasms in mouse', *Proc Natl Acad Sci U S A*, 105: 1003-8.

Ootani, A., X. Li, E. Sangiorgi, Q. T. Ho, H. Ueno, S. Toda, H. Sugihara, K. Fujimoto, I. L. Weissman, M. R. Capecchi, and C. J. Kuo. 2009. 'Sustained in vitro intestinal epithelial culture within a Wnt-dependent stem cell niche', *Nat Med*, 15: 701-6.

Ootani, A., S. Toda, K. Fujimoto, and H. Sugihara. 2000. 'An air-liquid interface promotes the differentiation of gastric surface mucous cells (GSM06) in culture', *Biochem Biophys Res Commun*, 271: 741-6.

———. 2003. 'Foveolar differentiation of mouse gastric mucosa in vitro', *Am J Pathol*, 162: 1905-12.

Owens, B. M. 2015. 'Inflammation, Innate Immunity, and the Intestinal Stromal Cell Niche: Opportunities and Challenges', *Front Immunol*, 6: 319.

Owens, Benjamin, Tessa Steevels, Michael Dudek, David Walcott, Mei-Yi Sun, Alice Mayer, Philip Allan, and Alison Simmons. 2013. 'CD90+ Stromal Cells are Non-Professional Innate Immune Effectors of the Human Colonic Mucosa', *Front Immunol*, 4.

Owens, P., M. W. Pickup, S. V. Novitskiy, J. M. Giltnane, A. E. Gorska, C. R. Hopkins, C. C. Hong, and H. L. Moses. 2014. 'Inhibition of BMP signaling suppresses metastasis in mammary cancer', *Oncogene*, 34: 2437.

P.J.Peters, Erik Bos and Alexander Griekspoor. 2006. 'Current Protocols in Cell Biology ', *John Wiley&Sons Inc.*: 4.7.1-4.7.19.

Pampaloni, Francesco, Emmanuel G. Reynaud, and Ernst H. K. Stelzer. 2007. 'The third dimension bridges the gap between cell culture and live tissue', *Nature Reviews Molecular Cell Biology*, 8: 839.

Papastergiou, Vasilios, Sotirios D. Georgopoulos, and Stylianos Karatapanis. 2014. 'Treatment of Helicobacter pylori infection: Past, present and future', *World J Gastrointest Pathophysiol*, 5: 392-99.

Parsonnet, J., G. D. Friedman, D. P. Vandersteen, Y. Chang, J. H. Vogelman, N. Orentreich, and R. K. Sibley. 1991. 'Helicobacter pylori infection and the risk of gastric carcinoma', *N Engl J Med*, 325: 1127-31.

Peek, Richard M., and Martin J. Blaser. 2002. 'Helicobacter pylori and gastrointestinal tract adenocarcinomas', *Nature Reviews Cancer*, 2: 28-37.

Pinchuk, I. V., E. J. Beswick, J. I. Saada, G. Boya, D. Schmitt, G. S. Raju, J. Brenmoehl, G. Rogler, V. E. Reyes, and D. W. Powell. 2011. 'Human colonic myofibroblasts promote expansion of CD4+ CD25high Foxp3+ regulatory T cells', *Gastroenterology*, 140: 2019-30.

Pinchuk, I. V., K. T. Morris, R. A. Nofchissey, R. B. Earley, J. Y. Wu, T. Y. Ma, and E. J. Beswick. 2013. 'Stromal cells induce Th17 during Helicobacter pylori infection and in the gastric tumor microenvironment', *PLoS One*, 8: e53798.

Portela-Gomes, Guida Maria, and Mats Stridsberg. 2002. 'Chromogranin A in the Human Gastrointestinal Tract: An Immunocytochemical Study with Region-specific Antibodies', *Journal of Histochemistry & Cytochemistry*, 50: 1487-92.

Powell, D. W., I. V. Pinchuk, J. I. Saada, Xin Chen, and R. C. Mifflin. 2011. 'Mesenchymal cells of the intestinal lamina propria', *Annual review of physiology*, 73: 213-37.

Powell, N., J. W. Lo, P. Biancheri, A. Vossenkamper, E. Pantazi, A. W. Walker, E. Stolarczyk, F. Ammoscato, R. Goldberg, P. Scott, J. B. Canavan, E. Perucha, N. Garrido-Mesa, P. M. Irving, J. D. Sanderson, B. Hayee, J. K. Howard, J. Parkhill, T. T. MacDonald, and G. M. Lord. 2015. 'Interleukin 6 Increases Production of Cytokines by Colonic Innate Lymphoid Cells in Mice and Patients With Chronic Intestinal Inflammation', *Gastroenterology*, 149: 456-67.e15.

Qi, Zhen, Yehua Li, Bing Zhao, Chi Xu, Yuan Liu, Haonan Li, Bingjie Zhang, Xinquan Wang, Xiao Yang, Wei Xie, Baojie Li, Jing-Dong Jackie Han, and Ye-Guang Chen. 2017. 'BMP restricts stemness of intestinal Lgr5+ stem cells by directly suppressing their signature genes', *Nature Communications*, 8: 13824.

Qiao, Xiaotan T., Joshua W. Ziel, Wendy McKimpson, Blair B. Madison, Andrea Todisco, Juanita L. Merchant, Linda C. Samuelson, and Deborah L. Gumucio. 2007. 'Prospective identification of a multilineage progenitor in murine stomach epithelium', *Gastroenterology*, 133: 1989-98.

Que, Jianwen, Tadashi Okubo, James R. Goldenring, Ki-Taek Nam, Reiko Kurotani, Edward E. Morrisey, Olena Taranova, Larysa H. Pevny, and Brigid L. M. Hogan. 2007. 'Multiple dose-dependent roles for Sox2 in the patterning and differentiation of anterior foregut endoderm', *Development*, 134: 2521-31.

R Core Team. 2013. 'R: A language and environment for statistical

computing.', *R Foundation for Statistical Computing, Vienna, Austria.*

Rahman, Md Shaifur, Naznin Akhtar, Hossen Mohammad Jamil, Rajat Suvra Banik, and Sikder M. Asaduzzaman. 2015. 'TGF-β/BMP signaling and other molecular events: regulation of osteoblastogenesis and bone formation', *Bone Res*, 3: 15005.

Ramsey, Victoria G., Jason M. Doherty, Christopher C. Chen, Thaddeus S. Stappenbeck, Stephen F. Konieczny, and Jason C. Mills. 2007. 'The maturation of mucus-secreting gastric epithelial progenitors into digestive-enzyme secreting zymogenic cells requires <em>Mist1</em&gt', *Development*, 134: 211.

Ritchie, M. E., B. Phipson, D. Wu, Y. Hu, C. W. Law, W. Shi, and G. K. Smyth. 2015. 'limma powers differential expression analyses for RNA-sequencing and microarray studies', *Nucleic Acids Res*, 43: e47.

Rock, Jason R., Mark W. Onaitis, Emma L. Rawlins, Yun Lu, Cheryl P. Clark, Yan Xue, Scott H. Randell, and Brigid L. M. Hogan. 2009. 'Basal cells as stem cells of the mouse trachea and human airway epithelium', *Proceedings of the National Academy of Sciences*, 106: 12771.

Rodriguez-Pineiro, A. M., J. H. Bergstrom, A. Ermund, J. K. Gustafsson, A. Schutte, M. E. Johansson, and G. C. Hansson. 2013. 'Studies of mucus in mouse stomach, small intestine, and colon. II. Gastrointestinal mucus proteome reveals Muc2 and Muc5ac accompanied by a set of core proteins', *Am J Physiol Gastrointest Liver Physiol*, 305: G348-56.

Rodriguez, P., S. Da Silva, L. Oxburgh, F. Wang, B. L. Hogan, and J. Que. 2010. 'BMP signaling in the development of the mouse esophagus and forestomach', *Development*, 137: 4171-6.

Romieu-Mourez, Raphaëlle, Moïra François, Marie-Noëlle Boivin, Manaf Bouchentouf, David E. Spaner, and Jacques Galipeau. 2009. 'Cytokine Modulation of TLR Expression and Activation in Mesenchymal Stromal Cells Leads to a Proinflammatory Phenotype', *The Journal of Immunology*, 182: 7963.

Saha, Arindam, Charles E. Hammond, Craig Beeson, Richard M. Peek, Jr., and Adam J. Smolka. 2010. 'Helicobacter pylori represses proton pump expression and inhibits acid secretion in human gastric mucosa', *Gut*, 59: 874-81.

Sapkota, Gopal, Claudio Alarcón, Francesca M. Spagnoli, Ali H. Brivanlou, and Joan Massagué. 2007. 'Balancing BMP Signaling through Integrated Inputs into the Smad1 Linker', *Mol Cell*, 25: 441-54.

Sato, T., D. E. Stange, M. Ferrante, R. G. Vries, J. H. Van Es, S. Van den Brink, W. J. Van Houdt, A. Pronk, J. Van Gorp, P. D. Siersema, and H. Clevers. 2011. 'Long-

term expansion of epithelial organoids from human colon, adenoma, adenocarcinoma, and Barrett's epithelium', *Gastroenterology*, 141: 1762-72.

Sato, T., R. G. Vries, H. J. Snippert, M. van de Wetering, N. Barker, D. E. Stange, J. H. van Es, A. Abo, P. Kujala, P. J. Peters, and H. Clevers. 2009. 'Single Lgr5 stem cells build crypt-villus structures in vitro without a mesenchymal niche', *Nature*, 459: 262-5.

Sato, Toshiro, and Hans Clevers. 2013. 'Growing Self-Organizing Mini-Guts from a Single Intestinal Stem Cell: Mechanism and Applications', *Science*, 340: 1190.

Schindelin, Johannes, Ignacio Arganda-Carreras, Erwin Frise, Verena Kaynig, Mark Longair, Tobias Pietzsch, Stephan Preibisch, Curtis Rueden, Stephan Saalfeld, Benjamin Schmid, Jean-Yves Tinevez, Daniel James White, Volker Hartenstein, Kevin Eliceiri, Pavel Tomancak, and Albert Cardona. 2012. 'Fiji: an open-source platform for biological-image analysis', *Nature Methods*, 9: 676-82.

Schlaermann, P., B. Toelle, H. Berger, S. C. Schmidt, M. Glanemann, J. Ordemann, S. Bartfeld, H. J. Mollenkopf, and T. F. Meyer. 2014. 'A novel human gastric primary cell culture system for modelling Helicobacter pylori infection in vitro', *Gut*.

Schneider, C. A., W. S. Rasband, and K. W. Eliceiri. 2012. 'NIH Image to ImageJ: 25 years of image analysis', *Nat Methods*, 9: 671-5.

Seshacharyulu, Parthasarathy, Moorthy P. Ponnusamy, Dhanya Haridas, Maneesh Jain, Apar K. Ganti, and Surinder K. Batra. 2012. 'Targeting the EGFR signaling pathway in cancer therapy', *Expert opinion on therapeutic targets*, 16: 15-31.

Shen, Shixuan, Jingyi Jiang, and Yuan Yuan. 2017. 'Pepsinogen C expression, regulation and its relationship with cancer', *Cancer cell international*, 17: 57-57.

Sherwood, R. I., T. Y. Chen, and D. A. Melton. 2009. 'Transcriptional dynamics of endodermal organ formation', *Dev Dyn*, 238: 29-42.

Sherwood, R. I., R. Maehr, E. O. Mazzoni, and D. A. Melton. 2011. 'Wnt signaling specifies and patterns intestinal endoderm', *Mech Dev*, 128: 387-400.

Shin, M., S. Noji, A. Neubuser, and S. Yasugi. 2006. 'FGF10 is required for cell proliferation and gland formation in the stomach epithelium of the chicken embryo', *Dev Biol*, 294: 11-23.

Shinohara, M., M. Mao, T. M. Keeley, M. El-Zaatari, H. J. Lee, K. A. Eaton, L. C. Samuelson, J. L. Merchant, J. R. Goldenring, and A. Todisco. 2010. 'Bone morphogenetic protein signaling regulates gastric epithelial cell development and proliferation in mice', *Gastroenterology*, 139: 2050-60.e2.

Shirai, Yo-taro, Shogo Ehata, Masakazu Yashiro, Kazuyoshi Yanagihara, Kosei Hirakawa, and Kohei Miyazono. 2011. 'Bone Morphogenetic Protein-2 and -4 Play Tumor Suppressive Roles in Human Diffuse-Type Gastric Carcinoma', *Am J Pathol*, 179: 2920-30.

Sigal, M., C. Y. Logan, M. Kapalczynska, H. J. Mollenkopf, H. Berger, B. Wiedenmann, R. Nusse, M. R. Amieva, and T. F. Meyer. 2017. 'Stromal R-spondin orchestrates gastric epithelial stem cells and gland homeostasis', *Nature*, 548: 451-55.

Sigal, M., M. D. M. Reines, S. Mullerke, C. Fischer, M. Kapalczynska, H. Berger, E. R. M. Bakker, H. J. Mollenkopf, M. E. Rothenberg, B. Wiedenmann, S. Sauer, and T. F. Meyer. 2019. 'R-spondin-3 induces secretory, antimicrobial Lgr5(+) cells in the stomach', *Nat Cell Biol*, 21: 812-23.

Sigal, M., M. E. Rothenberg, C. Y. Logan, J. Y. Lee, R. W. Honaker, R. L. Cooper, B. Passarelli, M. Camorlinga, D. M. Bouley, G. Alvarez, R. Nusse, J. Torres, and M. R. Amieva. 2015. 'Helicobacter pylori Activates and Expands Lgr5(+) Stem

Cells Through Direct Colonization of the Gastric Glands', *Gastroenterology*, 148: 1392-404 e21.

Sjollema, Klaas A., and Ben N. G. Giepmans. Oct. 24, 2016. 'Automated Annotating Label in Nanotomy', *Imaging & Microscopy*.

Slot, J. W., H. J. Geuze, S. Gigengack, G. E. Lienhard, and D. E. James. 1991. 'Immuno-localization of the insulin regulatable glucose transporter in brown adipose tissue of the rat', *J Cell Biol*, 113: 123-35.

Spence, J. R., C. N. Mayhew, S. A. Rankin, M. F. Kuhar, J. E. Vallance, K. Tolle, E. E. Hoskins, V. V. Kalinichenko, S. I. Wells, A. M. Zorn, N. F. Shroyer, and J. M. Wells. 2011. 'Directed differentiation of human pluripotent stem cells into intestinal tissue in vitro', *Nature*, 470: 105-9.

Spencer-Dene, B., F. G. Sala, S. Bellusci, S. Gschmeissner, G. Stamp, and C. Dickson. 2006. 'Stomach development is dependent on fibroblast growth factor 10/fibroblast growth factor receptor 2b-mediated signaling', *Gastroenterology*, 130: 1233-44.

Stange, D. E., B. K. Koo, M. Huch, G. Sibbel, O. Basak, A. Lyubimova, P. Kujala, S. Bartfeld, J. Koster, J. H. Geahlen, P. J. Peters, J. H. van Es, M. van de Wetering, J. C. Mills, and H. Clevers. 2013. 'Differentiated Troy+ chief cells act as reserve stem cells to generate all lineages of the stomach epithelium', *Cell*, 155: 357-68.

Stein, B. A., A. M. Buchan, J. Morris, and J. M. Polak. 1983. 'The ontogeny of regulatory peptide-containing cells in the human fetal stomach: an immunocytochemical study', *J Histochem Cytochem*, 31: 1117-25.

Steinberg, M. L., and V. Defendi. 1983. 'Transformation and immortalization of human keratinocytes by SV40', *J Invest Dermatol*, 81: 131s-6s.

Steinhart, Zachary, and Stephane Angers. 2018. 'Wnt signaling in development and tissue homeostasis', *Development*, 145: dev146589.

Stzepourginski, I., G. Nigro, J. M. Jacob, S. Dulauroy, P. J. Sansonetti, G. Eberl, and L. Peduto. 2017. 'CD34+ mesenchymal cells are a major component of the intestinal stem cells niche at homeostasis and after injury', *Proc Natl Acad Sci U S A*, 114: E506-e13.

Suerbaum, S., C. Josenhans, and A. Labigne. 1993. 'Cloning and genetic characterization of the Helicobacter pylori and Helicobacter mustelae flaB flagellin genes and construction of H. pylori flaA- and flaB-negative mutants by electroporation-mediated allelic exchange', *J Bacteriol*, 175: 3278-88.

Takasato, M., P. X. Er, H. S. Chiu, B. Maier, G. J. Baillie, C. Ferguson, R. G. Parton, E. J. Wolvetang, M. S. Roost, S. M. Chuva de Sousa Lopes, and M. H. Little. 2015. 'Kidney organoids from human iPS cells contain multiple lineages and model human nephrogenesis', *Nature*, 526: 564-8.

The Cancer Genome Atlas, Network, Donna M. Muzny, Matthew N. Bainbridge, Kyle Chang, Huyen H. Dinh, Jennifer A. Drummond, Gerald Fowler, Christie L. Kovar, Lora R. Lewis, Margaret B. Morgan, Irene F. Newsham, Jeffrey G. Reid, Jireh Santibanez, Eve Shinbrot, Lisa R. Trevino, Yuan-Qing Wu, Min Wang, Preethi Gunaratne, Lawrence A. Donehower, Chad J. Creighton, David A. Wheeler, Richard A. Gibbs, Michael S. Lawrence, Douglas Voet, Rui Jing, Kristian Cibulskis, Andrey Sivachenko, Petar Stojanov, Aaron McKenna, Eric S. Lander, Stacey Gabriel, Gad Getz, Li Ding, Robert S. Fulton, Daniel C. Koboldt, Todd Wylie, Jason Walker, David J. Dooling, Lucinda Fulton, Kim D. Delehaunty, Catrina C. Fronick, Ryan Demeter, Elaine R. Mardis, Richard K. Wilson, Andy Chu, Hye-Jung E. Chun, Andrew J. Mungall, Erin Pleasance, A. Gordon Robertson, Dominik Stoll, Miruna Balasundaram, Inanc Birol, Yaron S.

N. Butterfield, Eric Chuah, Robin J. N. Coope, Noreen Dhalla, Ranabir Guin, Carrie Hirst, Martin Hirst, Robert A. Holt, Darlene Lee, Haiyan I. Li, Michael Mayo, Richard A. Moore, Jacqueline E. Schein, Jared R. Slobodan, Angela Tam, Nina Thiessen, Richard Varhol, Thomas Zeng, Yongjun Zhao, Steven J. M. Jones, Marco A. Marra, Adam J. Bass, Alex H. Ramos, Gordon Saksena, Andrew D. Cherniack, Stephen E. Schumacher, Barbara Tabak, Scott L. Carter, Nam H. Pho, Huy Nguyen, Robert C. Onofrio, Andrew Crenshaw, Kristin Ardlie, Rameen Beroukhim, Wendy Winckler, Gad Getz, Matthew Meyerson, Alexei Protopopov, Juinhua Zhang, Angela Hadjipanayis, Eunjung Lee, Ruibin Xi, Lixing Yang, Xiaojia Ren, Hailei Zhang, Narayanan Sathiamoorthy, Sachet Shukla, Peng-Chieh Chen, Psalm Haseley, Yonghong Xiao, Semin Lee, Jonathan Seidman, Lynda Chin, Peter J. Park, Raju Kucherlapati, J. Todd Auman, Katherine A. Hoadley, Ying Du, Matthew D. Wilkerson, Yan Shi, Christina Liquori, Shaowu Meng, Ling Li, Yidi J. Turman, Michael D. Topal, Donghui Tan, Scot Waring, Elizabeth Buda, Jesse Walsh, Corbin D. Jones, Piotr A. Mieczkowski, Darshan Singh, Junyuan Wu, Anisha Gulabani, Peter Dolina, Tom Bodenheimer, Alan P. Hoyle, Janae V. Simons, Matthew Soloway, Lisle E. Mose, Stuart R. Jefferys, Saianand Balu, Brian D. O'Connor, Jan F. Prins, Derek Y. Chiang, D. Neil Hayes, Charles M. Perou, Toshinori Hinoue, Daniel J. Weisenberger, Dennis T. Maglinte, Fei Pan, Benjamin P. Berman, David J. Van Den Berg, Hui Shen, Timothy Triche Jr, Stephen B. Baylin, Peter W. Laird, Gad Getz, Michael Noble, Doug Voet, Gordon Saksena, Nils Gehlenborg, Daniel DiCara, Juinhua Zhang, Hailei Zhang, Chang-Jiun Wu, Spring Yingchun Liu, Sachet Shukla, Michael S. Lawrence, Lihua Zhou, Andrey Sivachenko, Pei Lin, Petar Stojanov, Rui Jing, Richard W. Park, Marc-Danie Nazaire, Jim Robinson, Helga Thorvaldsdottir, Jill Mesirov, Peter J. Park, Lynda Chin, Vesteinn Thorsson, Sheila M. Reynolds, Brady Bernard, Richard Kreisberg, Jake Lin, Lisa Iype, Ryan Bressler, Timo Erkkilä, Madhumati Gundapuneni, Yuexin Liu, Adam Norberg, Tom Robinson, Da Yang, Wei Zhang, Ilya Shmulevich, Jorma J. de Ronde, Nikolaus Schultz, Ethan Cerami, Giovanni Ciriello, Arthur P. Goldberg, Benjamin Gross, Anders Jacobsen, Jianjiong Gao, Bogumil Kaczkowski, Rileen Sinha, B. Arman Aksoy, Yevgeniy Antipin, Boris Reva, Ronglai Shen, Barry S. Taylor, Timothy A. Chan, Marc Ladanyi, Chris Sander, Rehan Akbani, Nianxiang Zhang, Bradley M. Broom, Tod Casasent, Anna Unruh, Chris Wakefield, Stanley R. Hamilton, R. Craig Cason, Keith A. Baggerly, John N. Weinstein, David Haussler, Christopher C. Benz, Joshua M. Stuart, Stephen C. Benz, J. Zachary Sanborn, Charles J. Vaske, Jingchun Zhu, Christopher Szeto, Gary K. Scott, Christina Yau, Sam Ng, Ted Goldstein, Kyle Ellrott, Eric Collisson, Aaron E. Cozen, Daniel Zerbino, Christopher Wilks, Brian Craft, Paul Spellman, Robert Penny, Troy Shelton, Martha Hatfield, Scott Morris, Peggy Yena, Candace Shelton, Mark Sherman, Joseph Paulauskis, Julie M. Gastier-Foster, Jay Bowen, Nilsa C. Ramirez, Aaron Black, Robert Pyatt, Lisa Wise, Peter White, Monica Bertagnolli, Jen Brown, Timothy A. Chan, Gerald C. Chu, Christine Czerwinski, Fred Denstman, Rajiv Dhir, Arnulf Dörner, Charles S. Fuchs, Jose G. Guillem, Mary Iacocca, Hartmut Juhl, Andrew Kaufman, Bernard Kohl Iii, Xuan Van Le, Maria C. Mariano, Elizabeth N. Medina, Michael Meyers, Garrett M. Nash, Phillip B. Paty, Nicholas Petrelli, Brenda Rabeno, William G. Richards, David Solit, Pat Swanson, Larissa Temple, Joel E. Tepper, Richard Thorp, Efsevia Vakiani, Martin R. Weiser, Joseph E. Willis, Gary Witkin, Zhaoshi Zeng, Michael J. Zinner, Carsten

Zornig, Mark A. Jensen, Robert Sfeir, Ari B. Kahn, Anna L. Chu, Prachi Kothiyal, Zhining Wang, Eric E. Snyder, Joan Pontius, Todd D. Pihl, Brenda Ayala, Mark Backus, Jessica Walton, Jon Whitmore, Julien Baboud, Dominique L. Berton, Matthew C. Nicholls, Deepak Srinivasan, Rohini Raman, Stanley Girshik, Peter A. Kigonya, Shelley Alonso, Rashmi N. Sanbhadti, Sean P. Barletta, John M. Greene, David A. Pot, Kenna R. Mills Shaw, Laura A. L. Dillon, Ken Buetow, Tanja Davidsen, John A. Demchok, Greg Eley, Martin Ferguson, Peter Fielding, Carl Schaefer, Margi Sheth, Liming Yang, Mark S. Guyer, Bradley A. Ozenberger, Jacqueline D. Palchik, Jane Peterson, Heidi J. Sofia, and Elizabeth Thomson. 2012. 'Comprehensive molecular characterization of human colon and rectal cancer', *Nature*, 487: 330.

Tiso, N., A. Filippi, S. Pauls, M. Bortolussi, and F. Argenton. 2002. 'BMP signalling regulates anteroposterior endoderm patterning in zebrafish', *Mech Dev*, 118: 29-37.

Todisco, A., M. Mao, T. M. Keeley, W. Ye, L. C. Samuelson, and K. A. Eaton. 2015. 'Regulation of gastric epithelial cell homeostasis by gastrin and bone morphogenetic protein signaling', *Physiol Rep*, 3.

Tyanova, S., T. Temu, and J. Cox. 2016. 'The MaxQuant computational platform for mass spectrometry-based shotgun proteomics', *Nat Protoc*, 11: 2301-19.

van den Brink, G R, J C H Hardwick, C Nielsen, C Xu, F J ten Kate, J Glickman, S J H van Deventer, D J Roberts, and M P Peppelenbosch. 2002. 'Sonic hedgehog expression correlates with fundic gland differentiation in the adult gastrointestinal tract', *Gut*, 51: 628-33.

Van Den Brink, Gijs R., James C. H. Hardwick, Maikel P. Peppelenbosch, Sander J. H. Van Deventer, Guido N. J. Tytgat, Menno A. Brink, and Fiebo J. Ten Kate. 2001. 'Sonic hedgehog regulates gastric gland morphogenesis in man and mouse', *Gastroenterology*, 121: 317-28.

van Es, Johan H., Andrea Haegebarth, Pekka Kujala, Shalev Itzkovitz, Bon-Kyoung Koo, Sylvia F. Boj, Jeroen Korving, Maaike van den Born, Alexander van Oudenaarden, Sylvie Robine, and Hans Clevers. 2012. 'A Critical Role for the Wnt Effector Tcf4 in Adult Intestinal Homeostatic Self-Renewal', *Molecular and Cellular Biology*, 32: 1918.

Vassallo, Gabriele, Carlo Capella, and Enrico Solcia. 1971. 'Endocrine cells of the human gastric mucosa', *Zeitschrift für Zellforschung und Mikroskopische Anatomie*, 118: 49-67.

Venerito, M., M. Varbanova, F. W. Rohl, D. Reinhold, K. Frauenschlager, D. Jechorek, J. Weigt, A. Link, and P. Malfertheiner. 2016. 'Oxyntic gastric atrophy in Helicobacter pylori gastritis is distinct from autoimmune gastritis', *J Clin Pathol*, 69: 677-85.

Verzi, M. P., A. H. Khan, S. Ito, and R. A. Shivdasani. 2008. 'Transcription factor foxq1 controls mucin gene expression and granule content in mouse stomach surface mucous cells', *Gastroenterology*, 135: 591-600.

Verzi, M. P., M. N. Stanfel, K. A. Moses, B. M. Kim, Y. Zhang, R. J. Schwartz, R. A. Shivdasani, and W. E. Zimmer. 2009. 'Role of the homeodomain transcription factor Bapx1 in mouse distal stomach development', *Gastroenterology*, 136: 1701-10.

Vries, Robert G. J., Meritxell Huch, and Hans Clevers. 2010. 'Stem cells and cancer of the stomach and intestine', *Molecular oncology*, 4: 373-84.

Wang, R. N., J. Green, Z. Wang, Y. Deng, M. Qiao, M. Peabody, Q. Zhang, J. Ye, Z. Yan, S. Denduluri, O. Idowu, M. Li, C. Shen, A. Hu, R. C. Haydon, R. Kang, J.

Mok, M. J. Lee, H. L. Luu, and L. L. Shi. 2014. 'Bone Morphogenetic Protein (BMP) signaling in development and human diseases', *Genes Dis*, 1: 87-105.

Wang, T. C., J. R. Goldenring, C. Dangler, S. Ito, A. Mueller, W. K. Jeon, T. J. Koh, and J. G. Fox. 1998. 'Mice lacking secretory phospholipase A2 show altered apoptosis and differentiation with Helicobacter felis infection', *Gastroenterology*, 114: 675-89.

Watt, Fiona M., and Wilhelm T. S. Huck. 2013. 'Role of the extracellular matrix in regulating stem cell fate', *Nature Reviews Molecular Cell Biology*, 14: 467.

Willey, J. C., A. Broussoud, A. Sleemi, W. P. Bennett, P. Cerutti, and C. C. Harris. 1991. 'Immortalization of normal human bronchial epithelial cells by human papillomaviruses 16 or 18', *Cancer Res*, 51: 5370-7.

Wisniewski, J. R., A. Zougman, N. Nagaraj, and M. Mann. 2009. 'Universal sample preparation method for proteome analysis', *Nat Methods*, 6: 359-62.

Wong, B. C., W. P. Wang, W. H. So, V. Y. Shin, W. M. Wong, F. M. Fung, E. S. Liu, W. M. Hiu, S. K. Lam, and C. H. Cho. 2001. 'Epidermal growth factor and its receptor in chronic active gastritis and gastroduodenal ulcer before and after Helicobacter pylori eradication', *Aliment Pharmacol Ther*, 15: 1459-65.

Wu, Peng, Ping Wee, Jennifer Jiang, Xinmei Chen, and Zhixiang Wang. 2012. 'Differential Regulation of Transcription Factors by Location-Specific EGF Receptor Signaling via a Spatio-Temporal Interplay of ERK Activation', *PLoS One*, 7: e41354.

Xia, Y., I. Sancho-Martinez, E. Nivet, C. Rodriguez Esteban, J. M. Campistol, and J. C. Izpisua Belmonte. 2014. 'The generation of kidney organoids by differentiation of human pluripotent cells to ureteric bud progenitor-like cells', *Nat Protoc*, 9: 2693-704.

Yan, F., H. Cao, R. Chaturvedi, U. Krishna, S. S. Hobbs, P. J. Dempsey, R. M. Peek, Jr., T. L. Cover, M. K. Washington, K. T. Wilson, and D. B. Polk. 2009. 'Epidermal growth factor receptor activation protects gastric epithelial cells from Helicobacter pylori-induced apoptosis', *Gastroenterology*, 136: 1297-307, e1-3.

Yao, X., and A. J. Smolka. 2019. 'Gastric Parietal Cell Physiology and Helicobacter pylori-Induced Disease', *Gastroenterology*.

Ye, Wei, Hidehiko Takabayashi, Yitian Yang, Maria Mao, Elise S. Hibdon, Linda C. Samuelson, Kathryn A. Eaton, and Andrea Todisco. 2018. 'Regulation of Gastric Lgr5+ve Cell Homeostasis by Bone Morphogenetic Protein (BMP) Signaling and Inflammatory Stimuli', *Cellular and Molecular Gastroenterology and Hepatology*, 5: 523-38.

Zeisberg, Elisabeth M., Oleg Tarnavski, Michael Zeisberg, Adam L. Dorfman, Julie R. McMullen, Erika Gustafsson, Anil Chandraker, Xueli Yuan, William T. Pu, Anita B. Roberts, Eric G. Neilson, Mohamed H. Sayegh, Seigo Izumo, and Raghu Kalluri. 2007. 'Endothelial-to-mesenchymal transition contributes to cardiac fibrosis', *Nat Med*, 13: 952.

Zeng, Fenghua, and Raymond C. Harris. 2014. 'Epidermal growth factor, from gene organization to bedside', *Semin Cell Dev Biol*, 28: 2-11.

Zorn, A. M., and J. M. Wells. 2009. 'Vertebrate endoderm development and organ formation', *Annu Rev Cell Dev Biol*, 25: 221-51.

7. APPENDIX

7.1. Electronic appendix

Complete data of the microarray and MS analysis are provided in the Electronic Appendix:

Folder EA.1: Microarray data gene expression – txt files and QC report

- EA.1.1.: ExpDesign – Excel table
- EA.1.2.: Raw data – txt files
- EA.1.3.: Differential expression results – txt files
- EA.1.4.: Expression analysis – html and rmd file
- EA.1.5.: Preprocessing and QC report – html and rmd file

Folder EA.2: MaxQuant MS data analysis

- EA.2.1.: Excel file of MaxQuant MS data analysis

7.2. MaxQuant MS data analysis

Table 25: Top 100 hits of the MaxQuant MS data analysis. The full list with all detected peptides/proteins is to be found in the electronic appendix EA.2. Displayed are the first 100 hits of the MaxQuant MS data analysis with the LFQ intensities of every sample for the respective protein. MS analysis of mucus from Noggin deprived corpuis mucosoids non-treated or MEKi treated for 12 days was performed. In blue are the control proteins used in the MS analysis. Hits displayed in this thesis are highlighted in red. LFQ: Lable free quantification

		LFQ Intensity							
Protein IDs	**Score**	GAT23C_1	GAT23C_2	GAT23C +MEKi_1	GAT23C +MEKi_2	GAT26C_1	GAT26C_2	GAT26C +MEKi_1	GAT26C +MEKi_2
sp|O00391|QSOX1_HUMAN	323,31	1,37E+10	1,13E+10	3,11E+09	2,42E+09	1,03E+10	9,82E+09	6,83E+09	2,65E+08
sp|O00560|SDCB1_HUMAN	323,31	1,50E+09	1,40E+09	9,57E+07	1,57E+08	1,62E+09	9,21E+08	1,03E+09	0,00E+00
sp|O00584|RNT2_HUMAN	323,31	4,75E+08	2,40E+08	3,12E+08	0,00E+00	3,97E+08	2,54E+08	4,58E+08	0,00E+00
sp|O43490|PROM1_HUMAN	323,31	1,38E+09	2,29E+09	6,65E+08	7,49E+08	1,26E+09	6,97E+08	1,57E+09	1,27E+08
sp|P00558|PGK1_HUMAN	323,31	1,13E+09	1,37E+09	5,07E+08	3,77E+08	1,26E+09	1,23E+09	1,30E+09	2,21E+08
sp|P00698|LYSC_CHICK	323,31	3,59E+09	3,55E+10	5,29E+09	7,53E+10	4,27E+09	4,33E+10	4,62E+09	4,66E+10
sp|P00751|CFAB_HUMAN	323,31	4,02E+09	3,02E+09	2,59E+09	1,69E+09	3,78E+09	2,55E+09	6,06E+09	1,34E+09
sp|P00921|CAH2_BOVIN	323,31	1,01E+09	3,57E+10	1,08E+09	5,87E+10	1,68E+09	1,36E+10	1,64E+09	4,45E+09
sp|P00995|ISK1_HUMAN	323,31	1,64E+09	4,59E+08	4,68E+09	1,71E+08	9,94E+08	1,07E+09	1,43E+09	3,10E+09
sp|P01009|A1AT_HUMAN	323,31	4,97E+10	3,48E+10	3,03E+09	1,14E+10	2,07E+10	6,60E+09	1,83E+10	6,43E+07
sp|P01011|AACT_HUMAN	323,31	5,67E+09	6,98E+09	1,37E+09	6,95E+09	5,63E+09	3,33E+09	7,34E+09	0,00E+00
sp|P01033|TIMP1_HUMAN	323,31	2,09E+09	1,96E+09	3,14E+08	3,29E+08	1,21E+09	6,57E+08	7,27E+08	1,49E+08
sp|P01034|CYTC_HUMAN	323,31	6,92E+09	2,66E+09	4,80E+09	2,22E+09	4,96E+09	4,20E+09	6,48E+09	3,99E+09
sp|P01833|PIGR_HUMAN	323,31	1,81E+11	1,95E+11	7,75E+10	1,01E+11	1,66E+11	1,33E+11	1,73E+11	3,13E+10
sp|P02754|LACB_BOVIN	323,31	4,26E+09	6,24E+10	3,48E+09	8,30E+10	4,40E+09	9,81E+10	4,24E+09	3,37E+10
sp|P02774|VTDB_HUMAN	323,31	2,34E+08	6,13E+07	3,04E+09	1,15E+09	2,49E+08	1,58E+08	4,67E+08	1,30E+09
sp|P02787|TRFE_HUMAN	323,31	9,27E+09	9,61E+09	1,21E+11	9,19E+10	1,37E+10	1,35E+10	3,28E+10	1,27E+11
sp|P02788|TRFL_HUMAN	323,31	4,34E+09	8,17E+08	7,32E+09	3,01E+09	7,28E+08	8,34E+08	1,67E+09	3,59E+09
sp|P02789|TRFE_CHICK	323,31	1,98E+10	3,03E+11	1,35E+10	3,19E+11	2,35E+10	3,22E+11	2,46E+10	6,60E+10
sp|P04075|ALDOA_HUMAN	323,31	1,17E+09	1,02E+09	7,79E+08	3,89E+08	1,66E+09	1,08E+09	1,28E+09	1,92E+08
sp|P05156|CFAI_HUMAN	323,31	8,25E+08	7,65E+08	8,26E+08	1,74E+08	1,04E+09	6,11E+08	1,38E+09	8,04E+08

sp|P05787|K2C8_HUMAN	323,31	9,77E+08	3,96E+08	8,83E+08	4,94E+08	1,26E+09	8,57E+08	1,26E+09	1,51E+09
sp|P06396|GELS_HUMAN	323,31	1,17E+09	1,39E+09	1,51E+09	4,09E+08	1,19E+09	1,97E+09	7,74E+08	4,61E+08
sp|P06733|ENOA_HUMAN	323,31	9,99E+08	9,01E+08	1,01E+09	6,17E+08	8,58E+08	7,62E+08	1,14E+09	9,80E+08
sp|P07355|ANXA2_HUMAN	323,31	7,25E+08	5,87E+08	2,05E+08	1,02E+08	9,00E+08	7,37E+08	7,93E+08	0,00E+00
sp|P07477|TRY1_HUMAN	323,31	7,02E+09	1,27E+10	1,03E+09	2,43E+09	7,29E+09	9,86E+09	3,63E+09	0,00E+00
sp|P07998|RNAS1_HUMAN	323,31	3,97E+09	1,32E+09	6,91E+09	3,24E+09	3,77E+09	2,59E+09	8,70E+09	4,44E+09
sp|P08727|K1C19_HUMAN	323,31	1,15E+09	4,79E+08	6,94E+08	4,68E+08	1,11E+09	9,29E+08	1,36E+09	1,47E+08
sp|Q99878|H2A1J_HUMAN	323,31	8,82E+08	6,52E+08	1,87E+09	1,09E+09	9,34E+08	7,66E+08	1,55E+09	4,49E+09
sp|P10909|CLUS_HUMAN	323,31	2,38E+10	1,07E+10	1,51E+10	1,02E+10	1,39E+10	4,15E+09	3,11E+10	6,90E+08
sp|P14618|KPYM_HUMAN	323,31	8,26E+08	5,00E+08	7,67E+08	5,29E+08	1,21E+09	7,13E+08	1,56E+09	1,24E+09
sp|P15311|EZRI_HUMAN	323,31	2,62E+09	2,08E+09	8,90E+08	4,68E+08	3,01E+09	3,51E+09	1,55E+09	2,50E+07
sp|P15328|FOLR1_HUMAN	323,31	1,63E+07	0,00E+00	0,00E+00	0,00E+00	9,58E+08	4,61E+07	1,45E+09	6,21E+07
sp|P15941|MUC1_HUMAN	323,31	3,87E+09	8,03E+09	1,94E+09	4,20E+09	5,78E+09	5,73E+09	2,06E+09	1,87E+08
sp|P18065|IBP2_HUMAN	323,31	1,83E+09	1,26E+09	4,40E+09	9,05E+08	3,54E+09	1,85E+09	3,76E+09	5,43E+08
sp|P20061|TCO1_HUMAN	323,31	4,78E+09	4,08E+09	2,68E+09	2,98E+09	4,13E+09	2,34E+09	6,83E+09	0,00E+00
sp|P25311|ZA2G_HUMAN	323,31	5,25E+09	4,37E+09	3,26E+09	1,46E+09	1,96E+09	1,54E+09	1,48E+09	8,83E+07
sp|Q99879|H2B1M_HUMAN	323,31	2,41E+09	4,36E+08	3,03E+09	7,26E+08	2,27E+09	1,17E+09	4,16E+09	2,80E+09
sp|P60174|TPIS_HUMAN	323,31	4,50E+08	5,55E+08	7,25E+08	6,06E+08	7,26E+08	6,83E+08	8,55E+08	6,80E+08
sp|P61626|LYSC_HUMAN	323,31	2,06E+11	6,70E+10	2,87E+11	7,21E+10	1,25E+11	6,17E+10	2,49E+11	1,08E+11
sp|P61769|B2MG_HUMAN	323,31	7,29E+09	2,71E+09	5,83E+09	7,32E+08	6,56E+09	4,81E+09	5,84E+09	3,57E+08
sp|P62873|GBB1_HUMAN	323,31	3,08E+08	2,93E+08	1,42E+08	1,41E+08	3,84E+08	2,35E+08	3,36E+08	0,00E+00
sp|P63261|ACTG_HUMAN	323,31	2,72E+09	2,22E+09	2,96E+09	3,19E+09	2,68E+09	1,91E+09	2,91E+09	1,75E+09
sp|P68082|MYG_HORSE;sp|P02144|MYG_HUMAN	323,31	3,35E+09	8,02E+10	1,21E+09	8,10E+10	3,66E+09	9,04E+10	3,70E+09	5,05E+09
sp|P80188|NGAL_HUMAN	323,31	6,46E+09	1,62E+10	7,62E+08	5,95E+09	8,28E+09	4,35E+09	8,36E+09	0,00E+00
sp|P98088|MUC5A_HUMAN	323,31	1,16E+11	1,19E+11	1,38E+09	1,56E+09	6,85E+10	1,20E+11	1,33E+09	2,76E+08
sp|Q03403|TFF2_HUMAN	323,31	3,66E+10	1,14E+10	5,65E+10	1,51E+10	1,34E+10	2,33E+10	6,58E+09	9,93E+09
sp|Q08380|LG3BP_HUMAN	323,31	1,17E+10	9,34E+09	6,75E+09	6,24E+09	1,16E+10	8,84E+09	1,15E+10	1,02E+09
sp|Q12929|EPS8_HUMAN	323,31	9,31E+08	1,01E+09	3,73E+08	4,56E+07	1,11E+09	5,75E+08	3,94E+08	6,56E+07
sp|Q14118|DAG1_HUMAN	323,31	1,48E+09	6,81E+08	7,68E+08	1,50E+08	1,23E+09	6,36E+08	8,94E+08	1,82E+08
sp|Q14508|WFDC2_HUMAN	323,31	6,41E+08	4,56E+08	7,80E+08	1,66E+08	1,39E+09	4,28E+08	1,51E+09	1,53E+08
sp|Q6UXY8|TMC5_HUMAN	323,31	1,09E+09	1,04E+09	9,32E+08	7,78E+07	1,97E+09	1,30E+09	8,52E+08	4,10E+08
sp|Q6W4X9|MUC6_HUMAN	323,31	9,05E+10	5,94E+10	4,18E+10	4,35E+10	8,22E+10	3,71E+10	1,05E+11	3,61E+10

sp|Q7Z404|TMC4_HUMAN	323,31	5,39E+08	5,45E+08	3,18E+08	0,00E+00	7,26E+08	5,45E+08	4,82E+08	0,00E+00
sp|Q86X29|LSR_HUMAN	323,31	2,87E+09	8,21E+08	1,81E+09	4,49E+08	2,31E+09	1,14E+09	2,84E+09	1,60E+08
sp|Q8NBJ4|GOLM1_HUMAN	323,31	3,59E+09	7,03E+09	1,91E+09	1,98E+09	4,15E+09	7,51E+09	3,64E+09	3,15E+09
sp|Q8TDL5|BPIB1_HUMAN	323,31	1,07E+10	2,40E+10	1,01E+10	1,25E+10	1,64E+10	2,38E+10	3,64E+10	3,82E+09
sp|Q92520|FAM3C_HUMAN	323,31	2,68E+09	1,26E+09	1,73E+09	4,53E+08	2,68E+09	1,77E+09	1,97E+09	3,47E+08
sp|Q92896|GSLG1_HUMAN	323,31	8,10E+09	4,10E+09	1,51E+10	5,54E+08	4,87E+09	5,17E+09	6,62E+09	0,00E+00
sp|Q99828|CIB1_HUMAN	323,31	2,88E+08	3,34E+08	6,74E+07	1,66E+08	1,76E+08	2,28E+08	2,02E+08	0,00E+00
sp|Q9HC84|MUC5B_HUMAN	323,31	2,61E+09	6,47E+09	6,96E+07	5,35E+07	1,52E+10	2,19E+10	3,44E+09	2,33E+08
sp|Q9UBP4|DKK3_HUMAN	323,31	9,34E+08	1,57E+08	8,45E+08	8,18E+07	7,07E+08	2,24E+08	2,07E+09	8,01E+07
sp|Q9UHR4|BI2L1_HUMAN	323,31	6,06E+08	7,22E+08	1,89E+08	1,51E+08	8,69E+08	5,24E+08	3,53E+08	0,00E+00
sp|Q9UQB8|BAIP2_HUMAN	323,31	9,55E+08	3,70E+08	5,30E+08	2,77E+08	7,05E+08	4,28E+08	4,54E+08	1,46E+08
sp|Q9Y6R7|FCGBP_HUMAN	323,31	9,54E+09	5,40E+09	8,07E+07	1,20E+08	2,92E+10	3,35E+10	5,16E+09	5,05E+08
sp|O60635|TSN1_HUMAN	321,72	1,29E+08	5,73E+08	0,00E+00	0,00E+00	1,57E+08	4,53E+08	0,00E+00	0,00E+00
sp|P02790|HEMO_HUMAN	321,51	0,00E+00	0,00E+00	7,90E+08	8,51E+08	0,00E+00	0,00E+00	0,00E+00	7,47E+08
sp|P04406|G3P_HUMAN	315,07	6,47E+08	3,76E+08	3,36E+08	6,41E+08	9,34E+08	3,80E+08	1,08E+09	1,20E+08
sp|P80303|NUCB2_HUMAN	314,1	5,06E+08	2,03E+08	8,82E+08	1,89E+08	1,38E+08	8,51E+07	1,68E+08	0,00E+00
sp|P35579|MYH9_HUMAN	313,71	4,29E+08	8,15E+07	4,80E+08	3,38E+07	4,38E+08	1,64E+08	7,31E+08	1,94E+08
sp|Q06828|FMOD_HUMAN	285,76	1,43E+09	7,89E+08	1,54E+09	1,01E+09	6,37E+08	2,27E+08	1,64E+09	1,68E+08
sp|Q02818|NUCB1_HUMAN	279,66	8,38E+08	8,74E+08	1,46E+09	4,27E+08	9,24E+08	6,47E+08	7,72E+08	1,30E+08
sp|P02750|A2GL_HUMAN	277,84	1,64E+09	8,49E+08	5,71E+08	3,19E+08	1,11E+09	7,72E+08	1,32E+09	0,00E+00
sp|P13987|CD59_HUMAN	276,99	3,93E+09	2,28E+09	1,94E+09	8,64E+08	3,02E+09	4,09E+09	1,99E+09	5,83E+08
sp|P62937|PPIA_HUMAN	276,76	7,14E+08	6,05E+08	7,72E+08	5,23E+08	8,57E+08	7,06E+08	9,01E+08	1,66E+09
sp|P07237|PDIA1_HUMAN	275,38	3,81E+08	3,19E+08	4,55E+08	2,65E+08	4,87E+08	2,97E+08	4,42E+08	8,90E+07
sp|P04155|TFF1_HUMAN	267,89	5,36E+08	2,62E+08	1,25E+08	0,00E+00	1,88E+08	5,34E+08	0,00E+00	0,00E+00
sp|P19075|TSN8_HUMAN	253,84	1,11E+08	3,35E+08	2,68E+07	0,00E+00	1,79E+08	2,53E+08	7,02E+07	0,00E+00
sp|Q8WUM4|PDC6I_HUMAN	249,71	5,10E+08	5,66E+08	2,94E+08	9,75E+07	4,98E+08	5,43E+08	4,18E+08	0,00E+00
sp|Q8TE68|ES8L1_HUMAN	245,14	1,86E+08	2,46E+08	5,81E+07	2,93E+07	3,97E+08	3,84E+08	1,07E+08	0,00E+00
sp|O00468|AGRIN_HUMAN	244,8	1,58E+08	2,86E+08	1,78E+08	0,00E+00	3,30E+08	3,79E+08	1,65E+08	1,51E+08
sp|P56856|CLD18_HUMAN	243,97	2,90E+08	5,34E+08	3,51E+08	2,15E+08	2,62E+08	3,30E+08	1,62E+08	2,60E+08
sp|P11021|BIP_HUMAN	238,29	4,99E+08	4,24E+08	5,11E+08	3,03E+08	4,68E+08	3,27E+08	3,11E+08	4,44E+08
sp|P63104|1433Z_HUMAN	237	4,26E+08	1,78E+08	4,95E+08	1,13E+08	2,46E+08	2,18E+08	4,77E+08	7,49E+08
sp|P02765|FETUA_HUMAN	236,84	1,73E+09	1,36E+09	4,08E+10	2,56E+10	2,37E+09	2,63E+09	5,46E+09	1,42E+10

sp|P25815|S100P_HUMAN	236,31	4,97E+07	6,93E+07	0,00E+00	5,74E+07	3,01E+07	5,97E+07	2,79E+07	0,00E+00
sp|Q9H6S3|ES8L2_HUMAN	231,89	4,52E+08	2,22E+08	4,04E+07	3,44E+07	4,87E+08	3,46E+08	1,62E+08	0,00E+00
sp|P07478|TRY2_HUMAN	228,03	1,82E+10	2,01E+10	6,58E+09	4,36E+09	9,85E+09	7,22E+09	9,10E+09	1,03E+08
sp|P20142|PEPC_HUMAN	224,55	3,24E+10	1,63E+10	2,48E+10	2,50E+10	8,81E+09	2,51E+09	3,66E+10	5,67E+08
sp|Q8NCL4|GALT6_HUMAN	223,87	3,87E+08	2,09E+08	4,95E+07	5,57E+07	2,74E+08	2,35E+08	2,47E+08	0,00E+00
sp|P00441|SODC_HUMAN	213,16	3,75E+08	9,00E+07	6,85E+08	1,21E+08	3,48E+08	1,46E+08	7,21E+08	2,54E+08
sp|P02768|ALBU_HUMAN	207,05	4,15E+10	1,79E+10	4,34E+11	2,10E+11	4,61E+10	4,83E+10	1,05E+11	1,60E+11
sp|Q16651|PRSS8_HUMAN	204,57	3,27E+08	4,46E+08	1,40E+08	1,70E+08	3,56E+08	2,36E+08	3,36E+08	0,00E+00
sp|Q16674|MIA_HUMAN	195,18	3,58E+08	2,36E+08	0,00E+00	0,00E+00	4,66E+08	2,07E+08	4,35E+08	0,00E+00
sp|P30101|PDIA3_HUMAN	192,31	4,95E+08	1,92E+08	7,65E+08	2,57E+08	4,85E+08	4,31E+08	4,97E+08	3,82E+08
sp|P0DP25|CALM3_HUMAN	190,73	5,27E+07	8,41E+07	5,11E+07	0,00E+00	4,67E+07	6,97E+07	7,06E+07	0,00E+00
sp|P37802|TAGL2_HUMAN	185,97	1,19E+08	1,70E+08	0,00E+00	5,66E+07	1,20E+08	8,31E+07	1,25E+08	0,00E+00
sp|P07996|TSP1_HUMAN	185,8	2,70E+08	1,23E+08	9,02E+08	3,99E+08	6,11E+08	1,79E+08	5,15E+08	1,95E+09
sp|P06731|CEAM5_HUMAN	185,63	1,60E+08	6,50E+07	0,00E+00	0,00E+00	3,30E+07	4,90E+08	0,00E+00	0,00E+00
sp|Q8N4A0|GALT4_HUMAN	183,36	1,88E+08	1,47E+08	0,00E+00	0,00E+00	1,12E+08	8,16E+07	9,60E+07	0,00E+00
sp|P05783|K1C18_HUMAN	181,25	2,89E+08	1,14E+08	1,62E+08	7,47E+07	2,69E+08	1,55E+08	3,74E+08	2,43E+08